# Modulation of mu-opioid receptor dynamics at the plasma membrane and its implications for signalling and trafficking

by Owen George Underwood

BSc (Hons)

Thesis submitted to the

University of Nottingham

For the Degree of

Doctor of Philosophy

December 2023

# I. Abstract

G Protein-Coupled Receptors (GPCRs) likely number more than 830, and much of their function is modulated by arrestins. Arrestins are cytosolic scaffolding proteins, of which only two isoforms mediate numerous signalling outcomes of most GPCRs, often in a ligand-dependent manner. This thesis focuses on how ligand-directed, arrestin-mediated signalling outcomes are selected for one particular GPCR, the μ-opioid receptor (MOR). The MOR is the target receptor for some of the strongest analgesics available in the clinic, including morphine and fentanyl, however these drugs have a number of highly limiting side effects. The MOR is known to couple to β-arrestin2 and has varying signalling and trafficking outcomes dependent on the activating opioid ligand. This has previously been linked to MOR C-tail phosphorylation patterns and their effects on β-arrestin2 such that different ligands exhibit differing receptor trafficking outcomes. G protein-coupled receptor kinases (GRKs) have been shown to be the main effectors in inducing the formation of these phosphorylation patterns, and their differing recruitment has been linked to different opioid ligands. In this thesis, we will assess the role of individual GRKs on MOR signalling, trafficking and regulation, and assess how different phosphosites, and MOR agonists affect the conformational landscape of arrestins.

In chapter 2, cells were screened with differential GRK expression (via CRISPR/Cas9 KO of single or multiple GRK isoforms) for their ability to activate two effector pathways, G protein and arrestin recruitment, when treated with different opioid ligands. Proximity-based bioluminescence resonance energy transfer (BRET) were used in assays measuring the recruitment of fluorescently tagged engineered G protein miniGsi and β-arrestin2 to a luciferase tagged MOR. Clear differences in β-arrestin2 recruitment were detected between HEK293 cell lines . We show that while GRK2 and 3 play the most significant role in β-arrestin2 recruitment to MOR, reintroduction of GRK5 into a GRK-null background rescued recruitment, albeit to a lesser extent than the GRK2/3 family, whereas reintroduction of GRK6 did not rescue recruitment. We also show a component of GRK-independent recruitment of arrestin in this null-GRK background. However, there was little effect of the knockout of GRKs on G protein activation of the MOR by DAMGO, morphine and fentanyl, as expected from kinases mostly affecting receptor regulation. Combined, our results highlight the differing roles of individual GRKs in the MOR-induced arrestin recruitment, and the differing preferences of opioid ligands for specific GRK isoforms.

After this, we build up from previous work in the lab suggesting the role of GRKs in MOR diffusion within the plasma membrane. Taking advantage of the GRK KO cells, a limited set of cells with differential GRK expression were screened for their MOR diffusion and trafficking characteristics at the plasma

membrane, both under basal conditions and following treatment with an agonist. We used fluorescence correlation spectroscopy (FCS) to assess diffusion speed, particle concentration, and clustering of the MOR. We did not observe changes in MOR in cells with differential GRK expression under basal conditions or upon incubation with the opioid agonist.

Finally, different MOR agonists as well as the effect of mutation of C-tail serine and threonine residues were assessed for their ability to induce conformational changes in β-arrestin2. To achieve this, a selection of BRET-based intramolecular conformational β-arrestin2 biosensors were used to show that while MOR agonist efficacy correlates strongly with conformational change in each sensor location, small differences in local conformations can be observed with differing MOR agonists. We also show that mutation of the C-tail phosphorylation motifs to alanine had a significant impact on the conformational changes of arrestin. Combined, these data suggest that β-arrestin2 adopts phosphorylation-dependent conformations, and opioid agonists are able to modulate these conformations.

Taken together, the data obtained in this thesis highlights the mechanisms by which MOR ligands are able to induce distinct patterns of receptor phosphorylation; by activating individual GRK isoforms and/or modulating arrestin conformations, leading to differences in receptor trafficking and potentially signalling.

## II. Publications During Enrolment

Underwood, O., Fritzwanker, S., Glenn, J., Batista-Gondin, A., Drube, J., Hoffman, C., Briddon, S., Schulz, S., Canals, M. (In Preparation). Key phosphorylation sites for robust β-arrestin2 binding at the MOR revisited.

Abstract: Desensitisation of the mu-opioid receptor (MOR) is proposed to underlie the initiation of opioid analgesic tolerance and previous work has shown that agonist-induced phosphorylation of the MOR C-tail contributes to its desensitisation. Moreover, we and others have shown that phosphorylation is important for β-arrestin recruitment to the receptor, and that ligands of different efficacies induce distinct patterns, or barcodes, of receptor phosphorylation. Within the MOR C-tail, the $^{370}$TREHPSTANT$^{379}$ harbours Ser/Thr residues important for these regulatory functions. $^{375}$Ser acts as a primary phosphorylation site of a ligand-dependent, hierarchical, and sequential process, whereby flanking $^{370}$Thr, $^{376}$Thr and $^{379}$Thr residues can get subsequently phosphorylated. Here we used HEK293 GRK KO cells in combination with phosphosite specific antibodies and site-directed mutagenesis of the MOR to evaluate the contribution of the different GRK subfamilies to ligand-induced phosphorylation barcodes and β-arrestin2 recruitment. We show that both GRK subfamilies (GRK2/3 and GRK5/6) promote phosphorylation of Thr$^{370}$ and Ser$^{375}$. However, only GRK2/3 induce phosphorylation of Thr$^{376}$ and Thr$^{379}$, which is required to promote robust β-arrestin recruitment to the receptor. Moreover, while DAMGO and fentanyl can engage all kinases to promote Thr$^{370}$ and Ser$^{375}$ phosphorylation, under endogenous GRK expression conditions, morphine-induced phosphorylation of these residues is specifically mediated by GRK5/6. These data provide insight into the mechanisms of MOR regulation and suggest that the cellular complement of the different GRK subfamilies plays an important role in determining the tissue responses of distinct opioid agonists.

Underwood, O., Haider, R.S., Sanchez, J., Canals, M. (In Preparation) Arrestin-centred interactions at the membrane and their conformational determinants.

Abstract: More than 30 years after their discovery, arrestins are recognised multiprotein scaffolds that play essential roles in G protein-coupled receptor (GPCR) regulation and signalling. Originally named for their capacity to hinder GPCR coupling to G proteins and facilitate receptor desensitisation, arrestins have emerged as key hubs for a myriad of other functions, including receptor internalisation and scaffolding of signalling complexes. Recent structural studies have started to provide snapshots of the complexes formed by GPCRs and arrestins, supporting a wealth of biochemical data delineating the molecular determinants of such interactions. Furthermore, biophysical

techniques have also provided key information with regards to the basal and active conformations of arrestins, and how these are affected upon GPCR activation. Here we review the most recent advances on our understanding of GPCR-arrestin complexes, from structure to interactions of arrestins with the lipid bilayer and other proteins. We also present an updated view on the development of tools to study the conformational flexibility of arrestins, with the potential to provide experimental data to describe the dynamic models of arrestin activation.

# III. Conference Attendance During Enrolment

## Oral Presentations:

Underwood, O, Haider, RS, Lane, JR, Hoffmann, C, Canals, M. 2021. Use of intramolecular biosensors to monitor mu-opioid receptor-induced conformational changes of β-arrestin2. First International iGPCR.net Meeting, Nov 2021, Online.

Underwood, O, Haider, RS, Lane, JR, Hoffmann, C, Canals, M. 2022. β-arrestin2 conformational changes are induced by mu-opioid receptor activation. 6th Ernest Online Conference, March 2022, Online.

Underwood, O. 2022. μ-Opioid phosphorylation patterns induce distinct β-arrestin 2 conformational shapes. 2022 IMPACT Student Symposium, April 2022, Birmingham, UK.

## Poster Presentations:

Underwood, O, Haider, RS, Lane, JR, Hoffmann, C, Canals, M. 2020. Use of intramolecular biosensors to monitor mu-opioid receptor-induced conformational changes of β-arrestin2. British Pharmacological Society: Pharmacology 2020, Dec 2020, Online.

Underwood, O, Haider, RS, Lane, JR, Hoffmann, C, Canals, M. 2021. Use of intramolecular biosensors to monitor mu-opioid receptor-induced conformational changes of β-arrestin2. 1st Transatlantic ECI GPCR symposium, July 2021, Online.

Underwood, O, Haider, RS, Lane, JR, Hoffmann, C, Canals, M. 2021. Use of intramolecular biosensors to monitor mu-opioid receptor-induced conformational changes of β-arrestin2. British Pharmacological Society: Pharmacology 2021, Sept 2021, Online.

Underwood, O, Haider, RS, Lane, JR, Hoffmann, C, Canals, M. 2021. Use of intramolecular biosensors to monitor mu-opioid receptor-induced conformational changes of β-arrestin2. First International iGPCR.net Meeting, Nov 2021, Online.

Underwood, O, Haider, RS, Lane, JR, Hoffmann, C, Canals, M. 2022. β-arrestin2 conformational changes are induced by mu-opioid receptor activation. 6th Ernest Online Conference, March 2022, Online.

Underwood, O, Haider, RS, Lane, JR, Hoffmann, C, Canals, M. 2022. β-arrestin2 conformational changes are induced by mu-opioid receptor activation. 2022 IMPACT Student Symposium, April 2022, Birmingham, UK.

# IV. Acknowledgements

My time as a PhD student has filled me with joy, both in experiencing real scientific research and with the people who have helped and shared in my time at COMPARE.

Firstly, I'd like to thank Prof. Meritxell Canals, who, without her brilliant guidance, kindness, immense knowledge, and encouragement this work would not exist. I realise how lucky I am to have such a caring and involved supervisory team helping and guiding me with the past 4 years of this work. With this, I'd also like to thank Dr Steve Briddon, for his similarly amazing guidance and expertise navigating both scientific discovery and the PhD process.

Another big thank you should go to the rest of the Molecular Neuropharmacology Lab group, Dr Rob Lane for his brilliant insights, and Dr Julie Sanchez and Jackie Glenn for their excellent tutelage teaching me how to work in such a wonderful lab, Thanks also to Raphael for his extensive work, expertise, and kindness in generating and gifting the constructs and cells used in this work, as well as Hannah, Noemi, George, Lucy, and Lauren, with which I've had the immense pleasure of working alongside for the past few years.

Thanks should also go to Dr Joëlle Goulding, for her role in introducing me to, and supporting me in, the world of imaging and COMPARE, which I would also like to thank as a whole for their unmatched sense of friendship, community, and belonging that I have felt since joining in 2018.

Thank you also to Prof. Jeanette Woolard for her support throughout my PhD and, alongside Prof. Eamonn Kelly, their time and insightful questions during my Viva.

For all their love and support during all my education, thank you to my family, my parents, my grandparents, and my sister. Thank you also to the Kerry family, for their care and support over the past few years.

Finally, thank you to my amazing partner Lucy, who continues to love and support me throughout the most difficult periods during this process and throughout our future.

# V. Abbreviations

β2AR – β2-adrenoceptor

AC – adenylyl cyclase

AC – autocorrelation

AIP – aryl hydrocarbon receptor interacting protein

ANOVA – analysis of variance

AP2 – adaptin protein subunit 2

ARF – ADP-ribosylation factor

ARNO – ARF nucleotide-binding site opener

ASK1 – Apoptosis signal-regulating kinase 1

ATP – adenosine triphosphate

BRET – bioluminescence resonance energy transfer

CaMKII – calcium/calmodulin-dependent protein kinase II

cAMP – cyclic adenosine monophosphate

CCR5 – C-C chemokine receptor type 5

CDC – Centre for Disease Control

CFP – cyan fluorescent protein

CLB – C-lobe base

Cmpd101 – Compound 101

CK – creatine kinase

CNS – central nervous system

Cryo-EM – cryo-electron microscopy

CRISPR – clustered regularly interspaced short tandem repeats

D2 – dopamine receptor D2

DAMGO – [D-Ala2,N-Me-Phe4,Gly5-ol]-enkephalin

DMEM – Dulbecco's modified Eagle's medium

DOR – δ-opioid receptor

ECL – extracellular loop

EDT – ethanedithiol

EDTA - ethylenediaminetetraacetic acid

EIF4E – eukaryotic translation initiation factor 4E

EGF – epidermal growth factor

eNOS – endothelial nitric oxide synthases

ERK – extracellular signal-regulated kinase

FAK – focal adhesion kinase

FBS – foetal bovine serum

FCS – fluorescence correlation spectroscopy

FDA – Food and Drug Administration

FlAsH – fluorescein arsenical hairpin

FRAP – fluorescence recovery after photobleaching

FRET – Forster resonance energy transfer

GABA - γ aminobutyric acid

GDP – guanosine diphosphate

GDS – GDP dissociation stimulator

GIRK – G protein-activated inwardly rectifying potassium channel

GEF – guanine-nucleotide exchange factor

GPCR – G protein-coupled receptor

GPR52 - G protein-coupled receptor 52

GRK – G protein-coupled receptor kinase

GSK – glycogen synthase kinase

GTP – guanosine triphosphate

hAGT – human O6-alkylguanine-DNA alkytransferase

HBSS – Hank's balanced salt solution

HEK – human embryonic kidney

ICL – intracellular loop

IKBa – nuclear factor of kappa light polypeptide gene enhancer in B-cells inhibitor, alpha

iNOS – cytokine-inducible nitric oxide synthases

JNK – c-Jun N-terminal kinase

KIF3A – kinesin family member 3A

KO – knock-out

KOR – κ-opioid receptor

MAPK – mitogen-activated protein kinase

MDM2 – mouse double minute 2

MEK – mitogen-activated protein kinase kinase

mG – mini-G protein

Mnk – mitogen-activated protein kinase interacting protein kinase

MKK1 – Mitogen-activated protein kinase kinase 1

MOR – μ-opioid receptor

NA – numerical aperture

NEDD – neural-precursor-cell-expressed developmentally down-regulated

NFkB – nuclear factor kappa B subunit

NK – Natural Killer Cells

NLuc – Nanoluciferase

NMR – nuclear magnetic resonance

NOR – nociception/orphanin FQ peptide receptor

PBS – phosphate buffered saline

PCH – photon counting histogram

PDB – Protein Data Bank

PDE – phosphodiesterases

PDL – poly-D-lysine

PEI – polyethyleneimine

PIP2 – phosphatidylinositol 4,5-biphosphate

PI3K – phosphoinositide 3 kinase

PKA – protein kinase A

PKC – protein kinase C

PLL – poly-L-lysine

PM – plasma membrane

PMA – phorbol 12-myristate 13-acetate

POMC – pro-opiomelanocortin

PP2a – protein phosphatase 2A

PRK2 – protein kinase C related kinase 2

PTEN - phosphatase and tensin homolog

Raf – Rapidly Accelerated Fibrosarcoma

RET – resonance energy transfer

RH domain – regulator of G-protein signaling (RGS) homology domain

RLuc – Renilla luciferase

ROCK2 – Rho associated coiled-coil containing protein kinase 2

RSK – ribosomal s6 kinase

SEM – standard error of the mean

SGK1 – serum- and glucocorticoid- inducible kinase 2

SHP – small heterodimer partner

TM – transmembrane

TRAF – Tumour necrosis factor receptor–associated factor

YFP – yellow fluorescent protein

WT – wild type

# VI. Table of Contents

# Chapter 1: Introduction

## 1.1 G Protein Coupled Receptors – Structure and Signalling

G protein-coupled receptors (GPCRs) are a diverse group of integral membrane proteins found in almost all tissues in the body. They encompass more than a quarter of all known receptors in humans. They respond to a huge range of stimuli (from large peptides and hormones, to ions and photons) and participate in virtually all physiological processes, from locomotion to vision, as well as pain perception and modulation. Not surprisingly, due to their important physiological roles, GPCRs are implicated in the pathophysiology of a wide range of clinical conditions, from cardiovascular diseases, to cancer, obesity, and neurological disorders. As a class GPCRs hold the largest share of drugs in the clinic when split by target, being the targets of up to 34% of FDA approved drugs (Pándy-Szekeres *et al.*, 2018; Alhosaini *et al.*, 2021). Pharmacological targeting of GPCRs is achieved using a variety of different strategies, from small molecule ligands to large biologics such as peptides and monoclonal antibodies.

### 1.1.1 GPCR Classification

GPCRs are classified into 6 families, and within these other groupings can be created based on their physiological effect or ligand type. These are the Rhodopsin (A) family, Secretin (B1) family, featuring receptors such as the parathyroid and glucagon receptors, the Adhesion (B2) family, the Glutamate (C) family encompassing some taste receptors and the GABA receptor, and finally the Frizzled (F) and the Taste 2 (T) families. The largest of these families, Family A, is made up of rhodopsin-like GPCRs, named for their sequence homology to the first GPCR to be characterised, Rhodopsin. Family A GPCRs are stimulated by a wide variety of stimuli, making them the most diverse family, and as a result, have been further divided by ligand type. These include the aminergic receptors, containing more high-profile receptors such as the dopamine, muscarinic, serotonin and adrenaline receptors. A large group in this class are the peptide receptors, which include the orexin, neuropeptide, and opioid receptors. Other GPCR families share more limited sequence homology, but still share broadly similar structures. Most of these families still have orphan receptors, namely receptors whose function has been discovered by experimental means, but for which their endogenous ligands have not yet been identified (Pándy-Szekeres *et al.*, 2018).

### 1.1.2 GPCR Structure and Conformations

Structurally, GPCRs are formed of 7 membrane spanning helical domains, connected by six alternating intra- and extra-cellular loops, with a free N- and C-terminal protruding into the extracellular and intracellular space, respectively (see figure 1.1.2.1). The size and composition of these protruding regions vary between GPCR families, and are involved in recruitment and

binding of ligands, trafficking and embedding of the receptor, and coupling to regulatory complexes (Pándy-Szekeres *et al.*, 2023).

The arrangement of the 7 transmembrane (TM) alpha-helical domains in an anticlockwise ring forms the hydrophobic core of GPCRs, allowing it to be impermeable to water and ions. Many family A GPCRs also contain helix 8, an intracellular helix with a palmitoylation site embedded in the membrane, residing at the base of TM helix 7 (Goddard and Watts, 2012). In family A GPCRs, this core also contains the binding site for most endogenous ligands, known as the orthosteric binding pocket. Upon binding of an activating ligand (agonist), the transmembrane domains of the GPCR change conformation, opening an intracellular binding pocket for the effectors of the receptor to bind, be activated and trigger intracellular signalling cascades (Lefkowitz, 2013).

The orthosteric binding site in family A GPCRs is formed by the outward protrusion of the ring of the transmembrane domains. The site faces the extracellular side of the membrane, and is generally accessed by this route, however some lipophilic molecules such as the opioid agonist fentanyl can enter through the side of the receptor, between the transmembrane domains (Erlandson, McMahon and Kruse, 2018; Kelly *et al.*, 2023). The pocket itself displays different residue side chains into the pocket dependent on the GPCR, thus generating the specificity of ligand required for activation. Different ligands can bind different areas of the pocket, thus allowing for a variety of activation states (Podlewska *et al.*, 2020; Kelly *et al.*, 2021; Vo *et al.*, 2021). Other than the orthosteric sites, some ligands can bind to GPCRs at other locations, and these can either function as a secondary binding site for agonists (in the case of bitopic ligands), or as binding sites for allosteric ligands, having different effects on orthosteric agonists (Christopoulos, 2002; Christopoulos and Kenakin, 2002; May, Avlani, *et al.*, 2007; May, Leach, *et al.*, 2007). Many family A GPCRs have an extracellular vestibule above the orthosteric binding site, in which small molecules can bind and have the effect of potentiating (positive allosteric modulators) or inhibiting (negative allosteric modulators) endogenous agonist effects. This has been shown to be the case for the muscarinic and adenosine receptors (Christopoulos, 2002; Christopoulos and Kenakin, 2002; May, Avlani, *et al.*, 2007; Christopoulos *et al.*, 2014).

Extracellular loops are involved in the recruitment, binding, and retention of ligands. In the glutamate family of GPCRs and some peptide binding GPCRs, the N termini and extracellular loops can be large, and are the main binding site for endogenous ligands (Erlandson, McMahon and Kruse, 2018). In other receptors, such as GPR52, the second extracellular loop is proposed to be the activating molecule, folding into the ligand binding pocket and inducing the conformational change that results in receptor activation (Sutkeviciute and

Vilardaga, 2020). In most other GPCRs, the extracellular loops are short, and are able to fold over the ligand binding region, either occluding the region entirely, as in the case of many lipid binding receptors such as the cannabinoid receptors (Erlandson, McMahon and Kruse, 2018), reducing binding affinity by occluding the region temporarily, or reducing the off rate of a ligand, by folding over after ligand binding and G protein activation, creating a lid to retain the ligand (DeVree *et al.*, 2016; Weis and Kobilka, 2018; Bock and Bermudez, 2021). The residues of the extracellular loop often interact with the ligand, stabilising the docking and participating in conformational changes (Sutkeviciute and Vilardaga, 2020; Bock and Bermudez, 2021).

At the base of the helical bundle are the 3 intracellular loops (ICLs), and these have variable lengths and sequences. Many GPCRs are able to have their intracellular loops phosphorylated, and this is thought to improve arrestin binding stability (Oakley *et al.*, 2001; Verweij *et al.*, 2020). In the inactive structure, ICLs occlude the effector binding pocket, however, upon agonist binding and receptor activation (see section 1.2), ICL2 is able to bind the highly conserved DRY motif in a different way, stabilising a helical rather than looped conformation, binding G proteins rather than occluding the pocket (Weis and Kobilka, 2018). Due to their flexibility, structures and functions of these loops are poorly understood, however it is known that removal of ICL3 (such as in the fusion of fluorophores) has effects on the conformational equilibrium of the receptor as a whole, forcing TM helices into specific conformations that may not normally be favoured by ligand binding (Weis and Kobilka, 2018).

Finally, GPCRs have varied C-terminal tail lengths, with some, such as the gonadotropin releasing hormone receptor, having essentially none, and others, such as the adrenoceptor family, can be around between 10 and 150 residues long. For most GPCRs, the main role of the C-tail is the recruitment of arrestin. Arrestins are recruited following phosphorylation of serine and threonine residues along the length of the C-terminal tail, by a variety of cellular kinases, but generally by G protein coupled receptor kinases. This region of GPCRs will be explored in more detail in section 4.1.2.

#### *1.1.2.1 Conformational changes upon receptor activation*

Accumulated evidence from the recent structural studies has revealed that GPCRs have a generally conserved process of activation. The contraction of the ligand binding pocket following agonist binding, leads to conformational change at the base of the pocket containing three generally conserved residues on helix 3, 5 and 6, which, when labelled with Ballesteros-Weinstein nomenclature (Ballesteros and Weinstein, 1995), are $I^{3.40}$, $P^{5.50}$, and $F^{6.44}$. This causes a further conformational change in a tryptophan residue, $W^{6.48}$,

causing helix 6 to kink, albeit to a different extent in different receptors, and the intracellular half of this helix to move away from the centre of the bundle. This opens the intracellular side of the helix bundle, allowing for the binding of the effectors into this cleft, including G proteins or arrestins, as discussed in section 1.1.3 and 1.1.5, respectively. Other conformational rearrangements, such as those occurring in the NPXXY and DRY motifs, enhance and stabilise G protein binding (Barak *et al.*, 1994, 1995; Oakley *et al.*, 2001; Marion *et al.*, 2006; Weis and Kobilka, 2018). These series of conformational rearrangements means changes can transduce across non-overlapping regions, such as the orthosteric site and the intracellular binding pocket, and these changes are caused by allosteric coupling, or the movement of one area of the protein forcing change in others by repulsion between side chains of the residues involved (Erlandson, McMahon and

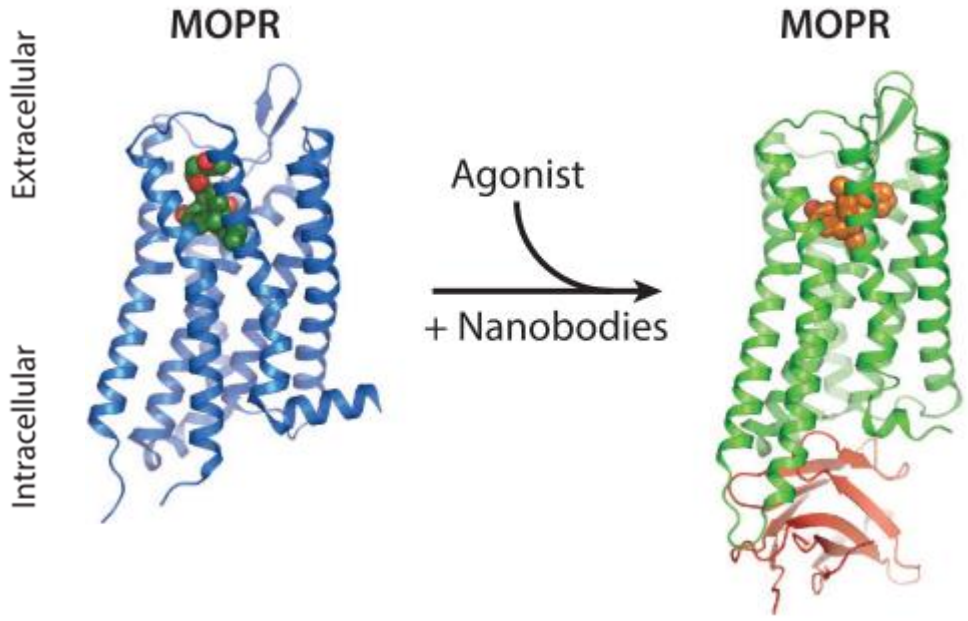


*Figure 1.1.2.1, Structure of opioid receptors. MOPR = μ-opioid receptor. Inactive structure in blue, active, ligand and nanobody bound structure in green. Taken from Corder, et al, 2018.*

Kruse, 2018; Weis and Kobilka, 2018; Bock and Bermudez, 2021). These changes have been shown to propagate in the reverse direction also, receiving allosteric changes from G protein binding that increase the binding affinity of the ligand through similar conformational changes (see figure 1.1.2.1) (DeVree *et al.*, 2016; Bock and Bermudez, 2021).G Proteins

Classical GPCR signalling occurs via guanine nucleotide binding proteins (G proteins), effectors that lend their name to the receptor family. G proteins form a heterotrimeric complex made up of α, β, and γ subunits, with the β and γ subunits existing as a constitutive dimer. Formation of an α-helix at the intracellular loops of the receptor has been shown to be one of the main methods of formation of the G protein-receptor complex, the other being the opening of the intracellular binding site upon activation by an agonist. The N-

terminal α-helix of the Gα subunit is able to insert itself into this binding site and given the variability of this helix between Gα subunit isoforms, this process is thought to be the main determinant of GPCR-G protein coupling specificity (Liu *et al.*, 1998; Flock *et al.*, 2017). The formation of the α-helix on the intracellular loop allows this region to embed in a hydrophobic pocket on the Gα surface. Gα also interacts with TM3, 5 and 6 upon insertion into the receptor core, however this is determined to be after activation of the Gα subunit. The shifts in conformation induced by the reciprocal binding of the helices frees GDP, which is quickly replaced by GTP, and this change induces conformational changes not yet studied, resulting in the disassociation between Gα, Gβγ, and the receptor (Calebiro *et al.*, 2021). The split and activated subunits (Gα-GTP and Gβγ) are released from the intracellular binding pocket of the receptor, allowing another G protein complex to bind, allowing for amplification of the signal transduced (Calebiro *et al.*, 2021). While activated, the G protein subunits can bind and activate downstream effectors, dependant on their isoform. The slow but inherent GTP-ase activity of the Gα subunit results in the conversion of GTP to GDP, and Gα signalling is halted, rebinding the Gβγ in a concentration dependent manner (Ross, 2008). This GTP-ase activity can be increased by regulators of G protein signalling (RGS), therefore attenuating Gα signalling and, indirectly, Gβγ (Berman, Kozasa and Gilman, 1996).

Gα subunits are membrane tethered via palmitoylation of their N-terminus. There are four families of Gα subunit, sorted depending on their first-described downstream effectors, and while different receptors generally have a strong preference for a single subclass, they can usually activate different types with varying affinities. Gαs acts a stimulator for adenylyl cyclase (AC), and as such increases local cyclic adenosine monophosphate (cAMP) concentration. Gαi and Gαo inhibit AC, reducing cAMP concentration. Gαq activates the enzyme phospholipase Cβ, promoting the inositol trisphosphate and diacylglycerol signalling pathways, affecting intracellular calcium ion concentrations. Gα12/13 activate Rho signalling and stimulate changes in the cytoskeleton of the cell. All Gα subunits have GTPase activity (albeit different rates of hydrolysis), resulting in the conversion of the bound GTP to GDP, and as such inactivation and rebinding to Gβγ (Wettschureck and Offermanns, 2005).

The Gβγ complex is also membrane bound, via the isoprenylated C-terminus of the Gγ subunit. There are 5 subtypes of Gβ subunits and 12 subtypes of Gγ subunits (Downes and Gautam, 1999). The signalling potential of the Gβγ subunit is much wider and still under investigation, with 60 different combinations of the two subunits possible. It is known to also activate phospholipase C and affect some ion channels, such as G protein-coupled inwardly rectifying potassium (GIRKs) channels (Atwood *et al.*, 2011), as well as binding RGS proteins, intracellular kinases, tubulin and calcium channels

(Smrcka, 2008). Importantly, Gβγ has been known to assist in the recruitment of G protein receptor kinases (GRKs) (Smrcka, 2008; Khan *et al.*, 2013; Hanlon and Andrew, 2015).

Lipid-binding modifications, such as palmitoylation and isoprenylation, retain both the Gα and Gβγ subunits at the membrane (Goddard and Watts, 2012).

### 1.1.3 G Protein-Coupled Receptor Kinases

G Protein-Coupled Receptor Kinases (GRKs) are a family of 6 kinases, GRK1-6, with GRK1 expression limited to retinal cells, and GRK4 to the testes. The rest are ubiquitously expressed in mammalian tissues (Premont *et al.*, 1996; Pitcher, Freedman and Lefkowitz, 1998). They are highly conserved proteins, with homologous variants also expressed in many model organisms such as *Drosophila* and *C. elegans* (Pitcher, Freedman and Lefkowitz, 1998). Canonically, GRKs phosphorylate serine and threonine residues at the intracellular motifs of the GPCR, which includes the C-terminal tail that extends into the cytosol, as well as the ICLs. GRKs work alongside other kinases to phosphorylate GPCRs, an important step in the modulation of GPCR signalling.

GRKs can be subdivided into families, based on their mechanism of membrane targeting. The GRK2/3 family resides in the cytosol, and have pleckstrin homology (PH) domains, able to bind Gβγ subunits that are themselves restricted to the membrane by prenylation (Pitcher, Freedman and Lefkowitz, 1998), discussed in section 4.1.1. GRK2 has also been crystallised in complex with Gαq, similarly recruiting the GRK to the membrane. Direct binding of the Gβγ complex to GRK2 has been suggested to inhibit the signalling function of the Gβγ subunit (Raveh *et al.*, 2010). GRK3 has been shown to be more likely to localise to the membrane than GRK2 in neuronal cells, but not in HEK cells (Gurevich *et al.*, 2012).

The GRK4/5/6 family have lipid binding domains; for GRK4 and 6 this is a palmitoylation site, for GRK5 this is a bundle of positively charged residues. With these domains, members of this family become tethered to the plasma membrane. However, GRK5 and 6 have also been detected in the nucleus, indicating a potential role as regulators of transcription (Gurevich *et al.*, 2012). The GRK1/7 family have short prenylation sequences targeting them to the plasma membrane. GRK1 and GRK7 expression is limited to rod and cone cells, and are the main phosphorylation partners for Rhodopsin and opsin, the GPCRs involved in vision (Gurevich *et al.*, 2012).

Each GRK is formed of a kinase domain, made up of a small and large lobe, and a regulator of G protein signalling homology domain (RH), made up of a terminal and bundle lobe. When inactive, these domains form an open structure, and in transitioning to a closed state, the bundle lobe rotates 8°, and the large lobe rotates 11.5°, closing the cleft between the two domains.

Upon these rotations, disordered regions become more ordered, with the formation of multiple α-helices. The first, the C-terminal tail of the GRK, forms the helix and binds the two domains together, stabilising the closed conformation. The kinase domain C-tail forms a helix as it passes over the top of the GRK, and thus shifts the active site tether into a position ready to aid in phosphorylation of a target. Finally, the N-terminal tail forms a helix, which is able to embed in the intracellular receptor core, between ICLs 2 and 3. This loop is shorter than that of the Gα subunit, however, is known to stabilise the GRK-receptor complex. At the tip of the RH domain, near the end of the N-terminal helix is a flat area of PIP2 binding residues, further stabilising the receptor bound complex. These positions allow for both the C-terminus of the receptor, as well as a sufficiently long ICL3 to lay between the lobes and become phosphorylated by the active site of the kinase domain (Boguth *et al.*, 2010; Gurevich *et al.*, 2012).

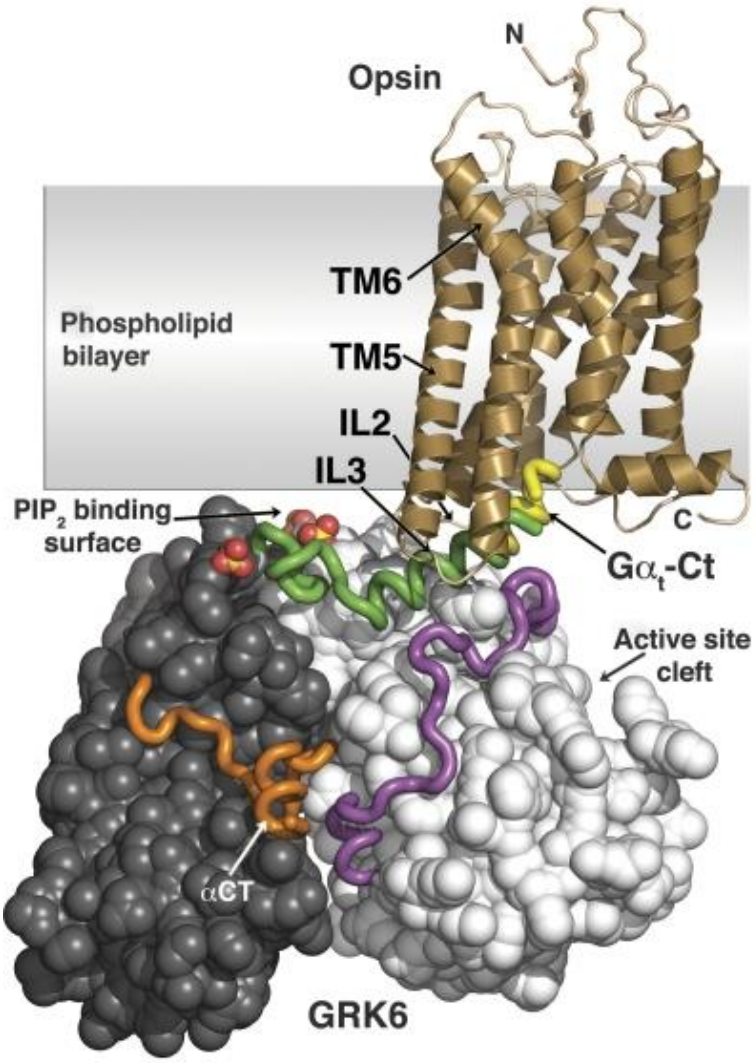


*Figure 1.1.4, figure depicting a model of the representative GPCR, opsin, bound to the representative GRK, GRK6, in the active state, with labelled GPCR secondary structure and GRK features (PDB entry 3DQB), with the kinase domain shown in white, and the RH domain shown in grey. The N-terminal helix is shown in green, superimposed over a G-protein α subunit C-tail to highlight differences in penetration into the GPCR intracellular cleft. The C-terminal tail of the RH domain is shown in orange, and the C-terminal tail of the kinase domain is shown in purple, with the atoms comprising the $PIP_2$ binding domain highlighted in red/yellow. Taken from Boguth, et al, 2010.*

The order of, and requirements for, GRK recruitment to the receptor, are still to be determined. Put forward by Pitcher, Freedman and Lefkowitz, in 1998,

the classical model suggests that GRKs are recruited before β-arrestin2. Evidence provided by kinetic experiments (Miess *et al.*, 2018) remain in keeping with this model. Traditionally, it is thought G proteins play a role in GRK recruitment, especially the Gβγ subunit. The binding of GRKs to the Gβγ subunit vastly increases their plasma membrane concentration, due to the prenylation of the Gγ subunit and its anchoring in the membrane. This brings GRK and GPCR in close proximity and greatly increases phosphorylation and desensitisation rates of activated receptors (Pitcher, Freedman and Lefkowitz, 1998; Li *et al.*, 2003). With the discovery of the membrane localisation mechanism for each GPCR, it is assumed that the conversion of the 'search' area for GRKs looking for active GPCRs from 3D to 2D increases the speed by which active GPCRs are found by a large magnitude, thus leading to apparent recruitment.

In addition to GPCRs, GRKs have been shown to interact with and phosphorylate many other proteins, some are similar to GPCRs, and are embedded in the membrane, such as toll-like receptors and single transmembrane domain tyrosine or serine/threonine kinases, although others include transcription factors. GRK5 and 6 are known to localise in the nucleus, and have been indicated to have a role in the cell life cycle, cancer, and immunity (Gurevich *et al.*, 2012). These roles appear to not require prior activation by GPCRs, indicating either low basal kinase activity of GRKs, or some alternative activation mechanism.

GRKs are also known to scaffold other proteins in a phosphorylation-independent manner. As discussed above, GRK2 and 3 can bind and sequester Gαq and promote the breakdown of GTP bound to Gαq, inhibiting its signalling potential. Other interactions are directly involved in the regulation of themselves or GPCRs, however others involve major signalling pathways, and the list appears to be growing (Ribas *et al.*, 2007; Penela *et al.*, 2010; Gurevich *et al.*, 2012).

### 1.1.4 Arrestins

The other signalling pathway of relevance to GPCRs is that of arrestins. There are 4 isoforms of arrestin (table 1.1.5), two of which are classed as visual, referring to their almost exclusive binding to opsin GPCRs (Smith and Rajagopal, 2016), and two are non-visual, the so called β-arrestins (Lohse and Hoffmann, 2014).

| **Arrestin #** | **Visual/Non-Visual** | **Alternative Name** |
|---|---|---|
| Arrestin-1 | Visual (Rhodopsin) | α-Arrestin-1 |
| Arrestin-2 | Non-Visual | β-arrestin1 |
| Arrestin-3 | Non-Visual | β-arrestin2 |
| Arrestin-4 | Visual (Colour Opsins) | α-Arrestin-2 |

*Table 1.1.5, Nomenclature of the different isoforms of Arrestin, and their general function.*

β-Arrestins are known to bind and become activated by the C-terminal tail of GPCRs. Following prolonged stimulation of the GPCRS, GRKs along with second messenger activated kinases are recruited and phosphorylate certain residues on the intracellular side of the receptor. This creates a high affinity binding site for the β-arrestin, which translocates from the cytosol to the membrane. Binding of arrestin occludes the G protein binding site, and thus, G protein-dependent signalling is uncoupled. At the same time, β-arrestin can scaffold the formation of an endocytic complex, interacting with proteins such as AP2 and clathrin, recruiting these proteins to the plasma membrane, and causing internalisation of the receptor. From here, the receptor can be either recycled back to the cell surface (resensitisation) or degraded (downregulation). Arrestins, as the name suggests, arrest, or stop, GPCR signalling, generally by sterically blocking access to the receptor by G proteins, and by promoting the internalisation of the receptors, moving them away from the cell surface and blocking access by the membrane-impermeable ligand.

Family A GPCRs have been further separated by subclass depending on their preferential binding to one form of arrestin, a major regulatory molecule, named for its ability to arrest GPCR signalling. Class A receptors preferentially bind arrestin-2, herein referred to as β-arrestin1. Class B receptors bind both β-arrestin1 and β-arrestin2.

#### *1.1.4.1 Structure and activation*

The four arrestin isoforms are similar in shape, essentially two crescent shaped domains each formed of 2 layers of β-sheets, referred to as the N and C terminal domains (Figure 1.1.5.1.1). The side-by-side orientation of these domains results in the central crest, composed of the finger loop, an important loop known to undergo significant conformational change upon activation of arrestin and to interact with GPCRs, as well as the middle loop and the C loop (Chen *et al.*, 2017; Scheerer and Sommer, 2017). Another important region is the polar core, a network of highly charged residues that stabilises the connection of the N- and C-domains. In the inactive state, the C-terminal tail of arrestin lays across the N-domain. Within the N-domain the C-tail displays hydrophobic interactions known to be sensitive to the 'three element domain', a region thought to be important for maintaining the inactive state of arrestin (Scheerer and Sommer, 2017). This tail also contributes a residue towards the formation of the polar core. Given its connection to other sites of the molecule, the disruption of the interactions of the C-tail is highly effective in changing the overall conformation of arrestin upon activation.

The theory that arrestins undergo large conformational change upon activation was first hypothesised by (Schleicher, Kühn and Hofmann, 1989), due to the large activation energy required for such a high affinity bond

between arrestin and receptor. This has been proven, and the main measure of activation since has been the large 20° rotation of the N- and C-domains relative to one another.

The displacement of the arrestin C-tail by that of the GPCR (C-tail exchange) and the disruption of the polar core are thought to be the main sources of this rotation. These two areas were described as sensors, the C-terminal binding named the phosphate sensor, and the central crest as the activation sensor.

The binding of a GPCR C-terminal tail to arrestin, displaces its own C-terminal tail, due to the phosphorylated residues of the GPCR repelling the acidic tail of the arrestin. This, in turn, triggers a multitude of more localised conformational effects. The residue contributed by the arrestin C-terminal is removed from the polar core, causing limited destabilisation. This causes repulsion of the gate loop, a region surrounding the polar core linked to the C-domain of the molecule. The gate loop translates towards the N-domain, and opens a positively charged crevice, in which the phosphorylated receptor tail then binds. This is supported by numerous lysine and arginine residues littered across the surface of the N-domain of arrestin, and their interaction with the phosphorylated sites of the receptor C-tail (Scheerer and Sommer, 2017; Chen, Iverson and Gurevich, 2018).

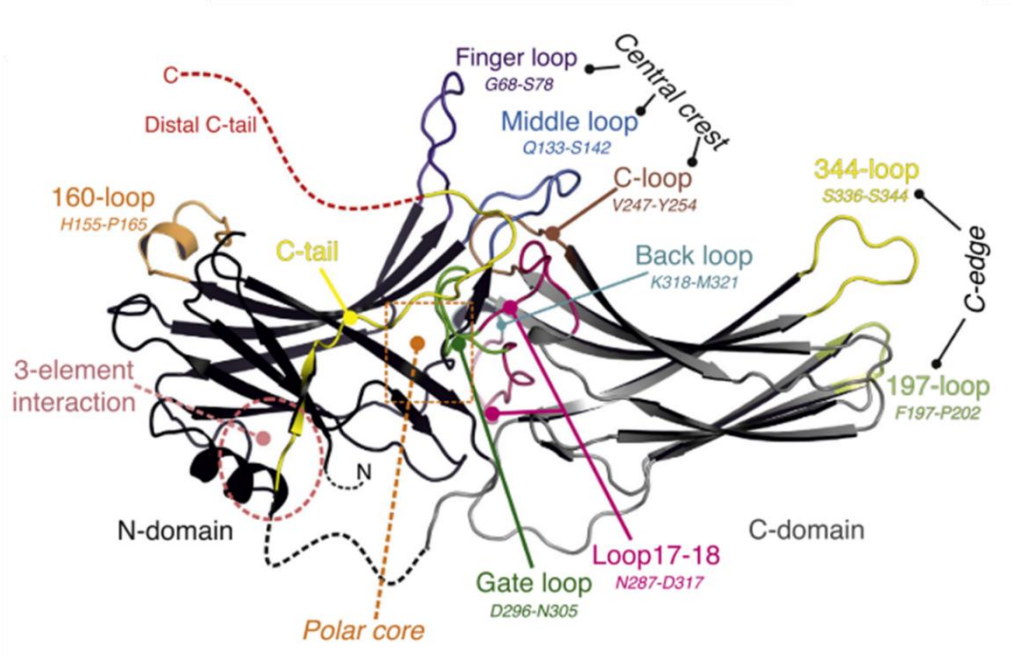


*Figure 1.1.5.1.1, General structure of Arrestins, with labelled motifs and features. Residue numbers are given for some motifs and relate to their position in the Arrestin-1 structure. Taken from Scheerer and Sommer, 2017.*

Classically, it was thought that this C-tail binding was a prelude, or an activating step, to allow the binding of the activation sensor, or the central crest, to the core of the activated receptor (Scheerer and Sommer, 2017; Chen, Iverson and Gurevich, 2018). Evidence from in silico and in vitro

structural studies (Kim *et al.*, 2013; Scheerer and Sommer, 2017; Latorraca *et al.*, 2018, 2020) show that, following C-tail binding, either weakened intramolecular forces at the base of this loop, or the introduction of a stabilising residue, guides the formation of a helical-like structure in the loosened loop, appearing similar to the C-terminal of a Gα subunit. This will then bind in the same GPCR pocket as the Gα subunit, stabilising the receptor arrestin conformation and blocking any further G protein activation. Breakdown of the polar core by the removal of the gate loop also causes many of the other loops of the central crest to break their intramolecular bonds and form binding clefts, into which the ICLs of the receptor can insert. The breaking of intramolecular bonds, as well as the displacement of the C tail, causes the 20 ° rotation of the C-domain, and arrestin is thought to be active at this point.

This classical model, however, has undergone a series of revisions, with a multitude of publications giving evidence that while the interactions between the receptor core and C-tail with the different arrestin domains are related, and improve the stability of one another, they are by no means essential for the other's function. This was suggested initially by Chen, Iverson and Gurevich, 2018, due to the numerous observations of binding of arrestins to active, unphosphorylated receptors.

In many studies using both biochemical and imaging assays, the idea of a stable interaction between β-arrestin and the C-terminal tail of the receptor has been shown. In Shukla *et al.*, 2014, electron microscopy shows β-arrestin1 bound in a stable manner to the C-terminal tail of a β2 adrenoceptor/Vasopressin 2 receptor chimera, and is described as "partially engaged". However, truncation of the chimera C-tail did not abolish β-arrestin activation, regardless of the length of truncation. This provided further evidence that the engagement of the core of the receptor is possible without the binding of the receptor C-tail (Eichel *et al.*, 2018a).

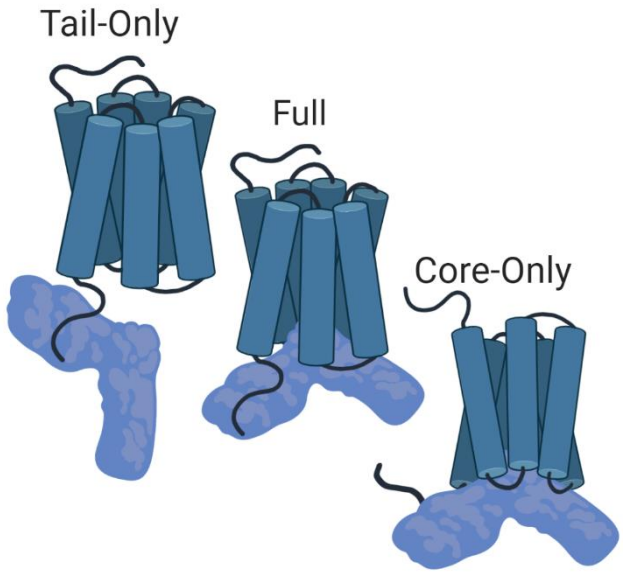


*Figure 1.1.5.1.2, Illustration of the different proposed conformations of arrestin binding to GPCRs.*

The hypothesis of two distinct modes of arrestin engagement by the GPCR was consolidated by Latorraca *et al.*, 2018, in which *in silico* molecular dynamics simulations showed that both the cytoplasmic tail of the receptor and the TM core can independently induce arrestin activation, which was determined by the relative rotation of the C- and N-domains with a threshold for activation of 18 ° (Latorraca *et al.*, 2018). Removal of the arrestin C-tail from the N-domain was shown to increase the conformational mobility of arrestin, however it remained mostly inactive. With only the receptor C-tail present, a twist angle of approximately 15.6 ° was observed, and with only the receptor core, a twist angle of 17 ° was observed, both with similar variability. When both core and C-tail were bound, a 20 ° rotation was observed, with slightly reduced variability. Transitions to the active state were observed when force was applied to arrestin loops that contacted the receptor tail or ICLs. The back loop of arrestin is known to interact with ICL3, the C-loop with ICL2, and the finger loop, which interacts with the receptor binding pocket. This latter interaction was observed to be the main mediator for the helicalisation of the finger loop, which remained unstructured regardless of activation state of the arrestin. Similarly, forcing the helicalisation of this region had no effect on the interdomain twisting. The receptor core was observed to have an immediate activating effect on the arrestin twist angle, so it is likely the disruption of the polar core by the ICLs that transduce the greatest effect. This is supported by increased arrestin binding and activation when ICL3 is phosphorylated or contains more acidic residues.

Finally, activation of arrestin by a phosphorylated tail also causes conformational shifts on the C-edge (Figure 1.1.5.1.1), a series of loops on the side of the C-domain furthest from the central crest. This causes rotation of the loop and allows for the shallow embedding of loops into the membrane, providing another source of complex stability (Scheerer and Sommer, 2017).

Despite all the wealth of information regarding the conformational changes of arrestin upon receptor activation, it is important to note that most of the

studies described above used model receptors such as rhodopsin, or highly modified GPCR C-tails with high affinities for arrestin such as the β2-adrenoceptor-vasopressin 2 receptor chimera. The conformational changes triggered by the activation of other GPCRs have started to be investigated using arrestin conformational biosensors (Lee *et al.*, 2016; Nuber *et al.*, 2016).

Given the kinetics of arrestin recruitment compared to G proteins and GRKs, it is likely that, unlike GRKs, arrestin is not first recruited to the membrane, and instead conducts a 3D 'search' for active receptors from the cytoplasm. However, this idea is challenged in a recent report, where arrestins are shown to exhibit short-lived interactions with the membrane and are able to diffuse across the membrane in a 2D movement (Grimes *et al.*, 2023). Altogether, this indicates arrestin is able to use both 3D and 2D searches, and it is likely the latter component can be modulated by altering membrane lipid content (Qiu *et al.*, 2011).

#### *1.1.4.2 Arrestin-interacting proteins*

Traditionally, β-arrestins were seen as molecules with a sole purpose of desensitising GPCRs and acting as a scaffold for clathrin-coated pit formation. This idea changed when yeast two hybrid and co-immunoprecipitation studies identified a huge variety of arrestin interacting partners, with one study identifying 337 different binding partners to activated arrestin (Xiao *et al.*, 2007). Table 1.1.5.2 summarises a selection of well-studied pathways affected in some way by β-arrestin2 (arrestin-3) binding, and their overlap with other arrestin isoforms.

| Effector | Arrestin | Reported Function | References |
|---|---|---|---|
| Clathrin heavy chain | 2, 3 | Clathrin dependent GPCR endocytosis | (Goodman *et al.*, 1996; Krupnick *et al.*, 1997; Laporte *et al.*, 1999, 2000) |
| β-Adaptin2 subunit of AP-2 | | | |
| Tubulin; microtubules | 1, 2, 3, 4 | Sequestration of arrestin, attenuation of MAPK activity, enhanced ubiquitination of cytoskeletal proteins | (Hanson *et al.*, 2006, 2007) |
| $Ca^{2+}$-calmodulin | 1, 2, 3, 4 | Cytosolic sequestration of Ca2+-calmodulin | (Wu *et al.*, 2006) |
| Inositol hexakisphosphate | 1, 2, 3, 4 | Arrestin oligomerization, receptor endocytosis, arrestin nuclear translocation | (Palczewski *et al.*, 1991; Gaidarov *et al.*, 1999; |

| | | | |
|---|---|---|---|
| | | | Milano *et al.*, 2006; Hanson *et al.*, 2008) |
| Src family tyrosine kinases<br>c-Src; c-Yes; c-Hck; c-Fgr;<br>c-Fyn | 1, 2, 3 | ERK1/2 activation, dynamin 1 phosphorylation, exocytosis/granule release, phosphorylation/destabilization of GRK2, FAK phosphorylation, EGF receptor transactivation, phosphorylation of β-Adaptin2 subunit of AP-2 | (Luttrell *et al.*, 1999; Barlic *et al.*, 2000; DeFea, Vaughn, *et al.*, 2000; Miller *et al.*, 2000; Imamura *et al.*, 2001; Penela *et al.*, 2001; Fessart *et al.*, 2007; Noma *et al.*, 2007; Galet and Ascoli, 2008; Zimmerman *et al.*, 2009) |
| c-Raf1-MEK1/2-ERK1/2 | 2, 3 | Activation of cytosolic ERK1/2, receptor internalization and trafficking, p90RSK phosphorylation, actin cytoskeletal reorganization/chemotaxis, ERK1/2-dependent transcription, Mnk1/eIF4E phosphorylation/protein translation | (Lin *et al.*, 1999; DeFea, Zalevsky, *et al.*, 2000; Luttrell *et al.*, 2001; Seta *et al.*, 2002; Ge *et al.*, 2003; Gesty-Palmer *et al.*, 2005; DeWire *et al.*, 2008; Khoury *et al.*, 2014) |
| ASK1-MKK4-JNK3 | 3 | Activation of cytosolic JNK3, sequestration of JNK outside the nucleus | (McDonald, 2000; Song *et al.*, 2006; Breitman *et al.*, 2012) |

| | | | |
|---|---|---|---|
| ASK1-MKK3/7-p38 MAPK | 2, 3 | Scaffolding/Activation of p38 MAPK, inhibition of p38 MAPK | (Sun *et al.*, 2002; Zhao *et al.*, 2004; Yang *et al.*, 2012) |
| IκBα–IκB kinase α/β | 2, 3 | Attenuation of NFκB signalling | (Gao *et al.*, 2004; Witherow *et al.*, 2004) |
| Casein kinase II | 3 | Activation of CK2 | (Kendall *et al.*, 2011) |
| cAMP phosphodiesterases PDE4D3; PDE4D5 | 2, 3 | Attenuation of cAMP signalling | (Perry, 2002; Baillie *et al.*, 2007) |
| Diacylglycerol kinases | 2, 3 | Attenuation of PKC signalling | (Nelson *et al.*, 2007) |
| PI 4-phosphate 5-kinase Iα | 2, 3 | Control of clathrin-dependent GPCR internalisation | (Nelson *et al.*, 2008) |
| Phosphatidylinositol 3-kinase PTEN | 2, 3 | Localized inhibition of PI3K, inhibition of Akt signalling and cell proliferation, increased cell migration | (Wang and DeFea, 2006; Lima-Fernandes *et al.*, 2011) |
| PP2A-Akt-GSK3β | 3 | Inactivation of Akt/GSK3β, activation of β-catenin signalling, activation of Akt | (Beaulieu *et al.*, 2005, 2008; Kendall *et al.*, 2011) |
| Nitric oxide synthases | 2, 3 | Suppression of stress-induced iNOS transcription, post-translational activation of iNOS, eNOS-dependent S-nitrosylation of β-arrestin2 | (Ozawa *et al.*, 2008; Kuhr *et al.*, 2010) |
| Cofilin; chronophin; LIM kinase | 3 | Actin cytoskeletal reorganization/chemotaxis | (Zoudilova *et al.*, 2007, 2010) |
| Filamin A | 2, 3 | Membrane ruffling | (Scott *et al.*, 2006) |
| SHP-1; SHP-2 | 3 | Inhibition of NK cell cytotoxicity | (Yu *et al.*, 2008) |

| | | | |
|---|---|---|---|
| E3 ubiquitin ligases Mdm2; parkin; Nedd4; AIP4; TRAF6 | 1, 2, 3 | Ubiquitination of β-arrestin2, stabilization of GPCR–arrestin complex, increased p53-mediated apoptosis, inhibition of Toll-like receptor signalling, stabilization of GPCR–arrestin–ERK1/2 signalosome, GPCR ubiquitination and downregulation | (Shenoy, 2001; Shenoy and Lefkowitz, 2003; Wang *et al.*, 2003, 2006; Bhandari *et al.*, 2007; Shenoy *et al.*, 2007, 2008) |
| Ubiquitin-specific protease 33 | 3 | Deubiquitylation of β-arrestin2, control of GPCR internalization | (Shenoy *et al.*, 2009) |
| Ral-GDS | 2, 3 | Cytoskeletal reorganization/granule exocytosis | (Bhattacharya *et al.*, 2002) |
| ARF6-ARNO | 2, 3 | GPCR endocytosis | (Claing *et al.*, 2001; Houndolo, Boulay and Claing, 2005) |
| Kif3A kinesin motor protein | 2, 3 | Targeting and internalization of Smoothened | (Kovacs *et al.*, 2008) |

*Table 1.1.5.2, the non-receptor β-arrestin2 interactome, annotated with arrestins involved, and function of interaction. Adapted from (Peterson and Luttrell, 2017).*

### 1.1.5 GPCR Internalisation

Following stable arrestin binding, GPCRs are further desensitised by internalisation. This process involves effectors such as the adaptor protein 2 (AP2) binding to effector binding surfaces of arrestin such as the C-tail, however recent study has revealed a further binding site at the C-lobe base (CLB) for an alternative mechanism of endocytosis.

Clathrin and AP2 mediated endocytosis relies on the interactions between arrestins and either the AP2 adaptor protein, which itself can also bind clathrin, or direct binding to the heavy chain. Arrestins, and subsequently the active receptor bound to arrestin, favourably interact with phosphatidylinositol-4,5-bisphosphate ($PIP_2$) rich membranes, and follows the concentration gradient of PIP2 towards clathrin coated pits (Janetzko *et al.*, 2022), where the arrestin can be held in place through binding AP2 or clathrin heavy chain (Sorkin and von Zastrow, 2002, 2009).

The mechanism of CLB mediated endocytosis has yet to be elucidated, however it has been shown that this region does not directly bind clathrin or

AP2. Class A receptors preferentially utilise CLB-mediated endocytosis, whereas Class B receptors are more balanced, and use both C-tail- and CLB-mediated endocytosis (Barsi-Rhyne, Manglik and von Zastrow, 2022).

Following the formation of a clathrin coated vesicle and the budding of the pit, clustered receptors are delivered to early endosomes. From here, two routes become available; the recycling of receptors back to the membrane, or further trafficking into the cell. Recycling of receptors from this compartment has been shown to have a half-life of around 10 mins and can involve endosome-associated phosphatases that strip phosphorylation from the GPCR C-tail, decreasing the affinity of arrestin and re-sensitising the receptor. Further trafficking of the receptor will lead to sequestration of receptors into multi-vesicular bodies, either on the surface of these bodies, or further sequestered by invagination of the membrane of these bodies for form lumen. From here, slower recycling may occur, returning to the membrane with a half-life of around 2 hours. The availability of surface receptors during these refractory periods are likely to be most important in neurons, where the inhibition or promotion of transmitted signals is tightly controlled by GPCRs and their ligands, most notably at the synapse.

The sorting of receptors is promoted by posttranslational modifications of the receptor-arrestin complex. De-phosphorylation of the receptor promotes recycling, either rapidly such as in the case of the β2-adrenoceptor, or more slowly, as is the case with the vasopressin receptor. Maintained phosphorylation of the receptor, as well as ubiquitination of the complex, promotes degradation by lysosomes (Sorkin and von Zastrow, 2002, 2009; Khoury *et al.*, 2014; Lay *et al.*, 2016).

## 1.2 Opioid Receptors: Structure to Physiology

Opioid receptors form a subset of family A GPCRs that bind endogenous opioids, a superfamily of peptides that derive from the proteolytic cleavage of larger protein precursors, shown in table 1.2.2.1 below (Corder *et al.*, 2018). Opioid receptors were originally divided into 3 subtypes, μ, κ, and δ, named for the drugs used to identify them and their localization (Brownstein, 1993). A later study identified the nociceptin opioid receptor, and its endogenous ligand, with high sequence homology with the other 'classical' opioid receptors (Toll *et al.*, 2016). While all four activate inhibitory G proteins such as $G\alpha_i$, subtle differences in expression and signalling are likely linked to observed differences in behavioural outcomes of selective ligands, with anti-nociception, antidepressant and anti-anxiolytic, and stress response being linked to the MOR, δOR, and κOR respectively (Al-Hasani and Bruchas, 2011a).

The structures of the inactive (antagonist-bound) states of all four opioid receptors have been determined (figure 1.2). Additionally, the structures of multiple active states of the MOR have been solved, with a variety of binding partners, such as nanobodies and agonists (Manglik *et al.*, 2016; Corder *et al.*, 2018; Wang *et al.*, 2023). The latest, and most complete of these structures (active MOR with G protein and agonist DAMGO) was obtained using cryo-electron microscopy and has shown the binding positions of Gαi and nanobodies to the MOR (Thomsen *et al.*, 2016).

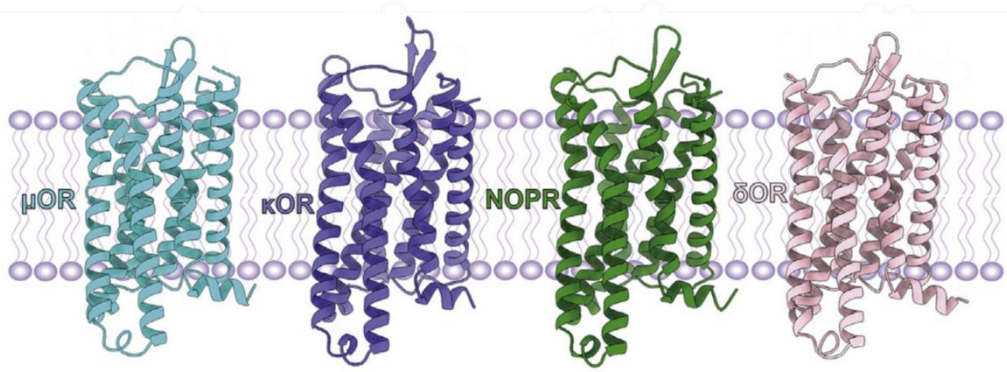


*Figure 1.2, structures of all four opioid receptors (μOR = μ-opioid receptor (cyan), κOR = κ-opioid receptor (purple), NOPR = Nociceptin receptor (green), δOR = δ-opioid receptor (pink)). Taken from Wang, et al, 2023.*

### 1.2.1 Mu-Opioid Receptor Physiology

The MOR system has a variety of tissue specific effects, broadly split between the central nervous system (CNS) and the periphery (table 1.2.1). Generally, MOR agonists inhibit functions in the CNS such as respiration and nociception, as well as inhibition of the gastrointestinal, urinary, cardiovascular, and immune systems, while increasing euphoria (Al-Hasani and Bruchas, 2011b).

*Table 1.2.1, Physiological effects of morphine and other clinically used opioids, split by tissue. Adapted from Al-Hasani and Bruchas, 2011. (Al-Hasani and Bruchas, 2011b). (+) indicates potentiation while (-) indicates reduction*

| | **Organ system** | **Effects** | **Change direction** |
|---|---|---|---|
| Central Nervous System | CNS | Analgesia | + |
| | | Euphoria | + |
| | | Sedation | + |
| | | Rate of Respiration | - |
| | | Cough Reflex | - |
| | | Miosis (constriction of the pupils) | + |
| | | Truncal Rigidity | + |
| | | Nausea and Vomiting | + |
| Periphery | Gastrointestinal System | Constipation | + |
| | | Gastric Motility | - |
| | | Digestion in Small Intestine | - |
| | | Peristalsis of the Colon | - |
| | | Constriction of Biliary Smooth Muscle | + |
| | | Oesophageal Reflex | + |
| | Other Smooth Muscle | Depression of Renal Function | + |
| | | Uterine tone | - |
| | | Urinary retention | + |
| | Skin | Itching and Sweating | + |
| | | Flushing of the face, neck, and thorax | + |
| | Cardiovascular system | Blood pressure and heart rate under stress | - |
| | Immune System | Formation of rosettes by human lymphocytes | - |
| | | Cytotoxic activity of natural killer cells | - |
| | Other | Behavioural Restlessness | + |

### 1.2.2 Mu-Opioid Ligands

The MOR has been exploited by humans for many thousands of years for its anti-nociceptive effect, when stimulated by endogenous (e.g. endorphins) and exogenous (e.g. morphine, heroin) ligands. The MOR is also responsible for the constipation, respiratory depression and addiction induced by these opioids.

The therapeutic interest in this receptor has led over the decades to improvements in specificity, and the creation of novel agonists and antagonists with widely varying pharmacological profiles. Attempts to remove side effects, such as addiction, tolerance, respiratory depression and

constipation, have progressed to some avail, however none have achieved the complete separation of antinociception from the more harmful effects (Groer *et al.*, 2007; Manglik *et al.*, 2016; Hill *et al.*, 2018; Kennedy *et al.*, 2018; Kliewer *et al.*, 2020).

Opioid receptors are the targets for endogenous peptides, referred to in three classes: endorphins, enkephalins, and dynorphins. These interact with varying affinities with all three opioid subtypes and are formed via the cleavage of precursor peptides (Pathan and Williams, 2012).

Unknowingly, the targets for these endogenous peptides were being utilised by civilised humans millennia ago, where the milk of the opium poppy, *Papaver somniferum*, generated pain relieving and euphoric effects. The alkaloids generating these effects were morphine and codeine, still commonly used today (Bryant and Knights, 2010).

Exogenous opioids have since expanded, and in the past few centuries new classes of opioids, semisynthetic, and synthetic, have expanded the repertoire of opioid drugs, and due to their varied pharmacology, are able to treat many different illnesses and ailments.

#### *1.2.2.1 Endogenous Ligands*

In 1975, it was shown that brain extracts inhibited acetylcholine release from nerves in the guinea pig ileum, an effect that was blocked with naloxone, a synthetic antagonist for the MOR. From these studies, endogenous peptide ligands and their precursor peptides were discovered for each of the opioid receptors (see table 1.2.2.1) (Kosterlitz and Waterfield, 1975; Brownstein, 1993; Pasternak and Pan, 2013).

It was later shown that altering the sequence of some of these peptides generated better stability and variable pharmacology and selectivity, the most important of which is DAMGO ([D-Ala$^2$,MePhe$^4$,Gly(ol)$^5$]enkephalin), a highly selective, and highly efficacious and potent MOR agonist, which functions as the main reference agonist in opioid work (Pasternak and Pan, 2013).

*Table 1.2.2.1, Human endogenous opioids by family, and their receptor specificity (Corder* et al.*, 2018).*

| **Peptide Family** | **Precursor Peptide** | **Peptide agonist** | **Receptor** |
|---|---|---|---|
| β-Endorphins | Proopiomelanocortin (POMC) | β-Endorphin | μ |
| Enkephalins | Preproenkephalin | Met-Enkephalin | δ, μ |
| | | Leu-Enkephalin | |
| Dynorphins | Prodynorphin | Dynorphin-A | κ |
| | | Dynorphin-B | |
| | | α-neoendorphin | |
| Nociceptins | Prepronociceptin | Nociceptin | Nociceptin |

#### 1.2.2.2 Naturally Derived Ligands

Many alkaloids can be isolated from the *P. somniferum* poppy which has been cultivated for at least 5000 years for these molecules. Morphine was the first alkaloid isolated nearly 200 years ago, and other opioids have been isolated from the opium mixture, namely codeine, papaverine and thebaine. Codeine must be converted to morphine in the body by cytochrome P450 2D6 to exert its opioid effects (Crews *et al.*, 2014). Morphine, the prototypical and partial agonist, transduces its effects mainly through the MOR, however has some degree of activity at the KOR and DOR (James and Williams, 2020).

#### 1.2.2.3 Semi-Synthetic Ligands

Small manipulations of the chemical structures of the alkaloids discussed above yield a more varied toolkit of opioids called semi-synthetic opioids. These include diamorphine, dihydromorphine, buprenorphine, tramadol, and oxycodone. Many of these ligands have off target effects, such as stimulation of opioid receptors other than the MOR, as well as roles affecting neurotransmitter reuptake and non-GPCR targets. Buprenorphine is a weak MOR partial agonist, and has a small analgesic effect, however, it also has moderate affinity for both the KOR and NOR, inhibiting analgesia at high doses. The metabolite of buprenorphine, norbuprenorphine, exhibits higher efficacy than its parent ligand (Brown *et al.*, 2011).

#### 1.2.2.4 Synthetic Ligands

Building on the understanding of the pharmacophores of the naturally derived and semi-synthetic ligands, the 20$^{th}$ century generated a large number of synthetic opioids for various uses. These include pethidine, tapentadol, methadone, and fentanyl and its derivatives. Fentanyl is highly lipophilic, and much more fat-soluble than other opioids (James and Williams, 2020). It is a high efficacy agonist, and is much more potent, and selective, than morphine at the MOR, with similar affinity (Comer and Cahill, 2019). Oliceridine is a synthetic partial agonist with efficacy between that of morphine and buprenorphine (Schneider, Provasi and Filizola, 2016; Pedersen *et al.*, 2019; Gillis, Batista-Gondin, *et al.*, 2020a; Beard *et al.*, 2021).

### 1.2.3 Mu-Opioid Signalling

The classical signalling described for the MOR is through its coupling to the Gαi G proteins. Activation of the Gαi inhibits adenylyl cyclase and causes a subsequent decrease of neuronal excitability (Galligan and Akbarali, 2014), inhibiting the transmission of pain signals. There is also some evidence the MOR couples weakly to Gαo, linked to attenuation of $Ca^{2+}$ release and stimulation of $K^{+}$ release, which prevent neurotransmitter release and cause hyperpolarisation respectively (Morita and North, 1982; Surprenant *et al.*, 1990). Both of these effects will attenuate nociceptive signalling; however, Gαo coupling requires much higher concentrations of MOR agonist.

The Gβγ subunit released upon activation of MOR, also has important signalling effects. Presynaptically, the Gβγ subunit inhibits voltage-gated calcium channels, inhibiting neurotransmitter release and therefore attenuating pain transmission across synapses. Postsynaptically, Gβγ couple to GIRK channels and activate them, causing hyperpolarization and inhibiting neural activity.

In recent years, it has become apparent that GPCR localisation within the plasma membrane, as well as throughout the endocytic compartments, is key for its signalling repertoire (Sternini *et al.*, 1996; Tsvetanova and von Zastrow, 2014; Halls *et al.*, 2016). This has also been illustrated with the MOR, with the suggestion of signalling from different subcellular locations being as relevant as the arrestin signalling described at these receptors (Halls *et al.*, 2016; Stoeber *et al.*, 2018). Two key players in the regulation and diffusion of the MOR are GRKs and arrestins (Halls *et al.*, 2016; Batista-Gondin *et al.*, 2019). As such, the following sections will address the role of these families of proteins in the context of the MOR.


*Figure 1.2.3, Amino acid residue sequence of the C-terminal tail of the mouse μ-opioid receptor, between residues numbered 350 and 398. Serine and Threonine residues highlighted in black, and residue number. Taken from Just, et al, 2013.*

The MOR has 11 serine and threonine residues that can be phosphorylated in its C-terminal tail, shown as the mouse MOR (mMOR) in figure 1.2.3 (Doll *et al.*, 2011; Just *et al.*, 2013; Miess *et al.*, 2018). It has previously been shown that MOR phosphorylation is hierarchical and sequential with the central serine of the $^{370}$THREPSTANT$^{379}$ motif, S375, essential for phosphorylation of the C-terminal (Just *et al.*, 2013) as mutation of that Ser prevents phosphorylation of other residues. There is evidence that recruitment of GRKs is at least partly controlled by retained integrity of key C-terminal motifs. Suggested in a paper by Miess *et al.*, 2018, the $^{370}$TREHPSTANT$^{379}$ motif of the MOR is essential for effective GRK2 recruitment, and the $^{354}$TSST$^{357}$ region is required for stable binding of GRK and arrestin (Fessart *et al.*, 2007; Miess *et al.*, 2018).

However, even when all the phosphorylation sites on the C-terminal were mutated to Ala, residual GRK2 binding was still detectable. This could suggest some initiation event that activates and brings GRKs in proximity to the activated receptor, which then relies on, or is cooperatively enhanced by, these phosphorylation sites. This is supported by the observation that a small molecule inhibitor of GRKs, compound 101, also eliminated GRK binding, highlighting the need for activated GRKs for efficient recruitment to the receptor. An alternative suggestion could be the involvement of the ICL3 of the MOR, which itself retains a number of phosphorylation sites that have been less studied. Pitcher, Freedman and Lefkowitz, 1998 suggested that GRKs may rely in some part on the presence of ICL3 to become activated,

although this was suggested for rhodopsin and muscarinic receptors, assessment of the role of ICL3 in GRK and arrestin recruitment at the MOR still remains to be investigated.

It has been suggested that the GRK isoforms that are recruited to MOR and the extent of receptor phosphorylation depend on the agonist, with DAMGO and enkephalins predominantly recruiting GRK2 and 3 and phosphorylating the motifs highlighted above (TREHPSTANT and TSST), while morphine recruits GRK5 and 6 and only promotes phosphorylation of S375 (Stoeber *et al.*, 2020). However, this still remains to be proven in physiologically relevant systems. PKC has been shown to phosphorylate particular sites on the MOR C-tail, namely S363 and T370 (C. Bailey *et al.*, 2009; Chen *et al.*, 2013). These different patterns of phosphorylation of the C-terminal gives rise to the hypothesis that different ligands exhibit varied signalling responses via a phosphorylation barcode on the intracellular side of the receptor (Just *et al.*, 2013; Yang *et al.*, 2015; Batista-Gondin *et al.*, 2019; Verweij *et al.*, 2020) whereby such barcode differentially engages with signalling effectors.

Altogether, this suggests that the recruitment of different GRKs to the MOR may be the first key step for the activation of a variety of signalling pathways, including the generation of different arrestin conformations. Moreover, a recent study by Batista-Gondin, et al (Batista-Gondin *et al.*, 2019) suggested that GRK2/3 controls MOR diffusion across the plasma membrane when activated by high efficacy agonists, diffusion that has been previously linked to different spatio-temporal signalling profiles (Halls *et al.*, 2016). This highlights the importance of this family of proteins in regulating MOR localisation and signalling.

More recent research has focused on the development of opioids with significantly reduced side effects. A particular avenue that has been exploited is the generation of ligands that preferentially activate the G protein signalling pathway over others.

It was observed early in cell-based opioid research that different ligands elicit different levels of receptor internalisation (Sternini *et al.*, 1996). These and following studies have demonstrated that endogenous peptides such as the aforementioned enkephalins produced high levels of internalisation, whereas morphine did not.

Importantly, arrestin has been linked to the more harmful effects of opioids (Raehal, Walker and Bohn, 2005; Manglik *et al.*, 2016) and recent research has been driven by the hypothesis that the side effects of opioid drugs are caused by a β-arrestin2 signalling pathway. The reasoning behind this is a series of papers from between 1999 and 2005, in which β-arrestin2 knockout mice exhibited reduced respiratory depression and improved analgesia when treated with morphine (Bohn *et al.*, 1999; Raehal, Walker and Bohn, 2005).

These results have led to the thought that, to reduce side effects, drugs must solely or preferentially activate the G protein pathway of opioid receptors, while not activating the β-arrestin2 pathway. Drugs such as oliceridine, SR17018, and PZM21 all showed G protein bias in initial cell-based assays (DeWire *et al.*, 2013; Manglik *et al.*, 2016; Schmid *et al.*, 2017) and also showed diminished side-effects in animal models.

However, independent tests have shown PZM21 did not have either the bias that was first assessed, nor the reduced respiratory depression (Hill *et al.*, 2018). Following this, SR17018 showed worsened side effects (Kliewer *et al.*, 2019), and oliceridine was initially rejected by the FDA for failing to show safety improvements over morphine (Azzam, McDonald and Lambert, 2019); however it has since been approved for use in clinic. More recently, the original observations described in the β-arrestin2 knockout mouse were independently tested by a consortium of three laboratories, which could not replicate the results of the original 1999 and 2005 papers. They speculated that the different results stemmed from the mice used in the original papers, which were early crosses of a mouse strain that had previously shown reduced responses to morphine (Sv129) (Kliewer *et al.*, 2020). As such, pharmacological research is starting to pivot away from G protein bias and searching for other strategies and explanations that may confer support improved side effect profiles.

A systematic study of clinically relevant opioids and a new synthetic opioid ligand library highlighted how opioid ligands can be grouped depending on pharmacological parameters of efficacy and functional affinity, and with this, clusters can be associated to physiological side effects (Benredjem *et al.*, 2019). This is supported by a paper from our lab (Gillis, Batista-Gondin, *et al.*, 2020b), in which the intrinsic efficacy of ligands (both in G protein and arrestin assays) inversely correlates to improved therapeutic windows, namely, the higher the intrinsic efficacy, the narrower the therapeutic window, suggesting that low intrinsic efficacy can be an alternative mechanism that explains the improvements of side effect profiles (Conibear and Kelly, 2019).

### 1.2.4 Opioid Epidemic and Crisis

Chronic use of opioids entails the development of tolerance, dependence and addiction. The use of increasing doses of opioids increases the chances of severe respiratory depression, which, in cases of overdose can be fatal. The harmful effects of opioids are no more apparent than in the present day, where opioid prescribing has rapidly increased in developed nations such as the USA. According to the CDC, there have been three waves of opioid overdose deaths. The first appears to begin in the late 1990s, where opioids that are commonly prescribed came to cause around 5 deaths per 100,000 Americans. Heroin rose the toll to similar levels beginning in 2010, followed in 2017 by other synthetic opioids which brought the third wave to 9 deaths per 100,000 (CDC Injury Center, 2018). This trend appears to still be rising, and as shown in figure 1.2.4, a large cause of this is prescription opioids. A similar pattern has been shown in the UK and Europe. This is likely due, in part, to the lack of opioids that achieve their goal of antinociception without the more dangerous side effects, such as dependence and addiction which eventually lead to respiratory depression, the main cause of death after overdose.

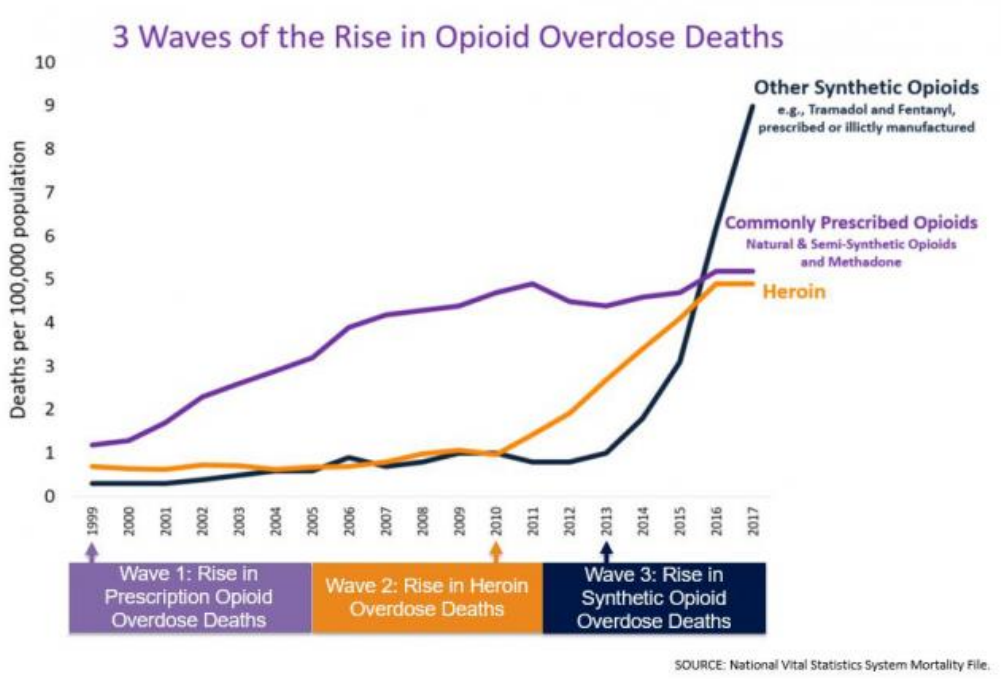


*Figure 1.2.4, Opioid Overdose deaths split by CDC classification, from 1999 to 2017. (CDC, 2018)*

One of the aims of intense opioid research is to separate the mechanisms of antinociception from the mechanisms of respiratory depression, addiction, and tolerance, and eventually create opioids that act on antinociception alone. Ideally, this would be achieved by a single drug, however, it may require combined therapeutics to reduce side effects.

## 1.3 Bioluminescence Resonance Energy Transfer

Resonance Energy Transfer (RET) is a concept first observed in 1922 (Cario and Franck, 1922), and later theoretically explained in 1927 (Perrin, 1927). It describes the phenomenon in which energy is transferred from a donor to an acceptor molecule. Crucially, this transfer does not involve the transfer of electrons, but the release of a photon from an electron relaxing into a lower energy state. This electron can then excite an electron some distance away to a higher energy state (Jones and Bradshaw, 2019).

Experimental developments (Kallmann and London, 1929) were later compiled into a simplified theoretical explanation (Fŏrster, 1959); provided the emission and absorbance spectra of the donor and acceptor respectively overlap sufficiently, the efficiency of energy transfer (E) is relative to the distance between the donor and acceptor through the function:

$$E = \frac{1}{1 + \left(\frac{r}{R_0}\right)^6}$$

where *r* is the distance between the donor and the acceptor, and $R_0$ is a coefficient for the distance at which transfer has 50% efficiency, for which each pair of donors and acceptors has a value. The value for each pair can be determined using the following equation:

$$R_0 = 0.21[\kappa^2 Q_D n^{-4} J(\lambda)]^{\frac{1}{6}}$$

where $J(\lambda)$ is the value for the spectral overlap between the donor emission and acceptor absorption spectra, $Q_D$ is the quantum yield of the donor, n is the refractive index of the medium in which the observation is conducted, and $\kappa^2$ is an orientation factor related to the relative orientation of the donor emission and acceptor absorption dipoles, which can be at any point between 0 (perpendicular) and 4 (collinear), with an average for freely rotational dipoles of 2/3, and a value of 1 when dipoles are parallel (Hwang, Song and Zhang, 2019).

Two main processes for inducing RET in biological settings has been either using fluorescence or bioluminescence as the energy donor. In fluorescence resonance energy transfer, FRET, fluorescent donors such as fluorescent proteins or dyes are excited, generally by lasers of specific wavelength, and subsequently these proteins or dyes emit photons of different wavelength than the excitation laser. Laser intensity can be varied, and the use of a laser allows for more spatially specific activation of FRET pair under observation. However, the use of lasers increases the likelihood of photobleaching of the donor, or direct excitation of the acceptor. BRET uses the action of an enzyme that, in the oxidation of a luciferin molecule, uses the energy released from this catalysis to emit photons of light at a spectrum of

wavelengths, generally with a particularly strong peak at a specific wavelength. Use of this process to excite the acceptor results in little to no photobleaching, and a reduced background noise, improving the signal to noise ratio. The lack of requirement of external illumination of a sample allows for more simple equipment for detection (Pfleger and Eidne, 2006; Pfleger, Seeber and Eidne, 2006; Salahpour *et al.*, 2012; Stoddart *et al.*, 2015).

BRET was facilitated by the discovery of a luciferase enzyme in a *Renilla reniformis* sea pansy, which is able to oxidise the chemical coelenterazine to generate the energy required for bioluminescence. Engineering and optimisation of luciferases and luciferins have yielded a large variety of emission spectra and intensities (Yeh *et al.*, 2017).

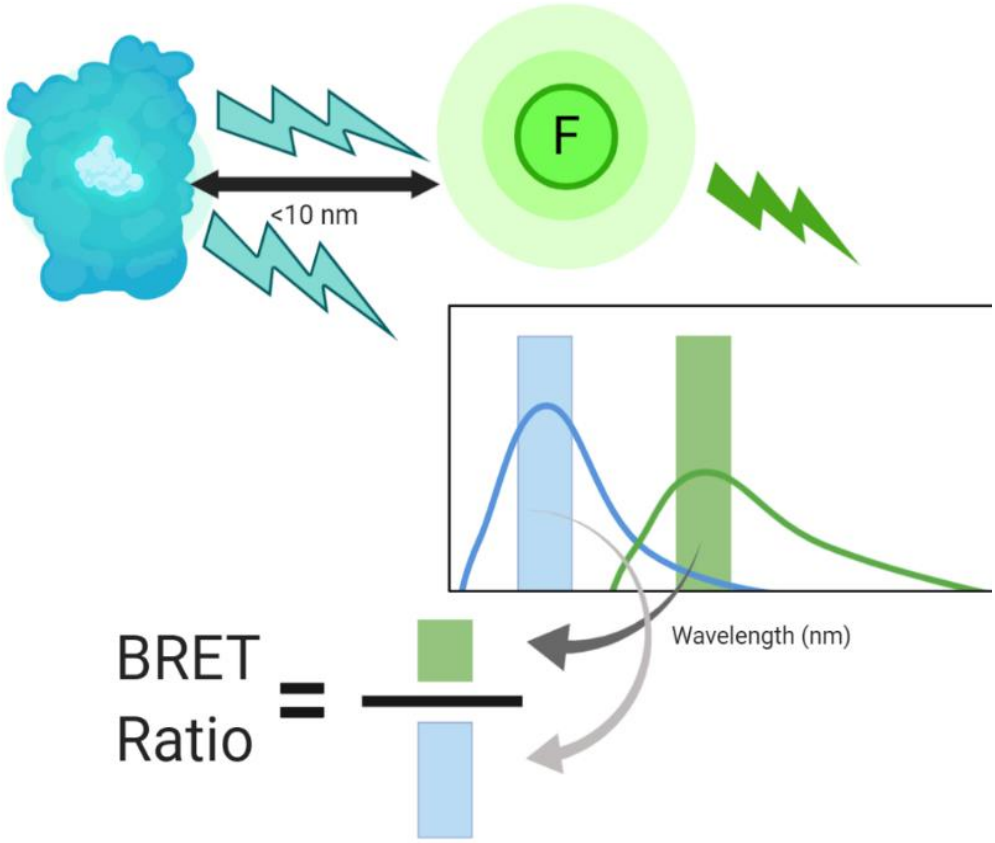


*Figure 1.3, a diagram showing Bioluminescence resonance energy transfer (BRET) as a method of observing proximity of tagged moieties. A bioluminescent donor, shown in blue emits a spectrum of photons as shown in the emission spectra. A fluorophore, shown in green, within 10 nm can then absorb a portion of these photons, using their energy to emit photons with a different spectrum. These two emissions are measured within a pre-defined range, usually around the peak emission of the two spectra. These measurements can then be used to create a BRET ratio, by dividing the measured fluorescence by the measured luminescence. This ratio will change if the distance between the acceptor and donor changes, as less energy is transferred.*

The dependence of FRET and BRET on the distance between fluorophores has made them particularly useful approaches to monitor protein-protein interactions as well as conformational changes (Ayoub and Pfleger, 2010; Nuber *et al.*, 2016). Importantly for this work, as shown in the equation for

energy transfer efficiency, distance between the acceptor and donor is one of the main factors in determining energy transfer, with an exponent of 6. As such, the changing distance between donor and acceptor, observed upon conformational change, can have a great effect on the level of energy transfer, and the limit of detectable transfer of energy is around 10 nm (White *et al.*, 2017). By measuring the level of donor emission, and the level of acceptor emission, we can gain an understanding of the relative distances between the two. To account for changing intensity due to number of donors or acceptors, the energy transfer ratio is calculated by dividing the measured fluorescence by the measured bioluminescence, shown in figure 1.3.

Changing distances between donor and acceptor can occur by the active recruitment of the donor- to the acceptor, by indirect recruitment of one of these to a nearby third partner, or by random diffusion. Bystander BRET can occur when random diffusion of tagged molecules leads to increased proximity and is characterised by a linear increase in BRET ratio upon increasing concentration of one of the BRET partners. Indirect BRET is the recruitment of a BRET partner to a similar cellular location as the other partner, such as a tagged plasma membrane marker. This indirect BRET generally has weaker signal to noise ratios, due to greater levels of bystander BRET occurring due to the high concentration of localisation marker needed. Direct BRET is the recruitment of a donor to an acceptor, or vice versa, usually resulting in much higher signal to noise ratios, due to the greater average proximity of the donor and acceptor, as well as a lower concentration requirement for both partners.

## 1.4 Aims and Objectives

As highlighted in this chapter, the role of phosphorylation of the receptor has wide ranging effects on the signalling and trafficking of GPCRs, and the MOR specifically. The role of β-arrestin2 as a trafficking and signalling molecule has been highlighted throughout opioid research. This work will assess the transduction of signals from the opioid ligand, through the phosphorylation of the receptor, to the arrestin, and the mechanisms of signalling pathway selection.

The hypothesis for my PhD is that the ***modulation of MOR signalling takes place at the level of the plasma membrane through effectors that cause differential redistribution of the receptor***. As part of this hypothesis, there are two main aims that the project will explore.

### 1.4.1 Effects of GRKs on MOR Translocation and Signalling

We set out to determine the differential effects of GRKs on the distribution and signalling of the MOR at the plasma membrane. Different ligands have shown a variety of internalisation effects, and, our lab has previously shown that the diffusion properties of the MOR differ depending on the agonist. These ligand-dependent effects on arrestin recruitment and signalling have been shown to be transduced by the phosphorylation states of the receptor C-tail, resulting in altered signalling effects in other family A GPCRs (Butcher, Tobin and Kong, 2011; Miess *et al.*, 2018; Latorraca *et al.*, 2020). Pharmacological and genetic strategies were used to explore the contributions of GRKs to G protein and arrestin recruitment as well as the diffusion and clustering of the MOR at the cell surface.

### 1.4.1 Mechanisms of Arrestin Conformational Selection

We also set out to determine the process by which signals are transmitted from these phosphorylation barcodes on to the arrestin, and the mechanism by which conformations of arrestin may be selected. β-arrestin2 biosensors were used, similar to the ones described in Nuber et al., 2016 (Nuber *et al.*, 2016), that are able to report a change in conformation of arrestin through the use of BRET signals, using bioluminescent and fluorescent tags along its sequence. These sensors were used to investigate differences across MOR agonists as well as across MOR phosphorylation mutants.

# Chapter 2: Characterisation of MOR function in CRISPR GRK-Knockout cells

## 2.1 Introduction

GRK-dependent phosphorylation of GPCR C-termini and intracellular loops (particularly ICL3) is the basis for high affinity arrestin binding, and subsequent internalisation. It has also been implicated as part of the phosphorylation barcode hypothesis (Nobles *et al.*, 2011) as an explanation for the limited number of effectors transducing varied signalling responses from hundreds of distinct GPCRs. This phosphorylation barcode hypothesis is the theory that GPCRs can undergo differential phosphorylation of the intracellular regions, especially the receptor C-tail, and that the repertoire of arrestin-dependant signalling pathways can subsequently be selected from dependant on the pattern presented. As such, assessment of the ability of GRKs to phosphorylate GPCRs and stimulate downstream events is important in understanding the mechanism for signalling pathway selection.

As discussed in section 1.2.3, the MOR has 11 serine and threonine residues that can be phosphorylated in its C-terminal tail (Doll *et al.*, 2011; Just *et al.*, 2013; Miess *et al.*, 2018). It has been suggested that the GRK isoforms that are recruited to MOR and the extent of receptor phosphorylation depend on the agonist, with DAMGO and enkephalins predominantly recruiting GRK2 and 3 and phosphorylating the TREHPSTANT and TSST motifs, while morphine recruits GRK5 and 6 and only promotes phosphorylation of S375 (Stoeber *et al.*, 2020). However, this still remains to be proven in physiologically relevant systems. PKC has been shown to phosphorylate particular sites on the MOR C-tail, namely S363 and T370 (C. Bailey *et al.*, 2009; Chen *et al.*, 2013).

### 2.1.1 Approaches to Studying GRKs

For the MOR, efforts to assess the role of GRKs in signalling pathways have been made through various methodological approaches. Previous efforts have included small molecule inhibitors, silencing RNAs, and *in vivo* knockouts, each of which has their strengths and weaknesses.

### 2.1.2 Small molecule inhibitors of GRKs

There are several small molecule inhibitors of GRKs, however their selectivity is generally poor. For instance, heparin and dextran sulphate inhibit GRK activity but are non-selective, inhibiting other kinases such as casein kinase, as well as being impermeable across the membrane (Benovic *et al.*, 1989). Balanol, a natural product derived from fungi, is a GRK2 inhibitor, but also inhibits other serine/threonine kinases such as PKA and PKC, albeit at lower potencies (Thal *et al.*, 2011). Compound 101 is the most commonly used, and is a selective GRK2/3 inhibitor (Ikeda, Kaneko and Fujiwara, 2007; Thal *et al.*, 2011) , although it has been shown to have moderate activity at other kinases, such as Rho-associated protein kinase 2 (ROCK2), protein kinase C–

related protein kinase (PRK2), PKC, PKA, mitogen- and stress-activated protein kinase 1 and serum and glucocorticoid-regulated kinase (SGK1) (Lowe *et al.*, 2015). Higher concentrations of compound 101 are required for cell-based assays than *in vitro* assays (3 – 100 µM), and off target inhibition has only been measured at 1 µM *in vitro*. At this concentration, PKC, which is known to phosphorylate MOR, retained its activity. Other inhibitors are available, such as amlexanox, a GRK5 inhibitor repurposed from its inhibitory effect on inflammatory kinases (Homan, Wu, Cannavo, *et al.*, 2014), with subsequently limited specificity (Reilly *et al.*, 2013), as well as paroxetine, a GRK2 inhibitor with 50 fold greater selectivity for GRK2 over other GRK isoforms (Homan, Wu, Wilson, *et al.*, 2014).

All of these small molecule inhibitors function as ATP mimetics (Kenski *et al.*, 2005; Ikeda, Kaneko and Fujiwara, 2007; Homan, Wu, Cannavo, *et al.*, 2014), and function as reversible inhibitors, displacing ATP when affinity is higher than that of ATP, or being displaced by ATP when affinity for the kinase is lower. This mechanism belies the lack of specificity in many inhibitors, because of the highly conserved nature of the ATP binding site in numerous kinases, reducing their usefulness.

### 2.1.3 *In vivo* Knockouts of GRKs

*In vivo* knockouts of GRKs have been achieved, most commonly GRK3, as homozygous GRK2 KO is embryonically lethal, however GRK2 inhibition by a mutant kinase knock-in that can be selectively inhibited by specific inhibitors has facilitated *in vivo* studies of the role of this kinase (Kenski *et al.*, 2005; Quillinan *et al.*, 2011). *In vivo* knockouts have allowed the testing of phosphorylation patterns and behaviour of GRK3 homozygous KO and GRK5 homozygous KO mice (Doll *et al.*, 2012; Glück *et al.*, 2014). They found supporting evidence for the role of GRK5 in morphine-induced phosphorylation or MOR, in which both sets of knockout animals (GRK3 and GRK5) lost some portion of their S375 phosphorylation upon treatment with morphine, whereas only the GRK3 knockout animal lost any portion of their S375 phosphorylation upon treatment with fentanyl. S375 is important, because, as pointed out in this paper and others (Schulz *et al.*, 2004; Doll *et al.*, 2011; Just *et al.*, 2013; Yousuf *et al.*, 2015; Miess *et al.*, 2018), S375 is the first site to be phosphorylated by GRKs, and its knockout reduces phosphorylation of other sites within the MOR C-terminal tail.

Glück et al., 2014 also highlighted the differing behavioural responses in the different knockout mice. GRK5 knockout mice exhibited reduced analgesic responses to morphine, but not fentanyl. Tolerance studies indicated that GRK5 plays a role in acute tolerance to morphine, supporting the fact that GRK5 is at least in part responsible for MOR phosphorylation with morphine, whereas there was no link between GRK5 knockout and chronic tolerance. Withdrawal symptoms were reduced in GRK5 knockout mice compared to

wildtype. GRK3 knockout mice exhibited no change in analgesia for either morphine or fentanyl but exhibited reduced acute and chronic tolerance for high efficacy agonists, pointing to the role of GRK3 in the development of tolerance but not in analgesia. Knockout of GRK5 for morphine, and GRK3 for fentanyl, resulted in reduced reward, that was shown to be not mediated by dopamine signalling, but likely by ERK signalling, indicating GRK5 is needed for, if not directly scaffolds or activates, ERK signalling. This is supported by the fact that S375/A knock-in mice retained reward function and indicates that while the phosphorylation barcode may be important for arrestin signalling, the GRKs selected by the ligand/receptor complex have their own signalling repertoire to add to the pathway.

*In vivo* knockout of GRK6 in mice has shown to increase locomotion with morphine, however, this has been suggested to be due to increased dopaminergic signalling rather than direct MOR effects. GRK6 knockout mice also showed reduced morphine-induced constipation, however exhibited no change in analgesia, tolerance, or dependence (Raehal *et al.*, 2009)

### 2.1.4 *In vitro* knockdown of GRKs

In cells, knockout of GRKs has previously been unavailable. Some studies into the roles of GRKs have been achieved using silencing RNAs in the delta opioid and angiotensin receptor, however while GRK levels were reduced as detected by western blot, expression remained detectable, indicating incomplete knockdown using this methodology (Kim *et al.*, 2005; Doll *et al.*, 2012; Mann *et al.*, 2019, 2020).

### 2.1.5 CRISPR Knockout of GRKs

The invention of CRISPR (clustered regularly interspaced palindromic repeat)/Cas (CRISPR associated)-9 technology (Doudna and Charpentier, 2014) has allowed the roles of specific genes to be investigated through their specific insertion or knockout. Evolved as adaptive immunity for bacteria against viruses, the CRISPR locus is comprised of repeated sequences of bases interspersed between spacers. The source of these spacers were sequences from viral genomes. These repeated sequences (CRISPR RNAs or crRNA) could then be cut alongside an associated space. The repeat would bind a palindromic tracer RNA that was transcribed from another section earlier in the locus, and together this would facilitate the binding of a Cas9 endonuclease. The single stranded viral sequence could then bind the complementary section in a viral genome, attaching the endonuclease and causing the double stranded cleavage of the viral genome, leading to its breakdown, and thus the death of the viral particle.

In its current form for use in molecular biology, the CRISPR sequences have been replaced by guide RNAs, which contain the repeated sequence and tracer RNA connected by a flexible loop region, allowing for self-association

and transcription as one sequence. A user can then fuse their target DNA to this sequence, and upon co-transfection with the Cas9 protein, can target specific genes or sequences in the transfected cell for alteration. This alteration can disrupt genes by causing small insertions or deletions during endogenous DNA repair, or repair or insert genes by assisted recombination.

As discussed earlier in this section, approaches to study GRKs have yielded interesting but varied results with regards to the role of these kinases in MOR phosphorylation and function. In the last three years, however, different groups have reported the generation of isoform specific GRK CRISPR/Cas9 KO cell lines, with two of these groups investigating the impact on MOR function.

CRISPR/Cas9 knockout cells were used to assess the roles of GRK2 and GRK3 with relation to β-arrestin2 recruitment to, and internalisation of, the MOR (Møller *et al.*, 2020). This highlighted that while GRK2 and 3 are the main isoforms involved in these functions, there remains a GRK2/3 independent component of β-arrestin2 recruitment. This also highlighted the greater contribution of GRK2 than GRK3 in these functions, as well as validating the use of compound 101 as a selective inhibitor of GRK2/3.

More recently, a more comprehensive suite of GRK knockout cells has been generated with single, double, triple and quadruple GRK deletions (Drube *et al.*, 2022). These cells will help elucidate more detailed information on GRK function and effects on MOR action.

The lentiCRISPR v2 plasmid used in the creation of the GRK Knockout cells used in this study was created by Sanjana et al., 2014 and allows for the transfection of both the Cas9 nuclease as well as the guide RNA (gRNA) selected on the same plasmid. Drube, et al, used these plasmids with oligo sequences targeting the double stranded break to a specific GRK isoform. To ensure knockout, four different gRNA oligos were created for each GRK isoform and were transfected simultaneously. Puromycin treatment then selected for successfully transfected cells and single cell clones were cultured and knockout confirmed by Western blot.

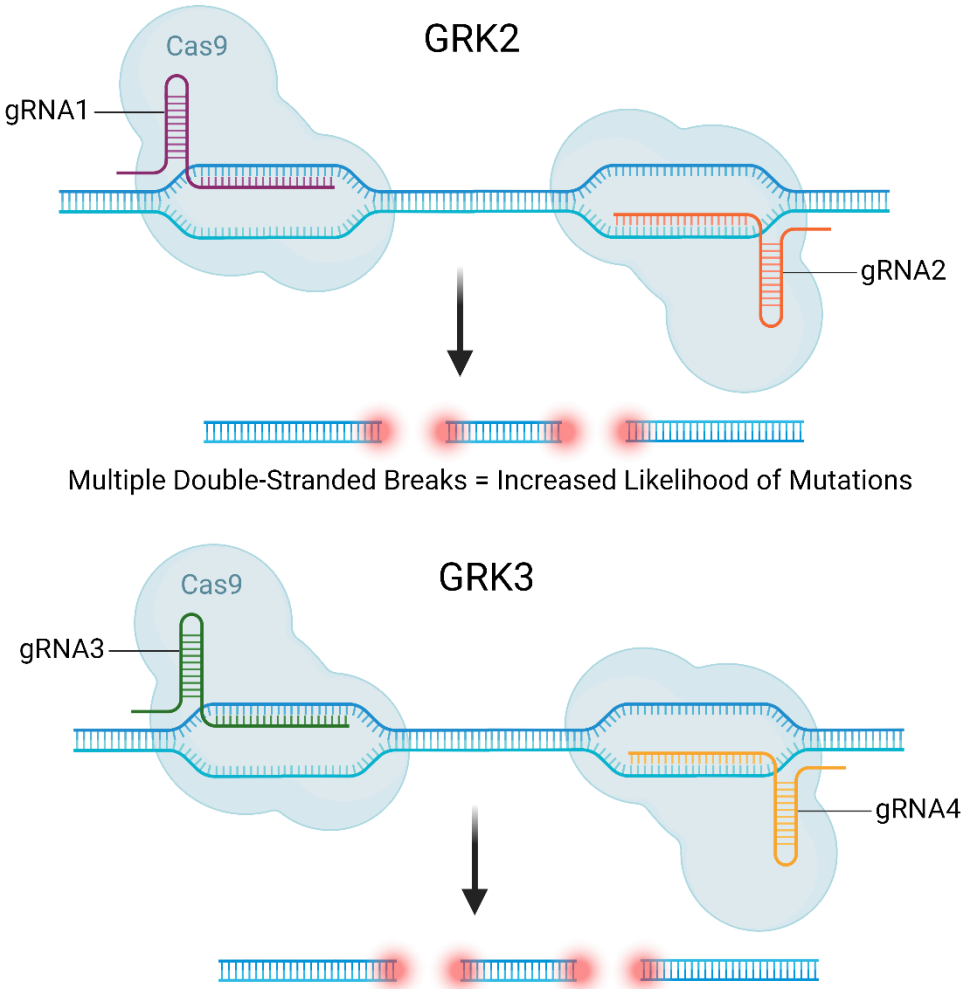


*Figure 2.1.5, diagram depicting the use of multiple guide RNAs to target the Cas9 endonuclease to both multiple genes and multiple locations within a specified gene, causing mutations and thus misfolded and/or degradation of translated proteins.*

As MOR phosphorylation patterns and specific MOR phosphosite antibodies are available, the MOR was used as a model receptor to describe the use of these new cell lines. It was found that, upon activation with the full agonist DAMGO, the GRK2/3 family is responsible for phosphorylation of T376, and that T370, T379, and S375 were able to be phosphorylated by all four GRKs. It was also shown that only GRKs phosphorylate T370, T379, and S375, although the strength of phosphorylation varies between the different GRK isoforms. S363 retained phosphorylation in quadruple GRK knockout cells, supporting the fact that S363 is a PKC phosphorylation site. While this data supports previous findings (Mann *et al.*, 2015; Møller *et al.*, 2020), the discovery that T376 is a GRK2/3 specific site was previously unknown. This site appears important for MOR internalisation, and it remains to be seen whether this site alone, or the degree of phosphorylation overall, is the main driver of MOR internalisation.

It was also shown that GRK5/6 have only limited effects in recruiting either of the β-arrestins to the receptor, and β-arrestin interactions with the MOR appears to be controlled by GRK2/3. However, all the experiments above were conducted with only the high efficacy agonist DAMGO, the impact of GRK KO in the action of other opioid agonists remains unknown.

As HEK293 cells have been reported to express the four GRKs (GRK2, GRK3, GRK5, GRK6) found ubiquitously in human tissues (Reichel *et al.*, 2022), alongside their ease of culture and transfection, these cells have most commonly been used to assess GRK function. While difficult to translate physiologically due to the wildly varying GRK expression found in human tissues(Usoskin *et al.*, 2015), as will be discussed later in this chapter, the molecular basis for these interactions can be described in cell models. This may then be used as a basis to predict molecular, cellular, and thus neuronal circuit outcomes in tissues with known expression levels.

### 2.1.6 Aims

In this chapter, the effects of the different GRK isoforms on MOR arrestin and G protein recruitment will be investigated using the GRK CRISPR/Cas9 KO cells described in Drube, et al, 2022, different opioid agonists and BRET approaches of arrestin and miniGsi recruitment.

## 2.2 Methods

### 2.2.1 Cell Culture

CRISPR generated GRK knockout cell lines received from Carsten Hoffmann's lab, and created as described in Drube et al., 2022, were stored at -80 °C in Foetal Bovine Serum (FBS) with 10% v/v DMSO. Human embryonic kidney 293 (HEK293) cells and knockout cell lines samples were thawed and seeded in T75 flasks and were maintained in 10 mL Dulbecco's Modified Eagle's Medium (DMEM) (Sigma Aldrich) supplemented with 10% v/v FBS (Sigma Aldrich) at 37 °C in a humidified atmosphere of 95% air and 5% $CO_2$. Cells were passaged using 1 mL 0.05% Trypsin-EDTA (Thermo Fisher Scientific, Loughborough, UK) to detach the cells from the flask, resuspended in 4 mL DMEM, and centrifuged at 1000 rpm for 3 mins. Supernatant was discarded, and the pellet was resuspended in 5 mL DMEM, and live cells were counted using a Countess II Automated Cell Counter (Thermo Fisher Scientific). Flasks were then seeded with 1:10 or 1:20 dilutions depending on growth rate and growth time. For assays, 10cm cell culture dishes were seeded with 750,000 live cells/dish.

### 2.2.2 Functional Assays

#### *2.2.2.1 mGsi Recruitment BRET Assay*

GRK knockout cell lines were transfected 24 hours post-seeding with 4 µg mGsi construct C-terminally tagged with a Venus fluorophore, and 1 µg hMOR tagged with a N-terminal FLAG tag and a C-terminal Nluc. 24 hours after transfection cells were re-plated in white 96 well plates coated with PDL. 24 hours post transfection cells had media replaced with 80 µL HBSS and was incubated for 30 mins at 37 °C at 5% $CO_2$ to acclimatise to the assay buffer. Cells were then treated with 10 µL of ligand at 10x final concentration and incubated for 5 mins, followed by 10 µL furimazine (final conc 5 µM) and incubated for 5 mins, to allow for maximal temporal response of opioid ligands (Miess *et al.*, 2018), as well as reaching furimazine equilibrium. Ligands used were either DAMGO, morphine, or fentanyl, at concentrations ranging between 100 µM and 0.1 nM in HBSS. Plates were read on a PHERAstar Plate Reader (BMG Labtech) using the BRET1 filter set (535 ± 30 (fluorescence), 475 ± 30 luminescence) for 3 cycles.

#### *2.2.2.2 β-arrestin2 Recruitment BRET Assay*

GRK knockout cell lines were transfected with 4 µg β-arrestin2 construct with a C-terminally tagged Venus fluorescent protein, and 1 µg hMOR tagged with a N-terminal FLAG tag and a C-terminal Nluc. These were plated, treated and read as described in the previous section.

### 2.2.3 Data Analysis

Bioluminescence and fluorescence data were exported using MARS (BMG Labtech) into Excel (Microsoft). BRET ratios were generated for each well in

each cycle by dividing measured fluorescence by luminescence. BRET ratios were exported to GraphPad Prism (version 9.1.1). Each BRET ratio for the well was then normalised by subtracting the average change observed in a vehicle control, and plotted (4 replicates, one experiment) as a function of the logarithmic function of the ligand concentration. Non-linear regression was then performed and fitted values obtained using the following equation:

$$y = Bottom + \frac{Top - Bottom}{1 + 10^{Log(EC50) - x}}$$

where y is the change in BRET ratio over vehicle, and x is the logarithmic function of the concentration of ligand in M. The mean of the 4 replicates were then taken and grouped together for the 5 repeats and plotted and analysed as described for the individual experiments.

## 2.3 Results

Ligand dependent phosphorylation of GPCRs, including the MOR, by GRKs has been widely reported (Nobles *et al.*, 2011; Glück *et al.*, 2014; Møller *et al.*, 2020; Drube *et al.*, 2022). However, the roles of the different GRK isoforms in the transduction of these ligand-dependent effects into downstream signalling and regulation pathways have not been comprehensively studied. Here, we were able to assess the effects of differential GRK expression on two major GPCR downstream effectors, G proteins and arrestin. Due to the important role of GRKs in creating conditions suitable for arrestin recruitment, we first undertook assays assessing the effects of GRK expression on β-arrestin2 recruitment at the MOR

### 2.3.1 β-arrestin2 Recruitment

To observe the effects of GRKs on MOR signalling, we tested the ability of the MOR to recruit β-arrestin2 under a variety of GRK conditions using a standard BRET protocol that measures β-arrestin2-Venus recruitment to Flag-MOR-NLuc.

#### *2.3.1.1 Role of Small Molecule Inhibition and Over Expression of GRKs on MOR Agonist Responses in a β-arrestin2 Recruitment Assay*

In order to link the results gained in the CRISPR knockout cells to current literature and the methods used to study GRK function previously, we conducted preliminary assays using the small molecule inhibitor of the GRK2/3 family, compound 101. This small molecule is commonly used to prevent arrestin interactions by inhibiting GRK2/3 and preventing receptor phosphorylation. We also studied the effects of overexpression of GRK2, a common strategy for β-arrestin2 assays with receptors with weak and transient interactions with arrestins. GRK2 overexpression increases the assay window and allows the user to delineate differences in opioid ligand efficacy. Of note, these preliminary assays were conducted in the HEK293T cell line maintained in the Canals/Lane lab.

β-arrestin2 recruitment to the MOR in WT HEKs (figure 2.3.1.1) shows a common pattern of responses, with DAMGO exhibiting the maximal effect, fentanyl reaching approximately 50% of DAMGO, and morphine achieving just over 10%. This is in agreement with extensive previous published data.

Overexpression of GRK2 (figure 2.3.1.1b) increases Emax for all ligands, with DAMGO response increasing 5-fold. Lower efficacy agonists achieve significantly higher responses when compared to DAMGO, with fentanyl achieving approximately 90% that of DAMGO, and morphine increasing to 65%. Potency also increases significantly, with DAMGO and morphine increasing by more than one log unit. Fentanyl responses are highly variable and therefore not significant.

GRK2/3 inhibition with compound 101 (figure 2.3.1.1c) had distinct effects depending on the agonist. Cpd101 induced a reduction of DAMGO's Emax (by a third) without affecting its potency, morphine's potency and Emax were increased while fentanyl responses were unchanged compared to the absence of the inhibitor.

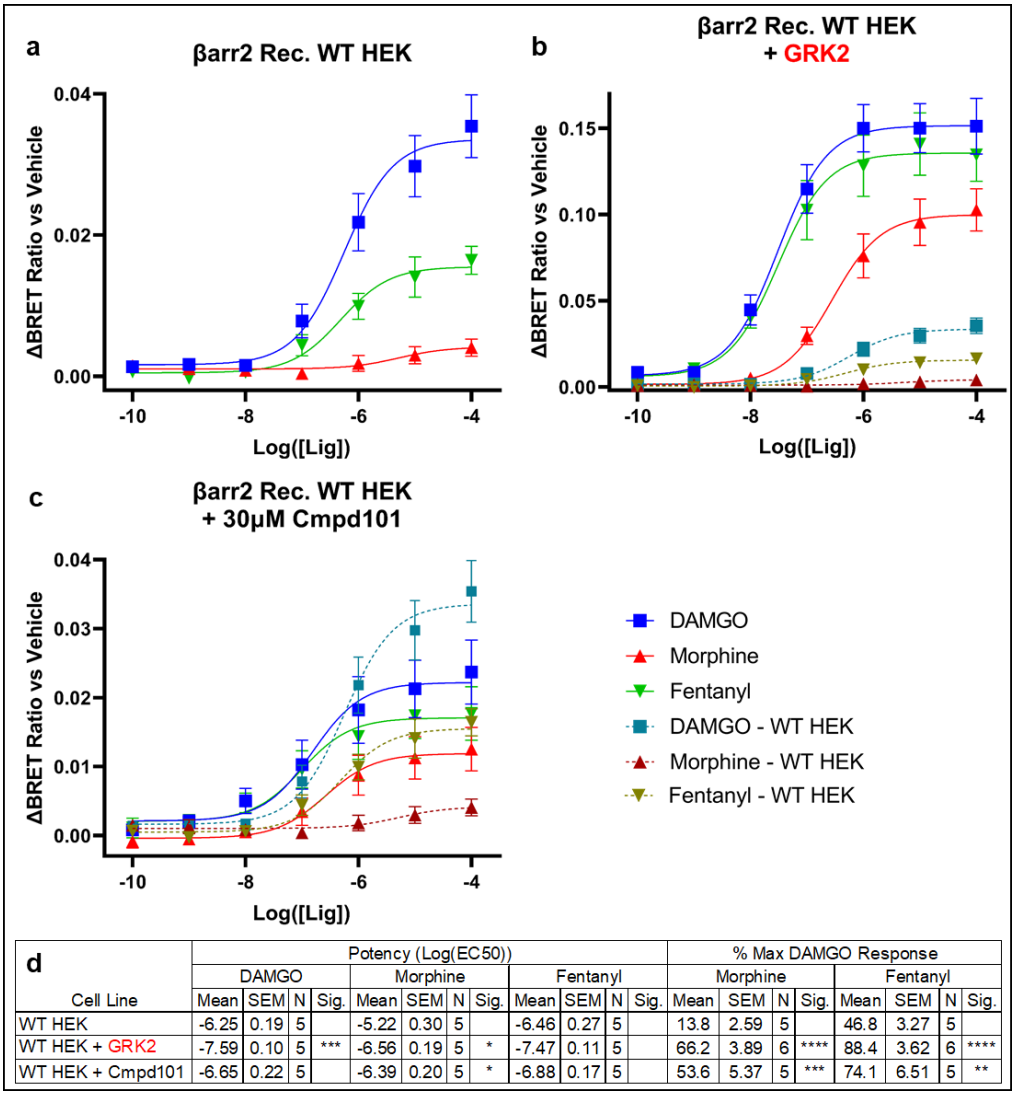


**d**

| Cell Line | Potency (Log(EC50)) | | | | | | | | | | | | % Max DAMGO Response | | | | | | | |
|---|---|---|---|---|---|---|---|---|---|---|---|---|---|---|---|---|---|---|---|---|
| | DAMGO | | | | Morphine | | | | Fentanyl | | | | Morphine | | | | Fentanyl | | | |
| | Mean | SEM | N | Sig. | Mean | SEM | N | Sig. | Mean | SEM | N | Sig. | Mean | SEM | N | Sig. | Mean | SEM | N | Sig. |
| WT HEK | -6.25 | 0.19 | 5 | | -5.22 | 0.30 | 5 | | -6.46 | 0.27 | 5 | | 13.8 | 2.59 | 5 | | 46.8 | 3.27 | 5 | |
| WT HEK + GRK2 | -7.59 | 0.10 | 5 | *** | -6.56 | 0.19 | 5 | * | -7.47 | 0.11 | 5 | | 66.2 | 3.89 | 6 | **** | 88.4 | 3.62 | 6 | **** |
| WT HEK + Cmpd101 | -6.65 | 0.22 | 5 | | -6.39 | 0.20 | 5 | * | -6.88 | 0.17 | 5 | | 53.6 | 5.37 | 5 | *** | 74.1 | 6.51 | 5 | ** |

*Figure 2.3.1.1, β-arrestin2-YFP recruitment to MOR-Nluc BRET mean ± SEM concentration response curves with varied opioid ligands (log(M)) (DAMGO (Blue), Morphine (Red), Fentanyl (Green) at 10 mins post-ligand addition in a) Wild Type (WT) HEK293T cells. b) HEK293T cells with GRK2 co-transfected, with WT HEK concentration response curves overlaid (DAMGO – Teal, Morphine – Crimson, Fentanyl – Mustard). c) WT HEK293T cells treated with 30 μM compound 101, a GRK2/3 family inhibitor, for 30 mins pre-ligand treatment, with WT HEK concentration response curves overlaid. d) Table showing EC50 and maximum response as a % of maximum DAMGO response for each ligand in each cell condition, with standard error of the mean (SEM), N-number (N), and significance as a difference from WT HEK in an unpaired T-Test, corrected for multiple comparisons using a Holm-Šídák test (*: p ≤ 0.05; **: p ≤ 0.005; ***: p ≤ 0.0005; ****: p ≤ 0.00005)*

#### *2.3.1.2 Comparison of MOR Agonist Responses in a β-arrestin2 Recruitment Assay in two different Parental Cell Lines*

In order to compare WT HEK responses to cells that have undergone CRISPR knockout, control HEK293 cells that have undergone CRISPR/Cas9 transfection with no guide RNA (Control HEK) were also tested in the β-arrestin2 assay. As shown in figure 2.3.1.2b, Emax values for DAMGO and fentanyl were significantly larger in Control HEK293 cells compared to WT HEK293 cells, but there was no significant change in potency of any of the agonists.

In fact, comparing the WT HEKs to GRK2 KO cells shown in figure 2.3.1.2c highlights greater similarities between the WT HEKs and GRK2 KO cells than between the WT HEKs and the Control HEKs; GRK2 KO cells showed slight but consistent decreases in response, no changes in potency, and no Emax change relative to DAMGO.

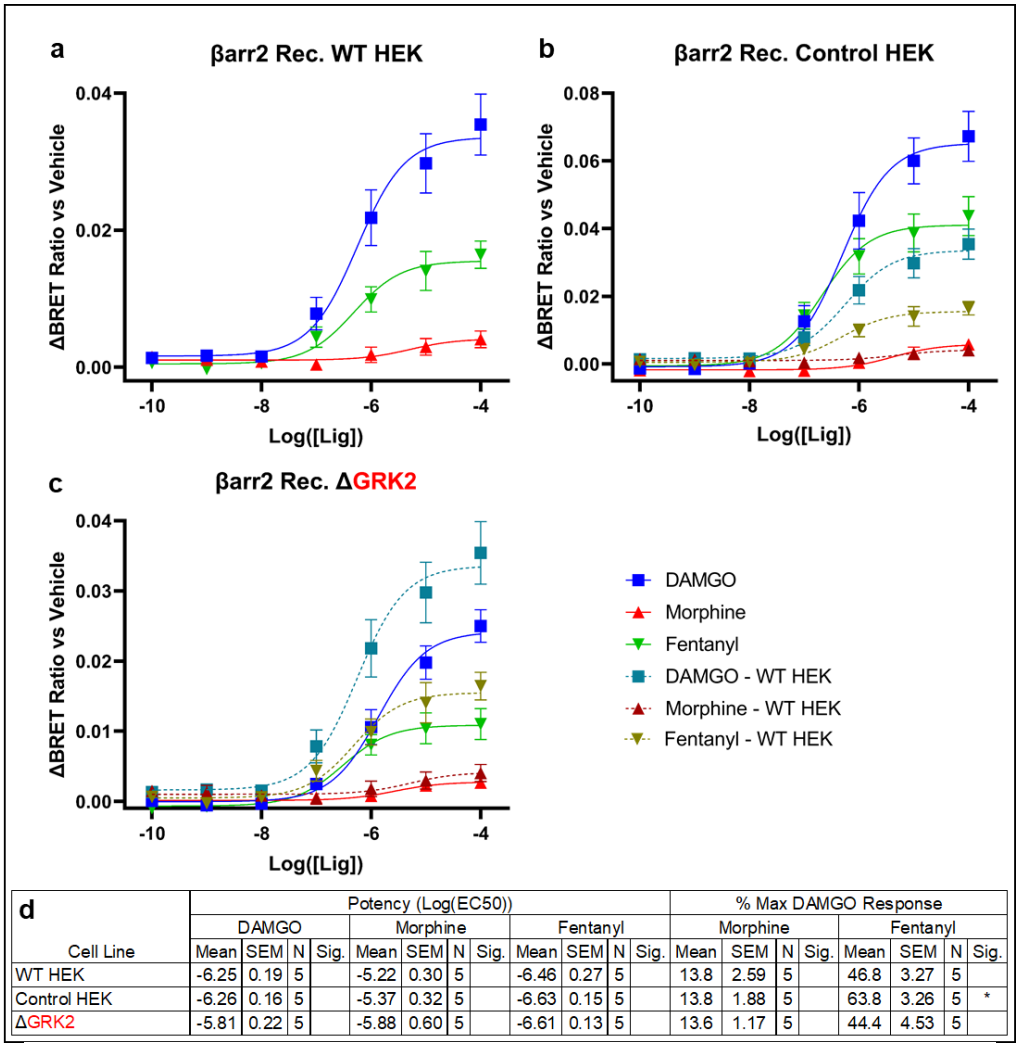


**d**

| Cell Line | Potency (Log(EC50)) | | | | | | | | | | | | % Max DAMGO Response | | | | | | | |
|---|---|---|---|---|---|---|---|---|---|---|---|---|---|---|---|---|---|---|---|---|
| | DAMGO | | | | Morphine | | | | Fentanyl | | | | Morphine | | | | Fentanyl | | | |
| | Mean | SEM | N | Sig. | Mean | SEM | N | Sig. | Mean | SEM | N | Sig. | Mean | SEM | N | Sig. | Mean | SEM | N | Sig. |
| WT HEK | -6.25 | 0.19 | 5 | | -5.22 | 0.30 | 5 | | -6.46 | 0.27 | 5 | | 13.8 | 2.59 | 5 | | 46.8 | 3.27 | 5 | |
| Control HEK | -6.26 | 0.16 | 5 | | -5.37 | 0.32 | 5 | | -6.63 | 0.15 | 5 | | 13.8 | 1.88 | 5 | | 63.8 | 3.26 | 5 | * |
| ΔGRK2 | -5.81 | 0.22 | 5 | | -5.88 | 0.60 | 5 | | -6.61 | 0.13 | 5 | | 13.6 | 1.17 | 5 | | 44.4 | 4.53 | 5 | |

*Figure 2.3.1.2, β-arrestin2-YFP recruitment to MOR-Nluc BRET mean ± SEM concentration response curves with varied opioid ligands (log(M)) DAMGO (Blue), Morphine (Red), Fentanyl (Green) at 10 mins post-ligand addition in a) Wild Type (WT) HEK293T cells. b) Control HEK293 cells transfected with CRISPR/Cas9 plasmids with no guide RNA co-transfected, with WT HEK concentration response curves overlaid (DAMGO – Teal, Morphine – Crimson, Fentanyl – Mustard). c) CRISPR-generated HEK293 ΔGRK2 cells, with WT HEK concentration response curves overlaid. d) Table showing EC50 and maximum response as a % of maximum DAMGO response for each ligand in each cell condition, with standard error of the mean (SEM), N-number (N), and significance as a difference from WT HEK in an unpaired T-Test, corrected for multiple comparisons using a Holm-Šídák test (*: $p \leq 0.05$)*

### *2.3.1.3 Effect of GRK2/3 CRISPR Knockout on MOR Agonist Responses in a β-arrestin2 Recruitment Assay*

In order to assess the role of the GRK2/3 family in β-arrestin2 recruitment to the MOR following agonist stimulation, cells engineered to lack GRK2, GRK3 or both GRK2 and 3 (Drube *et al.*, 2022) were assessed against the Control HEKs.

GRK2 knockout shown in figure 2.3.1.3b showed significant decreases in the responses of DAMGO and fentanyl, however morphine's response was unchanged. There was also no significant change in potency for all ligands assayed compared to control HEKs.

GRK3 knockout shown in figure 2.3.1.3c showed variable responses with all ligands, however, morphine exhibits significantly increased Emax and relative response to DAMGO compared to control HEKs, as well as a significant increase in potency.

The combined KO of GRK2 and 3 is shown in figure 2.3.1.3d. We observe decreases in both DAMGO and fentanyl Emax in the GRK2/3 knockout cells compared to the control HEKs, whose curves become overlaid, as well as the significant increase to both potency and response in morphine. While this increase in response is around half that of what is observed in GRK3 knockout, relative response is increased even further, from around 15% in the control HEK, to 45% in GRK3 knockout, to 60% in GRK2/3 knockout.

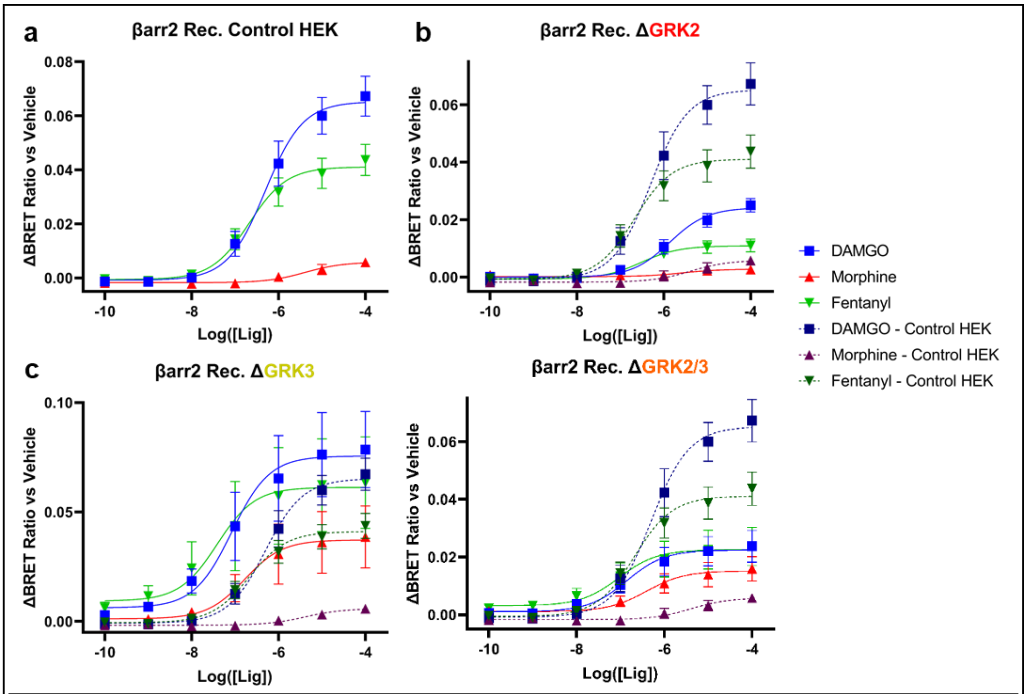


e

| Cell Line | Potency (Log(EC50)) | | | | | | | | | | | | % Max DAMGO Response | | | | | | | |
|---|---|---|---|---|---|---|---|---|---|---|---|---|---|---|---|---|---|---|---|---|
| | DAMGO | | | | Morphine | | | | Fentanyl | | | | Morphine | | | | Fentanyl | | | |
| | Mean | SEM | N | Sig. | Mean | SEM | N | Sig. | Mean | SEM | N | Sig. | Mean | SEM | N | Sig. | Mean | SEM | N | Sig. |
| Control HEK | -6.26 | 0.16 | 5 | | -5.37 | 0.32 | 5 | | -6.63 | 0.15 | 5 | | 13.8 | 1.88 | 5 | | 63.8 | 3.26 | 5 | |
| ΔGRK2 | -5.81 | 0.22 | 5 | | -5.88 | 0.60 | 5 | | -6.61 | 0.13 | 5 | | 13.6 | 1.17 | 5 | | 44.4 | 4.53 | 5 | * |
| ΔGRK3 | -6.73 | 0.26 | 6 | | -6.58 | 0.19 | 6 | * | -7.08 | 0.23 | 6 | | 43.9 | 8.67 | 6 | * | 73.3 | 10.11 | 6 | |
| ΔGRK2/3 | -6.72 | 0.21 | 5 | | -6.41 | 0.20 | 5 | * | -7.01 | 0.21 | 5 | | 61.3 | 9.62 | 5 | ** | 91.2 | 14.11 | 5 | |

*Figure 2.3.1.3, ß-arrestin2-YFP recruitment to MOR-Nluc BRET mean ± SEM concentration response curves with varied opioid ligands (log(M)) (DAMGO (Blue), Morphine (Red), Fentanyl (Green) at 10 mins post-ligand addition in a) control HEK293 cells. b, c, d) control HEK293 cell concentration response curves (dashed lines) overlaid (DAMGO – Dark Blue, Morphine – Purple, Fentanyl – Dark Green) on concentration response curves conducted in CRISPR-generated b) ΔGRK2 cells. c) ΔGRK3 cells. d) ΔGRK2/3 cells. e) Table showing EC50 and maximum response as a % of maximum DAMGO response for each ligand in each cell condition, with standard error of the mean (SEM), N-number (N), and significance as a difference from control HEK in an unpaired T-Test, corrected for multiple comparisons using a Holm-Šídák test (*: p ≤ 0.05; **: p ≤ 0.005)*

### 2.3.1.4 Effect of GRK5/6 CRISPR Knockout on MOR Agonist Responses in a ß-arrestin2 Recruitment Assay

In order to assess the role of GRK5/6 family knockout, single and double GRK knockout cells were assessed against the control HEKs described in section 2.3.1.2.

GRK5 knockout shown in figure 2.3.1.4b exhibited very little change in Emax, and no significant changes in potency when compared to control HEKs for any of the ligands. GRK6 knockout shown in figure 2.3.1.4c showed greater, but not significant decreases for DAMGO and fentanyl responses. In combination, GRK5/6 knockout shown in figure 2.3.1.4d exhibited similar effects, with no significant decreases in Emax, and no significant change in potency compared to control HEKs for any of the ligands.

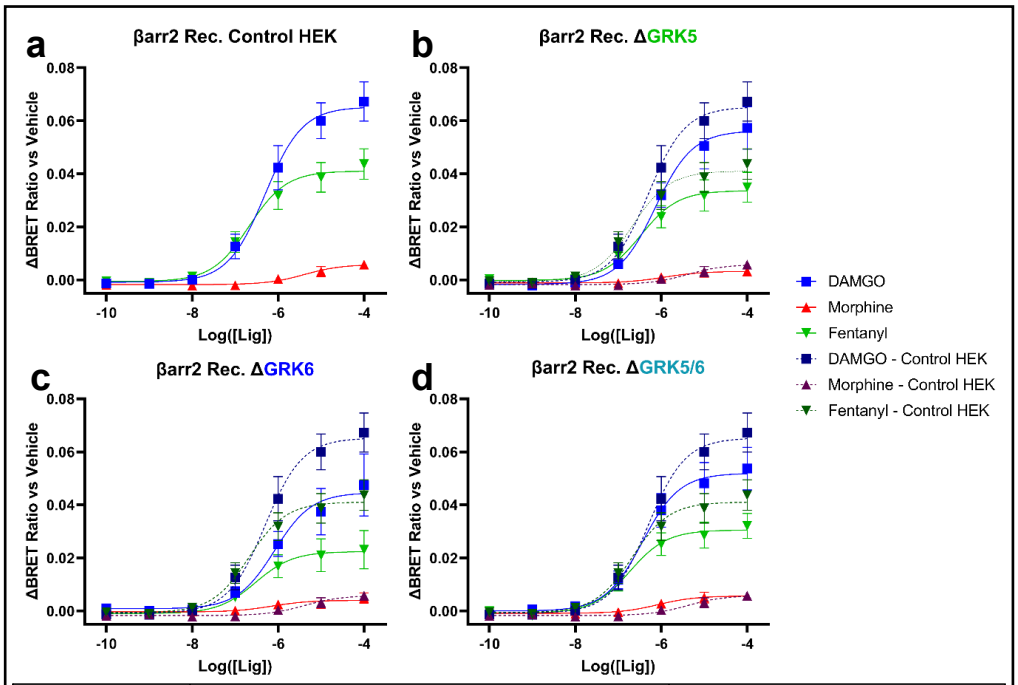


**e**

| Cell Line | Potency (Log(EC50)) | | | | | | | | | | | | % Max DAMGO Response | | | | | | | |
|---|---|---|---|---|---|---|---|---|---|---|---|---|---|---|---|---|---|---|---|---|
| | DAMGO | | | | Morphine | | | | Fentanyl | | | | Morphine | | | | Fentanyl | | | |
| | Mean | SEM | N | Sig. | Mean | SEM | N | Sig. | Mean | SEM | N | Sig. | Mean | SEM | N | Sig. | Mean | SEM | N | Sig. |
| Control HEK | -6.26 | 0.16 | 5 | | -5.37 | 0.32 | 5 | | -6.63 | 0.15 | 5 | | 13.8 | 1.88 | 5 | | 63.8 | 3.26 | 5 | |
| ΔGRK5 | -6.17 | 0.04 | 4 | | -6.16 | 0.33 | 4 | | -6.45 | 0.09 | 5 | | 9.5 | 1.02 | 5 | | 60.4 | 1.83 | 5 | |
| ΔGRK6 | -6.34 | 0.26 | 5 | | -6.25 | 0.28 | 5 | | -6.74 | 0.14 | 5 | | 20.9 | 10.70 | 5 | | 59.7 | 10.11 | 5 | |
| ΔGRK5/6 | -6.41 | 0.11 | 5 | | -5.94 | 0.33 | 4 | | -6.72 | 0.11 | 5 | | 14.1 | 1.45 | 4 | | 60.0 | 1.76 | 5 | |

*Figure 2.3.1.4, β-arrestin2-YFP recruitment to MOR-Nluc BRET mean ± SEM concentration response curves with varied opioid ligands (log(M)) (DAMGO (Blue), Morphine (Red), Fentanyl (Green) at 10 mins post-ligand addition in a) control HEK293 cells. b, c, d) control HEK293 cell concentration response curves (dashed lines) overlaid (DAMGO – Dark Blue, Morphine – Purple, Fentanyl – Dark Green) on concentration response curves conducted in CRISPR-generated b) ΔGRK5 cells. c) ΔGRK6 cells. d) ΔGRK5/6 cells. e) Table showing EC50 and maximum response as a % of maximum DAMGO response for each ligand in each cell condition, with standard error of the mean (SEM), N-number (N), and significance as a difference from control HEK in an unpaired T-Test, corrected for multiple comparisons using a Holm-Šídák test (*: p ≤ 0.05; **: p ≤ 0.005).*

### 2.3.1.5 Effect of Quadruple-GRK Knockout on MOR Agonist Responses in a β-arrestin2 Recruitment Assay

We next characterised the effects of a full GRK isoform knockout using the quadruple GRK KO cells (ΔQ-GRK). As shown in figure 2.3.1.5b, knockout of all four GRK isoforms showed a near complete abrogation of β-arrestin2 recruitment. As shown in figure 2.3.1.5c, we can detect very small levels of response, and at the top concentration of DAMGO (10 µM), results are significantly different from 0 (P = 0.0396) as measured by a one sample T-

test, whereas this is not the case for top concentrations of morphine or fentanyl (P = 0.2938, 0.1915 respectively).

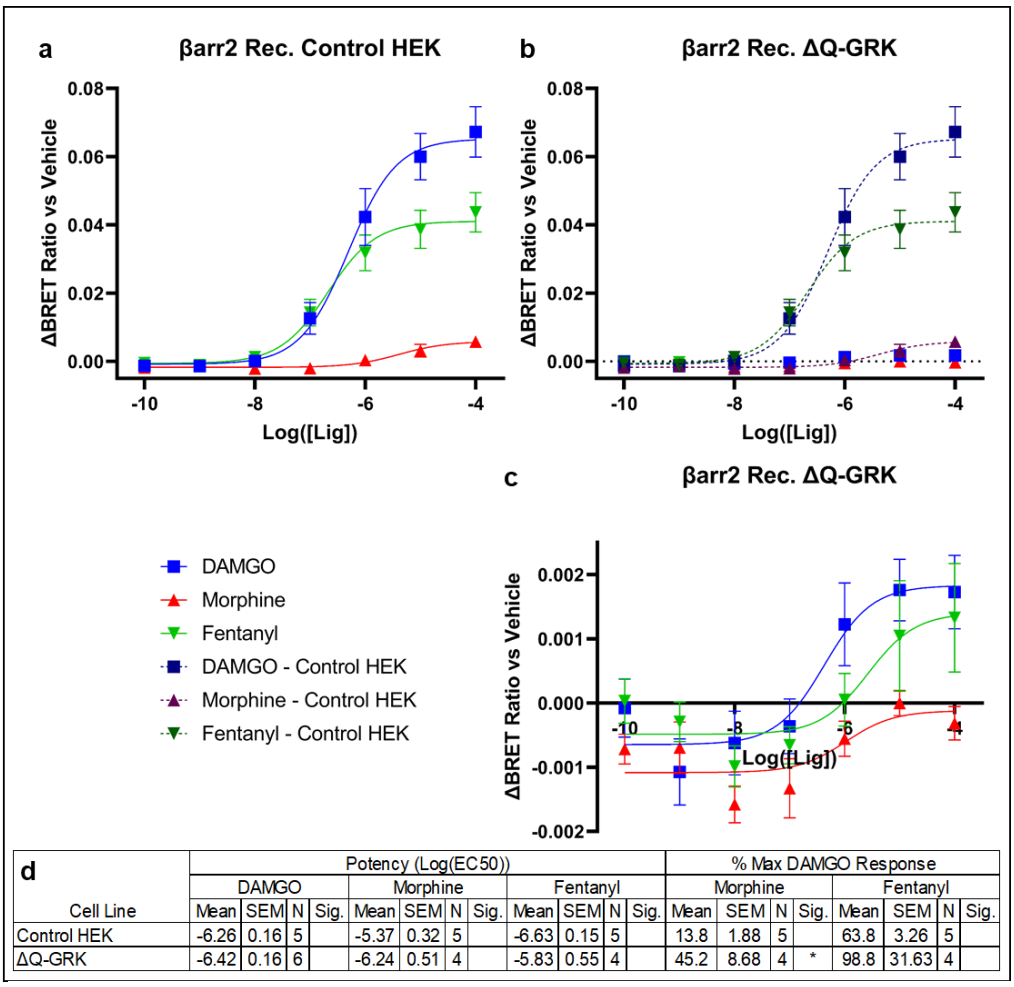


**d**

| Cell Line | Potency (Log(EC50)) | | | | | | | | | | | | % Max DAMGO Response | | | | | | | |
|---|---|---|---|---|---|---|---|---|---|---|---|---|---|---|---|---|---|---|---|---|
| | DAMGO | | | | Morphine | | | | Fentanyl | | | | Morphine | | | | Fentanyl | | | |
| | Mean | SEM | N | Sig. | Mean | SEM | N | Sig. | Mean | SEM | N | Sig. | Mean | SEM | N | Sig. | Mean | SEM | N | Sig. |
| Control HEK | -6.26 | 0.16 | 5 | | -5.37 | 0.32 | 5 | | -6.63 | 0.15 | 5 | | 13.8 | 1.88 | 5 | | 63.8 | 3.26 | 5 | |
| ΔQ-GRK | -6.42 | 0.16 | 6 | | -6.24 | 0.51 | 4 | | -5.83 | 0.55 | 4 | | 45.2 | 8.68 | 4 | * | 98.8 | 31.63 | 4 | |

*Figure 2.3.1.5, β-arrestin2-YFP recruitment to MOR-Nluc BRET mean ± SEM concentration response curves with varied opioid ligands (log(M)) (DAMGO (Blue), Morphine (Red), Fentanyl (Green) at 10 mins post-ligand addition in a) control HEK293 cells. b) control HEK293 cell concentration response curves (dashed lines) overlaid (DAMGO – Dark Blue, Morphine – Purple, Fentanyl – Dark Green) on concentration response curves conducted in CRISPR-generated quadruple GRK knockout cells. c) quadruple GRK knockout cells. d) Table showing EC50 and maximum response as a % of maximum DAMGO response for each ligand in each cell condition, with standard error of the mean (SEM), N-number (N), and significance as a difference from control HEK in an unpaired T-Test, corrected for multiple comparisons using a Holm-Šídák test (*: p ≤ 0.05)*

### 2.3.1.6 Effect of re-introducing individual GRK isoforms on MOR β-arrestin2 Recruitment

While individual KO of a single GRK isoform may suggest the contribution of that isoform to the response detected, it is still possible that in the absence of that particular isoform, other isoforms compensate its loss. To ascertain the role of individual GRKs, each GRK isoform was transfected alongside β-arrestin2-YFP and the MOR-NLuc into the ΔQ-GRK knockout background.

As shown in figure 2.3.1.6b, GRK2 reintroduction in a ΔQ-GRK KO background amplifies the response of all ligands even beyond the responses obtained in control HEK cells. Emax and potencies are significantly higher for all ligands. Interestingly, a similar effect was observed with GRK3 reintroduction,

suggesting that GRK3 may compensate the lack of GRK2. We observed a separation of ligand efficacies upon reintroduction of GRK5 with arrestin recruitment being rescued (above control responses) for all ligands, although maintaining the order of efficacies observed in the Control cells.

Interestingly, reintroduction of GRK6 shown in figure 2.3.1.6f marginally improved the responses of all ligands compared to Control cells.

*Figure 2.3.1.6, β-arrestin2-YFP recruitment to MOR-Nluc BRET mean ± SEM concentration response curves with varied opioid ligands (log(M)) (DAMGO (Blue), Morphine (Red), Fentanyl (Green) at 10 mins post-ligand addition in a) control HEK293 cells. b) quadruple GRK knockout HEK293 cells. c, d, e, f,) control HEK293 cell concentration response curves (dashed lines) overlaid (DAMGO – Dark Blue, Morphine – Purple, Fentanyl – Dark Green) on concentration response curves conducted in quadruple GRK knockout HEK293 cells co-transfected with c) ΔGRK2 cells. d) ΔGRK3 cells. e) ΔGRK5. f) GRK6. g, h, i) Maximal response values (Emax) taken from concentration response curves described in a-f, for each ligand used; g) DAMGO. h) Morphine. i) Fentanyl. j) Table showing EC50 and maximum response as a % of maximum DAMGO response for each ligand in each cell condition, with standard error of the mean (SEM), N-number (N), and significance as a difference from control HEK in an unpaired T-Test, corrected for multiple comparisons using a Holm-Šídák test (*: p ≤ 0.05; **: p ≤ 0.005; ***: p ≤ 0.0005; ****: p ≤ 0.00005)*

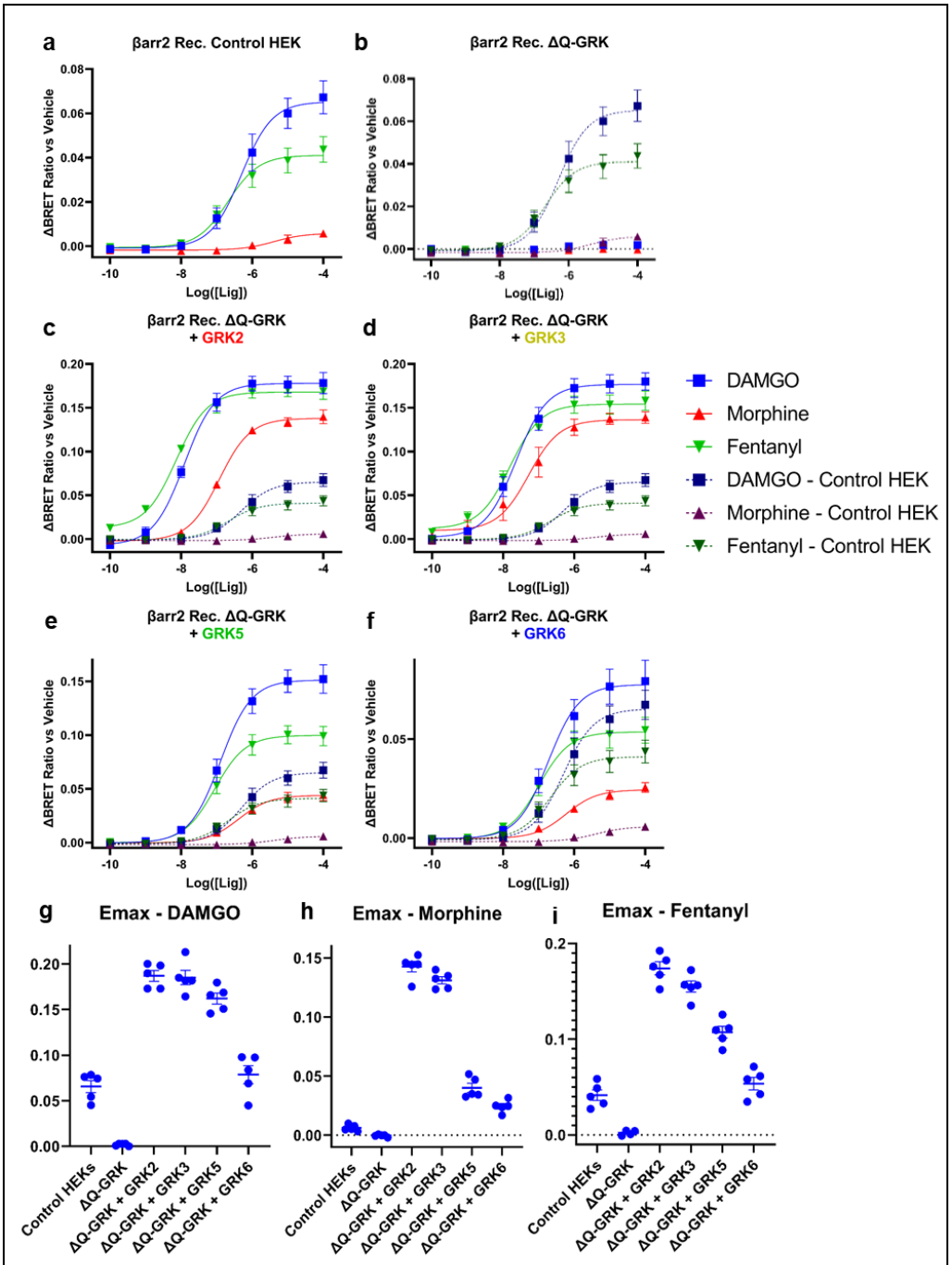


| | Potency (Log(EC50)) | | | | | | | | | | | | % Max DAMGO Response | | | | | | | |
|---|---|---|---|---|---|---|---|---|---|---|---|---|---|---|---|---|---|---|---|---|
| | DAMGO | | | | Morphine | | | | Fentanyl | | | | Morphine | | | | Fentanyl | | | |
| Cell Line | Mean | SEM | N | Sig. | Mean | SEM | N | Sig. | Mean | SEM | N | Sig. | Mean | SEM | N | Sig. | Mean | SEM | N | Sig. |
| Control HEK | -6.26 | 0.16 | 5 | | -5.37 | 0.32 | 5 | | -6.63 | 0.15 | 5 | | 13.8 | 1.88 | 5 | | 63.8 | 3.26 | 5 | |
| ΔQ-GRK | -6.42 | 0.16 | 6 | | -6.24 | 0.51 | 4 | | -5.83 | 0.55 | 4 | | 45.2 | 8.68 | 4 | * | 98.8 | 31.63 | 4 | |
| ΔQ-GRK + GRK2 | -7.92 | 0.05 | 6 | **** | -6.93 | 0.05 | 6 | *** | -8.15 | 0.10 | 6 | **** | 78.3 | 2.34 | 6 | **** | 94.7 | 3.67 | 6 | *** |
| ΔQ-GRK + GRK3 | -7.76 | 0.09 | 5 | **** | -6.97 | 0.02 | 5 | ** | -7.96 | 0.13 | 5 | *** | 71.5 | 2.34 | 5 | **** | 82.8 | 0.81 | 5 | *** |
| ΔQ-GRK + GRK5 | -6.87 | 0.09 | 6 | * | -6.40 | 0.06 | 6 | * | -7.04 | 0.08 | 6 | * | 29.8 | 2.86 | 6 | ** | 65.9 | 2.29 | 6 | |
| ΔQ-GRK + GRK6 | -6.71 | 0.15 | 5 | | -6.24 | 0.05 | 5 | * | -6.99 | 0.06 | 5 | | 33.3 | 2.51 | 5 | *** | 69.9 | 3.30 | 5 | |

### 2.3.2 Assessment of MOR ability to recruit miniGsi in GRK isoform KO cells

While GRKs have been implicated in scavenging of Gβγ subunits of the heterotrimeric G protein, they do not directly affect initial G protein binding to the GPCR. To assess the effects of GRKs on MOR activation and G protein signalling, we tested the effect of individual GRK KO on G protein recruitment to the MOR using a miniGsi recruitment assay in CRISPR generated GRK knockout cells. While GRKs are not thought to be involved in mGsi recruitment, any observed changes may give an indication on how the presence or absence of any GRK isoform affects MOR signalling and or expression. In general, we observed much more limited changes in the response in GRK knockout cells in mGsi recruitment compared to those observed in the arrestin recruitment assay described in section 2.3.1. Interestingly, similar changes were observed upon the reintroduction of individual GRK isoforms into the GRK-null background.

#### *2.3.2.1 Role of Small Molecule Inhibition and Over Expression of GRKs on MOR Agonist Responses in a miniGsi Recruitment Assay*

Similar to the β-arrestin2 assay, we used methods that allowed the study of the effects of GRKs in cells not altered by CRISPR, using the small molecule inhibitor compound 101, and transient overexpression of GRK2.

In HEK293T WT cells shown in figure 2.3.2.1a, DAMGO and fentanyl have similar potencies and Emax, while morphine exhibits around 65% of their maximal response and lower potency. For all ligands, potency for the mGsi pathway is higher than in the β-arrestin2 recruitment assay.

The HEK293T WT cells overexpressing GRK2 shown in figure 2.3.2.1b exhibit similar patterns of relative response, however the Emax for each ligand is increased for all ligands while only the increase in potency of fentanyl is significant. Interestingly, a similar change can be seen upon treatment with compound 101 shown in figure 2.3.2.1c, although in this case none of the potency shifts are significant for any of the ligands.

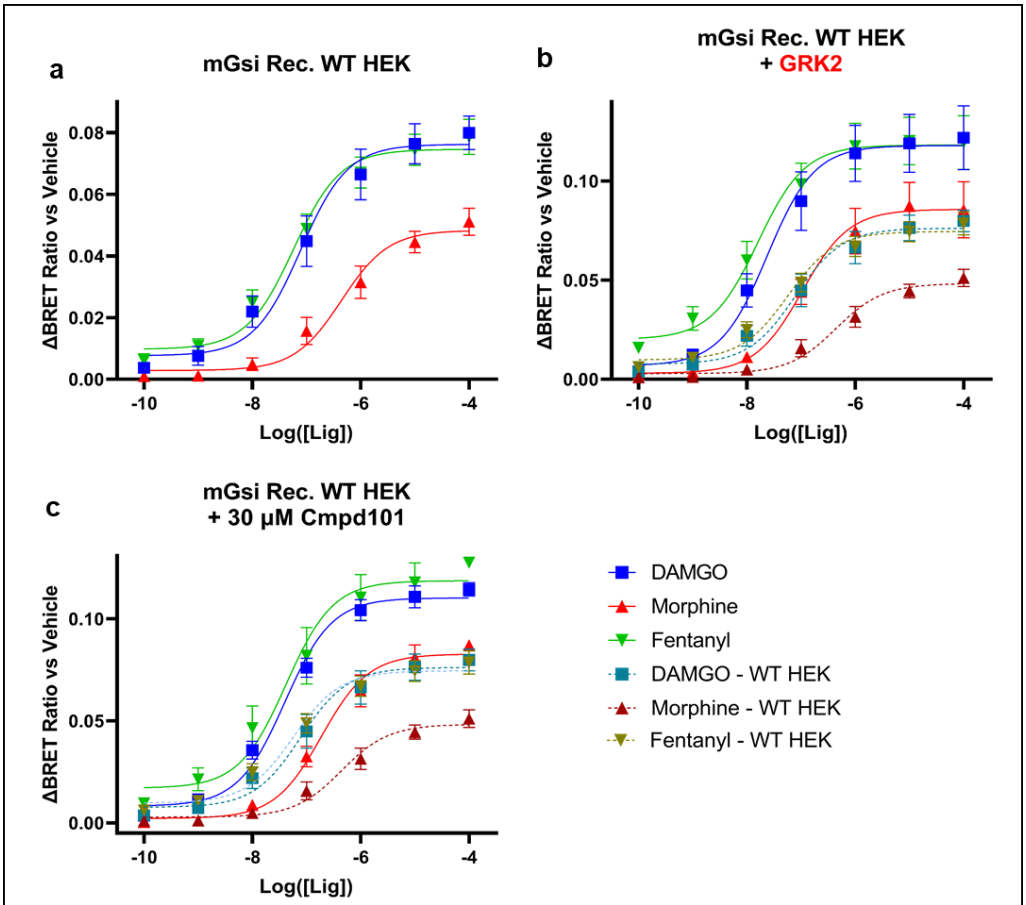


**d**

| Cell Line | Potency (Log(EC50)) | | | | | | | | | | | | % Max DAMGO Response | | | | | | | |
|---|---|---|---|---|---|---|---|---|---|---|---|---|---|---|---|---|---|---|---|---|
| | DAMGO | | | | Morphine | | | | Fentanyl | | | | Morphine | | | | Fentanyl | | | |
| | Mean | SEM | N | Sig. | Mean | SEM | N | Sig. | Mean | SEM | N | Sig. | Mean | SEM | N | Sig. | Mean | SEM | N | Sig. |
| WT HEK | -7.10 | 0.25 | 5 | | -6.36 | 0.33 | 5 | | -7.28 | 0.17 | 5 | | 64.2 | 1.45 | 5 | | 95.5 | 1.74 | 5 | |
| WT HEK + GRK2 | -7.58 | 0.14 | 6 | | -6.96 | 0.09 | 6 | | -7.78 | 0.08 | 6 | * | 71.2 | 3.84 | 6 | | 101.2 | 4.87 | 6 | |
| WT HEK + Cmpd101 | -7.44 | 0.10 | 5 | | -6.71 | 0.13 | 5 | | -7.46 | 0.20 | 5 | | 74.5 | 3.10 | 5 | * | 106.8 | 5.18 | 5 | |

*Figure 2.3.2.1, mGsi-Venus recruitment to MOR-Nluc BRET mean ± SEM concentration response curves with varied opioid ligands (log(M)) (DAMGO (Blue), Morphine (Red), Fentanyl (Green) at 10 mins post-ligand addition in a) Wild Type (WT) HEK293T cells. b) HEK293 cells transfected with CRISPR/Cas9 plasmids with no guideRNA co-transfected, with WT HEK concentration response curves overlaid (DAMGO – Teal, Morphine – Crimson, Fentanyl – Mustard). c) CRISPR-generated HEK293 ΔGRK2 cells, with WT HEK concentration response curves overlaid. d) Table showing EC50 and maximum response as a % of maximum DAMGO response for each ligand in each cell condition, with standard error of the mean (SEM), N-number (N), and significance as a difference from WT HEK in an unpaired T-Test, corrected for multiple comparisons using a Holm-Šídák test (*: p ≤ 0.05).*

### 2.3.2.2 Comparison of MOR Agonist Responses in a mGsi Recruitment Assay in two different Parental Cell Lines

As noted above, it is possible that the CRISPR process affects the signalling capacity of a cell. For this purpose, as for β-arrestin2 recruitment, we evaluated mGsi recruitment in Control cells, namely cells that have undergone the CRISPR selection process but retain full complement of GRK isoforms.

As shown in figure 2.3.2.2b, compared to HEK293T WT (above), the control HEK293 cells show slight increases in potency (although only significant for fentanyl). In terms of Emax, there is a significant increase for morphine from 65% to 90% of DAMGO.

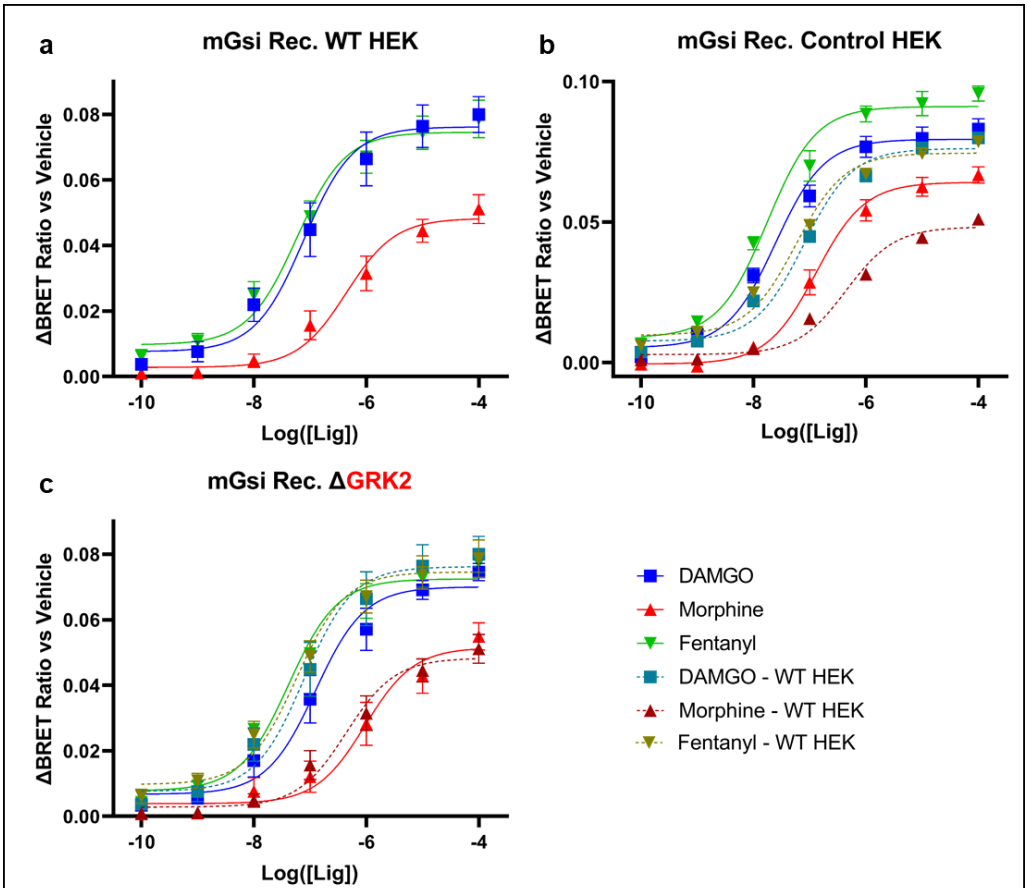


**d**

| Cell Line | Potency (Log(EC50)) DAMGO Mean | SEM | N | Sig. | Morphine Mean | SEM | N | Sig. | Fentanyl Mean | SEM | N | Sig. | % Max DAMGO Response Morphine Mean | SEM | N | Sig. | Fentanyl Mean | SEM | N | Sig. |
|---|---|---|---|---|---|---|---|---|---|---|---|---|---|---|---|---|---|---|---|---|
| WT HEK | -7.10 | 0.25 | 5 | | -6.36 | 0.33 | 5 | | -7.28 | 0.17 | 5 | | 64.2 | 1.45 | 5 | | 95.5 | 1.74 | 5 | |
| Control HEK | -7.61 | 0.05 | 5 | | -6.88 | 0.09 | 5 | | -7.74 | 0.04 | 5 | * | 89.7 | 8.68 | 5 | * | 108.3 | 6.50 | 5 | |
| ΔGRK2 | -6.86 | 0.25 | 5 | | -6.06 | 0.33 | 5 | | -7.38 | 0.05 | 5 | | 73.4 | 4.44 | 5 | | 101.3 | 3.73 | 5 | |

*Figure 2.3.2.2, mGsi-Venus recruitment to MOR-Nluc BRET mean ± SEM concentration response curves with varied opioid ligands (log(M)) (DAMGO (Blue), Morphine (Red), Fentanyl (Green) at 10 mins post-ligand addition in a) Wild Type (WT) HEK293T cells. b) HEK293 cells transfected with CRISPR/Cas9 plasmids with no guideRNA co-transfected, with WT HEK concentration response curves overlaid (DAMGO – Teal, Morphine – Crimson, Fentanyl – Mustard). c) CRISPR-generated HEK293 ΔGRK2 cells, with WT HEK concentration response curves overlaid. d) Table showing EC50 and maximum response as a % of maximum DAMGO response for each ligand in each cell condition, with standard error of the mean (SEM), N-number (N), and significance as a difference from WT HEK in an unpaired T-Test, corrected for multiple comparisons using a Holm-Šídák test (*: $p \leq 0.05$)*

### *2.3.2.3 Effect of GRK2/3 CRISPR Knockout on MOR Agonist Responses in a miniGsi Recruitment Assay*

In order to assess the role of GRK2/3 family knockout on mGsi recruitment, single and double GRK knockout cells were assessed against the control HEKs described in the previous section (figure 2.3.2.3a).

Compared to control HEK293 cells, GRK2 knockout significantly decreases potency in all ligands, however, although we observe decreases in the relative maximal response of all ligands, these are not significant. GRK3 knockout only significantly decreases the potency of fentanyl.

Combining these knockouts in the GRK2/3 KO cells has no significant effects in the potency of the three ligands.

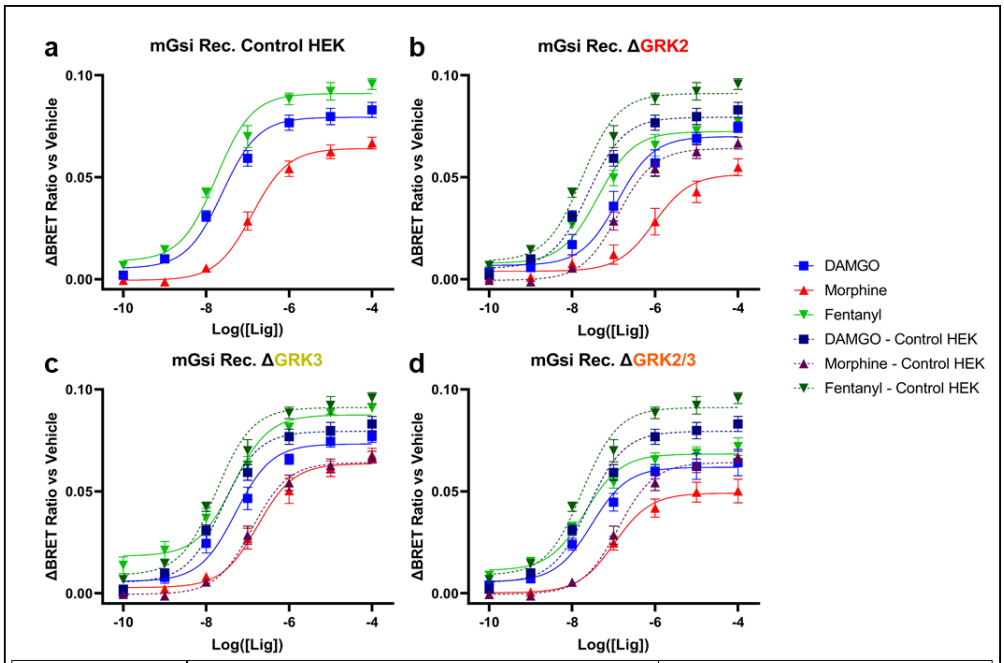


**e**

| | Potency (Log(EC50)) | | | | | | | | | | | | % Max DAMGO Response | | | | | | | |
|---|---|---|---|---|---|---|---|---|---|---|---|---|---|---|---|---|---|---|---|---|
| | DAMGO | | | | Morphine | | | | Fentanyl | | | | Morphine | | | | Fentanyl | | | |
| Cell Line | Mean | SEM | N | Sig. | Mean | SEM | N | Sig. | Mean | SEM | N | Sig. | Mean | SEM | N | Sig. | Mean | SEM | N | Sig. |
| Control HEK | -7.61 | 0.05 | 5 | | -6.88 | 0.09 | 5 | | -7.74 | 0.04 | 5 | | 89.7 | 8.68 | 5 | | 108.3 | 6.50 | 5 | |
| ΔGRK2 | -6.86 | 0.25 | 5 | * | -6.06 | 0.33 | 5 | * | -7.38 | 0.05 | 5 | ** | 73.4 | 4.44 | 5 | | 101.3 | 3.73 | 5 | |
| ΔGRK3 | -7.28 | 0.15 | 6 | | -6.57 | 0.20 | 6 | | -7.37 | 0.13 | 6 | * | 88.1 | 2.72 | 6 | | 118.5 | 3.21 | 6 | |
| ΔGRK2/3 | -7.52 | 0.12 | 5 | | -6.97 | 0.14 | 5 | | -7.66 | 0.10 | 5 | | 79.4 | 2.31 | 5 | | 114.4 | 6.55 | 5 | |

*Figure 2.3.2.3, mGsi-Venus recruitment to MOR-Nluc BRET mean ± SEM concentration response curves with varied opioid ligands (log(M)) (DAMGO (Blue), Morphine (Red), Fentanyl (Green) at 10 mins post-ligand addition in a) control HEK293 cells. b, c, d) control HEK293 cell concentration response curves (dashed lines) overlaid (DAMGO – Dark Blue, Morphine – Purple, Fentanyl – Dark Green) on concentration response curves conducted in CRISPR-generated b) ΔGRK2 cells. c) ΔGRK3 cells. d) ΔGRK2/3 cells. e) Table showing EC50 and maximum response as a % of maximum DAMGO response for each ligand in each cell condition, with standard error of the mean (SEM), N-number (N), and significance as a difference from control HEK in an unpaired T-Test, corrected for multiple comparisons using a Holm-Šídák test (*: $p \leq 0.05$; **: $p \leq 0.005$).*

### 2.3.2.4 Effect of GRK5/6 CRISPR Knockout on MOR Agonist Responses in a miniGsi Recruitment Assay

In order to assess the role of GRK5/6 family knockout, single and double GRK knockout cells were assessed against the control HEKs described in section 2.3.2.2 (figure 2.3.2.4)

GRK5 knockout does not change the potency of any ligand to recruit mGsi, however, fentanyl shows a significant increase in Emax relative to DAMGO. Similarly, GRK6 knockout showed no change in potency or Emax.

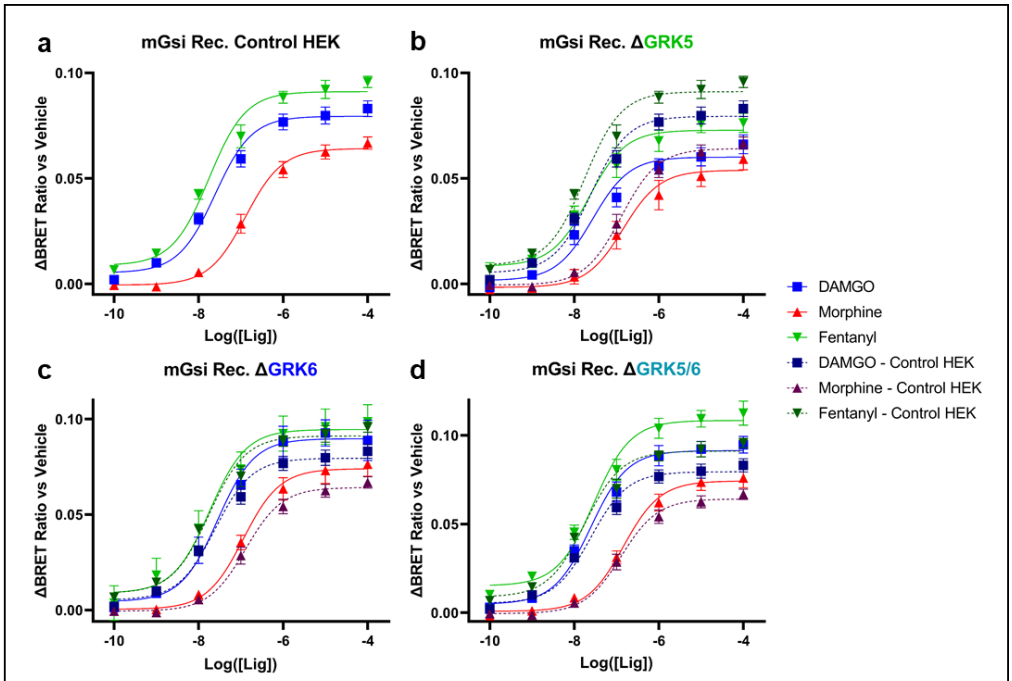


**e**

| Cell Line | Potency (Log(EC50)) | | | | | | | | | | | | % Max DAMGO Response | | | | | | | |
|---|---|---|---|---|---|---|---|---|---|---|---|---|---|---|---|---|---|---|---|---|
| | DAMGO | | | | Morphine | | | | Fentanyl | | | | Morphine | | | | Fentanyl | | | |
| | Mean | SEM | N | Sig. | Mean | SEM | N | Sig. | Mean | SEM | N | Sig. | Mean | SEM | N | Sig. | Mean | SEM | N | Sig. |
| Control HEK | -7.61 | 0.05 | 5 | | -6.88 | 0.09 | 5 | | -7.74 | 0.04 | 5 | | 89.7 | 8.68 | 5 | | 108.3 | 6.50 | 5 | |
| ΔGRK5 | -7.54 | 0.14 | 6 | | -6.73 | 0.17 | 6 | | -7.62 | 0.10 | 6 | | 91.3 | 3.71 | 6 | | 124.7 | 3.07 | 6 | * |
| ΔGRK6 | -7.52 | 0.10 | 5 | | -6.94 | 0.04 | 5 | | -7.70 | 0.10 | 5 | | 83.3 | 4.22 | 5 | | 112.6 | 11.39 | 5 | |
| ΔGRK5/6 | -7.59 | 0.08 | 5 | | -6.82 | 0.06 | 5 | | -7.53 | 0.09 | 5 | | 81.3 | 1.98 | 5 | | 121.4 | 5.91 | 5 | |

*Figure 2.3.2.4, mGsi-Venus recruitment to MOR-Nluc BRET mean ± SEM concentration response curves with varied opioid ligands (log(M)) (DAMGO (Blue), Morphine (Red), Fentanyl (Green) at 10 mins post-ligand addition in a) control HEK293 cells. b, c, d) control HEK293 cell concentration response curves (dashed lines) overlaid (DAMGO – Dark Blue, Morphine – Purple, Fentanyl – Dark Green) on concentration response curves conducted in CRISPR-generated b) ΔGRK5 cells. c) ΔGRK6 cells. d) ΔGRK5/6 cells. e) Table showing EC50 and maximum response as a % of maximum DAMGO response for each ligand in each cell condition, with standard error of the mean (SEM), N-number (N), and significance as a difference from control HEK in an unpaired T-Test, corrected for multiple comparisons using a Holm-Šídák test (*: $p \leq 0.05$)*

### 2.3.2.5 Effect of Quadruple-GRK CRISPR Knockout on MOR Agonist Responses in a miniGsi Recruitment Assay

We then conducted mGsi recruitment assays in quadruple GRK knockout cells (ΔQ-GRK), lacking GRK2,3,5 and 6 isoforms (figure 2.3.2.5b). In these cells can observe significant, but small decreases in Emax for all ligands. The potency of DAMGO and fentanyl also was significantly reduced, but not that of morphine.

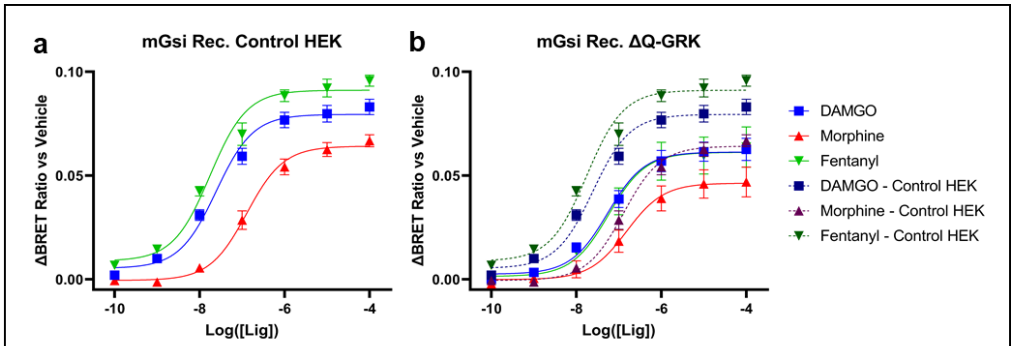


c

| Cell Line | Potency (Log(EC50)) | | | | | | | | | | | | % Max DAMGO Response | | | | | | | |
|---|---|---|---|---|---|---|---|---|---|---|---|---|---|---|---|---|---|---|---|---|
| | DAMGO | | | | Morphine | | | | Fentanyl | | | | Morphine | | | | Fentanyl | | | |
| | Mean | SEM | N | Sig. | Mean | SEM | N | Sig. | Mean | SEM | N | Sig. | Mean | SEM | N | Sig. | Mean | SEM | N | Sig. |
| Control HEK | -7.61 | 0.05 | 5 | | -6.88 | 0.09 | 5 | | -7.74 | 0.04 | 5 | | 89.7 | 8.68 | 5 | | 108.3 | 6.50 | 5 | |
| ΔQ-GRK | -7.29 | 0.09 | 5 | * | -6.81 | 0.09 | 5 | | -7.25 | 0.07 | 5 | *** | 75.9 | 6.67 | 5 | | 98.3 | 7.08 | 5 | |

*Figure 2.3.2.5, mGsi-Venus recruitment to MOR-Nluc BRET mean ± SEM concentration response curves with varied opioid ligands (log(M)) (DAMGO (Blue), Morphine (Red), Fentanyl (Green) at 10 mins post-ligand addition in a) control HEK293 cells. b) control HEK293 cell concentration response curves (dashed lines) overlaid (DAMGO – Dark Blue, Morphine – Purple, Fentanyl – Dark Green) on concentration response curves conducted in CRISPR-generated quadruple GRK knockout cells. c) quadruple GRK knockout cells. d) Table showing EC50 and maximum response as a % of maximum DAMGO response for each ligand in each cell condition, with standard error of the mean (SEM), N-number (N), and significance as a difference from control HEK in an unpaired T-Test, corrected for multiple comparisons using a Holm-Šídák test (*: p ≤ 0.05; **: p ≤ 0.005; ***: p ≤ 0.0005)*

### 2.3.2.6 Effect of re-introducing individual GRK isoforms on MOR a miniGsi Recruitment Assay

While individual KO of a single GRK isoform may suggest the contribution of that isoform to the response detected, it is still possible that in the absence of that particular isoform, other isoforms compensate its loss. To ascertain the role of individual GRKs, each GRK isoform was transfected alongside assay mGsi-Venus and MOR-NLuc into the ΔQ-GRK knockout background.

As shown in figure 2.3.2.6b, it was sufficient to overexpress GRK2 to revert the ΔQ-GRK mGsi response into a control HEK response, however, this was not the case when overexpressing GRK3, although the response was more variable. Similar to GRK3, GRK5 and GRK6 overexpression shows no change compared to quadruple knockout.

*Figure 2.3.2.6, mGsi-Venus recruitment to MOR-Nluc BRET mean ± SEM concentration response curves with varied opioid ligands (log(M)) (DAMGO (Blue), Morphine (Red), Fentanyl (Green) at 10 mins post-ligand addition in a) control HEK293 cells. b) quadruple GRK knockout HEK293 cells. a, c, d, e, f,) control HEK293 cell concentration response curves (dashed lines) overlaid (DAMGO – Dark Blue, Morphine – Purple, Fentanyl – Dark Green) on concentration response curves conducted in quadruple GRK knockout HEK293 cells co-transfected with c) ΔGRK2 cells. d) ΔGRK3 cells. e) ΔGRK5. f) GRK6. g, h, i) Maximal response values (Emax) taken from concentration response curves described in a-f, for each ligand used; g) DAMGO. h) Morphine. i) Fentanyl. j) Table showing EC50 and maximum response as a % of maximum DAMGO response for each ligand in each cell condition, with standard error of the mean (SEM), N-number (N), and significance as a difference from control HEK in an unpaired T-Test, corrected for multiple comparisons using a Holm-Šídák test (*: p ≤ 0.05; **: p ≤ 0.005; ***: p ≤ 0.0005)*

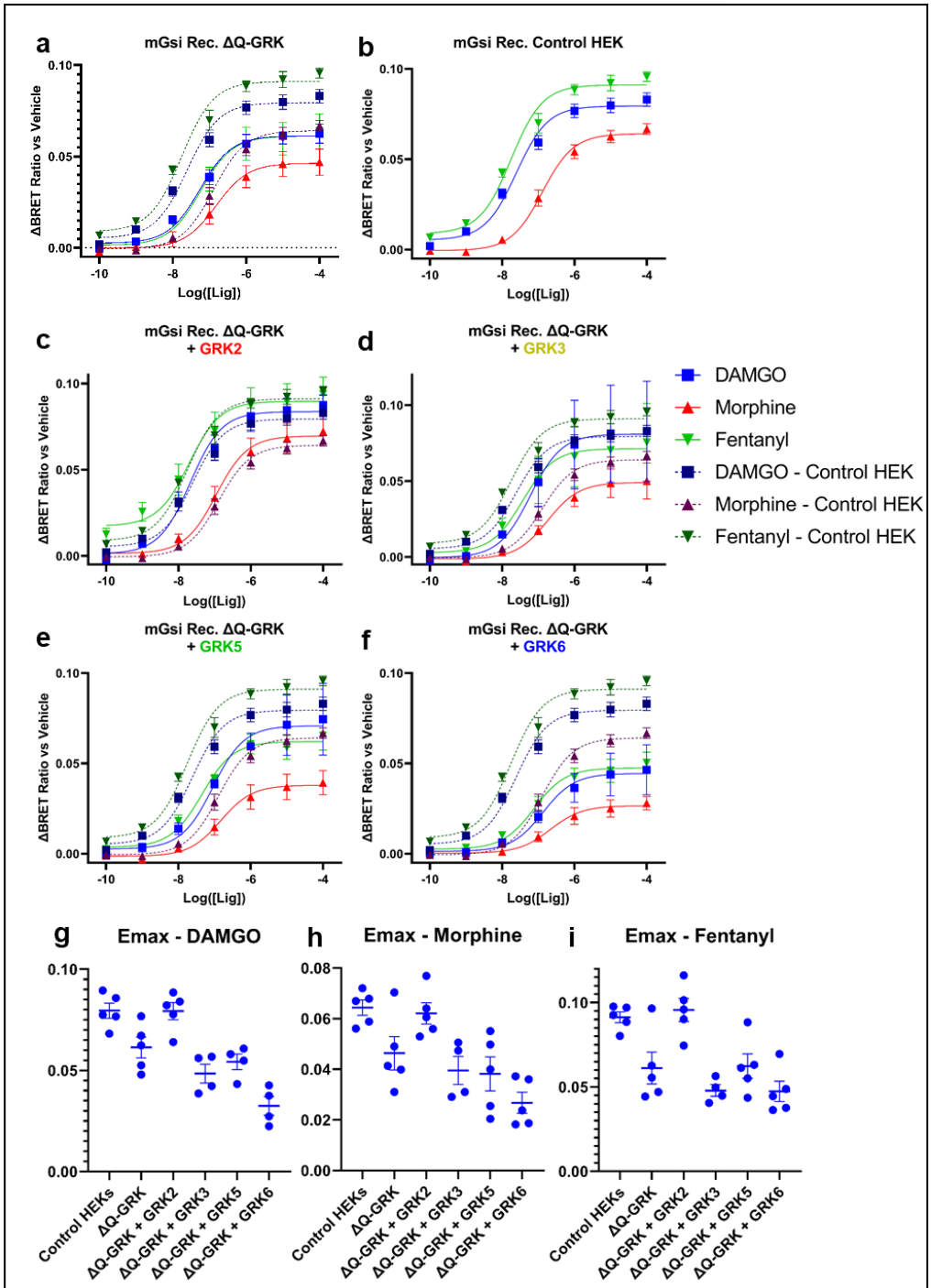


**j**

| Cell Line | Potency (Log(EC50)) | | | | | | | | | | | | % Max DAMGO Response | | | | | | | |
|---|---|---|---|---|---|---|---|---|---|---|---|---|---|---|---|---|---|---|---|---|
| | DAMGO | | | | Morphine | | | | Fentanyl | | | | Morphine | | | | Fentanyl | | | |
| | Mean | SEM | N | Sig. | Mean | SEM | N | Sig. | Mean | SEM | N | Sig. | Mean | SEM | N | Sig. | Mean | SEM | N | Sig. |
| Control HEK | -7.61 | 0.05 | 5 | | -6.88 | 0.09 | 5 | | -7.74 | 0.04 | 5 | | 89.7 | 8.68 | 5 | | 108.3 | 6.50 | 5 | |
| ΔQ-GRK | -7.29 | 0.09 | 5 | * | -6.81 | 0.09 | 5 | | -7.25 | 0.07 | 5 | *** | 75.9 | 6.67 | 5 | | 98.3 | 7.08 | 5 | |
| ΔQ-GRK + GRK2 | -7.64 | 0.09 | 6 | | -6.93 | 0.08 | 6 | | -7.73 | 0.12 | 6 | | 80.7 | 4.0 | 6 | | 109.5 | 6.4 | 6 | |
| ΔQ-GRK + GRK3 | -7.37 | 0.09 | 5 | * | -6.80 | 0.14 | 5 | | -7.51 | 0.05 | 5 | * | 74.3 | 8.2 | 5 | | 98.2 | 9.5 | 5 | |
| ΔQ-GRK + GRK5 | -7.25 | 0.26 | 5 | | -6.74 | 0.14 | 5 | | -7.46 | 0.15 | 5 | | 66.3 | 13.8 | 5 | | 94.3 | 8.7 | 5 | |
| ΔQ-GRK + GRK6 | -7.01 | 0.21 | 5 | * | -6.57 | 0.13 | 5 | | -7.16 | 0.19 | 5 | * | 74.9 | 13.9 | 5 | | 123.6 | 16.9 | 5 | |

## 2.4 Discussion

In this study, we used β-arrestin2 tagged with a Venus fluorescent protein on the C-terminal tail, first described by Angers et al., in 2000, to measure the level of recruitment of β-arrestin2 to the NLuc-tagged receptor upon agonist stimulation, indicated by an increase in BRET ratio.

We also used an engineered G protein that mimics G protein binding to the receptor. Originally used for structural studies and engineered as the miniGs protein (Carpenter and Tate, 2016), this protein comprises the GTPase domain of Gs, which binds and induces similar effects on the receptor as the original protein, however reduces its size and insolubility when compared to the full Gs protein. A similar rationale was used (Nehmé *et al.*, 2017) to generate a library of miniG proteins that mimic full sized G proteins. In this study, we used miniGsi (mGsi), a miniGs with the alpha5 helix, the main receptor binding surface, being mutated to that of Gi, forming a chimeric protein with Gi coupled receptor specificity, but miniGs stability. While these were generated to stabilise GPCRs for structural studies, the miniG proteins have been developed further for use in signalling assays (Wan *et al.*, 2018) such as the one demonstrated here, in which a Venus protein was tagged onto N terminus, to allow for BRET measurements to occur upon co-expression with luciferase-tagged receptors. Nuclear export sequences were also added to ensure localisations of miniG proteins to the cytosol for use in live cells.

These two assays provide unamplified, direct association data for the main two signalling and regulatory events selected by GPCRs, with good levels of sensitivity and previous literature of use in MOR studies and the GPCR field in general.

The MOR represents a prototypical GPCR where ligand-dependent regulation and signalling has been extensively described. While there is evidence of a phosphorylation barcode at the C-tail of the MOR, which varies depending on the agonist, it is still unclear which GRK isoforms participate in this mechanism. Here, we used 3 MOR agonists to address this question; DAMGO is a high efficacy reference agonist commonly used in lab settings, morphine is a clinically used opioid partial agonist which induces a distinct phosphorylation and regulation of the MOR when compared to other ligands, finally, fentanyl is a clinically use agonist, whose lipophilic properties have been recently highlighted (Comer and Cahill, 2019; de Waal *et al.*, 2020; Kelly *et al.*, 2023).

### 2.4.1 Functionality Assessment

In order to understand the role of each GRK in the transduction of ligand-dependent MOR signalling, we characterised each GRK knockout cell line for both their ability facilitate β-arrestin2 recruitment to the MOR, an event that

is directly affected by GRK activity, and the ability to recruit mGsi, an event that is not directly affected by the role of GRKs. We observed that knockouts of individual GRK isoforms and GRK families had differing responses in the two assays which were ligand-dependent. Similarly, we also observed distinct effects upon reintroduction of individual GRK isoforms into a GRK-null background.

#### *2.4.1.1 Previous Methods: Small Molecule and Over Expression*

In order to amplify β-arrestin recruitment BRET windows, multiple previous studies have commonly used overexpression of GRK2 to make the transient nature of the MOR-β-arrestin2 interaction more stable and robust, therefore detectable in assay methods (Zhang *et al.*, 1998; Miess *et al.*, 2018; Gillis, Batista-Gondin, *et al.*, 2020a). Comparing HEK293T WT with endogenous expression of GRKs to cells with GRK2 overexpression (figure 2.3.1.2c), the increased signal window obtained for all ligands, results in a loss of the differentiation between DAMGO and fentanyl observed in WT cells. However, it is under this condition (GRK2 overexpression), that morphine's response becomes more detectable.

The data gained from this comparison in the β-arrestin2 assay fit previous reports, with GRK2 overexpression allowing internalisation of the MOR upon treatment with morphine in imaging studies, an event that is much more limited with endogenous levels of GRK2 (Groer *et al.*, 2007). Interestingly, the role of fentanyl as a partial agonist compared to DAMGO in the β-arrestin2 assay under WT conditions is new, however, and does not match previously described responses when compared to DAMGO (Schmid *et al.*, 2017; de Waal *et al.*, 2020; Gomes *et al.*, 2020; Kelly *et al.*, 2023). Of note fentanyl has a series of outlying pharmacological characteristics affecting the results we see in these assays and making it especially prone to show differences in different assay systems. The main characteristic leading to these differences is its high lipophilicity, allowing fentanyl to embed in the plasma membrane (Kelly *et al.*, 2023). This can have varying effects, from increasing local concentration of fentanyl around MORs, to diluting the free pool of fentanyl through fat-sequestration or assay-vessel non-specific binding. These aspects may explain the differences observed between fentanyl's behaviour in this assay and fentanyl's behaviour in other assays.

As expected inhibition of GRK2 and 3 by compound 101 (figure 2.3.1.1c) decreases DAMGO and fentanyl response in the β-arrestin2 recruitment assay. However, the limited level of decrease is unexpected, as total inhibition of the main two GRK isoforms reported to act on MOR would be expected to almost abolish recruitment (Møller *et al.*, 2020; Pedersen *et al.*, 2020; Drube *et al.*, 2022). Similarly, the increase in response from morphine

compared to the Emax in wild type is unexpected. Reasons for this and comparisons to different cell lines will be explored in the next section.

Interestingly, overexpression of GRK2 increases responses of all ligands in the mGsi assay. An explanation for this effect could be that upon overexpression of GRK2, more MOR reaches the plasma membrane, effectively increasing receptor expression. However, this remains to be assessed. A similar effect is also observed upon inhibition of GRK2 and GRK3 by compound 101, however, this could be explained by the lack of receptor desensitisation; upon inhibition of phosphorylation, G protein recruitment may be less limited, hence more detectable.

#### *2.4.1.2 Parental Cell Line Comparison*

When comparing the WT HEK293T cells used in our lab, to the CRISPR transfected control HEK293 cells, we can see clear differences in responses, particularly for β-arrestin recruitment. While the response to morphine stays essentially the same, we see much greater responses to DAMGO and fentanyl in the control HEK293 cells. An explanation for this observation would be that both cell lines have differential endogenous expression of GRK isoforms, more likely GRK2. This is supported by the effects of GRK2/3 inhibition by compound 101, which is much less effective than would be expected. Assuming the low GRK2 expression by WT cells, the effect of a GRK2/3 inhibitor will be compromised.

The suggestion that WT cells express lower levels of GRK2 than control cells is also supported by the similarities observed between WT and GRK2 knockout cells, which have near identical relative responses for each ligand, a similarity is also seen in the mGsi assay.

Thus, we suggest that the endogenous GRK isoform complement between the two parental cell lines is different. This could be validated by RNAseq or quantitative Western blot experiments in the future. However, it highlights the importance of using the corresponding parental cell lines in comparative CRISPR studies.

#### *2.4.1.3 GRK2/3 Family CRISPR Knockout*

Knockout of GRK2 has the most profound effect on opioid ligand responses as described previously (Møller *et al.*, 2020), with a large decrease in Emax across the ligands in the β-arrestin2 recruitment assay. Fentanyl appears to be especially reliant on GRK2, as it regularly shows significant changes in its relative response compared to DAMGO when GRK2 is affected. Upon knockout of GRK2, it exhibits a response compared to maximal DAMGO response of 45%. In WT cells, with assumed low GRK2, this remains unchanged. In control cells, this significantly increases to 65%, and with GRK2 overexpression, this significantly increases to nearly 90%. Therefore, we can conclude that fentanyl arrestin recruitment is significantly affected by GRK2

expression. These changes are not as consistent with morphine, as only the overexpression of GRK2 results is significant changes in the β-arrestin2 recruitment assay, and no changes are seen in control or GRK knockout cells, implying morphine is much less reliant on GRK2 to phosphorylate the receptor upon activation, and only when high concentrations of GRK2 are present is this overcome.

The data obtained in GRK3 knockout cells is highly variable, making interpretations of effect challenging, however there appears to be no significant change in response or potency with DAMGO and fentanyl. Morphine however exhibits significantly increased response and potency. This remains to be validated.

The GRK2/3 double knockout appears to combine the effects of the two single knockouts in the β-arrestin2 recruitment assay, with the decrease in DAMGO and Fentanyl response similar to that of GRK2 single KO, and the significant rise in morphine response and potency observed upon GRK3 KO (although this effect is smaller in the double KO, likely by the knockout of GRK2). The effect of these single and double KOs supports the hypothesis that WT HEK293T cells express low levels of GRK2.

Interestingly, in combination, these responses to knockout suggest an inhibitory effect of GRK3 on morphine response as morphine is able to exhibit enhanced responses upon its single or double knockout, as well as upon small molecule inhibition. This effect does not appear to be completely reliant on GRK2 either, as although responses are reduced in GRK2/3 knockout over GRK3 knockout, the response exhibits similarly significant potency changes and responses above control. This could be explained by the role of GRK5/6, which will be explored later in this thesis, in section 4.1.1.

The effects of the GRK2/3 knockout in the mGsi assay are much less pronounced as would be expected from an assay which measures direct interactions of a miniaturised G protein and receptors, unlikely to be influenced by receptor phosphorylation.

Given the previous literature and the roles of GRK2 and GRK3 on MOR, the data gathered here is in general agreement. GRK2 has been previously shown to have greater effects on MOR desensitisation and arrestin recruitment then GRK3 (Møller *et al.*, 2020), and this is supported here, shown by the much clearer effects of GRK2 knockout on β-arrestin2 recruitment than GRK3. Similarly, the presence of GRK2/3 independent β-arrestin2 recruitment (Møller *et al.*, 2020) was here confirmed. The effects of GRK3 knockout on morphine however has not previously been shown and warrants further exploration as to the role of GRK3 in morphine-induced MOR desensitisation.

#### 2.4.1.4 GRK5/6 Family CRISPR Knockout

Comparing control cells to GRK5 and GRK6 family knockouts, we observe smaller effects than the ones observed in the GRK2/3 family knockouts. GRK5 knockout does not show significant effects on the ability of any ligand to recruit arrestin. Previous literature reports suggests that morphine-induced receptor phosphorylation relies on GRK5 (Glück *et al.*, 2014). It may be however that in single knockout cells, the effects of eliminating GRK5 are masked by the redundancy provided by the other GRK isoforms. Similarly, GRK6 showed no significant changes compared to control cells. In combination, knockout of both GRK5 and 6 produced no significant changes from control, suggesting redundancy from GRK6 is not the cause for the discrepancy between literature and the data here with regards to morphine and GRK5 (Glück *et al.*, 2014).

In the mGsi assay, as with GRK2/3 KOs, we see very limited changes in the ability of the ligands to recruit mGsi.

#### 2.4.1.5 Quadruple GRK CRISPR Knockout

While single and family knockouts provide insights as to what changes are observed when particular GRKs are removed, a full knockout background provides insights as to the role of other kinases within the cell on MOR function. The complete knockout of the main kinases that phosphorylate the MOR slightly reduces the ability of all ligands to recruit miniGsi. Given the importance of these GRKs, and the effect of their knockout on cell health (Drube *et al.*, 2022), the limited nature of the change in MOR ability to recruit mGsi highlights the limited size of direct effect we are likely observing. The reduced response in mGsi recruitment may be due to a multitude of factors, such as reduced cell surface expression of receptor, or more complicated factors, such as lack of Gβγ subunit scavenging, and therefore greater residency time of endogenous Gα subunits on the receptor, blocking mGsi recruitment. This could be investigated by imaging experiments or other methods of assessing cell surface expression such as radioligand binding, as well as directly assessing G protein activity using BRET constructs.

Quadruple-GRK knockout provides clear evidence of the important role of GRKs 2, 3 ,5 and 6 in arrestin recruitment to the MOR, however the small but concentration-dependent response in recruitment observed with increasing concentrations of DAMGO shown in figure 2.2.3.5b highlights that non-GRK kinases can still mediate a residual level of arrestin recruitment to the receptor. For example, this could suggest an effect of PKC, and its ability to phosphorylate the C-tail of arrestin at particular residues, namely S363 and T370 (El Kouhen *et al.*, 2001; C. Bailey *et al.*, 2009). These residues have been implicated in arrestin internalisation (Doll *et al.*, 2011; Feng, Li and Wang, 2011; Chen *et al.*, 2013) and may increase arrestin affinity for the receptor in the absence of GRKs. Another factor may be the inherent affinity of the

receptor core for arrestin increasing upon ligand activation and transition to an active conformation. Core binding with the finger loop region of arrestin is an important step in stable arrestin binding (Latorraca *et al.*, 2018; Haider *et al.*, 2022), and while transient, may account for the small changes we see in the quadruple-GRK knockout cells. Finally, another explanation may be the effects of GRK isoforms not removed by the CRISPR process, such as GRK4 (Premont *et al.*, 1996). While this is a possibility, examination of expression of these GRKs by transcriptomics or immunoblotting may exclude this possibility. However, the small nature of the changes seen highlights that any GRKs not knocked out have very little to no effect on MOR-arrestin interactions.

#### *2.4.1.6 GRK Rescue*

Quadruple knockout also provides a background to reintroduce GRK isoforms and study their effects individually. As we can see in figure 2.3.1.6, reintroduction of GRK2, 3 and 5 rescues the β-arrestin recruitment responses for all ligands, albeit to different extents, the effect of GRK5 overexpression being smaller. Re-introduction of GRK6, however, while it still rescues some arrestin recruitment is significantly less effective than the KO of the other three isoforms. These changes are expected, with GRK2 and GRK3 having been shown to have the greatest effects on MOR desensitisation (Doll *et al.*, 2012; Møller *et al.*, 2020), and GRK5 having a strong effect on a more limited set of phosphosites (Glück *et al.*, 2014), whereas GRK6 remains under-studied, and shows very little effect on MOR desensitisation.

### 2.4.2 Methods of Studying GRKs

As we have observed in the later sections of the results, we can see clear differences in the recruitment of arrestin with different opioid ligands in different GRK knockout lines. Morphine has shown, contradictory to literature reports (Glück *et al.*, 2014), a much lower recruitment of GRK5 over DAMGO or fentanyl, as exhibited in figure 2.3.1.6. We also see that fentanyl makes greater use of GRK2 over GRK3, shown by a drop in Emax between the two overexpression conditions.

Overexpression in a null GRK background such as that exhibited in the quadruple knockout cells appears to give clear information about the GRK isoforms that can contribute to the arrestin recruitment induced by different ligands. Screening ligands in this way may prove useful in generating data as to the GRK selectivity of different ligands, perhaps more so than in triple knockout cells that express endogenously a single GRK. Overexpression, however, does have disadvantages, affecting the transfection efficiency or expression of the assay machinery when co-transfecting a large amount of DNA and potentially forcing interactions that would not have high enough affinity to occur under native cellular conditions, making interpretations of selectivity challenging. In this way then, Triple knockout cells may provide

further information. However, it is important to note that certain pathophysiological conditions may exhibit heightened expression of GRKs, such as the overexpression of GRK2 in heart failure (Lymperopoulos, Rengo and Koch, 2012), thus overexpression of GRK isoforms can mirror such situations.

In the context of physiological relevance, it is important to consider GRK isoform expression in the areas where the MOR is expressed. RNA expression provides evidence for expression levels where direct protein measurements are unavailable and have been studied in many cell types in the brain. GRK2 appears to be the most common and is the most highly expressed in all regions of the brain, as shown in figure 2.4.2.1. Generally, this is followed by GRK3, then GRK6, and finally GRK5, however levels vary depending on brain region, highlighting the complexity and likely variability of responses that will arise endogenously (Karlsson et al., 2021; The Human Protein Atlas).

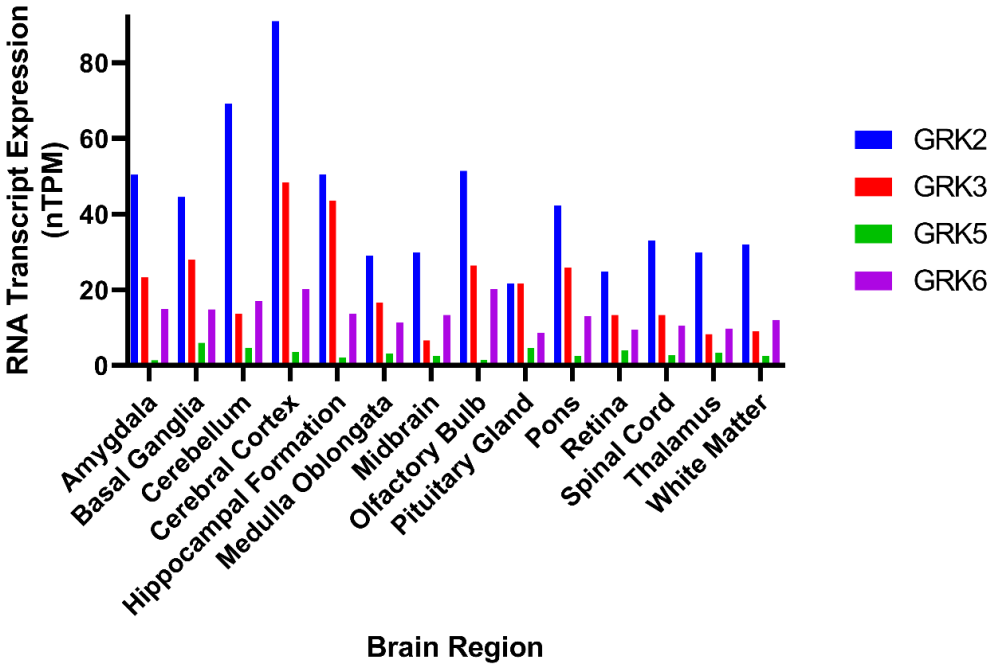


*Figure 2.4.2.1, RNA Transcript expression of GRKs split by brain region, adapted from Functional Annotation of Mammalian Genomes 5 (FANTOM5) data set, transcript expression levels summarized per gene in 14 brain regions, described in The Human Protein Atlas (proteinatlas.org).*

More specifically for MOR signalling, the dorsal root ganglion, or DRG, plays a major role in nociception, and has been studied to much greater depth (Usoskin *et al.*, 2015). Here, neuronal clusters were grouped by their expression of RNA markers identifying their function and highlight the variability of GRK expression.

As shown in figure 2.4.2.2, different neuronal clusters within the DRG structure have varying levels of GRK isoform expression, with some neurons exhibiting no expression of particular GRK isoforms depending on their function. This highlights the variability in GRK expression that is produced,

and with ligand specific GRK effects, may help to understand the different effects of varying opioid ligands in different brain regions and structures.

With these differences in mind, it may be justified to use GRK2 overexpression in opioid studies, due to the differences we see between neuronal populations with high GRK2 expression, and the data observed in WT HEKs, which behave more closely to GRK2 knockout cell lines.

| | Myelinated Neurons | | | | | Non-Petidergic Nociceptors | | | Peptidergic Nociceptors | | Unmyelinated Neurons |
|---|---|---|---|---|---|---|---|---|---|---|---|
| | NH | | | | | NP | | | PEP | | TH |
| | NF1 | NF2/3 | | NF4/5 | | NP1 | NP2/3 | | PEP1 | PEP2 | |
| | | NF2 | NF3 | NF4 | NF5 | | NP2 | NP3 | | | |
| GRK2 | 0.323 | 0.188 | 0.083 | 0.227 | 0.115 | 0.728 | 0.438 | 0.250 | 0.313 | 0.412 | 0.554 |
| GRK3 | 0 | 0 | 0.083 | 0.045 | 0.038 | 0.096 | 0 | 0 | 0.016 | 0.118 | 0.124 |
| GRK5 | 0.032 | 0.042 | 0 | 0 | 0 | 0.064 | 0.063 | 0.167 | 0.016 | 0 | 0.034 |
| GRK6 | 0.323 | 0.104 | 0.167 | 0 | 0.231 | 0.216 | 0.250 | 0.333 | 0.078 | 0.294 | 0.275 |

*Table 2.4.2.2, RNAseq data from 799 single cells from the mouse lumbar DRGs, clustered by neuron population, showing expression level in reads per million of different GRKs for each neuronal population. Adapted from Usoskin et al, 2015.*

# Chapter 3: Assessment of the role of GRKs in Mu-opioid receptor dynamics at the plasma membrane

## 3.1 Introduction

Subcellular localisation, both in different compartments within the cell, as well as different regions on the plasma membrane, has been shown to have significant effects on the signalling properties of GPCRs (Calebiro *et al.*, 2009; Irannejad *et al.*, 2017; Stoeber *et al.*, 2018; Crilly *et al.*, 2021). The processes by which GPCRs, including the MOR, are removed (internalisation) and returned (recycling) to the membrane have been well studied (Irannejad and von Zastrow, 2014; Eichel and von Zastrow, 2018). Building on previous work from our group, this chapter focuses on the effects of GRKs on the translocation of the MOR across the plasma membrane.

### 3.1.1 MOR Trafficking

The removal of the MOR from the membrane has been extensively described. To be internalised, the MOR must bind arrestin, allowing the arrestin to bind adaptor molecules, such as AP2, which pull the arrestin-receptor complex into clathrin coated pits. These pits form endosomes and move away from the plasma membrane into the cell. From here, receptors can be recycled back to the cell surface, or degraded in lysosomes. The time taken to recycle or be degraded can be dependent on effector binding and post-translational modification (Irannejad and von Zastrow, 2014; Irannejad *et al.*, 2017; Eichel and von Zastrow, 2018).

At the plasma membrane, the MOR has been shown to be distributed into different lipid domains, which appear to be dependent on the cholesterol content of the membrane (Rogacki *et al.*, 2018). The ability of the MOR to translocate within and outside of these lipid domains depends on the agonist activating the receptor, both in terms of receptor translocation (Saulière-Nzeh *et al.*, 2010; Melkes, Hejnova and Novotny, 2016), as the well-known agonist-dependent internalisation (Whistler and von Zastrow, 1998; El Kouhen *et al.*, 2001; Doll *et al.*, 2011; Just *et al.*, 2013). However, the mechanisms underlying this ligand-dependence are still not clear. Moreover, substances such as ethanol have been shown to affect MOR translocation, altering its mobility and surface density, possibly through effects on plasma membrane lipids (Vukojević *et al.*, 2008). More generally, several studies have highlighted the role of cytoskeletal structures in restricting GPCR movement, thus creating GPCR "hotspots" and possibly facilitating receptor clustering (Sungkaworn *et al.*, 2017), although this has not been specifically investigated for the MOR.

Previous studies have shown that agonist stimulation causes the MOR to transit from a diffuse distribution within the plasma membrane to a clustering of receptors in clathrin coated pits following the binding of arrestin

to the activated receptor (Halls *et al.*, 2016). Further details of this reorganisation upon agonist activation have been elucidated by our group (Halls *et al.*, 2016). Using super-resolution microscopy and FRET-based biosensors, it was shown that DAMGO, but not morphine stimulation of the MOR resulted in receptor redistribution across the membrane and receptor internalisation. This limited morphine-mediated redistribution was mediated by PKC-dependent phosphorylation of the MOR, via the G protein complex Gβγ. These differences in receptor reorganisation were associated with differences in signalling outputs, such as differential responses in cytoplasmic and nuclear ERK activation. While these different effects were shown to be independent of clathrin pit formation, they seemed to be phosphorylation dependent, as similar effects were not observed upon mutation of all 11 putative phosphosites of the MOR C-tail to alanine.

Further work by Batista-Gondin *et al.*, in 2019, using fluorescence correlation spectroscopy (FCS) and fluorescence recovery after photobleaching (FRAP) has shown that high efficacy agonists, but not low efficacy agonists, induce membrane reorganisation of the MOR in a pertussis toxin insensitive manner. MOR stimulation causes a decrease in lateral diffusion in an internalisation-independent manner, requiring GRK2/3.

Altogether, the findings above suggested that GRKs may play an important role in the distribution of the MOR within the plasma membrane. As the new CRISPR-KO cells deficient in GRKs have recently become available, we used these cellular backgrounds to provide further insight into the role of these kinases on MOR dynamics at the PM using FCS.

### 3.1.2 Use of Fluorescence Correlation Spectroscopy (FCS) to Investigate GPCR Translocation

Fluorescence Correlation Spectroscopy (FCS) is a spectroscopic technique which uses the measurement of fluctuations in fluorescence intensity of fluorescent molecules over time from a small defined, open, illumination volume of ~0.2fL. These fluctuations in the detected fluorescence intensity occur when fluorescent molecules move into or out of the detection volume. From the time-dependency of these fluctuations, multiple parameters can be determined that provide information on the speed of movement and concentration of these fluorescent molecules. When the volume is located at the plasma membrane of the cell, and the fluorescent molecule is a fluorescently tagged receptor, FCS can therefore be used to quantify the dynamics of movement and number GPCRs at the cell surface (Briddon, Kilpatrick and Hill, 2018; Batista-Gondin *et al.*, 2019).

### 3.1.1 Development

Counting molecules as a function of time was first conducted in 1911 by Theodor Svedberg, who visually counted colloidal gold particles over time as

a method of assessing concentration (Inouye and The Svedberg, 1911). This process was of limited use, generally in chemistry, for assessing the rate of reaction for the creation of fluorescent or visually observable molecules. In 1972, the term Fluorescence Correlation Spectroscopy was first used, in its use for assessing the diffusion of DNA and the rate of binding of ethidium bromide, as it increased fluorescence intensity upon its conjugation to DNA (Magde, Elson and Webb, 1972, 1974). This increased detectability of the particles, with the fluorescent ethidium bromide able to produce large numbers of photons per molecule. Since then, improvements in optics have allowed smaller detection volume, from the order of 10s of picolitres (Magde, Elson and Webb, 1974) to tenths of femtolitres (Briddon, Kilpatrick and Hill, 2018), as well as improving both precision and accuracy of its positioning. Detectors are now more sensitive and can count single photons have shorter dead times and much lower dark counts. Shorter read times were facilitated by these changes, and cell measurements became possible without membrane drift, with the first report describing membrane based experiments published in 1999 (Schwille *et al.*, 1999).

### 3.1.2 FCS Configuration

In order to measure fluorescence fluctuations in a sufficiently small volume, the most commonly used method is using a confocal optical set up. First, a laser of a wavelength chosen that would excite the fluorophore in use is focused through an objective lens, which focuses the light onto the area under observation, creating a hyperboloid light pattern with a centre area defined by the diffraction limit. These objectives are selected for minimal aberrations in the lens and have a high numerical aperture. Emission light of longer wavelength is collected by the same objective lens, passing through the dichroic mirror, before passing through a confocal pinhole. Light from any fluorophores excited outside of the focal plane of the confocal volume will not pass through the pinhole and thus will not be detected. After the pinhole, a detector sensitive enough to detect single photons records the fluctuations in fluorescence intensity over time. By choosing the region on which the confocal volume is placed, fluorescence fluctuations can be measured in free solution, or on 2D structures such as a plasma membrane. The confocal volume is an ellipsoid volume, made up of approximately 0.2 femtolitres volume (~1 x0.3μm, depending on wavelength), however this volume is variable dependant on the numerical aperture of the lens and the wavelength of the laser used.

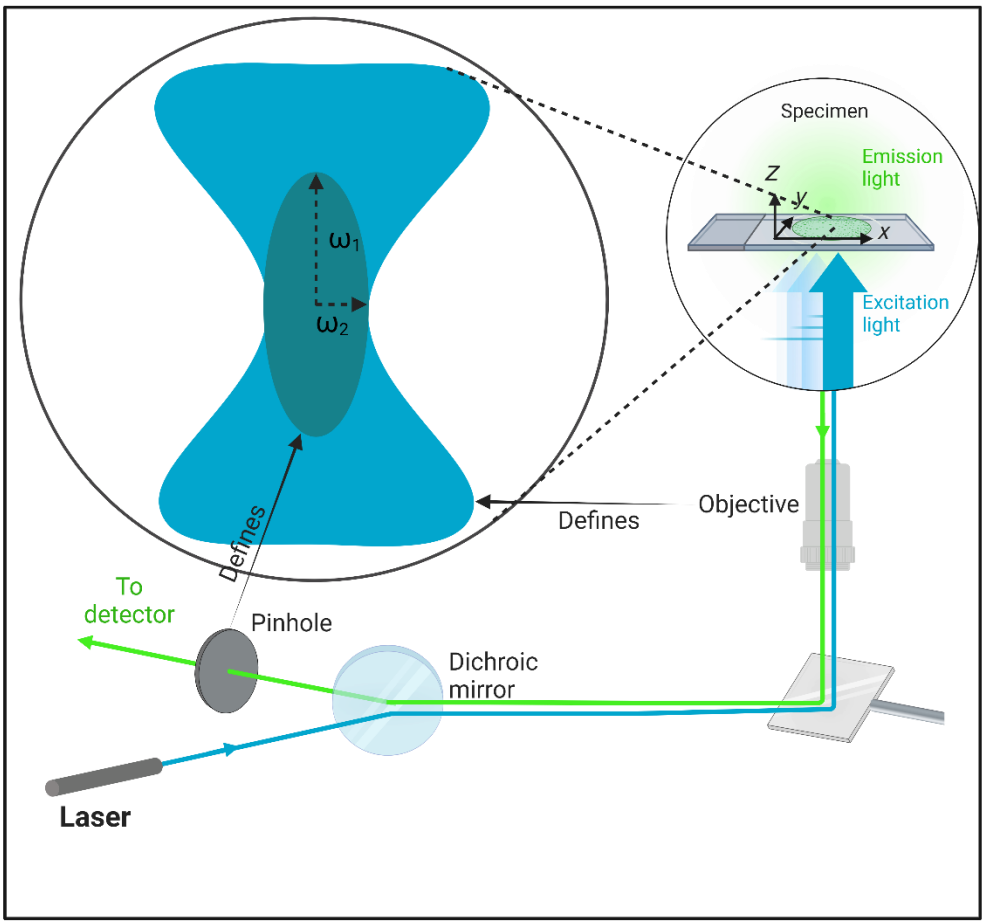


*Figure 3.1.2, diagram depicting the principles of defining a confocal volume. Laser light of a specific wavelength is emitted, passes through a dichroic mirror and is focussed by an objective lens on a specimen, producing the hyperboloid volume shown in blue. Upon excitation of a fluorophore within this hyperboloid volume, emitted photons will travel through the objective lens and be reflected by a dichroic mirror towards a pinhole. This pinhole will exclude all photos not emitted from within a defined focal plane, defining the dark cyan volume depicted. Photons emitted from this volume will pass through the pinhole and on to a detector.*

### 3.1.3 FCS Data Analysis

Calibration of the confocal volume is required to account for small variations in instrument alignment and is carried out daily. The dimensions of the detection volume can be calculated following calibration measurements using a standard solution of known concentration and diffusion co-efficient. Fitting a 3D free diffusion autocorrelation model to these data and using the known diffusion coefficient of the fluorophore and the average dwell time allows calculation of the radius of the volume. Using this radius, the structural parameter, i.e. the ratio of the volume height to the volume diameter can be fit to the calibration autocorrelation curve, and with both the diameter and the height, volume can then be calculated. Once the confocal detection volume is known, average dwell time and particle number can be determined and converted into diffusion coefficient and particle concentration.

#### 3.1.3.1 Autocorrelation

Autocorrelation analysis is applied to the fluorescence fluctuations generated by the free movement of individual particles through the detection volume. Autocorrelation analysis uses the time decay and dependency for the fluorescence fluctuations. It compares the similarity between the intensity at each time point to the intensity at a range of time points (100ns to 10s) later and does this for each time point on the trace.

The autocorrelation analysis is represented by the normalised autocorrelation function (G(τ)):

$$G(\tau) = 1 + \frac{\langle \delta I(t) \cdot \delta I(t+\tau) \rangle}{\langle I \rangle^2}$$

where I is the average intensity, δ is the change in intensity from the time averaged intensity, t is a time point and τ is the time difference between which the two comparisons are made. G(τ) is calculated for each timepoint and a range of time differences, and the resulting autocorrelation functions (G(τ)) can be plotted as a sigmoidal decay function of τ vs G(τ), where the mid-point of the decay indicates the average dwell time of the fluorescent species in the volume ($\tau_D$), and the intercept on the y-axis (G(0)) is inversely proportional to the number of particles in the volume during the measurement (N).

This autocorrelation function can be then fitted an appropriate biophysical model of the system (e.g. 3D diffusion for ligand, 2D diffusion for membrane) to obtain values for $\tau_D$ and N for the species of interest. Once the volume has been calibrated, this allows conversion of the N and $\tau_D$ to concentration and diffusion co-efficient, respectively. (Briddon *et al.*, 2004; Batista-Gondin, 2018; Briddon, Kilpatrick and Hill, 2018).

#### 3.1.3.2 Photon Counting Histogram

Photon Counting Histogram is an alternative method to analyse fluorescence fluctuations that allows the quantification of the brightness of individual particles within the sample by observing differences between expected distributions of photons generated by equally bright particles and distributions of photons generated by particles of varying brightness, explained further in section 3.3.3.2. In GPCR research, this brightness can be indicative, for example, of the oligomeric state of the GPCR in question, or clustering. For example, a cluster of four receptors diffusing as one particle will have a molecular brightness value of four-fold that of a monomeric receptor, assuming each receptor is labelled with one fluorophore.

## 3.2 Aims

In this chapter, we will assess the effects of GRKs on MOR diffusion and organisation at the cell surface by stably expressing a SNAP-tagged MOR in

the CRISPR generated GRK knockout cells characterised in Chapter 2. We will use FCS and PCH analysis to quantify receptor number at the cell surface, their diffusion across the cell membrane, and the formation of receptor clusters. The use of GRK knockout cells will provide complementary insight to highlight the role of these kinases in MOR dynamics.

## 3.3 Methods

### 3.3.1 Generation of Mixed Population Stable Cell Line – Selection and Assessment

In order to assess the role of GRKs on the diffusion and trafficking of the MOR, we required a fluorescently labelled MOR to be expressed at the cell surface of cell lines with different GRK expressions levels. Dr Carsten Hoffman's lab (Drube *et al.*, 2022) has recently generated HEK293 cells with different combinations of GRK2, 3, 5, and 6 knocked out via CRISPR/Cas9 technology, discussed in more detail in section 2.1.5. Using these cells, we generated cell lines that stably express the SNAP-tagged human MOR (hMOR). While the CRISPR process also required antibiotic (puromycin) selection for correctly knocked out clones, the G418 resistance gene *neoR* used in our plasmid provided an alternative resistance mechanism to select for SNAP-hMOR expressing cells.

The stable cell line did not undergo clonal selection, rather, it is a mixed population. This mixed population is useful for confocal microscopy-based techniques used in this chapter as cells of a particular brightness can be chosen from a variety of expression levels to gather the images better suited for analysis.

WT HEK293T, control HEK293, GRK2 knockout and quadruple GRK knockout cells were grown to 70% confluency in a 25 mL flask and transfected with 3 µg pcDNA 3.1 containing N-terminally SNAP tagged human MOR (SNAP-hMOR), using PEI. 24 hours later, G418 was added to the media at a concentration of 1 mg/mL, and cells were passaged upon reaching 90% confluency. Cells were maintained under G418 until growth matched that of untransfected cells.

### 3.3.2 SNAP Label Imaging

Fluorescent proteins such as green, yellow, and cyan fluorescent proteins (G, Y, C FP respectively) have poor photophysical properties for single molecule spectroscopy, such as rapid photobleaching and low quantum yield (Crivat and Taraska, 2012). To combat this, small molecule fluorescent dyes have been generated. These dyes bind covalently to the tagged protein of interest, either to a binding sequence introduced into the protein sequence (as is the case for Fluorescein Arsenical Hairpin (FlAsH) dyes, used in chapter 4), or to engineered enzyme tags. These engineered enzyme tags catalyse auto-attachment of the fluorescent dye in question and are similar in size to the aforementioned fluorescent proteins. The SNAP tag used here is a 20 kDa DNA repair protein called human $O^6$-alkylguanine-DNA alkytransferase, or hAGT, whose normal role is to catalyse the removal of the alkyl group from an $O^6$-alkylated guanine, binding the group to itself on a cysteine residue, and subsequently inactivating the enzyme (Juillerat *et al.*, 2003). Thus, by adding

a fluorophore to a $O^6$-alkyl or $O^6$-benzyl guanine, one can label the hAGT with this fluorophore. This process has been marketed by New England Biolabs as SNAP-tag® and have developed a variety of labels for this process, including membrane permeable and impermeable versions with a variety of fluorophores.

Labelled SNAP-tagged hMOR was imaged on a Zeiss LSM880F confocal microscope. Following selection, cells were plated into Nunc Labtek #1.0 glass bottomed 8 well plates coated with PDL. For the coating, 100 µL of 20 µg/ml PDL in Phosphate Buffered Saline (PBS) was added to each well of the 8 well plate and incubated at room temperature for 1 hour. Plates were then washed with PBS twice and stored at -4 °C before seeding.

Cells were seeded at 10,000 cells per well and incubated at 37 °C for 48 hours. Media was aspirated and cells were washed with PBS. Glucose was added to PBS at a final concentration of 5 mM, and this PBS/Glucose was added to each well. SNAP-Surface Alexa Fluor® 488 was dissolved in DMSO to a stock concentration of 1 mM and added to each well to achieve a final concentration of 1 µM. Plates were then incubated at 37 °C for 30 mins. Wells were then washed with PBS/glucose twice, with 5-min incubation in between addition and aspiration, followed by a final wash with a 20-min incubation. 100 µL PBS/glucose were then added to each well and plates were transferred to the Zeiss LSM880F confocal fluorescence microscope for imaging. 4096 x 4096 pixel images were captured at 24 °C using a 40x c-Apochromat 1.2 numerical aperture lens on zoom 1, with a 1 Airy unit pinhole, and a 488nm wavelength argon laser, using a BP505-610IR emission filter and a detector gain of 696. Gain and laser power were maintained between experiments.

### 3.3.3 FCS

After assessing stable transfection efficiency, we were able to assess receptor diffusion in cell lines with GRK profile expression, and the effects that opioid ligand treatment had in receptor translocation in these cell lines.

The confocal volume was calibrated each experimental day using a standard solution of 20 nM ATTO488 with a known diffusion coefficient of $4x10^{-6}$ $cm^2/s$ (Dertinger and Ewers, 2008), taking 10 x 10s calibration reads and fitting each of these to a 1 x 3D free component function, incorporating a pre-exponential term to account for triplet state photophysics. The average value of dwell time is used to calculate confocal radius, and the fitted structural parameter is used to calculate the half height of the volume. The radius and half height are then used to calculate confocal volume (Briddon, Kilpatrick and Hill, 2018). A 1 x 60s calibration read for PCH calibration was also taken.

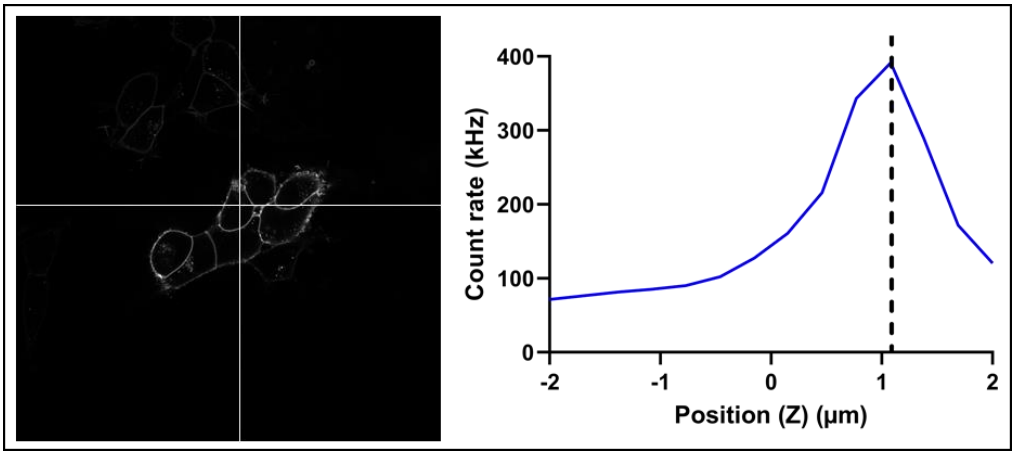


*Figure 3.3.3, use of live confocal images and z-intensity scan for positioning of a confocal volume on a cell plasma membrane containing SNAP-labelled hMOR. Crosshair used to position confocal volume on the cell in the x and y direction, with a zoom of 3 to observe membrane shape and avoid protrusions. Upon rough positioning in z based on observation of the membrane, a z-intensity scan at the position selected by the crosshair indicates peak fluorescence and thus membrane.*

Cells stably expressing SNAP-hMOR were plated and labelled as described in section 3.3.2 and transferred to the Zeiss LSM880F Confocal Fluorescence Microscope. Cells were equilibrated to 24 °C room temperature to reduce membrane drift. Following calibration, SNAP-hMOR expressing cells were located and the confocal volume positioned in x-y on a flat region of the upper plasma membrane using live confocal imaging, followed by an intensity based Z-scan of ±2 µm at 0.25 µm intervals. The peak intensity as an indication of membrane location for optimal positioning of the confocal volume.

Once the confocal volume was positioned at the plasma membrane, fluorescence fluctuations were collected for 30 s, excited by a 488 nm argon laser with an excitation power of 1% (approximately 0.08 kW/cm$^2$), and a pinhole of 1 Airy unit, with a BP505-610IR emission filter. Laser power and microscope settings were optimised as discussed in Batista-Gondin *et al.*, 2019. Data analysis was conducted as described in section 3.1.3, using the Zen 2010 Black software (Carl Zeiss, Jena, Germany), for both AC and PCH analyses. The initial 5 s of each trace were discarded to remove bleaching artefacts. Autocorrelation traces were fitted to a model containing a 1x 3D plus 1x or 2 x 2D components, including a pre-exponential to account for fluorophore triplet state and photophysics. For AC curves which did not have a clear asymptote at 1, an offset was added to the fit. Goodness of fit was assessed using residuals of the fit from the data. Similarly, PCH histograms were analysed in ZenBlack 2010, using a 20 µs time bin.

For each cell line under the basal condition, at least 20 different cells were measured over 3 independent experiments. For DAMGO treated conditions, at least 5 cells were measured over 2 independent experiments. Fluorescence fluctuation measurements were taken over 2 hours following labelling.

### 3.3.3.1 Autocorrelation Analysis

The autocorrelation curve generated was best described by a number of different fluorescent species, and yielded dwell time and particle number for each of these components in each cell line. Figure 3.3.3.1a shows a representative calibration trace using a known concentration of a freely moving dye in solution. The subsequent autocorrelation curve fit a model containing one component, yielding the dwell time ($\tau_{D1}$) and particle number (N) of the ATTO488 dye within the detection volume.

As indicated in figure 3.3.3.1, autocorrelation analysis of fluorescence fluctuations obtained on the upper cell membrane of SNAP-MOR-expressing basal cells yielded a complex AC curve as shown in figure 3.3.3.1e. As previously demonstrated for the SNAP-MOR receptor (and other SNAP-GPCRs), this curve was best fit by a model containing two diffusion components. The first 3D component ($\tau_{D1}$) accounted for unwashed SNAP-488 label, and generally constituted around 18% of the curve. The second, slower, 2D component ($\tau_{D2}$) represented diffusion of the SNAP-MOR in the membrane. For fitting purposes, the diffusion time of $\tau_{D1}$ was fixed in the fit to 20-60μs, which is the known diffusion time of free SNAP label when measured in solution. SNAP-MOR particle number ($N_2$) was calculated from total N as the fractional contribution of the $\tau_{D2}$ component to the total curve amplitude. Where AC curves reached an asymptote, but this was not at 1, a simple offset term was added to the fit equation to allow a more accurate fitting.

In some instances, autocorrelation curves required a second 2D component to better describe the curve, as shown in figure 3.3.3.1i. This component may represent slower moving receptors or aggregates, described by a longer dwell time ($\tau_{D3}$) and particle number ($N_3$). This additional component was added based on fit residuals and goodness of fit data.

Component diffusion coefficients (D; $\mu m^2/s$) and particle density ($N/\mu m^2$) were calculated from the dwell time and fractional particle number for each component based on the size of the confocal volume calculated from the calibration data.

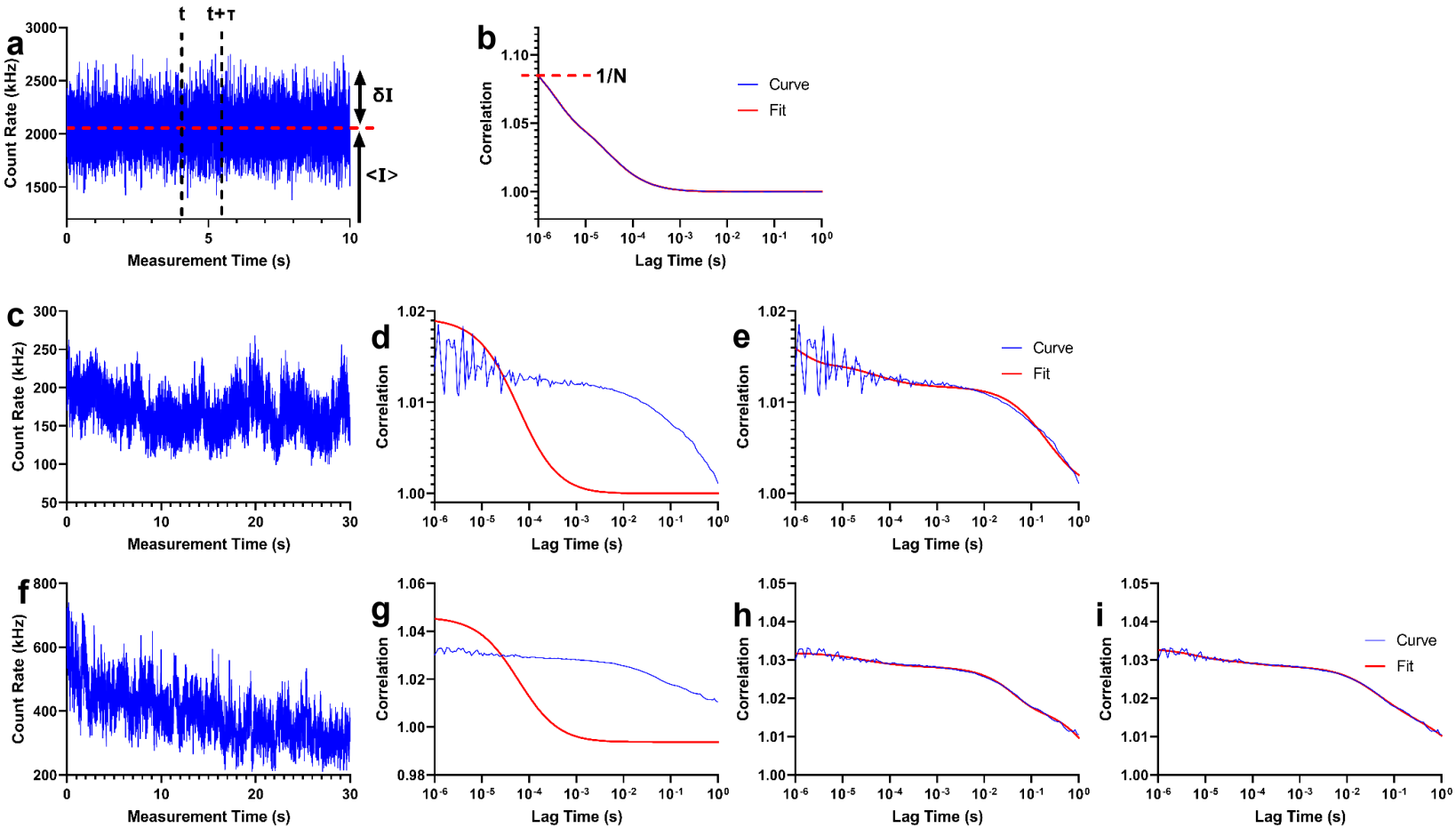


*Figure 3.3.3.1, a, c, f) fluorescence fluctuation traces, b, d, e, g-i) autocorrelation curves, and b, d, g) 1 component autocorrelation model fits e, h) 2 component autocorrelation model fits, i) 3 component autocorrelation model fits of a, b) ATTO488 dye in solution or c-i) SNAP-labelled hMOR at the membrane. The first 5 s of the traces shown here are removed to remove photobleaching artefacts.*

### 3.3.3.2 Photon Counting Histogram Analysis

Fluorescence fluctuation traces can also be analysed using PCH analysis, yielding average brightness values for fluorescent species. Similar to the autocorrelation analysis, the histogram generated by each trace can be used generate a fit, from which data on the molecular brightness ($\varepsilon_x$, Hz) of fluorescent species within the confocal volume can be determined. As shown in figure 3.3.3.2, in some occasions, the model used may generate a better fit using a second component, component 2, which describes a brighter species than the first component. The presence and brightness of this second component can be used to draw conclusions as to the presence of oligomeric forms of fluorescently labelled species.

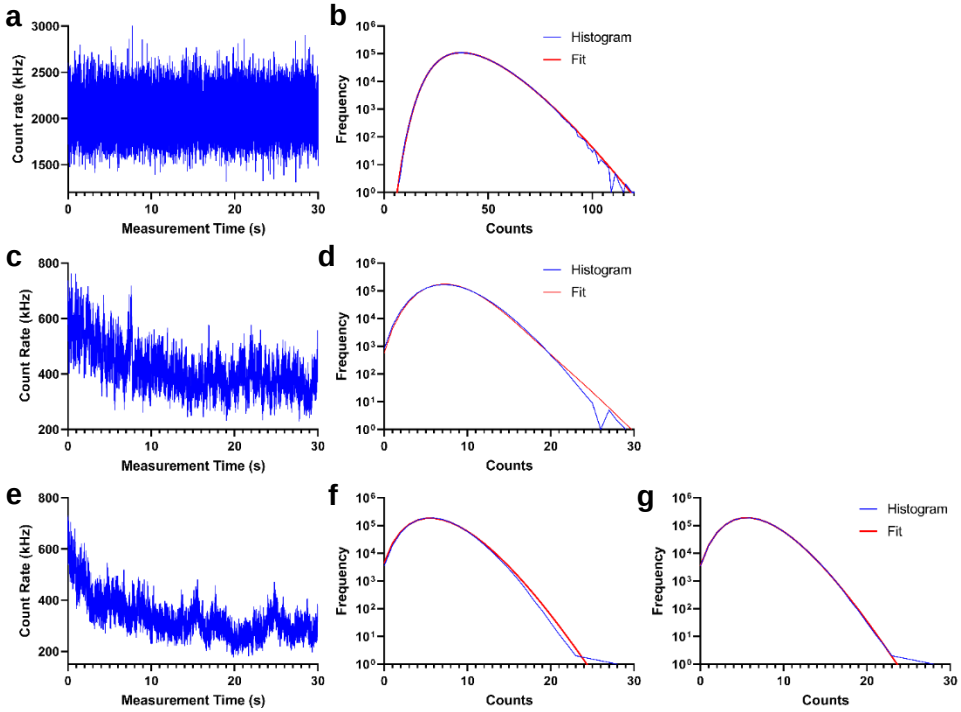


*Figure 3.3.3.2, a, b) ATTO488 dye in solution or c-g) SNAP-labelled hMOR at the membrane a, c, e) fluorescence fluctuation traces, with b, d, f, g) photon counting histograms generated from the respective traces. b, d, f, g) PCH fits generated using b, d, f) 1 component or g) 2 components. The first 5 s of the traces shown here are removed to remove photobleaching artefacts.*

In PCH analysis, fluorescence fluctuation traces are divided into time bins and a frequency histogram is generated of number of photons per time bin. The length of this bin time is required to be shorter than the dwell time of an average receptor, usually 20 - 1000 µs, so that diffusion of the species out for the volume isn't probable during a single time bin. The larger the amplitude of the fluctuations (brighter particles) the more this derived frequency histogram will deviate from Poissionian statistics. This deviation can be fitted to determine the molecular brightness, termed ε, and the particle number.

Conducting this binning on a calibration trace and fitting a PCH model allows for the generation of a first order correction, which corrects for the fraction of photons coming from outside the detection volume, due to the imperfect

Gaussian nature of the detection volume. This is then kept fixed for subsequent reads. Fitting a PCH model to the super-Poissionian histogram generated by the binning using this correction to the experimental reads allows the determination of concentration and brightness parameters for a given read (Briddon, Kilpatrick and Hill, 2018).

## 3.4 Results

### 3.4.1 Imaging of SNAP-hMOR stably expressed in HEK293T cells

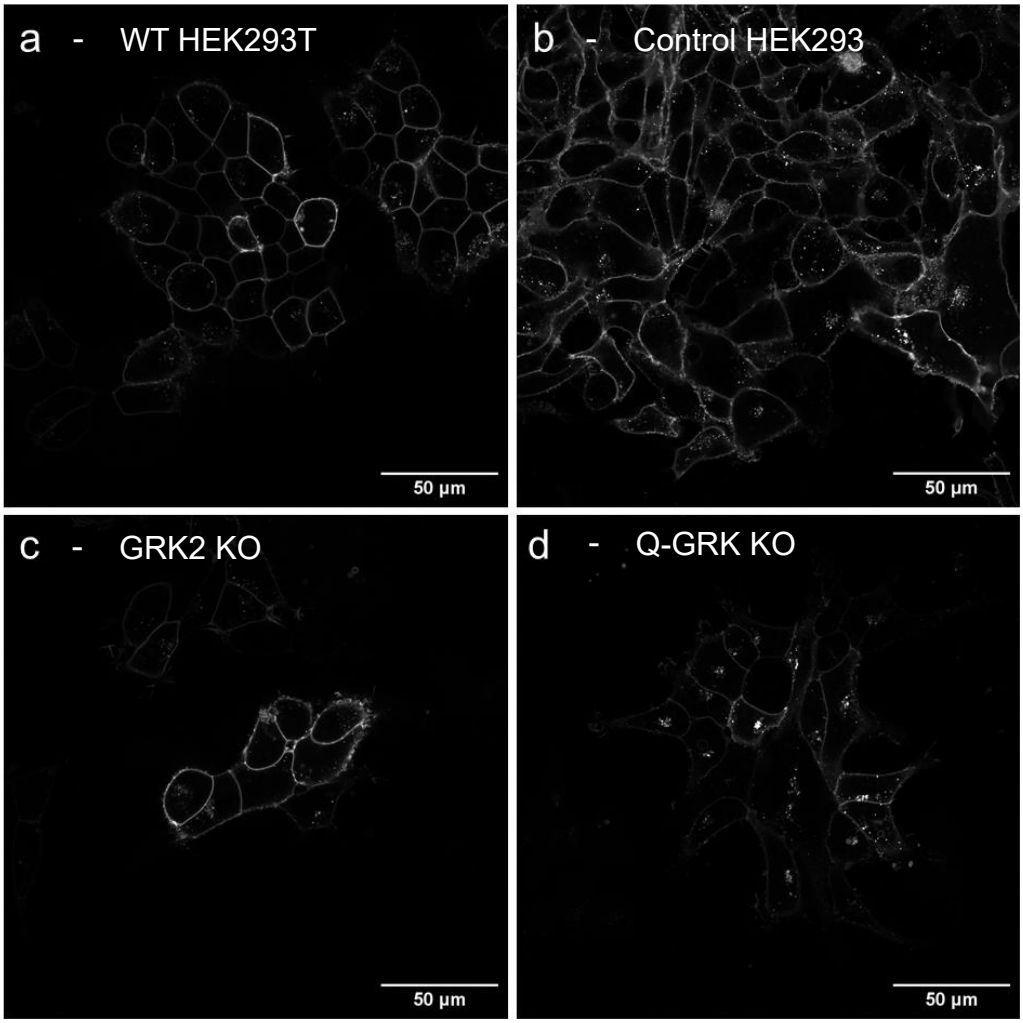


*Figure 3.4.1, single equatorial confocal slice fluorescence images taken on a Zeiss LSM880 using 40x magnification (NA 1.2, water immersion) of SNAP-Surface Alexa Fluor® 488 labelled stably transfected SNAP-hMOR in a) HEK293T cells from the Canals/Lane lab b) HEK293 Control cells created by Drube, et al, having undergone CRISPR/Cas9 expression with no guideRNA c) HEK293 cells with GRK2 knocked out by CRISPR/Cas9 d) HEK293 cells with GRK2, 3, 5, and 6 knocked out by CRISPR/Cas9 (Quadruple KO or Q-GRK KO). Scale bar shows 50 µm, N = 1.*

Initially, confocal imaging was used to determine the successful expression of SNAP-hMOR and differences in MOR distribution in unmodified HEK293T cells and CRISPR/Cas9 control and GRK knockout HEK293 cells. As shown in figure 3.4.1, in all cell lines fluorescence is predominantly localised to the membrane, with some fluorescence localised to isolated intracellular vesicles. As labelling was conducted with a cell impermeable label, any fluorescence localised to intracellular vesicles indicates recently internalised receptor. In the Q-GRK knockout cells, we see reduced membrane fluorescence and thus cell surface expression of the MOR, as well as increased vesicle fluorescence, and thus receptor internalisation.

### 3.4.2 Membrane Dynamics of the MOR in CRISPR/Cas9 GRK Knockout Cells

Following successful selection of stable SNAP-hMOR mixed population cell lines, in order to understand the effects of differential GRK expression on MOR membrane dynamics, we assessed the receptor diffusion and clustering under basal and ligand-treated cellular conditions in each of the cell lines generated using FCS

We collected fluorescence fluctuation measurements of the cell membrane following labelling of cell surface receptors in each of the cell lines generated by positioning the confocal volume over a flat region of the upper cell membrane in the x and y directions, and in the z direction using a z scan and positioning the confocal volume at the peak intensity, as shown in figure 3.3.3. Fluorescence fluctuations were recorded for 30 s, with the first 5 s being discarded from each of the traces to account for photobleaching.

#### *3.4.2.1 Effects of differential GRK expression on basal receptor organisation*

In order to assess the effects of differential GRK expression on receptor organisation under unstimulated conditions, FCS measurements were performed in cell lines with different GRKs knocked out by CRISPR.

As shown in figure 3.4.2.1a, number of SNAP-MOR (as determined by N) was not significantly different between cell lines with differential GRK expression as tested by Brown-Forsythe and Welch ANOVA tests (P = 0.2456, 0.3717, respectively). Wildtype HEK293T cells exhibited a mean particle number of 440.3 ± the standard error of the mean (SEM) of 58.8 particles/$\mu m^2$ compared to GRK2 knockout cells which exhibited 482.6 ± 71.6 particles/$\mu m^2$. The quadruple knockout cells exhibited 576.1 ± 81.3 particles/$\mu m^2$, and the Control HEK293 cells exhibited 383.0 ± 75.9 particles/$\mu m^2$.

Similarly, the diffusion coefficient for component 2 was not significantly different between cell lines with differential GRK expression as tested by Brown-Forsythe and Welch ANOVA tests (P = 0.2323, 0.0881 respectively). Wildtype HEK293T cells exhibited a mean diffusion coefficient of 0.17 ± 0.03 $\mu m^2/s$ compared to GRK2 knockout cells which exhibited 0.12 ± 0.02 $\mu m^2/s$. The quadruple knockout cells exhibited 0.18 ± 0.02 $\mu m^2/s$, and the Control HEK293 cells exhibited 0.21 ± 0.03 $\mu m^2/s$.

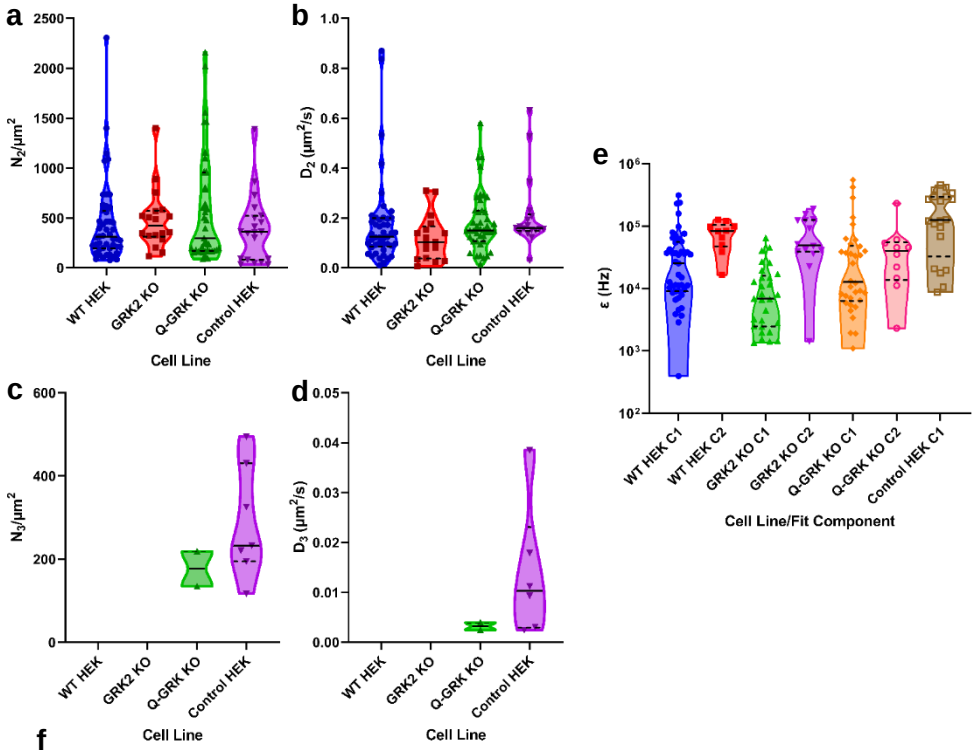


| Cell Line | Autocorrelation Analysis Parameters | | | | | | | | | | | Photon Counting Histogram Analysis Parameters | | | | | | |
|---|---|---|---|---|---|---|---|---|---|---|---|---|---|---|---|---|---|---|
| | $N_2/\mu m^2$ | | $D_2$; $\mu m^2/s$ | | $N_3/\mu m^2$ | | $D_3$; $\mu m^2/s$ | | No. Cells | Fit with C3 | %Fit with C3 | $\varepsilon_1$ (Hz) | | $\varepsilon_2$ (Hz) | | No. Cells | Fit with C2 | %Fit with C2 |
| | Mean | ± SEM | Mean | ± SEM | Mean | ± SEM | Mean | ± SEM | | | | Mean | ± SEM | Mean | ± SEM | | | |
| WT HEK | 440.3 | 58.8 | 0.17 | 0.03 | - | - | - | - | 48 | 0 | 0 | 46067 | 9832 | 78114 | 11250 | 48 | 11 | 23 |
| GRK2 KO | 482.6 | 71.6 | 0.12 | 0.02 | - | - | - | - | 18 | 0 | 0 | 12662 | 2799 | 78068 | 15097 | 31 | 14 | 45 |
| C-HEK | 383.0 | 75.9 | 0.21 | 0.03 | 288.2 | 51.2 | 0.0138 | 0.0055 | 20 | 7 | 35 | 183803 | 32921 | - | - | 20 | 0 | 0 |
| Q-KO | 576.1 | 81.3 | 0.18 | 0.02 | 176.9 | 41.9 | 0.0032 | 0.0007 | 43 | 2 | 5 | 61155 | 20675 | 51960 | 20680 | 39 | 10 | 26 |

*Figure 3.4.2.1, a) Number of particles per μm² and b) diffusion coefficient (μm²/s) of particles described by the second component, c) Number of particles per μm² and d) diffusion coefficient (μm²/s) of particles described by the third component and of a model fit to autocorrelation curve generated by fluorescence fluctuation measurements of SNAP-labelled hMORs in wildtype HEK293T cells from the Canals/Lane lab, as well as HEK293 cells with GRK2 knocked out by CRISPR/Cas9 (GRK2 KO), GRK2/3/5/6 knocked out by CRISPR/Cas9 (Q-GRK KO), or control cells transfected with CRISPR/Cas9 and no guide RNA (Control HEK). e) molecular brightness of each component in each of the cell lines under basal conditions, as measured by photon counting histogram. Black lines indicate median, dashed lines indicate upper and lower quartiles. f) table summarising autocorrelation analysis parameters and photon counting histogram analysis parameters for each cell line (mean ±SEM). Data collected from at least 20 individual cells per cell line over 3 independent experimental days.*

A small number of traces for some cell lines were best described with a model with a 3rd component. As shown by the table in figure 3.4.2.1f, none of the traces in either the wild type HEK 293T cells or the GRK2 knockout cells exhibited traces that fit a 3 component autocorrelation function over a 2 component version. Of the quadruple knockout cell traces, only 5% exhibited 3 component traces, whereas the control HEK293 cells exhibited around 35%. Of these traces, the average particle number for the 3rd component was 176.9 ± 41.9 particles/μm² for the quadruple knockout cells, and 288.2 ± 51.2 particles/μm² for the Control HEK293 cells, with no significant difference between these particle numbers as determined by Welch's t test (P = 0.1592). The average diffusion coefficient for the 3rd component was 0.0032 ± 0.0007 μm²/s for the quadruple knockout cells, and 0.0138 ± 0.0055 μm²/s for the Control HEK293 cells, with no significant difference between these diffusion coefficients as determined by Welch's t test (P = 0.1125).

As shown in figure 3.4.2.1e, the average molecular brightness of the particles in WT HEK293T cells described by the first component was 46,067 ± 9,832 Hz, compared to the molecular brightness of particles described in the second component, which was 78,114 ± 11,250 Hz, with 23% of PCH curves generated being best fit by a 2 component model. The particles in GRK2 knockout cells described by the first component had an average molecular brightness of 12,662 ± 2799 Hz, statistically significantly lower than the component 1 brightness of the WT HEK293T cells as determined by Brown-Forsythe and Welch ANOVA tests (adjusted P value (Dunnett's T3 multiple comparisons test) = 0.0390). The component 2 average molecular brightness for the GRK2 knockout cells was 78,068 ± 15,097 Hz, statistically greater than the component 1 average molecular brightness in the same cells (adjusted P value = 0.0145), with 45% of PCH curves generated in these cells being best fit with a 2 component model. The average molecular brightness of the particles in Quadruple GRK knockout cells described by the first component was 61,155 ± 20,675 Hz, compared to the molecular brightness of particles described in the second component, which was 51,960 ± 20,680 Hz, with 26% of PCH curves generated in these cells being best fit by a 2 component model. None of the PCH curves generated in the control HEK293 cells were best fit with a 2 component model, and the average molecular brightness of the particles in these cells was 183,803 ± 32,921 Hz, statistically greater than both the component 1 molecular brightness WT HEK293T cells and GRK2 knockout cells (adjusted P value = 0.0116, 0.0011 respectively).

#### *3.4.2.2 Effects of DAMGO treatment on receptor organisation in Control HEK293 cells*

The effects of a high efficacy MOR ligand, DAMGO, on MOR organisation in control cells (HEK293 cells, which have undergone CRISPR/Cas9 transfection, though without transfection of guideRNA) measured by FCS were obtained, in preparation for comparison to a cell line with 4 GRKs knocked out by CRISPR. Measurements were taken in control cells stably expressing SNAP-hMOR at varying time points post ligand addition and compared to the basal data shown above.

As shown in figure 3.4.2.2a, number of component 2 particles/$\mu m^2$ was not significantly different between the time points as tested by Brown-Forsythe and Welch ANOVA tests (P = 0.5151, 0.5494 respectively). Untreated basal cells exhibited a mean particle number of 383.0 ± 75.9 particles/$\mu m^2$ compared to treated cells 10 mins post ligand addition which exhibited 276.2 ± 62.76 particles/$\mu m^2$. At 20 mins cells exhibited 248.4 ± 47.7 particles/$\mu m^2$, and at 30 mins cells exhibited 288.3 ± 93.9 particles/$\mu m^2$.

Similarly, the diffusion coefficient for component 2 was not significantly different between time points as tested by Brown-Forsythe and Welch ANOVA tests (P = 0.2476, 0.3989 respectively). Untreated basal cells exhibited a mean diffusion coefficient of 0.21 ± 0.03 $\mu m^2/s$ compared to treated cells 10 mins post-ligand addition which exhibited 0.32 ± 0.08 $\mu m^2/s$. At 20 mins cells exhibited 0.23 ± 0.03 $\mu m^2/s$, and at 30 mins cells exhibited 0.48 ± 0.18 $\mu m^2/s$.

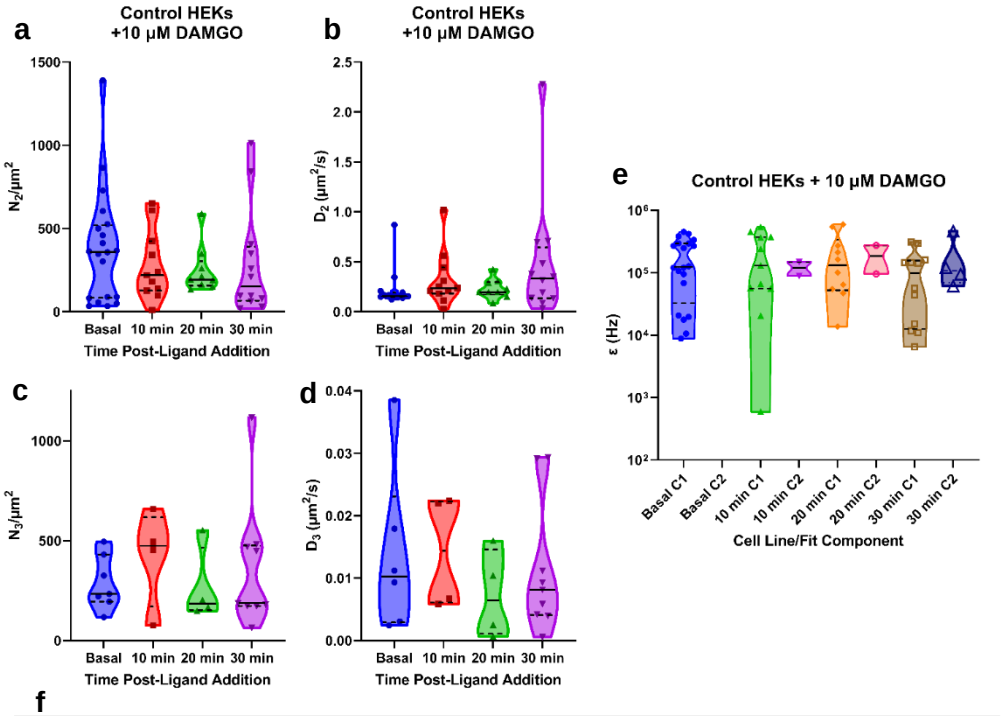


f

| Cell Line/Timepoint | Autocorrelation Analysis Parameters | | | | | | | | | | | Photon Counting Histogram Analysis Parameters | | | | | | |
|---|---|---|---|---|---|---|---|---|---|---|---|---|---|---|---|---|---|---|
| | $N_2/\mu m^2$ | | $D_2$; $\mu m^2/s$ | | $N_3/\mu m^2$ | | $D_3$; $\mu m^2/s$ | | No. Cells | Fit with C3 | %Fit with C3 | $\varepsilon_1$ (Hz) | | $\varepsilon_2$ (Hz) | | No. Cells | Fit with C2 | %Fit with C2 |
| | Mean | ± SEM | Mean | ± SEM | Mean | ± SEM | Mean | ± SEM | | | | Mean | ± SEM | Mean | ± SEM | | | |
| C-HEK - Basal | 383.0 | 75.9 | 0.21 | 0.03 | 288.2 | 51.2 | 0.0138 | 0.0055 | 20 | 7 | 35 | 183803 | 32921 | - | - | 20 | 0 | 0 |
| C-HEK+D 10min | 276.2 | 62.8 | 0.32 | 0.08 | 420.9 | 123.1 | 0.014 | 0.005 | 12 | 4 | 33 | 208679 | 58173 | 119750 | 30250 | 11 | 2 | 18 |
| C-HEK+D 20min | 248.4 | 47.7 | 0.23 | 0.03 | 266.9 | 95.67 | 0.007 | 0.004 | 10 | 4 | 40 | 206572 | 65820 | 184750 | 89250 | 10 | 2 | 20 |
| C-HEK+D 30min | 288.3 | 93.9 | 0.48 | 0.18 | 365.7 | 107.2 | 0.011 | 0.004 | 12 | 9 | 75 | 112021 | 31016 | 185325 | 94029 | 12 | 4 | 33 |

*Figure 3.4.2.2, a) Number of particles per $\mu m^2$ and b) diffusion coefficient ($\mu m^2/s$) of particles described by the second component, c) Number of particles per $\mu m^2$ and d) diffusion coefficient ($\mu m^2/s$) of particles described by the third component and of a model fit to autocorrelation curve generated by fluorescence fluctuation measurements of SNAP-labelled hMORs in control cells transfected with CRISPR/Cas9 and no guide RNA (Control HEK) before and at time points following treatment with 10 μM of the high efficacy MOR agonist DAMGO. e) molecular brightness of each component at each time point, as measured by photon counting histogram. Black lines indicate median, dashed lines indicate upper and lower quartiles. f) table summarising autocorrelation analysis parameters and photon counting histogram analysis parameters for each timepoint (mean ±SEM). Data collected from at least 5 individual cells per timepoint over 3 independent experimental days.*

A small number of traces for some time points were best described with a model with a 3rd component, as shown by the table in figure 3.4.2.2f. Of the untreated basal cell traces, 35% exhibited 3 component traces, with the 10, 20, and 30 min time point traces exhibiting 33%, 30%, and 75% of traces best fit with a 3rd component. Of these traces, the average particle number for the 3rd component was 288.2 ± 51.2 particles/$\mu m^2$ for the untreated basal cells, 420.9 ± 123.1 particles/$\mu m^2$ for the 10 min time point, 266.9 ± 95.67

particles/$\mu m^2$ for the 20 min time point, and 365.7 ± 107.2 particles/$\mu m^2$ for the 30 min time point, with no significant difference between these particle numbers as determined by Brown-Forsythe and Welch ANOVA tests (P = 0.7187, 0.7439 respectively). The average diffusion coefficient for the 3rd component was 0.014 ± 0.005 $\mu m^2/s$ for the untreated basal cells, 0.014 ± 0.005 $\mu m^2/s$ for the 10 min post ligand time point, 0.007 ± 0.004 $\mu m^2/s$ for the 20 min post ligand time point, and 0.011 ± 0.004 $\mu m^2/s$ for the 30 min post ligand time point, with no significant difference between these diffusion coefficients as determined by Brown-Forsythe and Welch ANOVA tests (P = 0.7508, 0.6796 respectively).

As shown in figure 3.4.2.2e, the average molecular brightness of the particles in component 1 of the curves generated in the basal control HEK293 cells was 183,803 ± 32,921 Hz, with none of the curves modelled best with a 2 component model. In comparison, following DAMGO treatment, there was no significant change in component 1 molecular brightness at any time point, with the 10 min post-ligand addition time point exhibiting an average brightness of 208,679 ± 58,173 Hz, and the 20 and 30 min time points exhibiting an average molecular brightness of 206,572 ± 65,820 Hz and 112,021 ± 31,016 Hz. Of the curves generated at each time point, as mentioned previously, none of the curves generated in basal cells were best fit by a 2 component model, whereas 18%, 20% and 33% of curves in the 10, 20, and 30 min time point were best fit by a two component model. The particles described by the 2nd component were similarly not significantly different in average molecular brightness, with the 10 min post-ligand addition time point exhibiting an average brightness of 119,750 ± 30,250 Hz, and the 20 and 30 min time points exhibiting an average molecular brightness of 184,750 ± 89,250 Hz and 185,325 ± 94,029 Hz.

### *3.4.2.3 Effects of DAMGO treatment on receptor organisation in Quadruple-GRK Knockout Cells*

In order to assess the effects of a high efficacy MOR ligand, DAMGO, on MOR organisation in the absence of GRK phosphorylation, we undertook FCS measurements in DAMGO-treated quadruple GRK knockout cells stably expressing the SNAP-hMOR. Measurements were taken at varying time points post ligand addition and compared to previous untreated quadruple GRK knockout cell data.

As shown in figure 3.4.2.3a, number of component 2 particles/$\mu m^2$ was not significantly different between the time points as tested by Brown-Forsythe and Welch ANOVA tests (P = 0.3368, 0.4463 respectively). Untreated basal cells exhibited a mean particle number of 576.1 ± 81.3 particles/$\mu m^2$ compared to treated cells 10 mins post ligand addition which exhibited 307.6 ± 107.8 particles/$\mu m^2$. At 20 mins cells exhibited 399.4 ± 128.6 particles/$\mu m^2$, and at 30 mins cells exhibited 390.2 ± 129.8 particles/$\mu m^2$.

Similarly, the diffusion coefficient for component 2 was not significantly different between time points as tested by Brown-Forsythe and Welch ANOVA tests (P = 0.6429, 0.7164 respectively). Untreated cells exhibited a mean diffusion coefficient of 0.18 ± 0.03 $\mu m^2/s$ compared to treated cells 10 mins post-ligand addition which exhibited 0.21 ± 0.06 $\mu m^2/s$. At 20 mins cells exhibited 0.17 ± 0.04 $\mu m^2/s$, and at 30 mins cells exhibited 0.14 ± 0.02 $\mu m^2/s$.

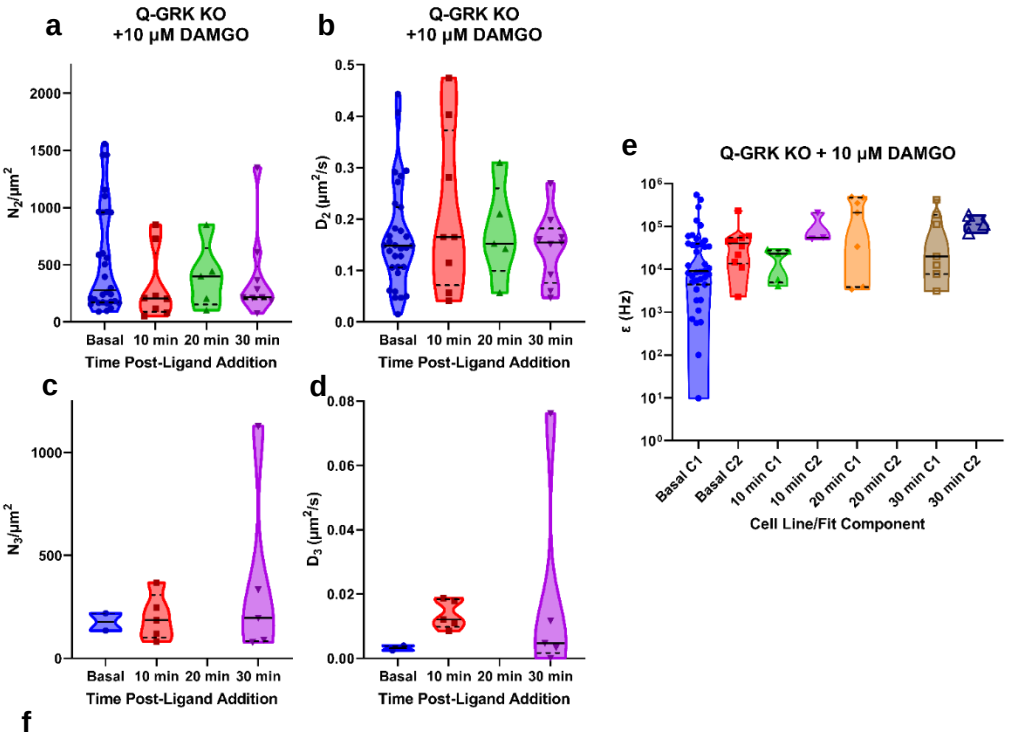


f

| Cell Line/Timepoint | Autocorrelation Analysis Parameters | | | | | | | | | | | Photon Counting Histogram Analysis Parameters | | | | | | |
|---|---|---|---|---|---|---|---|---|---|---|---|---|---|---|---|---|---|---|
| | $N_2/\mu m^2$ | | $D_2$; $\mu m^2/s$ | | $N_3/\mu m^2$ | | $D_3$; $\mu m^2/s$ | | No. Cells | Fit with C3 | %Fit with C3 | $\varepsilon_1$ (Hz) | | $\varepsilon_2$ (Hz) | | No. Cells | Fit with C2 | %Fit with C2 |
| | Mean | ± SEM | Mean | ± SEM | Mean | ± SEM | Mean | ± SEM | | | | Mean | ± SEM | Mean | ± SEM | | | |
| Q-KO - Basal | 576.1 | 81.3 | 0.18 | 0.02 | 176.9 | 41.9 | 0.0032 | 0.0007 | 43 | 2 | 5 | 61155 | 20675 | 51960 | 20680 | 39 | 10 | 26 |
| Q-KO+D 10min | 307.6 | 107.8 | 0.21 | 0.06 | 200.6 | 50.57 | 0.01367 | 0.001995 | 8 | 5 | 63 | 17680 | 5320 | 105139 | 51946 | 5 | 3 | 60 |
| Q-KO+D 20min | 399.4 | 128.6 | 0.17 | 0.04 | - | - | - | - | 5 | 0 | 0 | 223584 | 82110 | 280000 | 0 | 7 | 1 | 14 |
| Q-KO+D 30min | 390.2 | 129.8 | 0.14 | 0.02 | 364.8 | 196.3 | 0.019 | 0.014 | 9 | 5 | 56 | 108798 | 57875 | 121733 | 32353 | 7 | 3 | 43 |

*Figure 3.4.2.3, a) Number of particles per µm² and b) diffusion coefficient (µm²/s) of particles described by the second component, c) Number of particles per µm² and d) diffusion coefficient (µm²/s) of particles described by the third component and of a model fit to autocorrelation curve generated by fluorescence fluctuation measurements of SNAP-labelled hMORs in HEK293 cells with GRK2/3/5/6 knocked out by CRISPR/Cas9 before and at time points following treatment with 10 µM of the high efficacy MOR agonist DAMGO. e) molecular brightness of each component at each time point, as measured by photon counting histogram. Black lines indicate median, dashed lines indicate upper and lower quartiles. f) table summarising autocorrelation analysis parameters and photon counting histogram analysis parameters for each timepoint (mean ±SEM). Data collected from at least 5 individual cells per timepoint over 3 independent experimental days.*

A small number of traces for some time points were best described with a model with a 3rd component. As shown by the table in figure 3.4.2.3f, each of the conditions exhibited traces that fitted a 3 component autocorrelation function over a 2 component version. Of the untreated basal cell traces, 5% exhibited 3 component traces, with the 10 and 30 min time point traces exhibiting 63% and 56% of traces best fit with a 3rd component. The 20 min time point exhibited no traces best fit with a 3rd component. Of these traces,

the average particle number for the 3rd component was 176.9 ± 41.9 particles/$\mu m^2$ for the untreated basal cells, 200.6 ± 50.6 particles/$\mu m^2$ for the 10 min time point, and 364.8 ± 196.3 particles/$\mu m^2$ for the 30 min time point, with no significant difference between these particle numbers as determined by Brown-Forsythe and Welch ANOVA tests (P = 0.5411, 0.6807 respectively). The average diffusion coefficient for the 3rd component was 0.0032 ± 0.0007 $\mu m^2/s$ for the untreated basal cells, 0.014 ± 0.002 $\mu m^2/s$ for the 10 min post ligand time point, and 0.019 ± 0.014 $\mu m^2/s$ for the 30 min post ligand time point, with no significant difference between these diffusion coefficients as determined by Brown-Forsythe ANOVA test (P = 0.5910). However statistically significant differences between the diffusion coefficients were observed as determined by the Welch ANOVA. Dunnett's T3 multiple comparisons test shows a statistically significant increase in diffusion coefficients between the basal and 10 min time point (adjusted P = 0.0117).

As shown in figure 3.4.2.3e, the average molecular brightness of the particles in component 1 of the curves generated in the basal quadruple knockout cells was 61,155 ± 20,675 Hz, with the average molecular brightness of the particles in component 2 of the curves generated in the same cells being 51,960 ± 20,680. In comparison, following DAMGO treatment, there was no significant change in component 1 molecular brightness between any time point, with the 10 min post-ligand addition time point exhibiting an average brightness of 17,680 ± 5,320 Hz, and the 20 and 30 min time points exhibiting an average molecular brightness of 223,584 ± 82,110 Hz and 108,798 ± 57,875 Hz. Of the curves generated at each time point, as mentioned previously, 26% of the curves generated in basal cells were best fit by a 2 component model, whereas 60%, 14% and 43% of curves in the 10, 20, and 30 min time point were best fit by a two component model. The particles described by the 2nd component were similarly not significantly different in average molecular brightness, with the 10 min post-ligand addition time point exhibiting an average brightness of 105,139 ± 51,946 Hz, and the 20 and 30 min time points exhibiting an average molecular brightness of 280,000 Hz (1 curve) and 121,733 ± 32,353 Hz.

## 3.5 Discussion

Previous work from our lab using FCS and FRAP had suggested that receptor diffusion induced by high efficacy ligands such as DAMGO was GRK2/3 dependent (Batista-Gondin *et al.*, 2019), however, this work was conducted using small molecule inhibitors of GRK2 and GRK3. Here we extend this work using the recently developed CRISPR/Cas9 GRK knockout cells, which provide more specific and more complete removal of active GRKs within the cell. For this, we were able to successfully generate control and GRK knockout cell lines stably expressing SNAP-tagged MOR. Using these cell lines, however, our data suggests very limited changes in receptor diffusion and cell surface concentration, in both basal and DAMGO treated cells with differential GRK expression.

### 3.5.1 SNAP labelling and Imaging

We saw that stable transfection of SNAP-hMOR into each of the cell lines was successful, as we can observe clear membrane and vesicle localised fluorescence characteristic of specific binding to a SNAP-tagged receptor. Interestingly, while intracellular vesicles could be hypothesised to be endosomes, there were increased numbers of bright vesicles in the Q-GRK KO cells (figure 3.4.1d) compared to the control cells (figure 3.4.1b), despite GRKs being involved in the internalisation of the MOR. The distribution of these vesicles is markedly different however, as in the Q-GRK KO, the vesicles appear clustered and brighter closer to the centre of the cell, possibly around the nucleus or Golgi, however, this should be confirmed using a nuclear or Golgi co-stain. Distribution of vesicles in the control cells, as in the other imaged cells, appears more distributed across the cytoplasm, in less bright clusters. This suggests that phosphorylation of the receptor by non-GRK kinases (El Kouhen *et al.*, 2001; C. Bailey *et al.*, 2009) can stimulate different trafficking and recycling destinations, or that the constitutive internalisation of the MOR is affected by the knockout of GRKs in other ways.

During cell culture and image acquisition, the Q-GRK KO cells appeared rounded and proliferated more slowly than other CRISPR KO cell lines, both before and after stable cell line generation. The lack of GRKs in this cell line appears to have a profound effect on cell health and growth, supported by previous reports that knockout of certain GRKs can be embryonically lethal in animal models (Kenski *et al.*, 2005; Quillinan *et al.*, 2011). The lack of GRKs may thus be affecting the larger endocytotic processes occurring in the cells, leading to the differences observed in this imaging study.

### 3.5.2 FCS

Upon finding that SNAP-hMOR stable selection was successful, we moved on to assessing the differences in membrane organisation under differential GRK expression. For this we used FCS and evaluated the diffusion coefficient and brightness parameters using AC and PCH analysis.

We first assessed membrane organisation of hMOR in cell lines with differential GRK expression to understand the effects of GRKs on receptor number and distribution under basal conditions. The diffusion coefficient obtained for the SNAP-hMOR in WT HEK293T cells is similar to that previously reported. In the present study we obtained a diffusion coefficient of 0.17 ± 0.03 $\mu m^2/s$ which is not significantly different to that previously recorded in our lab described (Batista-Gondin, in 2018), of 0.146 ± 0.016 $\mu m^2/s$, as determined by unpaired t-test (P = 0.6726). We also observed statistically higher average particle number (440.3 ± 58.8 particles/$\mu m^2$ vs 157 ± 19 particles/$\mu m^2$) for the WT HEK293T (P = 0.0125). This may be due to increased SNAP-Surface Alexa Fluor® 488 label concentration used during the labelling process (1 µM vs 200 nM), or differences in plasmid copy number and thus cell surface expression. The diffusion coefficient obtained in both our studies was significantly lower than that observed using a YFP tagged MOR in HMY-1 cells, which recorded approximate values of 0.28 $\mu m^2/s$ (P = 0.0009) (Markova *et al.*, 2021). These differences may be due to differences in membrane constitution in different cell types as well as the different fluorescent tag used (YFP vs SNAP) (Vukojević *et al.*, 2008; Rogacki *et al.*, 2018).

As shown in figure 3.4.2.1, there were no significant differences in the particle number or diffusion co-efficient between the cell lines used. This indicates that GRKs have limited if any effect on receptor number or organisation at the membrane under basal conditions. This may not be surprising as GRKs main functions rely on receptor activation.

Assessing differences in the component 1 (free label) of the autocorrelation analysis in these basal cell lines provides good evidence that the washing and labelling process, as well as environmental controls, were consistent across experimental days, due to similar shaped violin plots and similar mean values for both the average concentration and diffusion coefficients for this fast component. Due to the average diffusion coefficient of approximately 200 $\mu m^2/s$, we can exclude that these species are receptors, as GPCR diffusion speed has previously been reported to be between 0.1 and 1 $\mu m^2/s$ (Briddon, Kilpatrick and Hill, 2018), and thus particles described by component 1 are free SNAP label that has either remained in the buffer solution following labelling or been released from non-specific binding following the washing process.

As shown in figure 3.4.2.1, some of the traces obtained with the control HEK and Q-GRK knockout cell lines exhibit autocorrelation curves best fit with a 3$^{rd}$ component (35% and 5% of the traces, respectively). The particles described by the 3$^{rd}$ component exhibit more than 10 fold slower diffusion coefficients compared to the particles described by the 2$^{nd}$ component, with the particles described by the 3$^{rd}$ component in the control HEK293 cells

exhibiting a diffusion coefficient of 0.0138 ± 0.0055 $\mu m^2/s$, compared to the particles described by the 2nd component in the same cells which exhibit a diffusion coefficient of 0.21 ± 0.03 $\mu m^2/s$. In the quadruple knockout cells, diffusion coefficients for particles described by the 3rd and 2nd component were 0.0032 ± 0.0007 $\mu m^2/s$ and 0.18 ± 0.02 $\mu m^2/s$, respectively. The particles described by the 3rd component may be oligomers of receptors due to the requirement of an increase in size difference by 8-fold to produce a detectable change in receptor diffusion coefficient (Briddon, Kilpatrick and Hill, 2018), something more likely to be achieved by receptor oligomers or multiple arrestin-bound receptors clustering together for internalisation than a single receptor bound to multiple effectors. Other explanations for this phenomenon are interactions between the receptor and the cytoskeleton, or transition into membrane domains with a different lipid constitution, both of which would slow receptor diffusion, and would not increase brightness, as observed in the PCH analysis.

In the WT HEK293T and GRK2 knockout cells there was no need to add a third component to obtain a good fit to the traces, this may indicate that GRK2 induces receptor oligomerisation, as both GRK2 KO but also WT HEK293 have been shown to lack this isoform in chapter 2 where the similar behaviour of the WT HEK293T and GRK2 knockout cells in, a β-arrestin2 recruitment assay upon DAMGO stimulation were shown to be very similar compared to control HEK293 cells (figure 3.5.2).

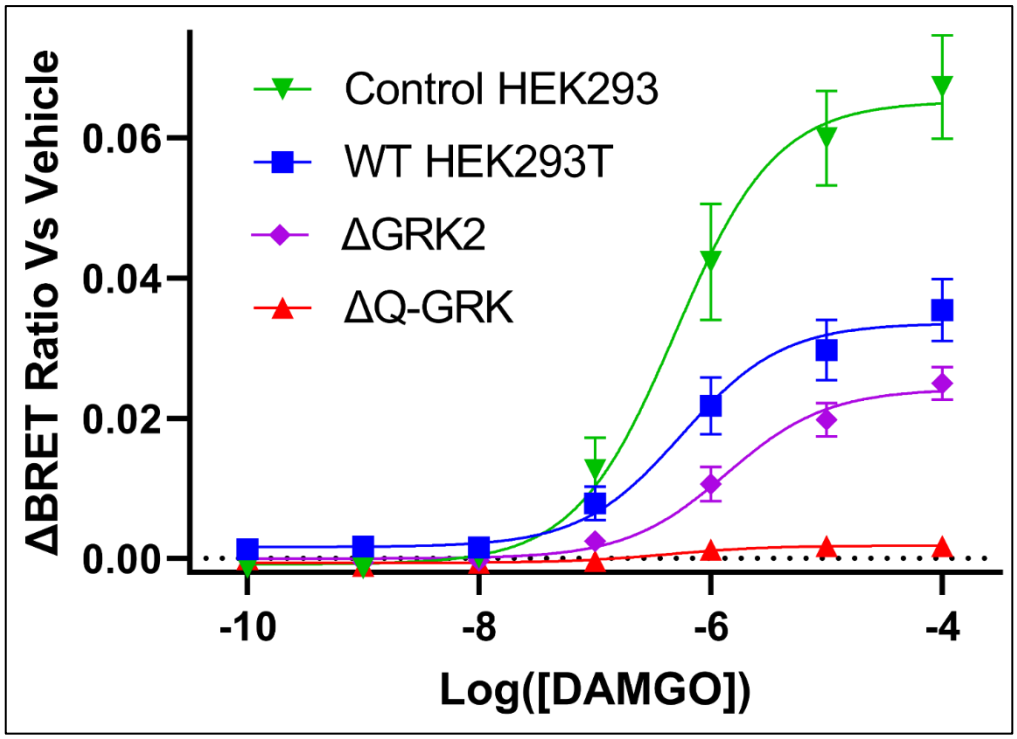


*Figure 3.5.2, Concentration-response curves showing β-arrestin-YFP recruitment to FLAG-MOR-Nluc stimulated by varying concentrations of DAMGO, in different cell lines: Wild Type HEK293T (blue), HEK293 cells with: CRISPR knockout of GRK2 (purple), CRISPR knockout of GRKs 2, 3, 5, and 6 (Quadruple GRK or Q-GRK) (red), and control cells that have undergone the CRISPR process though with no guideRNA (green). N=5, error bars show ± SEM.*

Only 2/43 autocorrelation curves generated in the basal quadruple knockout cells were best described with a 3 component model. While the mechanism of formation of receptor clusters in the Q-GRK knockout cells is difficult to rationalise, due to the limited number of curves best described by a 3rd component. However, the formation of receptor oligomers could be supported by the imaging experiments conducted in section 3.4.1, in which bright intracellular vesicles were observed in both the quadruple knockout cells as well as the control HEK293 cells, suggesting the presence of processes that drive receptor clustering that may be upregulated in cells lacking all GRKs, but not in cells lacking only GRK2.

As shown by the PCH analysis in figure 3.4.2.1e, none of the PCH curves generated in the control HEK293 cells were best modelled by a 2nd component. 23% of PCH curves generated in WT HEK293T cells were best fit with a second component, however on average the particles described by this component are not significantly brighter than the particles described by the 1st component (adjusted P value = 0.5234. In contrast, the average brightness of particles described by component 2 is significantly greater in the GRK2 knockout cells than the average brightness of particles described by component 1 (adjusted P value = 0.0145), suggesting potentially increased clustering of receptors in this cell line (the number of PCH curves generated in the GRK2 knockout cell line best described with a second component being 45%). Finally, the Q-GRK knockout cell line exhibits 26% of PCH curves best described with a 2nd component, and no significant difference in average molecular brightness between particles described by each of the two components (adjusted P value >0.9999). While this may not support the hypothesis raised using the AC analysis, further experiments are required to investigate this. Of note, the autocorrelation curves and PCH curves best described with an additional component may differ between analyses due to the aforementioned requirement for an 8-fold change in mass for the diffusion coefficient to be altered detectably in the AC analysis, whereas in the PCH analysis, a brightness change of 2-fold or greater is detectable (Briddon, Kilpatrick and Hill, 2018). This, however, assumes the slower moving component is also the brighter component, which may not be the case.

To summarise the possible explanations for the patterns shown by the different cell lines in their basal state, without GRK2, the expression of GRK3, 5 and 6 is able to induce clustering of the receptor, shown by the increase in brightness, but not to great enough levels to reduce the diffusion coefficient detectably.

After observing small differences in receptor organisation in basal cell lines with differing GRK expression, we moved on to assessing the effects of a highly-internalising agonist, DAMGO, on the diffusion of the MOR. Due to

time constrains, this was only assessed in the control and Q-GRK knockout cells, two ends of the GRK expression spectrum.

We first assessed the effects of DAMGO (10 µM) treatment on SNAP-hMOR diffusion at varying time points in the control HEK293 cells, in order to observe the effects of this agonist in a fully functional GRK system. This would allow us to compare to previous works using the MOR and DAMGO (Batista-Gondin *et al.*, 2019), as well as to the full knockout cells.

Surprisingly, we observed no difference in average particle number or diffusion coefficient for particles described by both component 2 and component 3 in any of the time points after DAMGO addition. This suggests that DAMGO treatment has little effect on receptor organisation at the plasma membrane. This is not supported by imaging experiments to be discussed in section 4.3.2.2 of chapter 4, which show increased clustering of SNAP-labelled MOR in both WT HEK293T and HEK293T cells co-transfected with GRK2. The data in the present study is different to the one obtained in our group and reported in Batista-Gondin, 2018 in that the DAMGO-induced decreases in particle number and diffusion coefficient observed previously, were not detected here. This difference may be due to the sample size of both experiments; for this work, 20 traces were generated in basal cells, and 10 at the 20 min time point, compared to 99 and 107 traces respectively for the work by Batista-Gondin. The small sample of traces obtained in the present study was due to time constrains, therefore, it should be increased before making further interpretations. With the small number of traces in mind, we do however observe an increasing percentage of autocorrelation curves best described by a 3 component model. Previous studies did not report the need of a 3$^{rd}$ component in AC analysis in either the basal or DAMGO treated cells. This may be due to the use of cells similar to that of the WT HEK293 cells used, which also exhibited no curves best described by 3 components in the basal state, likely due to low GRK expression.

When using PCH analysis, and different from Gondin et al, the data here shows no significant changes in brightness between each time point. However, consistent to previous data (Batista-Gondin, 2018), we do observe increases in number of PCH curves best fit with a second component, with no curves best fit with a second component in curves generated in basal cells, compared to 33% of curves best fit with a second component in curves generated at the 30 min timepoint.

When we assessed SNAP-hMOR organisation in quadruple GRK knockout cells upon addition of DAMGO, we did not observe differences in average particle number or diffusion coefficient for particles described by both component 2 and component 3 in any of the time points, except for the average diffusion coefficient of particles described by component 3 in the 10 min time point, which was significantly faster diffusing than particles described by

component 3 in basal cells (adjusted P value = 0.0117). However, due to the low number of curves generated at each time point, interpretation of these data is limited. This belies the main limitation of this work, the small numbers of curves generated. In order to ascertain differences, greater N numbers would be required, nearer 100 cells, as seen in other studies using FCS (Briddon *et al.*, 2004; Batista-Gondin, 2018; Rogacki *et al.*, 2018; Batista-Gondin *et al.*, 2019). Future work may use the preliminary data generated here to both extend the assays conducted here as well as assess other cell lines with GRKs knocked out, made available in recent work by Drube *et al.*, 2022. Of interest may be GRK2/3 family knockout, which may mimic effects similar to that observed previously with compound 101 (Batista-Gondin, 2018), a GRK2/3 family small molecule inhibitor (Thal *et al.*, 2011). The use of this inhibitor highlighted the role of GRK2/3 in mediating the changes in receptor organisation induced by DAMGO, which was shown to induce no significant change from vehicle following compound 101 treatment.

Other work may focus on the role of GRK 5/6, shown previously to be somewhat important for morphine mediated receptor desensitisation, and whether GRK5/6 alone might induce differences in receptor organisation following morphine treatment.

In conclusion, we do not observe the GRK dependent changes in receptor diffusion reported in previous work and observed differences in the number of components used to model traces observed in cell lines with differential GRK expression. The differences in observations between this study and work by Batista-Gondin *et al.* are likely due to reduced number of traces recorded in each condition in this study.

# Chapter 4: β-arrestin Conformational Signatures Induced by μ-Opioid Receptor Ligands

## 4.1 Introduction

GPCRs have been shown to recruit and activate arrestins, inducing a conformational change in the arrestin. This process allows effectors to bind the now active arrestin, mediating both receptor desensitisation and internalisation, as well as arrestin-dependent signalling, as discussed in section 1.1.5. This process, at least in part, is stimulated by the phosphorylation of the GPCR C-terminal tail by GRKs and other kinases.

The transition of β–arrestin from inactive to active has been shown to involve multiple conformational changes within its structure. The 20 ° twist between the N- and C-domains of arrestin has been a hallmark of activation, but more recently smaller conformational changes have been shown, such as the formation of helices in the finger loop region, the movements of other loops in the central crest, and the exposure of membrane binding residues at the C-edge (see figure 1.1.5.1.1). These changes have been shown to be dependent on structures in the active GPCR, including the receptor core and the phosphorylated C-tail (Gurevich and Gurevich, 2004; Latorraca *et al.*, 2018, 2020).

### 4.1.1 Phosphorylation Barcode Hypothesis

The phosphorylation barcode hypothesis, first suggested as early as 2004 (Gurevich and Gurevich, 2004; Kim *et al.*, 2005; Ren *et al.*, 2005), proposes that the phosphorylation of sites along the C-terminal tail of the receptor can be arranged in patterns, and each of these distinct patterns can transduce different intracellular signalling outcomes, mainly through β-arrestins. This was first shown in the ability of different GRKs to cause distinct signalling outcomes for the angiotensin 2 type 1A receptor and the vasopressin receptor in the ERK signalling pathway. Phosphorylation of the activated receptor C-tail by GRK2/3 upon knockdown of GRK5 or 6 by silencing RNAs exhibited no ERK activation, whereas phosphorylation by GRK5/6 upon GRK2/3 knockdown was shown to promote ERK activation. Interestingly, the reverse was true for receptor internalisation (Kim *et al.*, 2005; Ren *et al.*, 2005). This was then taken further, showing that different GRKs are able to phosphorylate specific phosphorylation sites, that some sites are exclusive to particular GRKs, and that selection of these sites can be ligand directed. This was shown for the β2AR as well as the muscarinic-m3 receptor (Butcher *et al.*, 2011; Nobles *et al.*, 2011). Since then, differential signalling outcomes dependent on phosphorylation patterns have been described for multiple GPCRs including the histamine 4 receptor (Verweij *et al.*, 2020), as well as the vasopressin 2 and β2AR (Ghosh *et al.*, 2019; Baidya, Kumari, Dwivedi-Agnihotri, *et al.*, 2020). It was also shown that β-arrestins can adopt multiple active conformations following activation by different GPCRs, rather than the

interdomain twist accepted previously as active β-arrestin (Shukla *et al.*, 2008), and this was shown to be dependent on receptor C-tail phosphorylation. Thus, in combination, it is theorised that ligand-directed receptor C-tail phosphorylation barcodes induce distinct β-arrestin conformations, and signalling pathways are selected by these conformations.

This work has continued, showing the effects of differing phosphorylation barcodes on β-arrestin conformation in both atomic level simulations and site directed spectroscopy (Latorraca *et al.*, 2020). Simulating the vasopressin receptor C-tail with a variety of phosphorylation patterns, it was shown that individual phosphosites can have positive or negative effects on arrestin binding, and this was independent of their role in β-arrestin activation. It was also shown that the number of phosphosites was not necessarily the driving force behind arrestin binding and activation, but the location of the phosphorylated residues was much more important. Alongside this, it was shown that phosphorylation of individual phosphosites can have major effects on local conformational changes of β-arrestin, such as finger loop movement, interdomain crevice opening, and C-tail displacement. Partial displacement of the β-arrestin C-tail by the receptor C-tail was also shown to be possible, leaving the C-tail of β-arrestin free of the N-domain groove, but still bound at the proximal end.

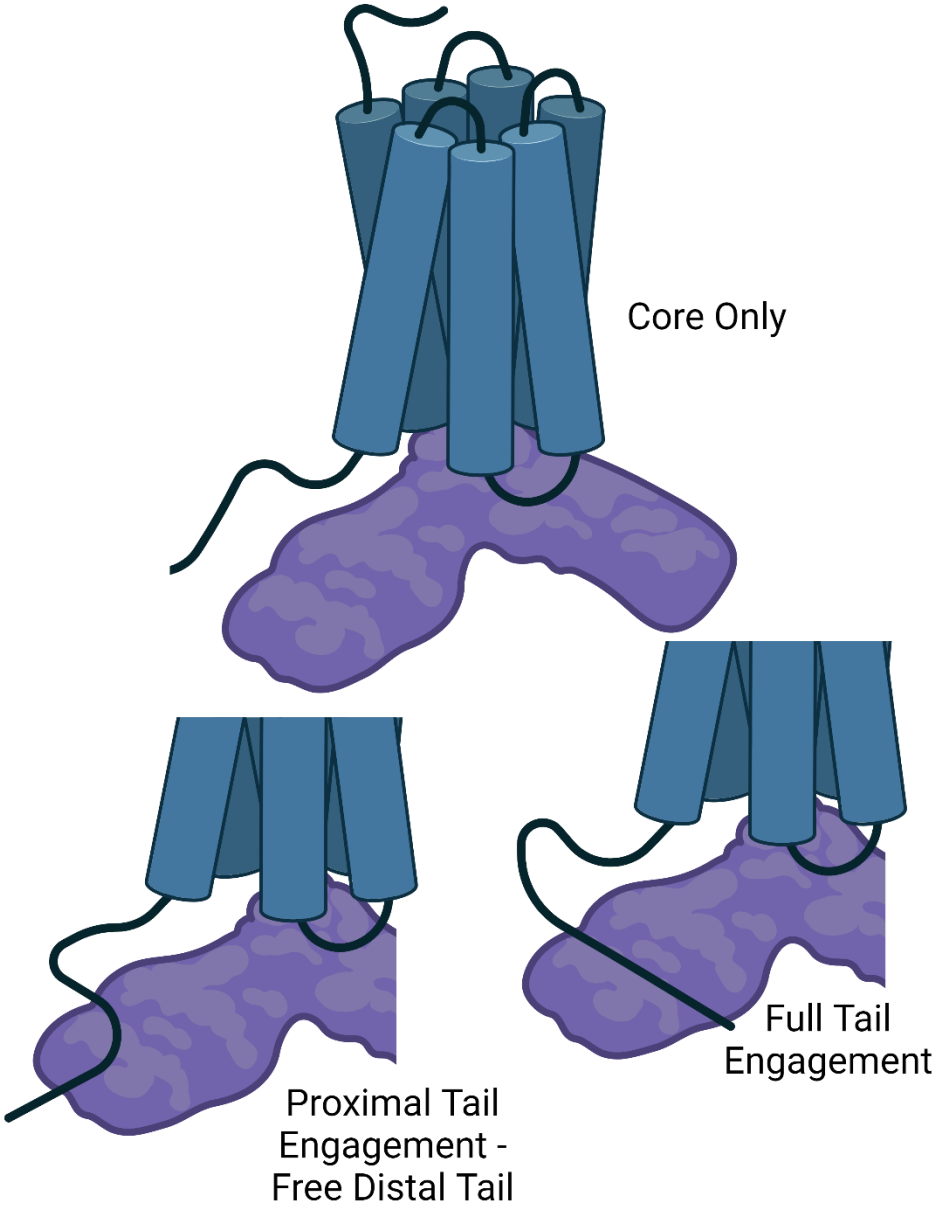


*Figure 4.1.1, diagram depicting engagement modes of arrestin when binding the GPCR C-terminal tail. Core Only engagement may induce conformational changes at the central crest of arrestin, such as the finger loop region. Proximal tail engagement may induce conformational changes in the N-domain, whereas full engagement may induce both conformational changes in the N-domain as well as causing the collapse of the polar core of arrestin, inducing conformational change across both N- and C-domains.*

Mechanisms for the transduction of ligand-dependent β-arrestin conformational change has been recently proposed. First, the formation of secondary structure in the receptor C-tail around the phosphorylation motifs upon their modification has been shown to occur for multiple receptor C-tails (Guillien *et al.*, 2023). The transition of pre-formed secondary structure, or short linear motifs, into specific secondary conformations upon

phosphorylation of certain sites has been shown to increase β-arrestin binding affinity and cause activation, by bringing phosphosites into specific pockets in the a β-arrestin N-domain groove. Different levels and locations of phosphorylation are thought to promote the formation of different secondary structures of the receptor C-tail, either upon phosphorylation itself, or by promoting β-arrestin binding. This allows the receptor C-tail residues to bind different pockets or β-arrestin and potentially elicit a different signalling outcome. Another mechanism proposed for the transduction of ligand-directed β-arrestin conformational change is the embedding of phosphorylation motifs, rather than residues, in pockets along the N-domain groove of β-arrestin. Specific phosphosites have been suggested to have inhibitory or activating effects on β-arrestin by forming salt bridges with the gate loop of β-arrestin, which, by drawing the gate loop into activating or inhibitory positions, can modulate the interdomain twist angle and control the global activation state of β-arrestin (Latorraca *et al.*, 2018, 2020). Other pockets along the N-domain groove of arrestin hold negatively charged residues, forming strong interactions with the receptor C-tail, stabilising binding rather than activating β-arrestin. In opposition to this, other phosphosites are drawn to pockets further out of the groove of β-arrestin, peeling the other sites away and reducing binding stability. The actual mechanism of ligand-directed arrestin conformational change may be a combination of these two processes, selection by secondary structures of C-tail of receptor and/or positive/negative effects of specific residues. Additionally, different GPCRs may rely on these mechanisms to different extents.

In order to propose a general mechanism for β-arrestin binding and activation an effort has been made to find consensus motifs for GPCR phosphosites. It has been suggested that specific phosphorylation codes are present across several GPCRs, and that these phosphorylation patterns will result in defined signalling outcomes (Zhou *et al.*, 2017; Baidya, Kumari, Dwivedi-Agnihotri, *et al.*, 2020). Two codes have been originally linked to high affinity β-arrestin binding, PxPxxP and PxxPxxP, the short and long codes respectively, in which P is either serine or threonine, and x is any residue other than proline (however the final P can be substituted for a phosphomimetic residue such as glutamic acid or aspartic acid). Mutation of residues within these sequences reduces visual and β-arrestin1 recruitment to both rhodopsin and the vasopressin 2 receptors, respectively. The three phosphorylated residues bind in three pockets in the N-domain of β-arrestin reported to be highly conserved across arrestin isoforms and different species (Gurevich and Gurevich, 2006; Zhou *et al.*, 2017). The reported codes have been shown to be present at least once in the C-tail of some GPCRs, however they have also been shown to repeat multiple times in a variety of receptors, such as adrenoceptors, chemokine receptors, as well as the

parathyroid hormone 1 receptor and the glucagon like peptide 1 receptor. However, the mutation of these codes in the β2-adrenoceptor to mimic that of the vasopressin receptor converts the normally ERK-excitatory role of β-arrestin1 to an ERK-inhibitory role, as is the case with the vasopressin receptor. This indicates for signalling, the long and short codes (PxPxxP and PxxPxxP) discussed in Zhou *et al.*, 2017 are dispensable, and in fact the formation of double threonine motifs affects signalling, and the PxPP code is responsible for changing ERK phosphorylation so dramatically (Baidya, Kumari, Dwivedi-Agnihotri, *et al.*, 2020). Supporting this, original work on the chemokine receptor CCR5 has reported the PxPP code to be responsible for the recruitment of β-arrestin1 in many other receptors. The titration of binding affinities detected by trypsin proteolysis and NMR by individual phosphosites shows a reliance on certain phosphosites over others in the CCR5 and vasopressin 2 receptor. These phosphosites form the PxPP motif in both the receptors assayed, and this motif is present across a selection of class B receptors (Isaikina *et al.*, 2022).

### 4.1.2 MOR Phosphorylation Sites and Patterns

The MOR has 11 serine/threonine residues on the C-terminal tail. The mouse (*Mus* musculus) MOR (mMOR) sequence is two amino acids shorter and has three differences from the human (homo sapiens) MOR (hMOR) in the C-tail region; namely, the C-terminal T of the TSST motif in mMOR, at the proximal end of the C-tail (closer to the helical domains), is exchanged for N in the hMOR, however the number of phosphosites are maintained by the exchange of A364 of the mMOR for T366 in the hMOR. The other difference between mMOR and hMOR is the exchange of E372 in the mMOR for D374 in the hMOR, located in the first section of the THREPSTANT motif described as important for arrestin binding and MOR signalling (Schulz *et al.*, 2004; Doll *et al.*, 2011; Pándy-Szekeres *et al.*, 2023). The C-tail of hMOR and mMOR are shown in figure 4.1.2.1, and the mMOR numbering will be used for the remainder of this work, due to the majority of studies using this homolog.

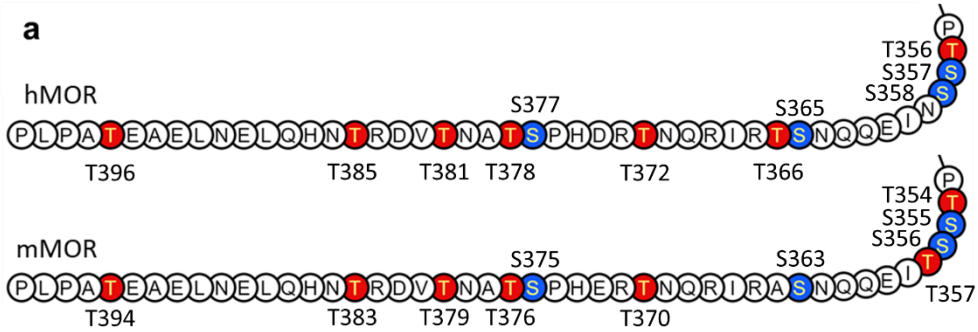


*Figure 4.1.2.1, Snake plots of the C-terminal tail region after helix 8 of MOR homologs human MOR (hMOR, top) and mouse MOR (mMOR, bottom) with serine and threonine residues highlighted in blue and red respectively.*

In contrast to the receptors discussed in the previous section, neither the Px(x)PxxP(D/E) or PPxP codes appear in the hMOR C-tail, although the PPxP motif appears in the TSST motif of the mMOR, though much more proximal

than described for other receptors (Zhou *et al.*, 2017; Baidya, Kumari, Dwivedi-Agnihotri, *et al.*, 2020; Isaikina *et al.*, 2022).

S363 has been shown to be constitutively phosphorylated by PKC in MORs expressed in HEK293 cells and in mouse brain *in vivo*, however GRKs are have been shown to phosphorylate this site in the presence of PKC inhibition, (El Kouhen *et al.*, 2001; Illing, Mann and Schulz, 2014). PKCα has also been shown to be able to phosphorylate T370, the first T in the THREPSTANT motif, when activated directly or by activation of nearby GPCRs. However, again, in the absence of PKC, GRKs are able to phosphorylate this residue. In fact, GRKs were shown to be faster than PKC at phosphorylating T370, indicating a preference for agonist-driven phosphorylation. However, T370 has been shown to be critical for PKC driven internalisation of the MOR, which, under endogenous GRK expression, can be induced to some degree by the PKC activator PMA. In contrast, DAMGO-mediated internalisation remains unaffected when T370 is individually mutated. Both S363 and T370 have been shown to be constitutively phosphorylated by mass spectrometry (Chen *et al.*, 2013). S363 mutation to alanine has been shown to increase the rate of DAMGO-mediated internalisation but not its extent, and the additional T370A mutation further increased rate and extent of receptor internalisation, indicating that phosphorylation of some sites may have inhibitory effects on different β-arrestin mediated processes (El Kouhen *et al.*, 2001).

| Amino Acid | Residue No. | | Motif | Phospho-site | Kinase | Ligand | Effect | Reference |
|---|---|---|---|---|---|---|---|---|
| | Mouse | Human | | | | | | |
| T | 354 | 356 | TSST | N | - | - | - | (Wang *et al.*, 2002) |
| S | 355 | 357 | TSST | Y | GRK2 (3?) | DAMGO | Reduced Agonist Dissociation, Sustained Desensitisation | (Wang *et al.*, 2002; Lau *et al.*, 2011; Birdsong *et al.*, 2015; Arttamangkul *et al.*, 2018, 2019; Miess *et al.*, 2018) |
| S | 356 | 358 | TSST | Y | GRK2 (3?) | DAMGO | Agonist Dissociation, Sustained Desensitisation | (Chen *et al.*, 2013; Birdsong *et al.*, 2015; Yousuf *et al.*, 2015; Arttamangkul *et al.*, 2018, 2019; Miess *et al.*, 2018) |
| T | 357 | - | TSST | Y | GRK2 (3?) | DAMGO | Agonist Dissociation, Sustained Desensitisation | (Wang *et al.*, 2002; Lau *et al.*, 2011; Chen *et al.*, 2013; Yousuf *et al.*, 2015; |

| | | | | | | | | |
|---|---|---|---|---|---|---|---|---|
| | | | | | | | | Arttamangkul *et al.*, 2018, 2019; Miess *et al.*, 2018) |
| S | 363 | 365 | - | Y | PKC | PKC Activators | Internalisation | (Doll *et al.*, 2011; Feng, Li and Wang, 2011; Chen *et al.*, 2013; Illing, Mann and Schulz, 2014; Mann *et al.*, 2015) |
| T | - | 366 | - | ? | - | - | ? | |
| T | 370 | 372 | THREP-STANT | Y | PKC, GRK2/3, CAMKII | DAMGO | Internalisation | (Doll *et al.*, 2011; Chen *et al.*, 2013) |
| S | 375 | 377 | STANT | Y | GRK2/3, GRK5* | DAMGO, Morphine* | Hierarchical Phosphorylation, Acute Desensitisation, Arrestin Recruitment, Internalisation | (Deng *et al.*, 2000; El Kouhen *et al.*, 2001; Schulz *et al.*, 2004; Doll *et al.*, 2011; Chen *et al.*, 2013; Glück *et al.*, 2014; Lowe *et al.*, 2015; Møller *et al.*, 2020) |
| T | 376 | 378 | STANT | Y | GRK2/3 | DAMGO | Internalisation, Desensitisation, Arrestin Recruitment | (Lau *et al.*, 2011; Moulédous *et al.*, 2012; Yousuf *et al.*, 2015; Gillis, Batista-Gondin, *et al.*, 2020a; Møller *et al.*, 2020; Fritzwanker, Schulz and Kliewer, 2021) |
| T | 379 | 381 | STANT | Y | GRK2/3 | DAMGO, Morphine | Internalisation, Desensitisation, Arrestin Recruitment | (Lau *et al.*, 2011; Moulédous *et al.*, 2012; Yousuf *et al.*, 2015; Gillis, Batista-Gondin, *et al.*, 2020a; Møller *et al.*, 2020; Fritzwanker, Schulz and Kliewer, 2021) |

| | | | | | | | | |
|---|---|---|---|---|---|---|---|---|
| T | 383 | 385 | - | N | - | - | - | (Lau *et al.*, 2011) |
| T | 394 | 396 | - | Y? | ? | ? | Internalisation | (Wolf *et al.*, 1999; Deng *et al.*, 2000; El Kouhen *et al.*, 2001; Lau *et al.*, 2011; Kliewer *et al.*, 2019) |

*Table 4.1.2.2, table showing the serine and threonine sites of the mouse and human MOR, their numbering within each homolog. Table also shows role of each residue in phosphorylation motifs, and the ability of each residue to become phosphorylated and by what kinase. Table also highlights ligands known to induce phosphorylation at each residue, and the effect phosphorylation of each residue contributes to. ? = unknown/under-studied*

Perhaps the most important motif for MOR regulation is the STANT motif. S375 is the most important residue for MOR internalisation; mutation of S375 has been shown to reduce internalisation rate and extent upon DAMGO treatment (El Kouhen *et al.*, 2001). Seminal work using phosphosite specific antibodies showed that this is the first residue to be phosphorylated upon receptor activation by all agonists. S375 phosphorylation is necessary for the subsequent phosphorylation of other residues within the MOR C-tail, which is consistent with the role of S375 in its hierarchical phosphorylation (Just *et al.*, 2013; Miess *et al.*, 2018). GRK2/3 or GRK5 have also been proposed to phosphorylate this site in an agonist-dependent manner (Schulz *et al.*, 2004; McPherson *et al.*, 2010). Once S375 is phosphorylated, GRK2/3 but not GRK5 go on to phosphorylate T376, T379, and T370 (Doll *et al.*, 2012; Mann *et al.*, 2015). Recent work with HEK293T cells lacking GRK2/3 have shown reduced but still detectable phosphorylation at T370 and T379 in response to high efficacy agonists (Fritzwanker, et al, unpublished data). Thus, while phosphorylation of T376 by GRK2/3 was confirmed, it remains unclear which kinases may phosphorylate T370 and T379 in the absence of GRK2/3 (Møller *et al.*, 2020; Drube *et al.*, 2022).

Closer to the helix 8, there is the TSST motif. TSST mutation to alanine has been shown to not affect the phosphorylation of other residues along the remainder of the C-tail (El Kouhen *et al.*, 2001; Just *et al.*, 2013; Birdsong *et al.*, 2015; Yousuf *et al.*, 2015; Miess *et al.*, 2018). Upon the mutation to alanine of sites other than the TSST motif and T394 , there was no observed internalisation, indicating the dominance of the THREPSTANT motif, and S363, for this process (Yousuf *et al.*, 2015). Further to this, while mass spectrometry has shown the TSST motif to be phosphorylated (Chen *et al.*, 2013), the site has been shown to be dispensable for internalisation by its mutation to alanine (Lau *et al.*, 2011). Two phosphosites in TSST were shown to have redundant control over acute desensitisation, in that phosphorylation of S355 and/or S357 induces acute desensitisation of the receptor. Mutation of both these sites to alanine exhibited inhibition ability to desensitise the

MOR (Wang *et al.*, 2002). Intriguingly, Birdsong, *et al.,* showed that for acute desensitisation of the MOR, TSST and STANT provide redundant control, requiring both motifs to be mutated in order to prevent desensitisation (Birdsong *et al.*, 2015). Furthermore, another role for the TSST motif in slowing agonist unbinding in an agonist-dependent manner has been suggested. Agonists able to phosphorylate this motif (such as Met-enkephalin or DAMGO) strongly induced the receptor to remain in a conformation with higher affinity for agonists after agonist unbinding, an effect that was attenuated upon mutation of TSST, but not STANT (Birdsong *et al.*, 2015).

Phosphorylation of other potential phosphosites in the C-tail, such as T383 and T394 has been less well studied, with suggestions that these sites are not phosphorylated. However, mutation of T394 to alanine reduced phosphorylation of other sites on the C-tail slightly, suggesting a potential role in C-tail phosphorylation (El Kouhen *et al.*, 2001). This differs in CHO cells, where this site is shown to be phosphorylated, and mutation of this site leads to a large reduction in phosphorylation of other residues in the C-tail (Deng *et al.*, 2000). Truncation of the MOR C-tail including this site exhibits no change in internalisation (Trapaidze *et al.*, 2000), and maintenance of this site when others are mutated does not retain internalisation. (Yousuf *et al.*, 2015).

As expected, when all potential phosphosites within the C-tail of MOR are removed by mutation, acute receptor desensitisation, as well as internalisation are significantly reduced or abolished (Yousuf *et al.*, 2015; Arttamangkul *et al.*, 2018; Miess *et al.*, 2018; Kliewer *et al.*, 2019). Importantly, this effect has also been shown for long-term tolerance (Arttamangkul *et al.*, 2018; Kliewer *et al.*, 2019), suggesting the desensitisation and internalisation of the MOR plays a significant role in increasing tolerance of opioid ligands.

Finally, splice variants of the MOR have also been shown to alter the C-terminal tail sequence , introducing substantially differing phosphorylation sites and subsequently causing different signalling, in both G protein and β-arrestin2 (Abrimian, Kraft and Pan, 2021). This has been suggested to be due to the introduction of sequences of generic motifs by many of the splice variants commonly seen in GPCRs that induce β-arrestin2 binding, although the physiological relevance of this is still unclear (Kliewer *et al.*, 2019)

Intracellular loop phosphorylation has been included in the phosphorylation barcode hypothesis (Nobles *et al.*, 2011), and clear evidence that they play a role in β-arrestin activation has been shown for some GPCRs (Latorraca *et al.*, 2018). However, the MOR has relatively short intracellular loops and the role intracellular loop phosphorylation plays in the recruitment and activation of β-arrestins by the MOR has not been extensively studied. It has been shown that polar interactions between the intracellular loops 2 and 3 and β-arrestin

leads to coupling of β-arrestin to the MOR, however the phosphorylation state of the phosphosites on MOR ICL3 has not been ascertained. It has been suggested that no phosphorylation of the ICLs of the MOR occurs even upon high efficacy agonist stimulation (El Kouhen *et al.*, 2001). While there are three possible sites for phosphorylation, S263, S268, and S270, phospho-antibodies for these sites have not been generated. Their role is yet to be elucidated.

### 4.1.3 Opioid ligand-directed phosphorylation

As discussed in section 1.2.2, there are a variety of pharmacologically diverse ligands for the MOR, and each has shown different effects on the phosphorylation of the MOR C-terminal tail.

High efficacy ligands, such as DAMGO and fentanyl, have been shown to internalise the MOR readily (Just *et al.*, 2013; Batista-Gondin *et al.*, 2019), and exhibit high degrees of phosphorylation, with the THREPSTANT motif becoming phosphorylated within a min, and, for fentanyl, at nanomolar concentrations (Doll *et al.*, 2011; Gillis, Batista-Gondin, *et al.*, 2020a). Morphine, a partial agonist, exhibits very limited internalisation (C. P. Bailey *et al.*, 2009; Glück *et al.*, 2014; Batista-Gondin *et al.*, 2019) but does cause phosphorylation of S375 and weak phosphorylation at T370 and T379 (Doll *et al.*, 2011; Gillis, Batista-Gondin, *et al.*, 2020a). Lower efficacy agonists, such as oliceridine, and buprenorphine, both exhibit weak phosphorylation of S375, and weak but detectable phosphorylation at T370, with no internalisation detected in imaging studies (Just *et al.*, 2013; Gillis, Batista-Gondin, *et al.*, 2020a; Fritzwanker, Schulz and Kliewer, 2021).

Upon GRK overexpression, as shown in section 2.3.1.2 and previously (Batista-Gondin *et al.*, 2019; Gillis, Batista-Gondin, *et al.*, 2020a), β-arrestin recruitment and receptor internalisation are much increased, and ligands such as morphine become able to internalise the receptor, likely by increased phosphorylation of the THREPSTANT motif.

The varied changes in phosphorylation patterns exhibited by MOR ligands across the length of the C-tail may have effects not only on β-arrestin recruitment, but on the conformations formed by the β-arrestin.

### 4.1.4 Arrestin Conformational Biosensors

#### *4.1.4.1 Early Arrestin Conformational Sensors*

The first use of BRET to monitor arrestin conformational changes was published in 2005, using a single conformational change sensor with the luciferase and YFP on each of the extremes of the N-and C-termini respectively (Charest, Terrillon and Bouvier, 2005). The data indicated that arrestin conformational change was dependent on the binding of effectors, such as the AP2 complex or downstream signalling proteins such as ERK, rather than activation by a receptor, due to the time taken for conformation

to change (Charest, Terrillon and Bouvier, 2005). This conformational sensor was subsequently used to investigate the effects of G protein and β-arrestin biased agonists for the angiotensin 1 and parathyroid hormone receptors, their biased mutants, and ligands of different efficacies for the β2 adrenoceptor. This study highlighted that arrestin could form multiple conformations, as shown by opposing changes in BRET upon treatment with different ligands (Shukla *et al.*, 2008).

#### *4.1.4.2 Latest Generation Arrestin Conformational Sensors*

The creation of intramolecular biosensors in which the fluorophore sites could be located in different regions of arrestin allowed for the more detailed study of conformational changes of this protein (Lee *et al.*, 2016; Nuber *et al.*, 2016). In these papers, the cyan fluorescent protein (CFP), or *renilla* luciferase (rLuc) was fused to the C- or N-terminus respectively, similar to the original Charest sensor. However, as opposed to tagging another large fluorescent protein partner to the opposing domain, Fluorescein Arsenical Hairpin (FlAsH) binding sites were inserted into the periphery of the arrestin molecule to detect conformational changes across the molecule, rather than a single point, and assuming global activation.

These locations were selected due to their lack of reported involvement in interaction of β-arrestin1 with the receptor, and as such are situated on the outer loops of the N- and C-domain. While the C-edge has now been shown to be involved in membrane binding (Lally *et al.*, 2017; Grimes *et al.*, 2022), this had not been reported at time of construct generation.

The use of FlAsH replaces fusion proteins such as YFP, or acyl carrier proteins such as HALO or SNAP tags, which are large, and can cause steric hinderance to changes in conformation (Fernandes *et al.*, 2017). The mutation of the protein sequence in the loops to that of the tetra-cysteine motif, in this case CCPGCC (Nuber *et al.*, 2016), provides the required binding site for the FlAsH molecule, which, upon binding the peptide, exhibits a red-shift of 16 nm and a significant increase in brightness when excited (Fernandes *et al.*, 2017).

The BRET rLuc–β-arrestin2–FlAsH sensors were able to generate population average data on the conformations formed across multiple cells. Six sensors were created with different FlAsH binding locations (Lee *et al.*, 2016). The FRET β-arrestin2–FlAsH-CFP sensors on the other hand had 8 sensors with different FlAsH binding sites, and using FRET, could observe single cell changes, and with higher temporal resolution, could also observe conformational change kinetics (Nuber *et al.*, 2016).

Using BRET-based assays, Lee *et al.*, 2016, showed that individual GPCRs, as well as structurally diverse ligands acting through the same GPCR, can induce distinct conformational changes, resulting in a conformational signature

specific to that receptor or ligand. This conformational heterogeneity might highlight a possible mechanism as to how arrestins can transduce different effects despite being effectors for hundreds of different GPCRs. This was later supported by showing very different conformational signatures upon activation by the Galanin receptor treated with differing endogenous ligands (Reyes-Alcaraz *et al.*, 2018). More mechanistically, the FRET sensor developed by Nuber *et al.*, 2016, delineated the distinct steps of arrestin binding, activation, and unbinding, as well as the changes in conformation that occurs with each step. This work also suggested that arrestin can remain activated upon unbinding from the receptor, a concept further highlighted in later reports (Eichel *et al.*, 2018b).

Conformationally selective antibody fragments have also been used as conformational biosensors. These have shown the similarities between β-arrestin1 and β-arrestin2 conformations, mainly when they bind to the C-tail of the receptor, however when binding to the receptor core the conformation adopted by arrestins is dramatically distinct, to the point where the antibody fragment cannot recognise them (Ghosh *et al.*, 2019). This work suggests that the main differences in signalling between the two β-arrestin isoforms is either determined by epitopes that do not engage the antibody fragment, or by conformational changes that are induced by receptor core interaction.

These findings were later supported in a paper by Oishi, Dam and Jockers, in 2020*,* using arrestin mutants which allowed further separation of these canonical arrestin binding steps. Deletion of the finger loop region prevented core interactions, and mutation of R170 to glutamic acid created a constitutively partially active arrestin similar to that used previously (Potter *et al.*, 2002; Charest, Terrillon and Bouvier, 2005; Scheerer and Sommer, 2017). This study used sensors more similar to(Charest, Terrillon and Bouvier, 2005), in which only a single donor and acceptor were used, on the N and C terminals of arrestin, however, overcame the weakness of the earlier sensors by being able to measure changes in basal BRET, therefore highlighting the difference between the WT and 'phosphorylation independent' constitutively active mutant (Oishi, Dam and Jockers, 2020).

### 4.1.5 β-arrestin2-FlAsH-Nluc Conformational Biosensors

The β-arrestin conformational sensors used in this chapter was developed from the FRET sensors described in Nuber *et al.*, 2016 (Charest, Terrillon and Bouvier, 2005). This second generation of intramolecular biosensors have improved high throughput capabilities through the replacement of the FRET donor CFP with a bright BRET donor Nanoluciferase (Nluc). These sensors have been used in several studies to date, in a variety of receptors (Moritz *et al.*, 2021; Boldizsar *et al.*, 2022; Drube *et al.*, 2022)

### 4.1.6 Aims

In this chapter, we intend to use previously described β-arrestin2-FlAsH-Nluc conformational biosensors (Nuber *et al.*, 2016; Haider, 2021) to understand the mechanism by which arrestin conformations are transduced by different opioid ligands. To understand these mechanisms, we will assess the conformational changes in β-arrestin2 upon activation by the MOR following treatment with a diverse set of opioid ligands. Following this, we will assess the role of the MOR C-tail in the transduction of these conformational changes by directly manipulating the MOR C-tail. Mutation of previously identified phosphosites (Miess *et al.*, 2018) to alanine will provide evidence for the involvement of these sites in the formation of different β-arrestin2 conformations.

## 4.2 Methods

### 4.2.1 β-arrestin2-FlAsH-Nluc sensor Expression and Functionality

#### *4.2.1.1 Luminescence Assay*

Plasmids for the β-arrestin2-FlAsH-Nluc sensors (F0 to 10) were a gift from Carsten Hoffman, from the University of Jena (Germany) [119]. Each of these were transfected into HEK293T cells as described in section 2.2.2.1. 24h after transfection cells were re-plated into PDL coated 96 well plates. 24 hours later, media was aspirated, and cells were washed once with PBS and then incubated with 90 µL/well PBS for 30 mins at 37 °C. Coelenterazine H was added to relevant wells, to achieve a final concentration of 5 µM, along with a PBS control. Following a 5-min incubation, plates were read in a CLARIOstar Plate Reader (BMG Labtech) to detect luminescence at 450 – 475 nm. These plates then underwent two more washing steps, before luminescence was read again.

#### *4.2.1.2 Luciferin Spectral Scan*

Cells were plated in 6 well plates and transfected using β-arrestin2-FlAsH-Nluc construct F0, then re-plated into 96 well plates, incubated as described above, and treated with coelenterazine H or furimazine as described. Plates were incubated for 5 mins, and a spectral scan at 3nm intervals was obtained for each substrate in a CLARIOstar Plate Reader.

#### *4.2.1.3 Luminescence Imaging*

Cells were plated in 6 well plates and transfected using β-arrestin2-FlAsH-Nluc constructs F0 to F10. Cells were then transferred into 3.5 cm polymer imaging dishes coated with poly-L-lysine (PLL, prepared adding 1 mL of 50 µg/mL PLL in Phosphate Buffered Saline (PBS) and incubated for 1hr, then washed with 1 mL PBS). Following re-plating, cells were incubated at 37 °C in a 5% $CO_2$ humidified environment for 24 hours. Media was aspirated and cells were incubated with 1 mL Hank's Buffered Saline Solution for 30 mins and 5 µM furimazine for 10 mins. Images were captured using an LV200 Bioluminescence Microscope (Olympus) with a 60x 1.35NA objective lens; brightfield images taken with 100 ms exposure, bioluminescence images were taken with 5 s exposure and images processed using ImageJ.

#### *4.2.1.4 K-Ras Membrane Recruitment Assay*

HEK293T cells were transfected with each of the β-arrestin2-FlAsH-Nluc constructs, GRK2, and hMOR, as well as either an empty vector or a membrane tethered K-Ras construct tagged with a Venus fluorophore. Cells were replated into PDL coated 96 well white plates, and 24 hours later media was replaced with 80 µL HBSS and cells incubated for 30 mins at 37 °C at 5% $CO_2$. Cells were then treated with 10 µM DAMGO and incubated for 5 mins at 37 °C, followed by addition of furimazine at a final concentration of 5 µM,

and incubated for 5 mins. Plates were read on a PHERAstar Plate Reader (BMG Labtech) using the BRET1 filter set (535 ± 30 nm (fluorescence), 475 ± 30 nm (luminescence)).

#### *4.2.1.5 β-Adaptin2-YFP Recruitment Assay*

HEK293T cells were transfected with each of the β-arrestin2-FlAsH-Nluc constructs, GRK2, and hMOR, as well as either an empty vector or β-Adaptin2 tagged with a YFP fluorophore (kind gift from Jonathan Javitch, Columbia University, NYC, USA). 24 hours post-transfection, cells were re-plated into PDL coated 96 well white plates, and 24 hours later media was replaced with 80 µL HBSS and cells were incubated for a further 30 mins at 37 °C at 5% $CO_2$. Cells were then treated with 10 µM DAMGO and incubated for 5 mins, followed by furimazine at a final concentration of 5 µM, and incubated for 5 mins. Plates were read on a PHERAstar Plate Reader (BMG Labtech) using the BRET1 filter set (535 ± 30 nm (fluorescence), 475 ± 30 nm (luminescence)).

### 4.2.2 Effects of Opioid Ligand on MOR regulation

#### *4.2.2.1 β–arrestin2-YFP Recruitment Assay*

HEK293T cells were transfected with a β-arrestin2 construct tagged with a C-terminally Venus fluorescent protein, and hMOR tagged with a N-terminal FLAG tag and a C-terminal Nluc. 24 hours after transfection cells were plated in white 96 well plates, had media replaced with 80 µL HBSS, and were incubated for 30 mins at 37 °C at 5% $CO_2$. Cells were then treated with agonist at increasing concentrations and incubated for 5 mins, followed by furimazine at a final concentration of 5 µM, and incubated for 5 mins. Plates were read on a PHERAstar Plate Reader (BMG Labtech) using the BRET1 filter set (535 ± 30 nm (fluorescence), 475 ± 30 nm (luminescence)).

#### *4.2.2.2 β-Adaptin2-YFP Recruitment Assay*

Assay was conducted as described in 4.2.2.1, transfecting β-arrestin2-Nluc (F0) as opposed to the β-arrestin2-FlAsH-Nluc constructs and treating with agonist at increasing concentrations.

#### *4.2.2.3 SNAPsurface Internalisation Imaging*

To assess opioid ligand ability to internalise the MOR with and without GRK2 overexpression, HEK293T cells stably expressing SNAP-hMOR were plated in 10cm dishes and 24 hours later transiently transfected with GRK2-Venus. 24 hours later cells were re-plated into PDL coated, Nuntek #1.0 chambered coverglass imaging slides, and incubated for a further 24 hours. Cells were SNAP-labelled with AlexaFluor647 as described in section 3.3.2 and imaged at 24°C on a Zeiss LSM880 confocal microscope, using a 633 nm and 488 nm laser, as described in section 3.3.2. Images taken before ligand addition and 20 mins post-ligand addition.

### 4.2.3 Intramolecular BRET Conformational Change Assay and Optimisation

To assess the conformational changes of β-arrestin2 induced by MOR activation by various ligands, cells were transfected with one of the β-arrestin2-FlAsH-Nluc constructs (F0 to F10) alongside MOR. Cells were washed twice with 100 µL/well HBSS, and then incubated with 100 µL of label solution (250 nM FlAsH-EDT2, 12.5 µM ethanedithiol (EDT) in HBSS) for 60 mins at room temperature. Wells were then aspirated and incubated for 10 mins with 100 µL wash solution (250 µM EDT). Cells were then incubated with 80 µL HBSS, before furimazine at a final concentration of 5 µM was added, incubated for 5 mins, and baseline BRET read in a PHERAstar Plate Reader (BMG Labtech) using the BRET1 filter set (535 ± 30 nm (fluorescence), 475 ± 30 nm (luminescence)) for 5 mins. 10 µL of ligand at the stated final concentrations of in HBSS or a HBSS vehicle control were then added. The plate was read every min as described above for a further 15 mins.

### 4.2.4 Data analysis

Data generated in the above assays were analysed using Prism v9.5.1 (GraphPad Software Inc., San Diego, CA). To determine maximal responses (Emax) and potencies (Log(EC50)), concentration–response curves were analysed using the three-parameter equation using the model:

$$y = Bottom + \frac{Top - Bottom}{1 + 10^{(Log(EC50) - x)}}$$

where Top and Bottom are the maximal and minimal responses in the y axis respectively, and EC50 is the ligand concentration that gives the response halfway between the maximal and minimal response.

The data generated in the conformational change assays were normalised to their own baseline and corrected for spectral overlap between the Nluc and FlAsH emission spectra through the following process. The BRET ratio was calculated by dividing the measured fluorescence by the measured luminescence for each sensor, and the F0 BRET ratio response was subtracted from the baseline (pre-ligand addition) and ligand response BRET ratios generated by the other sensors. The response BRET ratios were then normalised to generate the baseline BRET ratios to correct for differences in starting BRET ratio by calculating the percentage difference:

$$\Delta net\ BRET\ ratio(\%\ Baseline) = 100\ \times \frac{(ligand\ response - baseline)}{baseline}$$

Statistical differences were determined using T tests to assess significant changes from zero via one-sample t test. Unpaired t-tests were conducted to

assess significant differences from WT in the phosphomutant conformational change assay.

#### 4.2.4.1 Transfection Schema

| Assay | Plate | Media (mL) | DNA (µg) | | | | | | | | PDL (µL) |
|---|---|---|---|---|---|---|---|---|---|---|---|
| | | | Receptor | | | | βarrestin | | | β- | |
| | | | MOR-Nluc | PM/WT MOR | GRK2 | GRK2-Venus | 2-FlAsH-Nluc | βarrestin 2-YFP | K-Ras Venus | Adaptin 2-YFP | |
| Luminescence Assay | 6 well | 3 | | | | | 0.05 | | | | 6 |
| Luciferin Spectral Scan | 6 well | 3 | | | | | 0.05 | | | | 6 |
| Luminescence Imaging | 6 well | 3 | | | | | | | | | 6 |
| K-Ras Recruitment | 6 well | 3 | | 0.5 | 2 | | 0.3 | | 2 | | 6 |
| β-Adaptin2 Recruitment | 6 well | 3 | | 0.5 | 2 | | 0.3 | | | 2 | 6 |
| βarrestin2 Recruitment | 10 cm | 3 | 1 | | 2 | | | 4 | | | 30 |
| Internalisation Imaging | 10 cm | 10 | | | | 5 | | | | | 30 |
| Conformational Change | 24 well | 1 | | 0.5 | 0.5 | | 0.05 | | | | 2 |

*Table 4.2.4.1, table showing transfection volumes and micrograms of DNA of each plasmid for each assay used in this chapter.*

## 4.3 Results

### 4.3.1 β-arrestin2-FlAsH-Nluc sensor Expression and Functionality

In order to validate β-arrestin2-FlAsH-Nluc sensor expression and functionality, a selection of assays were conducted to examine the key characteristics of arrestin function (figure 4.3.1.1).

To assess expression, we first examined the ability of each β-arrestin2-FlAsH-Nluc construct to exhibit luminescence when treated with coelenterazine in transiently transfected HEK293 cells as described in section 4.2.1.1. Luminescence was read on a PHERAstar plate reader and determined relative to F0, which is a biosensor that harbours the Nluc tag but not the FlAsH sequence. As shown in fig. 4.3.1.1a, all constructs exhibit luminescence, except F8, which showed no luminescence above pcDNA empty vector (EV) control. This suggested that F8 was not expressed, and therefore was not used in further assays.

These experiments were extended by washing the cells three more times in assay buffer, and comparing the luminescence, thus simulating the future protocol which would involve labelling the β-arrestin2-FlAsH-Nluc sensors with FlAsH reagent. We saw a reduction in luminescence of between 80 and 95% upon successive washes. Despite this reduction, due to the brightness of Nluc, and the use of a brighter, more stable luciferin substrate, furimazine (see fig. 4.3.1.1d) in the BRET protocol, the remaining luminescence was still deemed sufficient moving forwards.

To determine the efficiency and homogeneity of transfection, and the localisation of the β-arrestin2-FlAsH-Nluc sensors in the cell, images of HEK239T cells transiently transfected with each β-arrestin2-FlAsH-Nluc construct following addition of furimazine were captured by an Olympus LV200 Bioluminescence microscope. Figure 4.3.1.1e shows that most of the cells in the field of view exhibited luminescence, albeit to different extents as expected from a transient transfection, showing a high transfection efficiency. The luminescence signal was confined to the cytoplasm of cells, highlighted by the clearly defined, darker, nuclei, confirming that the β-arrestin2-FlAsH-Nluc sensors retain the localisation of the original protein. These results show that the β-arrestin2-FlAsH-Nluc constructs were successfully translated, transcribed, and exported to the cytoplasm retaining the properties of the parent protein. Cells appeared healthy following transfection and proliferated well.

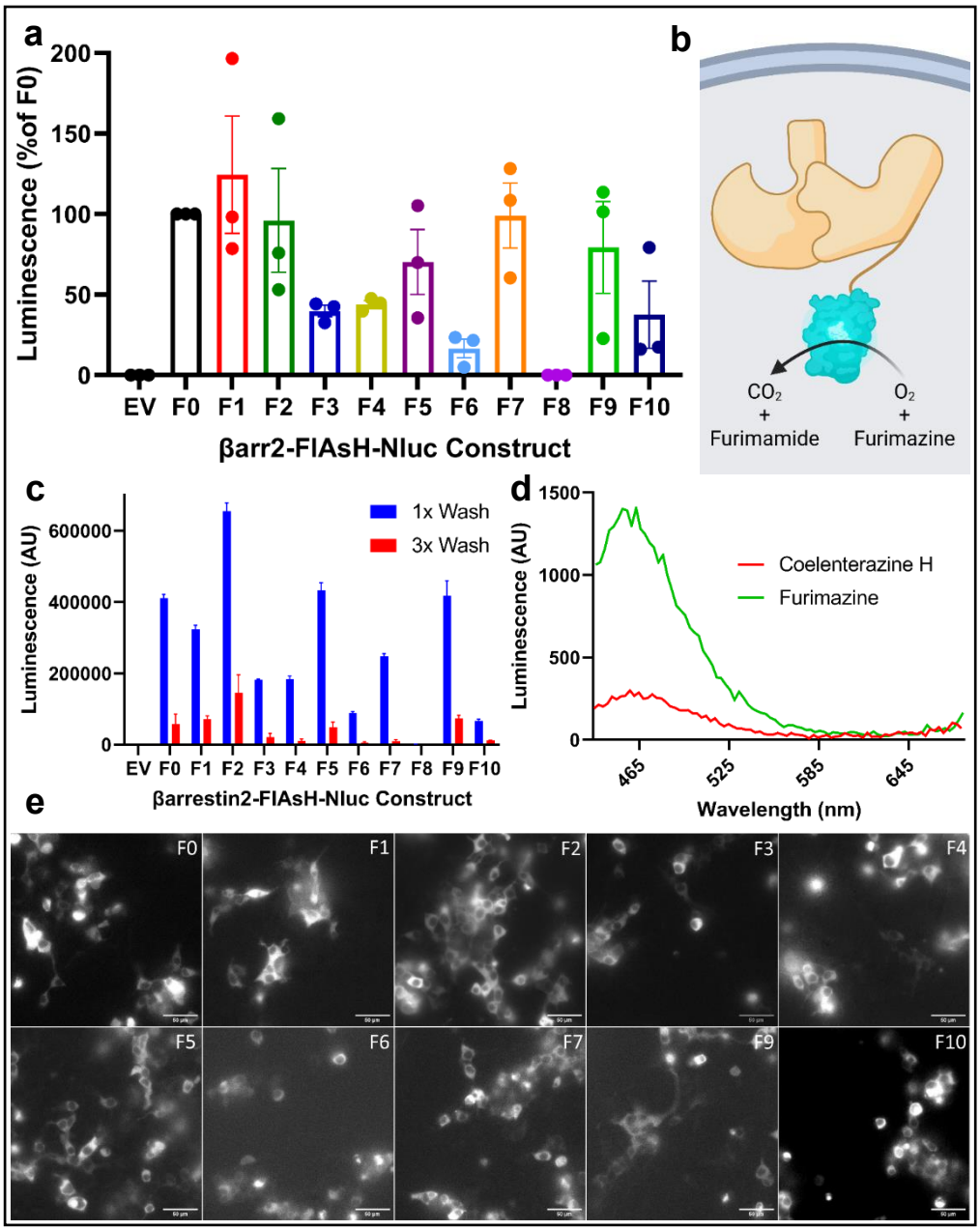


*Figure 4.3.1.1, a) β-arrestin2-FlAsH-Nluc Luminescence Assay measured by a population-based change in luminescence compared to an empty vector (EV) upon addition of the substrate Coelenterazine H (F0 to F10, normalised for each N to construct F0. N=3, error bars show ± SEM). b) Schematic depicting β-arrestin2-FlAsH-Nluc luminescence, with the luciferin reaction requirements and by-products. c) β-arrestin2-FlAsH-Nluc change in luminescence compared to an empty vector (EV) upon treatment with Coelenterazine H. Assay exhibits sensors F0 to F10, with luminescence shown after 1 wash of plated cells with HBSS, and 3 washes, mimicking FlAsH labelling conditions. N=1, error bars show ± SD. d) Luminescence emission spectra of β-arrestin2-FlAsH-Nluc upon addition of two luciferin substrates, Coelenterazine H and Furimazine. e) Bioluminescence images of β-arrestin2-FlAsH-Nluc transfected HEK293T cells treated with 5 µM furimazine, labelled by sensor F number (top right, F0 to F10), with luminescence limited to the cytoplasm. Scale bar shows 50 µm.*

To determine the ability of the β-arrestin2-FlAsH-Nluc constructs to be recruited by ligand-activated MOR, we transfected HEK293T cells with mMOR and a membrane marker described previously (Wan *et al.*, 2018), K-Ras, tagged with a Venus fluorescent protein. In cells treated with 10 µM DAMGO for 10 mins, recruitment of the constructs to the receptor was observed via bystander BRET (or the BRET signal from the Nluc tag coming in close

proximity to K-Ras-Venus at the plasma membrane). As shown in figure 4.3.1.2, all β-arrestin2-FlAsH-Nluc sensors used in this assay showed an increase in BRET ratio over vehicle when treated with DAMGO, apart from F6, which showed no significant increase over vehicle. Responses were variable however, with F1, F7, and F9 exhibiting similarly reduced responses compared to other sensors, possibly due to reduced expression or ability to embed in the membrane.

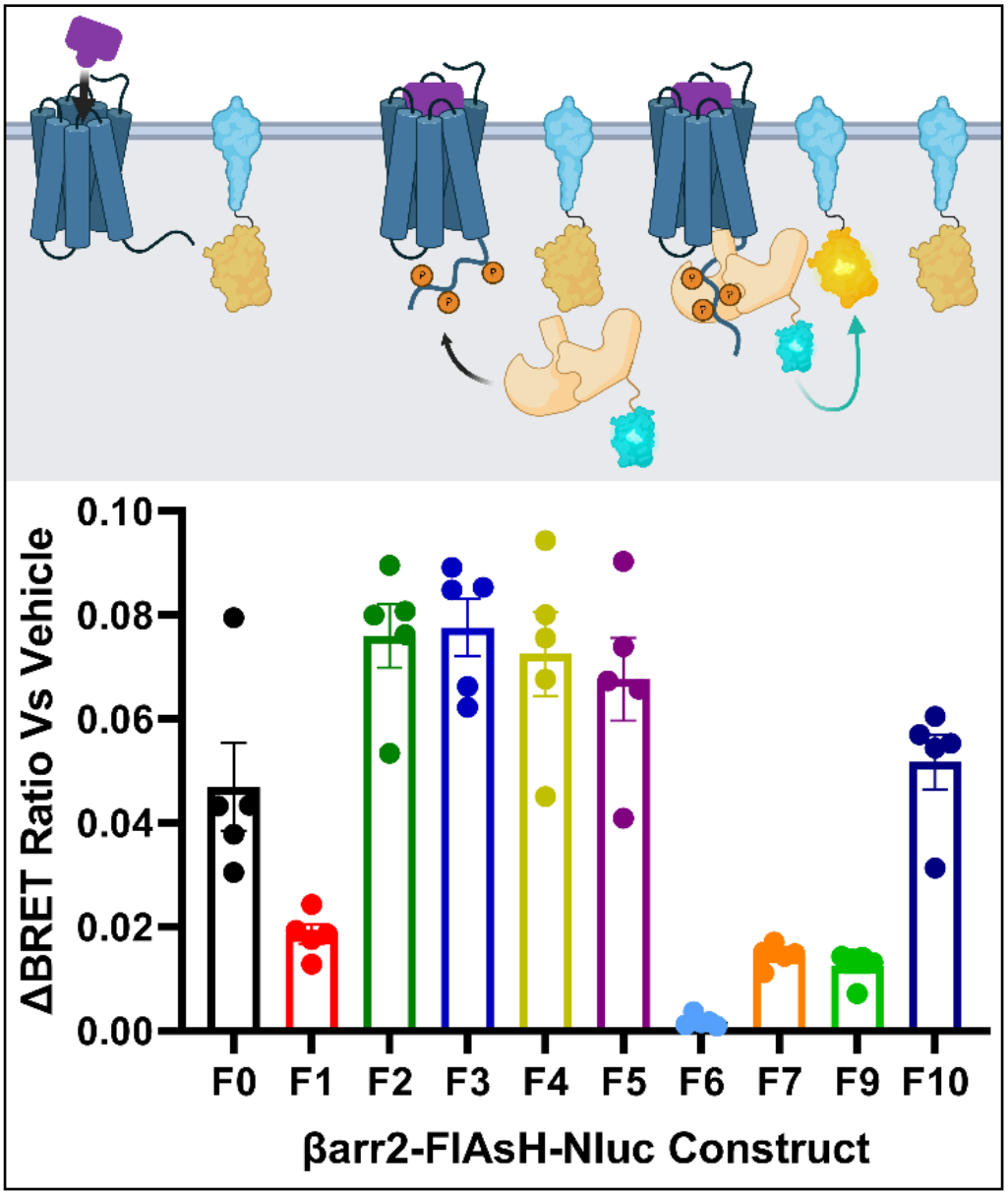


*Figure 4.3.1.2, a) Schematic depicting MOR (blue) induced intermolecular BRET assays involving β-arrestin2-FlAsH-Nluc (β-arrestin2 - beige, Nluc - light blue) recruitment to the membrane, measured by bystander BRET with the membrane bound, Venus (yellow) tagged K-Ras (light blue), following stimulation by MOR ligands (purple). b) β-arrestin2-FlAsH-Nluc recruitment to the plasma membrane measured by change in bystander BRET with Venus tagged K-Ras, a membrane marker, upon treatment with 10μM DAMGO vs vehicle control. N=5, error bars show ±SEM.*

Finally, to assess the ability of the β-arrestin2-FlAsH-Nluc constructs to recruit internalisation effectors, we utilized a β-Adaptin2 recruitment assay described in (Beautrait *et al.*, 2017). β-Adaptin2 functions as the accessory binding subunit of the AP2 complex, an adaptor molecule facilitating interaction between arrestin and clathrin, a major step in the internalisation of GPCRs. As described, upon receptor activation and subsequent internalisation, a YFP tag on the β-Adaptin2 will come into close proximity to the Nluc tag on the β-arrestin2-FlAsH-Nluc constructs in the event of functional recruitment and binding. Similar to the assay described in 4.2.2.1, cells were transfected with mMOR, the β-arrestin2-FlAsH-Nluc constructs, and β-Adaptin2-YFP, and exposed to 10 µM DAMGO for 10 min. As shown in figure 4.3.1.3, the change in BRET ratio against a vehicle control showed similar increases to those seen in the K-Ras assay, with F2, 3, 4, 5, and 10 showing the greatest recruitment, and F6 showing no significant difference from vehicle.

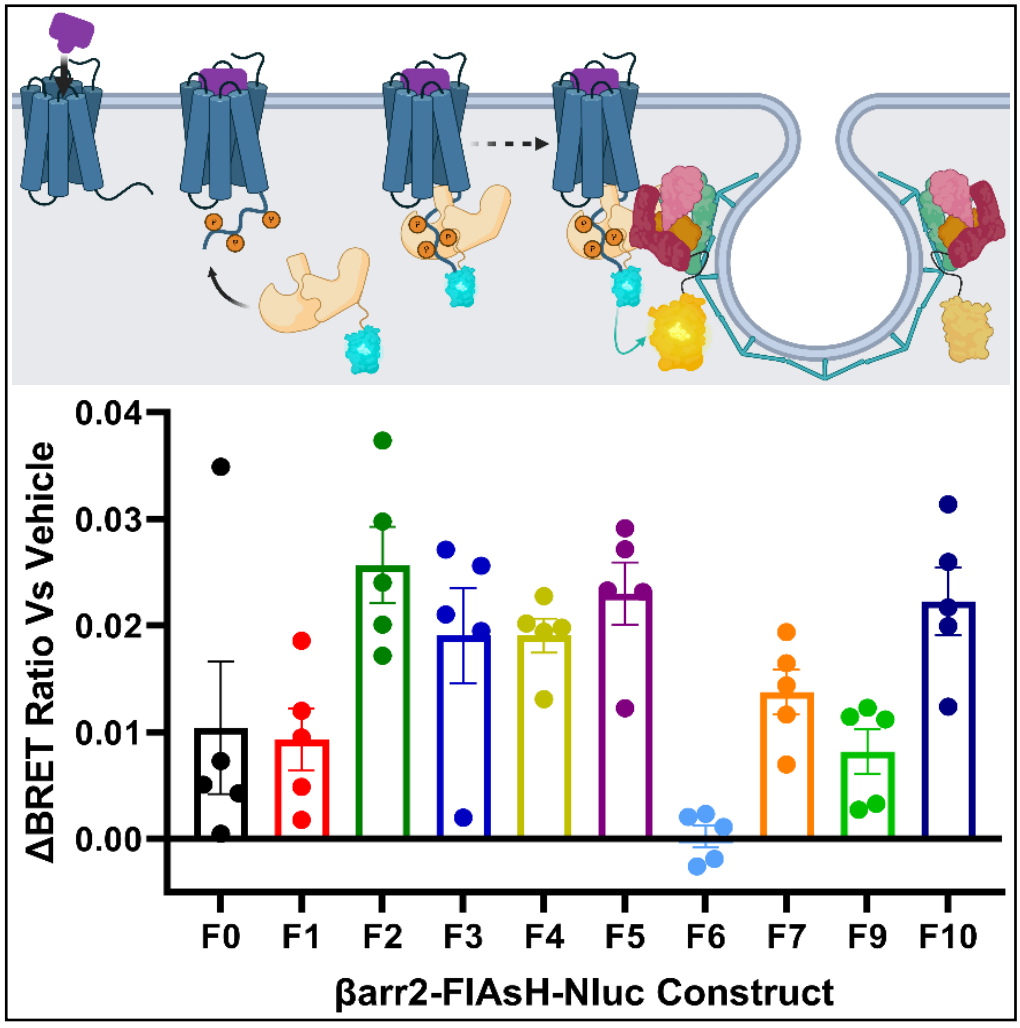


*Figure 4.3.1.3, a) β-arrestin2-FlAsH-Nluc recruitment of YFP-tagged β-Adaptin2 measured by difference in BRET Ratio upon treatment with 10µM DAMGO or vehicle control. N=5, error bars show ±SEM. b) Schematic depicting mu-opioid (blue) ligand (purple) induced intermolecular BRET assays involving β-arrestin2-FlAsH-Nluc (β-arrestin2 - beige, Nluc - light blue) recruitment of YFP (yellow) tagged β-Adaptin2 (red), an accessory binding subunit of the AP2 complex (red, orange, pink, green, bottom right), responsible for receptor translocation to clathrin coated pits.*

### 4.3.2 Selection of Opioid Ligands for the Assessment of Arrestin Conformational Changes

In order to investigate ligand-dependent arrestin conformational changes, we aimed to select ligands with different abilities to activate the receptor and induce β-arrestin recruitment. As such, further BRET-based and imaging-based assays were conducted with a variety of opioid ligands described in section 1.2.2. Ligands were assessed for their ability to induce arrestin recruitment to the membrane, recruitment of adaptin to arrestin, and internalisation of the receptor. Based on previous literature the ligands selected were DAMGO, a high efficacy opioid reference agonist, fentanyl, a high efficacy clinically used opioid, morphine, a prototypical opioid with partial efficacy, oliceridine (TRV130), a recently approved partial efficacy opioid, buprenorphine, a weak partial agonist, and naloxone, an antagonist (Comer and Cahill, 2019; Gillis, Kliewer, *et al.*, 2020; James and Williams, 2020). The data from the BRET assays used are shown in figure 4.3.2.1, using the β-Adaptin2-YFP recruitment assay shown previously, as well as an arrestin recruitment assay based on direct interaction between MOR-Nluc and β-arrestin2-YFP. Internalisation (figure 4.3.2.2) was assessed by imaging of the SNAP-tagged MOR.

To test the ability of the selected opioid ligands to recruit β-arrestin2 to the receptor, we transfected a Nluc-tagged mMOR alongside YFP-tagged β-arrestin2, as well as GRK2. After addition of the substrate furimazine, cells were incubated with opioid ligands for 10 mins at a concentration range between 100 µM and 0.1 nM. Change in BRET ratio over vehicle is shown for each ligand at each concentration, creating the concentration response curves shown in figure 4.3.2.1. DAMGO, oliceridine and naloxone exhibit similar potencies, with fentanyl exhibiting a potency approximately half a log unit greater, and morphine exhibiting a potency 1 log unit less than the other ligands. DAMGO and fentanyl exhibit similar maximal responses, and morphine exhibits responses around 80% of this. Oliceridine exhibited around 50% of the high efficacy agonist response, whereas naloxone showed a decrease in response at its higher concentrations.

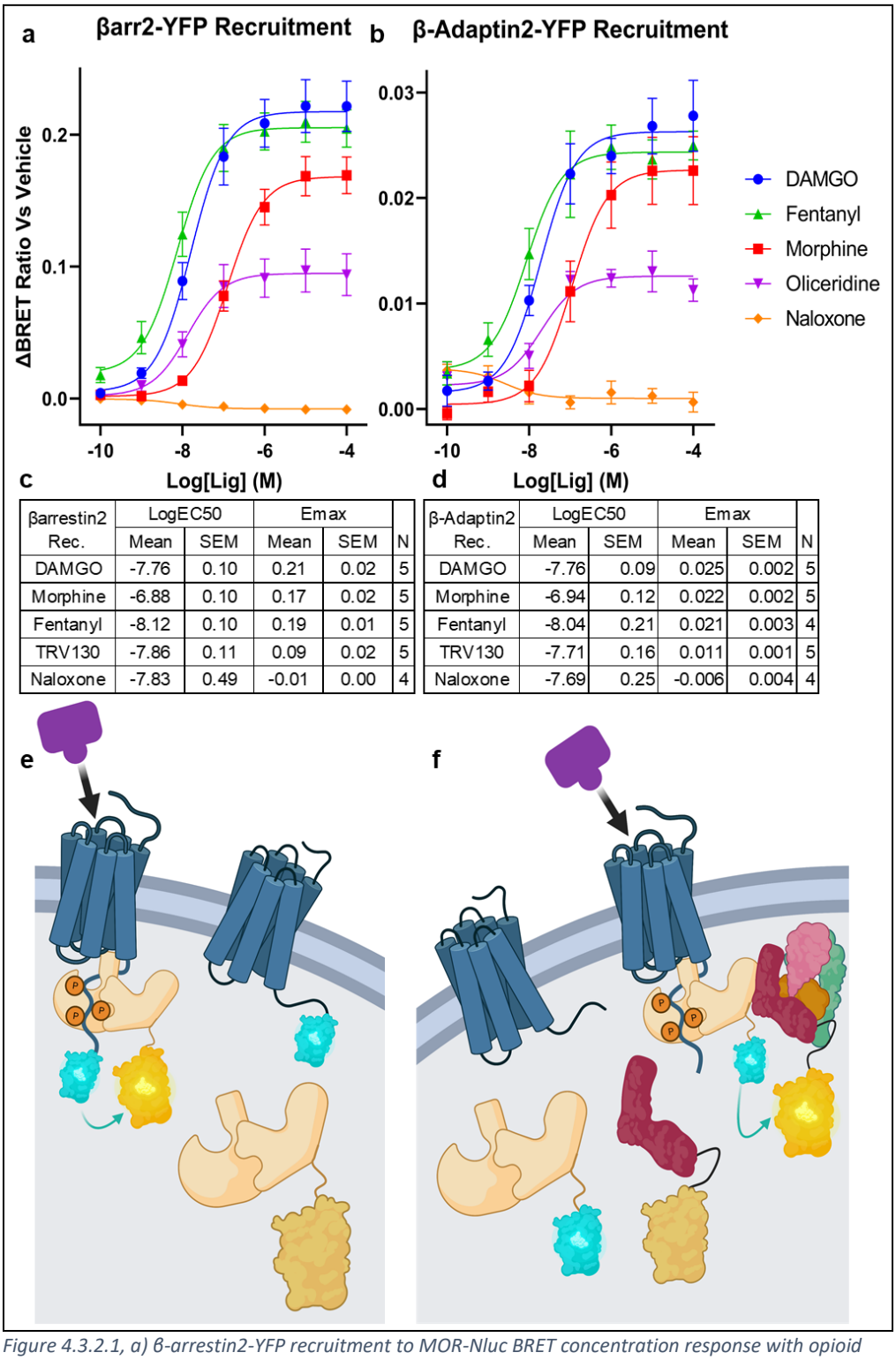


| βarrestin2 Rec. | LogEC50 | | Emax | | |
|---|---|---|---|---|---|
| | Mean | SEM | Mean | SEM | N |
| DAMGO | -7.76 | 0.10 | 0.21 | 0.02 | 5 |
| Morphine | -6.88 | 0.10 | 0.17 | 0.02 | 5 |
| Fentanyl | -8.12 | 0.10 | 0.19 | 0.01 | 5 |
| TRV130 | -7.86 | 0.11 | 0.09 | 0.02 | 5 |
| Naloxone | -7.83 | 0.49 | -0.01 | 0.00 | 4 |

| β-Adaptin2 Rec. | LogEC50 | | Emax | | |
|---|---|---|---|---|---|
| | Mean | SEM | Mean | SEM | N |
| DAMGO | -7.76 | 0.09 | 0.025 | 0.002 | 5 |
| Morphine | -6.94 | 0.12 | 0.022 | 0.002 | 5 |
| Fentanyl | -8.04 | 0.21 | 0.021 | 0.003 | 4 |
| TRV130 | -7.71 | 0.16 | 0.011 | 0.001 | 5 |
| Naloxone | -7.69 | 0.25 | -0.006 | 0.004 | 4 |

*Figure 4.3.2.1, a) β-arrestin2-YFP recruitment to MOR-Nluc BRET concentration response with opioid ligands (N=5, error bars show ± SEM) b) β-Adaptin2-YFP recruitment to β-arrestin2-FlAsH-Nluc BRET concentration response with varied opioid ligands (N=5, error bars show ± SEM). c) β-arrestin2-YFP recruitment to MOR-Nluc BRET Log(EC50) and Emax values with varied opioid ligands (N=5, means ± SEM) d) ) β-Adaptin2-YFP recruitment to β-arrestin2-FlAsH-Nluc BRET Log(EC50) and Emax values with varied opioid ligands (N=5, mean ± SEM from independent experiments each performed in quadruplicate). e,f) Schematic depicting mu-opioid ligand (purple) induced intermolecular BRET assays involving e) MOR-Nluc (Blue, light blue) recruitment of Venus (yellow) tagged β-arrestin2 (beige). f) β-arrestin2-FlAsH-Nluc (beige, light blue) recruitment of YFP (yellow) tagged β-Adaptin2 (red), an accessory binding subunit of the AP2 complex (red, orange, pink, green, bottom right), responsible for receptor translocation to clathrin coated pits. error bars show ± SEM).*

We then assessed the ability of the selected opioid ligands to stimulate the recruitment of β-Adaptin2 to β-arrestin2. As described in 4.2.2.2, cells were transfected with mMOR, β-Adaptin2-YFP, GRK2, and one of the β-arrestin2-FlAsH-Nluc constructs with no FlAsH binding motif, F0. These were then treated with furimazine and opioid ligands as described in 4.2.2.2. As shown in figure 4.3.2.1b, the change in BRET ratio against a vehicle control after 10 mins generates very similar responses to those shown in the β-arrestin2-YFP recruitment assay in terms of both potency and maximal response, although with more varied responses. The negative efficacy of naloxone in the β-Adaptin2 response is, relatively, much greater than in the β-arrestin2 recruitment assay, although more variable. Maximal changes in BRET ratio are around 1/10$^{th}$ that of those observed in the β-arrestin2 recruitment assay.

To assess the ability of the selected opioid ligands to induce receptor internalisation, we utilised HEK293T cells stably transfected with SNAP-tagged hMOR and transiently transfected GRK2-Venus, both to assess opioid ligand ability to internalise under GRK2 overexpression, as well as locate cells with GRK2 expression. Labelling of SNAP-tagged receptors was performed using a cell impermeable SNAPSurface-AlexaFluor647, and confocal images were taken 20 min post-ligand addition, incubating at room temperature during this time. Under unstimulated conditions, the SNAP-MOR was predominantly visualised on the plasma membrane with a few intracellular vesicles visible. Cells treated with DAMGO show bright, central clustering in cells co-expressing SNAP-hMOR and GRK2-Venus, as well as cells expressing only SNAP-hMOR, whereas exposure to fentanyl causes more diffuse but increased clustering in both cell types. Morphine appears to exhibit similarly bright central clustering to DAMGO, however only in cells co-expressing both SNAP-hMOR and GRK2-Venus. Oliceridine and buprenorphine exhibit little central or diffuse clustering, however there is limited cell number in the oliceridine images, making co-expression rare. Naloxone treated cells exhibit high levels of diffuse clusters in the baseline images, however these appear to reduce after 20 mins post-naloxone addition

To summarise, opioid ligands tested here behaved in agreement with previous reports (Gillis, Batista-Gondin, *et al.*, 2020a) with ligands displaying a spectrum of efficacies and potencies.

*Figure 4.3.2.2, confocal images of HEK293T cells stably transfected with SNAP-tagged hMOR, and transiently transfected Venus-tagged GRK2. SNAP-hMOR labelled with SNAPSurface-AlexaFluor647, and imaged before and 20 mins after 10 μM opioid ligand treatment using a Zeiss LSM880 confocal microscope and a 633nm laser. GRK2-Venus imaged 20 mins post ligand addition using 488 nm argon laser. N = 1.*

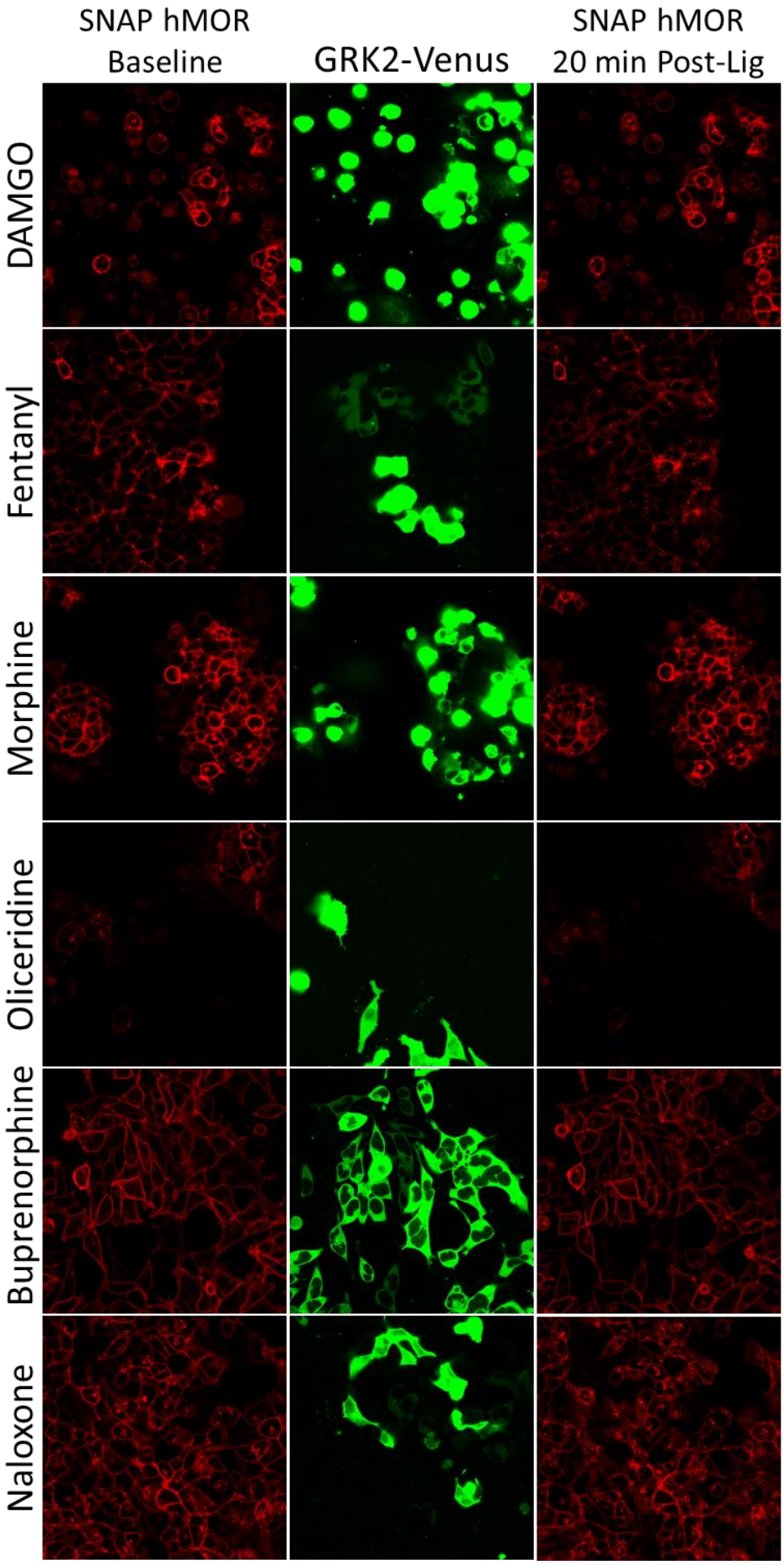
SNAP hMOR
Baseline
GRK2-Venus
SNAP hMOR
20 min Post-Lig
DAMGO
Fentanyl
Morphine
Oliceridine
Buprenorphine
Naloxone

### 4.3.3 Intramolecular BRET to Assess β-arrestin Conformational Changes

To assess the conformational changes in β-arrestin induced by MOR activation, we used the intramolecular BRET-based biosensors described in Haider et al., 2022. This assay measured the BRET change between the Nluc tagged to the C-terminal tail of the arrestin, and the FlAsH molecule, bound to a tetra-cysteine motif inserted into one of the protruding loops along the arrestin sequence. The position of this motif is noted in the cartoon in figure 4.3.3.3b for each construct, and the starting amino acid is listed at the bottom. As the conformation changes, the distance between the Nluc and FlAsH changes, increasing or decreasing the BRET efficiency as it does so, and changing the subsequent BRET ratio. To eliminate the role of spectral overlap between the emissions from Nluc and the FlAsH molecule, we conduct an identical assay with F0, a β-arrestin2-Nluc construct with no FlAsH binding sequence inserted, and thus no fluorophore binding. The BRET ratio measured in this control was then subtracted from subsequent measurements to account for spectral overlap and the BRET emission from unwashed FlAsH molecules. This is expressed as "net BRET ratio" in the following data.

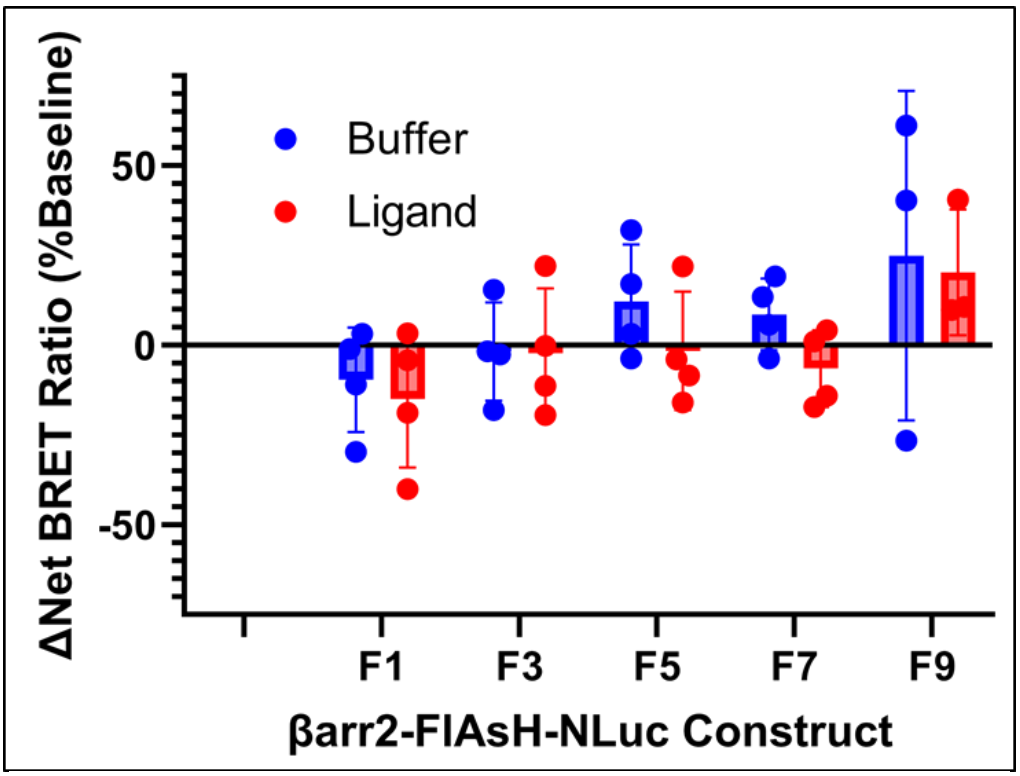


*Figure 4.3.3.1, Change as a percentage of baseline of net BRET ratio of β-arrestin2-FlAsH-Nluc intramolecular BRET conformational biosensors, with varying FlAsH binding sites after treatment with 1 µM DAMGO (red) or vehicle (blue) in the absence of GRK2 overexpression (n=1, error bars show ± SD)*

Initially, the intramolecular BRET conformational change assay was performed as described in 4.2.3 in wild type HEK293T cells, with no GRK2 overexpression, to assess whether these conformational changes could be detected under endogenous conditions. As shown in figure 4.3.3.1, 10 µM

DAMGO induced no significant conformational change in the net BRET ratio in odd numbered β-arrestin2-FlAsH-Nluc constructs compared to a vehicle control.

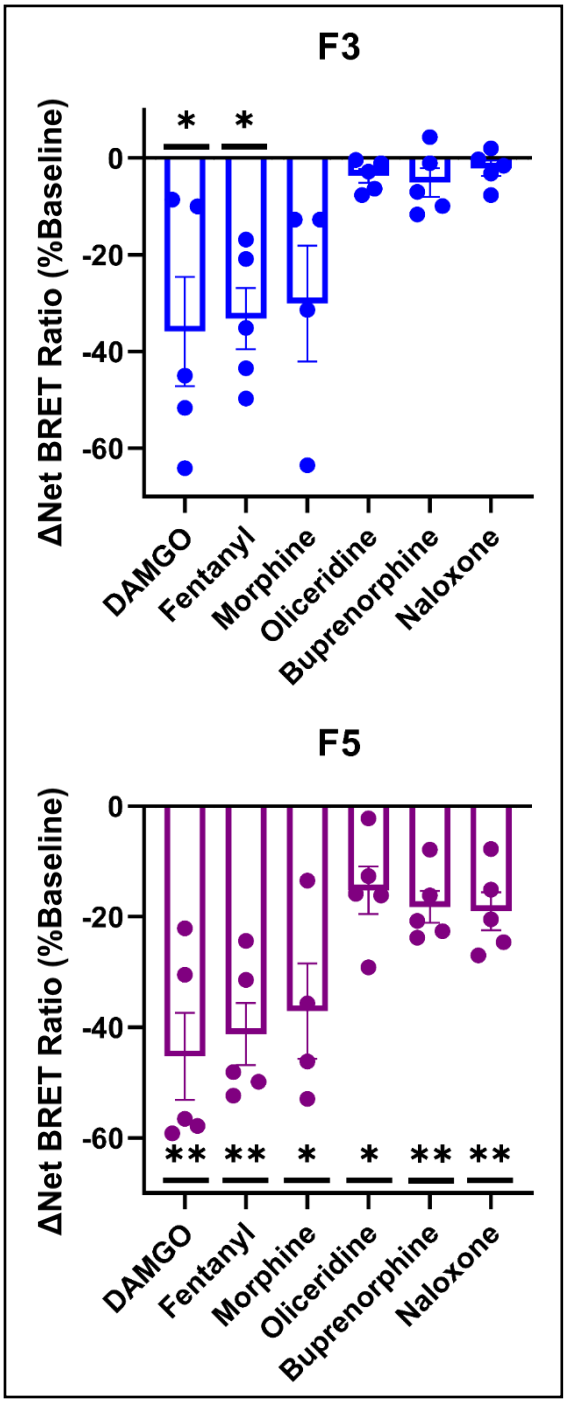


*Figure 4.3.3.2, Change as a percentage of baseline of net BRET ratio of β-arrestin2-FlAsH-Nluc intramolecular BRET conformational biosensors, with varying FlAsH binding sites (Top - F3, Dark Blue, residue 49; Bottom - F5, Purple, residue 157;), following treatment with 1 μM opioid ligands (n=5, average ± SEM, T-Test for significant difference from 0: *: p ≤ 0.05; **: p ≤ 0.005).*

We subsequently conducted similar assays in the presence of GRK2 overexpression to enhance arrestin recruitment to detect subsequent conformational changes (figure 4.3.3.2). Following treatment with 1 μM opioid ligand, we observed clear decreases in Net BRET ratio that was much greater with higher efficacy ligands. Construct F5 exhibited the greatest change, with most ligands assessed achieving a decrease significantly different from 0 (see appendix 4.3.3.2). F3 exhibited a threshold effect, in which partial agonists exhibited no significant change in net BRET ratio from 0, whereas high efficacy agonists do. In order to reduce variability, and ensure results were taken at saturating ligand concentrations (see figure 4.3.2.1), we increased the ligand concentration to 10 μM for all subsequent assays.

The ability of β-arrestin1 to undergo conformational changes under the conditions described above was also tested using the same sensors developed by Haider in 2021.However no change in net BRET ratio was observed (data not shown), in contrast to the window observed with β-arrestin2, and in combination with reports of weak coupling of the MOR to β-arrestin1 (Zhang *et al.*, 1998;

Bohn, Gainetdinov and Caron, 2004), we did not continue to study the βarrestin1 isoform.

To summarise the final form of the assay conducted, to more clearly assess the role of opioid ligands in conformational changes of arrestin, cells expressing all β-arrestin2-FlAsH-Nluc sensors were treated with 10 µM of each opioid ligand under overexpression of GRK2. While results are still variable, changes were observed in each β-arrestin2-FlAsH-Nluc sensor.

Once conditions to detect conformational changes had been optimised, we measured the effect of 10µM ligands on the different constructs after 10 min incubation. These data are summarised in figure 4.3.3.3.

As with 1 µM of opioid ligand, the F5 β-arrestin2-FlAsH-Nluc sensor exhibited the greatest BRET change in an efficacy-dependent pattern, with the amount of BRET signal decrease increasing as ligand efficacy increases. Of note, changes observed following treatment with naloxone and oliceridine were not significantly different to 0. β-arrestin2-FlAsH-Nluc sensors F1 to 3 exhibit similar patterns, where DAMGO, morphine, and fentanyl displayed significant decrease in BRET ratio, whereas lower efficacy agonists oliceridine, buprenorphine and naloxone caused no significant changes. This was similar in F4 and F10, although DAMGO produced a lower response than fentanyl in these β-arrestin2-FlAsH-Nluc sensors. Interestingly, the only significant response in F9 was with fentanyl treatment. F6 and F7 exhibit no significant BRET changes to any ligand.

*Figure 4.3.3.3, a) Schematic depicting BRET changes upon β-arrestin2-FlAsH-Nluc conformational change induced by activated GPCR binding. Arrows indicate changing distance between BRET donor Nluc (light blue) and BRET acceptor FlAsH (green). b) Cartoon depiction of β-arrestin2-Nluc-FlAsH conformational change biosensors described in Nuber et al., 2016. Inserted FlAsH-binding domains are shown as coloured loops superimposed on β-arr2 inactive structure (PDB: 3P2D). FlAsH-binding domain (CCPGCC) amino acid starting number are listed. Adapted from Haider, 2021 c) Change as a percentage of baseline of net BRET ratio of β-arrestin2-FlAsH-Nluc intramolecular BRET conformational biosensors, with varying FlAsH binding sites (F1, Red, residue 331; F2, Dark Green, residue 154; F3, Dark Blue, residue 49; F4, Yellow, residue 150; F5, Purple, residue 157; F6, Teal, residue 326; F7, Orange, residue 335; F9, Light Green, residue 225; F10, Blue, residue 263), following treatment with 10 µM opioid ligands (n=5, average ± SEM, T-Test for significant difference from 0: *: $p \leq 0.05$; **: $p \leq 0.005$; ***: $p \leq 0.0005$).*

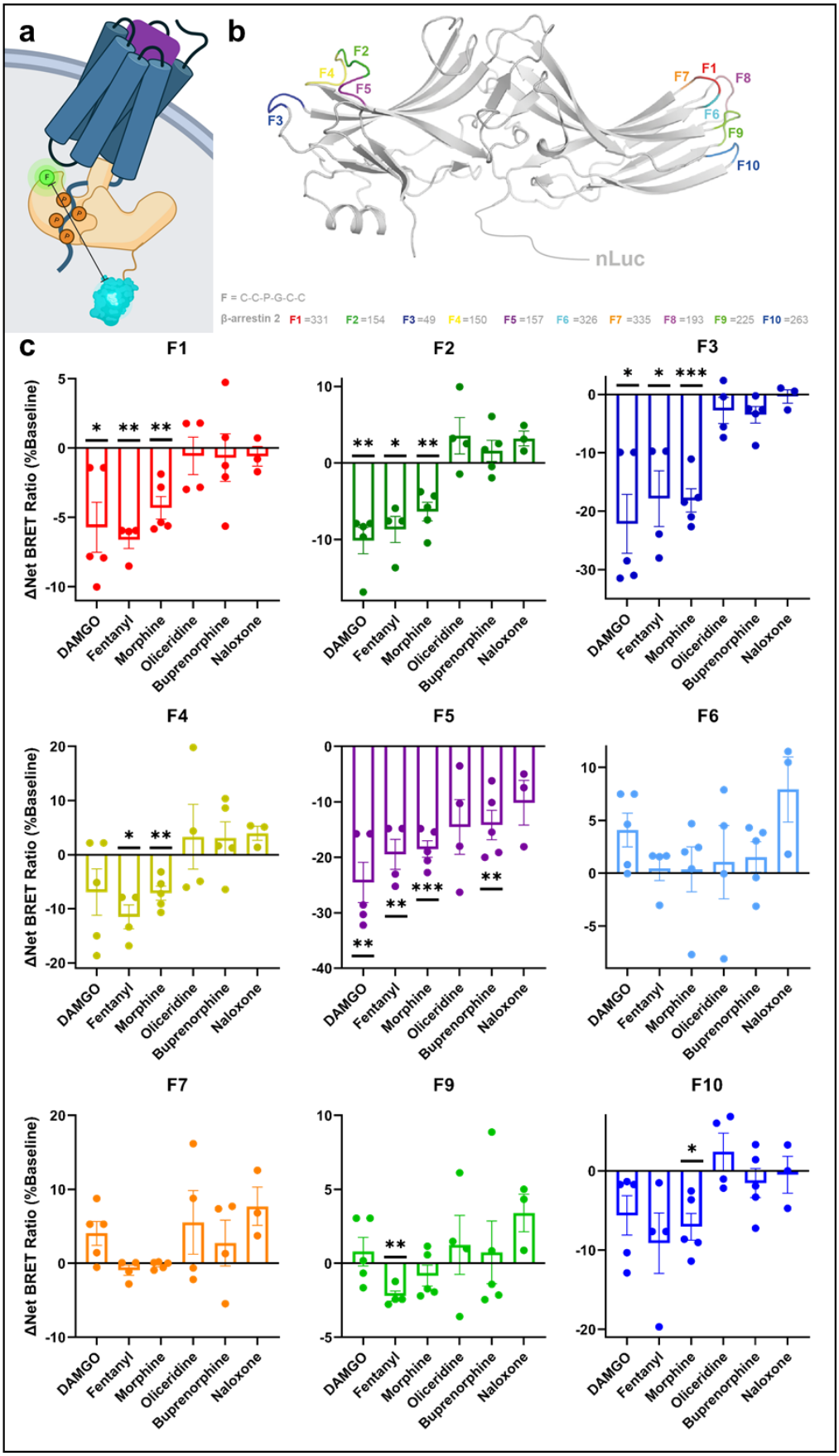
a
b
F1
F2
F3
F4
F5
F6
F7
F8
F9
F10
nLuc
F = C-C-P-G-C-C
β-arrestin 2 F1 =331 F2 =154 F3 =49 F4 =150 F5 =157 F6 =326 F7 =335 F8 =193 F9 =225 F10 =263
c
ΔNet BRET Ratio (%Baseline)
DAMGO
Fentanyl
Morphine
Oliceridine
Buprenorphine
Naloxone

### 4.3.4 Ligand-Induced β-arrestin2-Nluc-FlAsH Sensor Recruitment to the MOR

As the results above showed an efficacy dependent effect of the different ligands on the detected changes with the β-arrestin2-Nluc-FlAsH sensors, we moved on to assess whether this efficacy-related effect was due to the reduced level of recruitment of the β-arrestin2-Nluc-FlAsH sensor to the plasma membrane upon activation of the MOR by lower efficacy ligands. To check this, K-Ras bystander BRET recruitment assays were conducted with each ligand with the β-arrestin2-FlAsH-Nluc sensors that showed the most significant BRET changes, F0 to F5. The profile of recruitment was similar for all β-arrestin2-FlAsH-Nluc sensors tested, with recruitment decreasing as efficacy decreased. Of note, the β-arrestin2-FlAsH-Nluc sensor F1, which displays significantly lower BRET signal window of all β-arrestin2-FlAsH-Nluc sensors tested, retained detectable recruitment with the higher efficacy agonists tested. Thus, when measuring the ability of the different sensors to be recruited to the MOR the same efficacy threshold effect is observed as that seen for these sensors in the conformational change assay, where ligands of lower efficacy than morphine exhibit very little if any conformational change. This suggests that the lack of (or limited) conformational change with ligands such as oliceridine and buprenorphine is

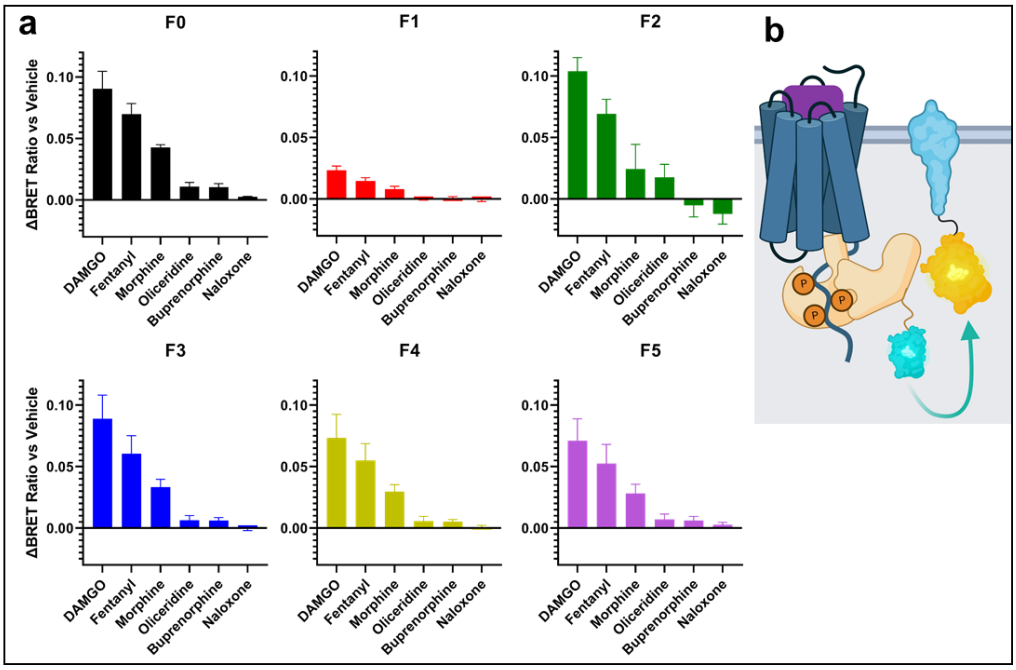


*Figure 4.3.4, a) β-arrestin2-FlAsH-Nluc conformational biosensors, with varying FlAsH binding sites (F0, Black, no FlAsH binding site; F1, Red, residue 331; F2, Dark Green, residue 154; F3, Dark Blue, residue 49; F4, Yellow, residue 150; F5, Purple, residue 157), recruitment to the membrane measured by change in bystander BRET with Venus tagged K-Ras, a membrane marker, upon treatment with 10μM opioid ligands vs vehicle control. N=5, error bars show ±SEM. b) Schematic depicting mu-opioid (blue) ligand (purple) induced intermolecular BRET assays involving β-arrestin2-FlAsH-Nluc (β-arrestin2 - beige, Nluc - light blue) recruitment to the membrane, measured by bystander BRET with the membrane bound, Venus (yellow) tagged K-Ras (light blue).*

likely to derive from these β-arrestin2-FlAsH-Nluc sensors not being recruited to the receptor.

### 4.3.5 Effect of MOR Phosphorylation on Arrestin Conformations.

To assess the role of the different phosphorylation motifs at the C-tail of MOR on agonist-induced arrestin conformations, previously described MOR

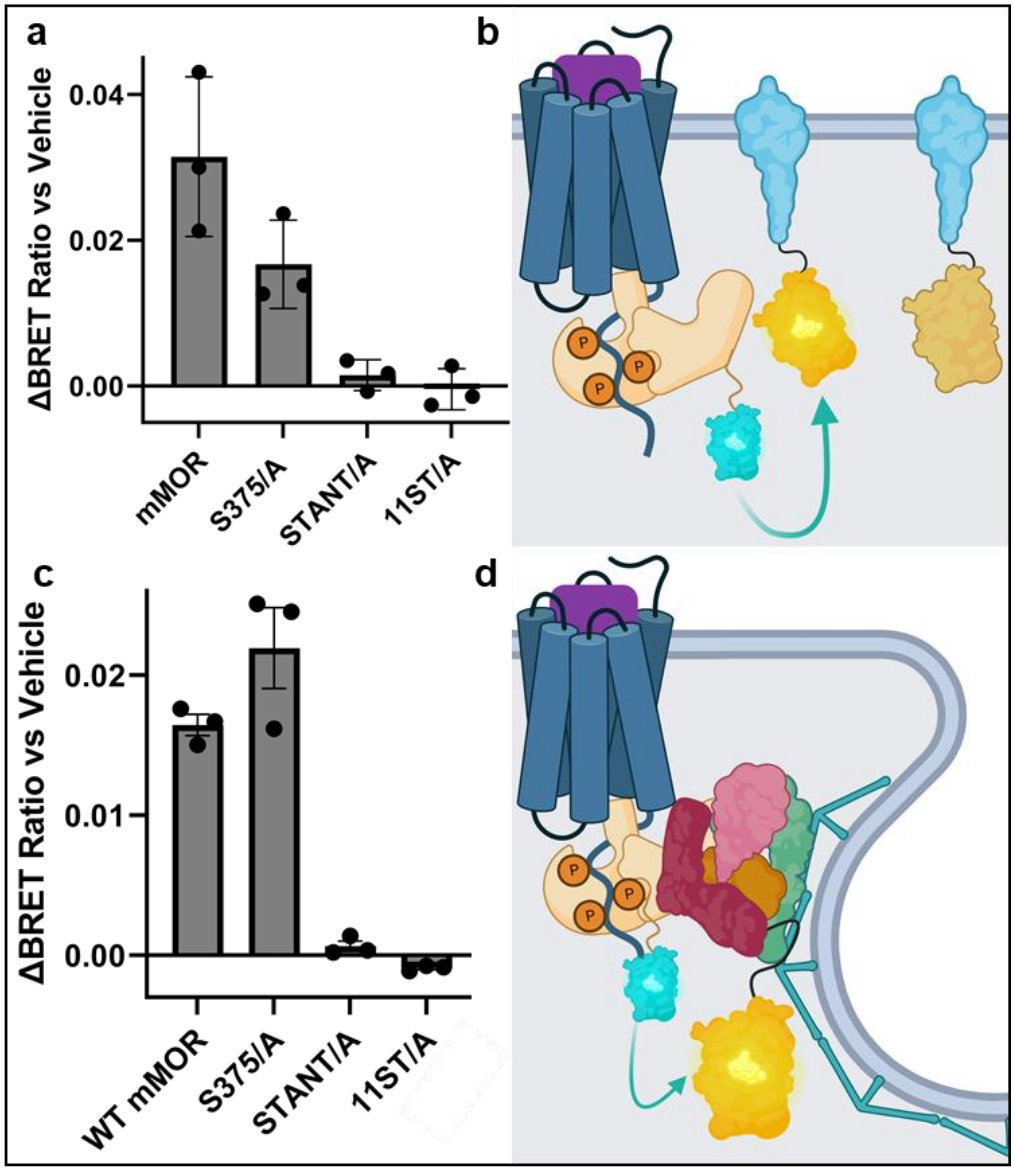


*Figure 4.3.5.1, a) Recruitment of β-arrestin2-FlAsH-Nluc measured by change in bystander BRET with K-Ras-Venus, a membrane marker, induced by vehicle control, in HEK293T cells transfected with WT mMOR, C-tail phosphodeficient mMOR, or an empty vector. (n=3, error bars show ± SEM). b) Schematic depicting mu-opioid (blue) ligand (purple) induced intermolecular BRET assays involving β-arrestin2-FlAsH-Nluc (β-arrestin2 - beige, Nluc - light blue) recruitment to the membrane, measured by bystander BRET with the membrane bound, Venus (yellow) tagged K-Ras (light blue). c) β-arrestin2-FlAsH-Nluc recruitment of YFP-tagged β-Adaptin2 measured by change in BRET, induced by opioid ligands activating WT or C-tail phosphodeficient MOR. (n=3, error bars show ± SEM). d) Schematic depicting mu-opioid (blue) ligand (purple) induced intermolecular BRET assays involving β-arrestin2-FlAsH-Nluc (β-arrestin2 - beige, Nluc - light blue) recruitment of YFP (yellow) tagged β-Adaptin2 (red), an accessory binding subunit of the AP2 complex (red, orange, pink, green, bottom right), responsible for receptor translocation to clathrin coated pits.*

mutants were used in which specific phosphosites have been mutated to alanine.

We first sought to confirm previous data and tested the different MOR phosphomutants for their capacity to recruit arrestin and induce receptor internalisation. The mutants used were S375A; shown to previously to reduced internalisation and hierarchical phosphorylation; STANT/A, a triple serine/threonine to alanine mutation shown to have greater effects on internalisation; and 11ST/A, a serine/threonine to alanine mutation of the 11 phosphosites on the mMOR C-tail, shown to abolish internalisation and receptor desensitisation (El Kouhen *et al.*, 2001; Just *et al.*, 2013; Yousuf *et al.*, 2015; Miess *et al.*, 2018).

To assess the ability of each of the phosphomutants to recruit β-arrestin2, we conducted a K-Ras bystander BRET recruitment assay, using the aforementioned F0 β-arrestin2-Nluc construct, transfected alongside K-Ras Venus, and overexpressed GRK2, depicted in figure 4.3.5.1b. As shown in figure 4.3.5.1a, with progressive removal of the number of phosphosites, the level of β-arrestin-2-Nluc recruitment decreased as shown by smaller changes in bystander BRET, with the single mutant S375/A exhibiting around half the change in BRET ratio when compared to the wild type MOR. Both STANT/A and 11ST/A exhibited no significant change when compared to vehicle.

To assess the ability of each of the phosphomutants to induce receptor internalisation, B-Adaptin2 BRET recruitment was measured, using the aforementioned F0 β-arrestin2-Nluc construct, transfected alongside β-Adaptin2-YFP, and overexpressed GRK2, depicted in figure 4.3.5.1d. As shown in figure 4.3.5.1c, neither 11ST/A or STANT/A showed any recruitment of β-Adaptin2-YFP compared to vehicle, with changes in BRET ratio similar to that of control with no MOR transfected. S375/A exhibited slightly higher BRET change than WT, in contrast to the previous assay. This supports previous findings that show that internalisation is abolished upon mutation the STANT motif to alanine, or the mutation of the 11 serine/threonine residues to alanine (Yousuf *et al.*, 2015).

Altogether the functionality data obtained in these assays with these phosphomutants agrees with previous reports (Just *et al.*, 2013; Yousuf *et al.*, 2015; Miess *et al.*, 2018), and thus we were able to confirm the roles of the phosphosites mutated. To ensure there were no sensor specific effects on recruitment to the individual phosphomutants, we conducted K-Ras recruitment assays, similar to those used in section 4.3.1.

The ability of each phosphomutant to recruit the different β-arrestin2-FlAsH-Nluc sensors was assessed using K-Ras Bystander BRET recruitment assays with all the β-arrestin2-FlAsH-Nluc sensors (F0-F10).

The recruitment in the WT MOR was similar to that obtained previously (figure 4.3.5.2a), confirming these data, and replicating the poor recruitment of F1 and F6, which was also seen with all phosphomutants. In general, S375/A exhibited weaker recruitment of each of the sensors when compared to WT but retained the general pattern of recruitment. Both the STANT/A and 11ST/A MORs were unable to recruit any of the sensors. This confirms the pattern observed in figure 4.3.5.1a is applicable to all sensors.

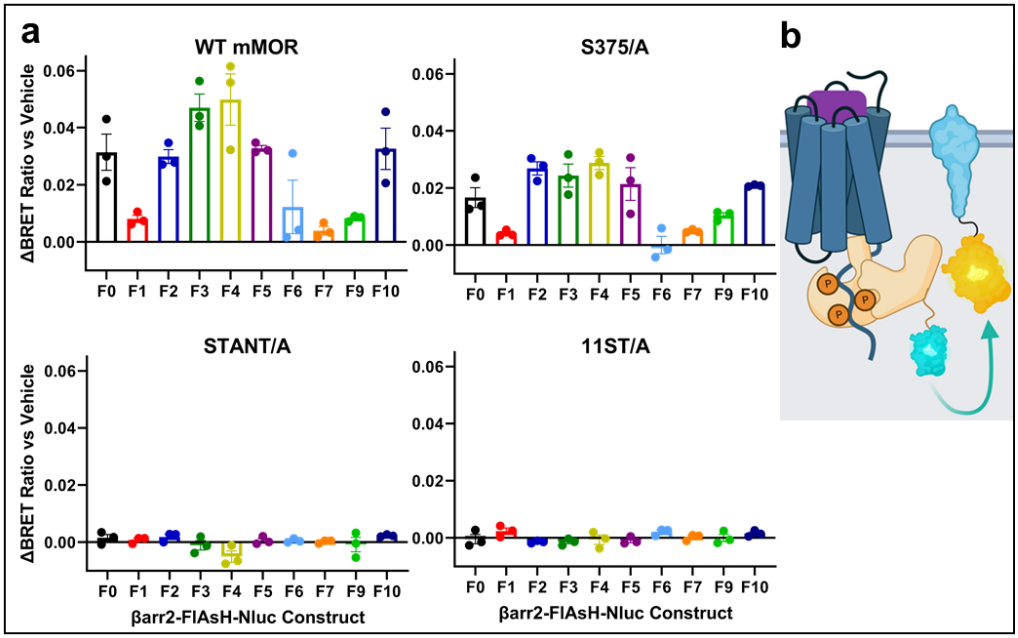


*Figure 4.3.5.2, a) Recruitment of β-arrestin2-FlAsH-Nluc measured by change in bystander BRET with K-Ras-Venus, a membrane marker, induced by vehicle control, in HEK293T cells transfected with WT or C-tail phosphodeficient mMOR. (n=3, error bars show ± SEM). b) Schematic depicting mu-opioid (blue) ligand (purple) induced intermolecular BRET assays involving β-arrestin2-FlAsH-Nluc (β-arrestin2 - beige, Nluc - light blue) recruitment to the membrane, measured by bystander BRET with the membrane bound, Venus (yellow) tagged K-Ras (light blue).*

### 4.3.6 MOR Phosphomutant Induced Conformational Change

Despite the poor performance of STANT/A and 11ST/A in our arrestin recruitment assays in the previous section, previous reports from more sensitive assays show that recruitment is detectable, albeit at a lower level. We continued on to assess the role of the mutated phosphosites in arrestin conformation.

To observe the effects of different phosphomutants on β-arrestin2 conformational change, the ability of DAMGO to induce conformational change in the different MOR phosphosite mutants was assessed. The effects observed upon knockout of S375 are not significantly decreased compared to unaltered MOR.

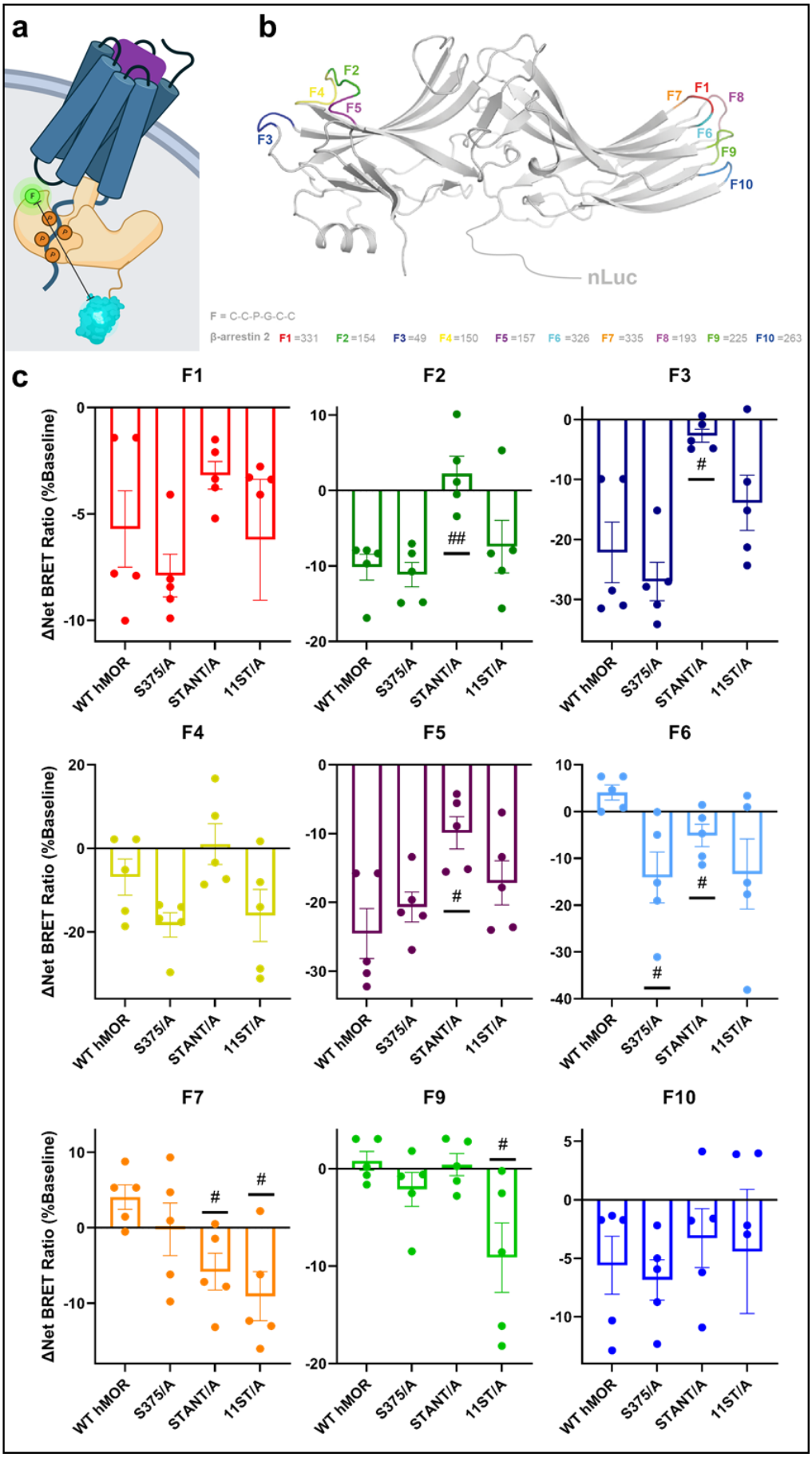
a
b
F2
F4
F5
F3
F7
F1
F8
F6
F9
F10
nLuc
F = C-C-P-G-C-C
β-arrestin 2 F1 =331 F2 =154 F3 =49 F4 =150 F5 =157 F6 =326 F7 =335 F8 =193 F9 =225 F10 =263
c
F1
F2
F3
F4
F5
F6
F7
F9
F10
ΔNet BRET Ratio (%Baseline)
WT hMOR
S375/A
STANT/A
11ST/A
#
##

*Figure 4.3.6.1, a) Schematic depicting detectable BRET changes upon β-arrestin2-FlAsH-Nluc conformational change induced by activated GPCR binding. Arrows indicate changing distance between BRET donor Nluc (light blue) and BRET acceptor FlAsH (green). b) Cartoon depiction of β-arrestin2-Nluc-FlAsH conformational change biosensors described in Nuber et al., 2016. Inserted FlAsH-binding domains are shown as coloured loops superimposed on β-arrestin2 inactive structure (PDB: 3P2D). FlAsH-binding domain (CCPGCC) amino acid starting number are listed. Adapted from Haider, 2021. c) Change as a percentage of baseline of net BRET ratio of β-arrestin2-FlAsH-Nuc intramolecular BRET conformational biosensors, with varying FlAsH binding sites (F1, Red, residue 331; F2, Dark Green, residue 154; F3, Dark Blue, residue 49; F4, Yellow, residue 150; F5, Purple, residue 157; F6, Teal, residue 326; F7, Orange, residue 335; F9, Light Green, residue 225; F10, Blue, residue 263), following treatment of MORs with phosphosites mutated to alanine with 10 μM DAMGO (n=5, average ± SEM).*

STANT/A mutation produced significantly reduced conformational change, however, upon knockout of the remaining phosphosites, the change observed was not significantly different to WT. A large response in 11ST/A was common across all β-arrestin2-FlAsH-Nluc sensors. This is notable in F7 and 9, where BRET ratio significantly increased. F7 also exhibits a significant change from WT in STANT/A, with a similar decrease in 11ST/A. F6 exhibits similar decreases in S375/A and STANT/A that are significantly different to the insignificant response in WT.

In summary this shows that conformational change in the β-arrestin2-FlAsH-Nluc sensors does not necessarily correlate with arrestin recruitment or internalisation as detected with the assays described in section 4.3.2. However, this assay was conducted at 10 min, and having observed previous reports as to the kinetic changes in arrestin recruitment over time for each of the phosphomutants, especially S375/A and STANT/A, we wanted to assess the conformational change over time.

To observe the changes in conformation over time, we assessed the change in net BRET ratio over a 30-min period. As shown in the representative time courses in figure 4.3.6.2, we see similar changes as those observed in the endpoint assays, with peaks reached within 5 mins of ligand addition, except STANT/A, which remains variable but around 0. All other phosphomutants then exhibit a similar plateau effect for the remaining period. Therefore, this suggests that conformational change is stable following activation of arrestin, and the changes that occur remain in place for more than 20 mins, possibly after arrestin has been released from the receptor.

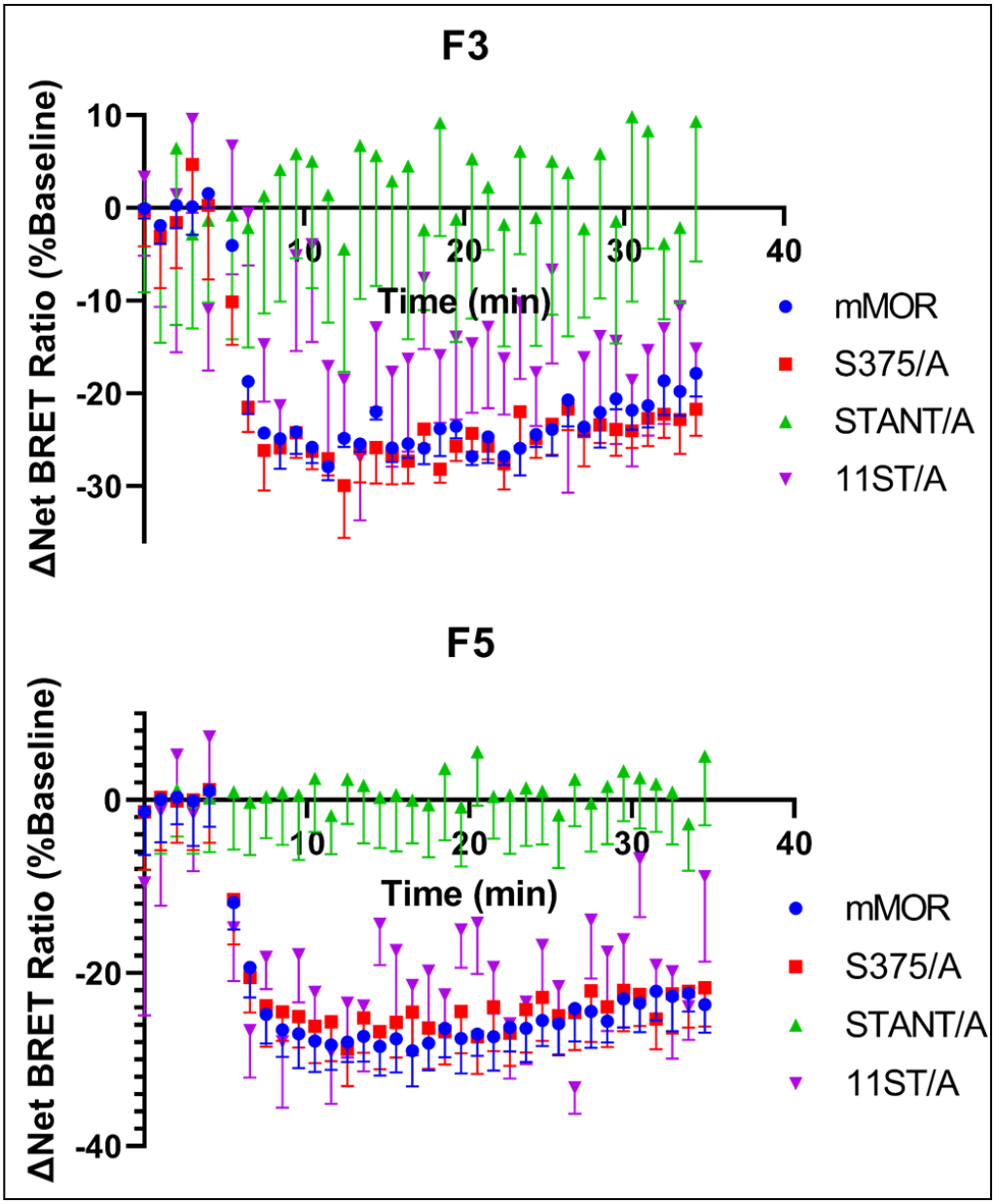


*Figure 4.3.6.2, Change as a percentage of baseline over time of net BRET ratio of β-arrestin2-FlAsH-Nluc intramolecular BRET conformational biosensors, with varying FlAsH binding sites (F3, Dark Blue, residue 49; F5, Purple, residue 157), following treatment of MORs with phosphosites mutated to alanine with 10 μM DAMGO (n=1, average of quadruplicate wells, error bars show SD).*

## 4.4 Discussion

### 4.4.1 β-arrestin2-FlAsH-Nluc Sensor Functionality

In order to assess conformational change in arrestin, we first had to ensure that the β-arrestin2-FlAsH-Nluc sensors retained similar functions to wildtype β-arrestin2. We assessed the level of expression of each β-arrestin2-FlAsH-Nluc sensor by measuring the luminescence produced by the Nluc tag upon treatment of transiently transfected HEK293T cells with furimazine, the Nluc substrate. Each β-arrestin2-FlAsH-Nluc sensor exhibited similar levels of bioluminescence. As expected, luminescence shown in these β-arrestin2-FlAsH-Nluc biosensors was highly variable, as there are many parameters could alter total luminescence of a population, such as transfection efficiency, cell homogeneity, and copy number, which may also vary between experiments. While an issue in luminescence-based experiments, the results generated in BRET studies are ratiometric between fluorescence and luminescence, which are consistent when distance and wavelength are maintained, regardless of the luminescence intensity, therefore mitigating many of the issues described above. The exception to these patterns was β-arrestin2-FlAsH-Nluc sensor F8, which showed no luminescence over that of empty vector, and F6, which showed very limited luminescence. Following communications with Carsten Hoffman, it was determined that this β-arrestin2-FlAsH-Nluc sensor is not expressed, and therefore was excluded from further assays.

We then wanted to ensure the β-arrestin2-FlAsH-Nluc sensors were expressed and exported to the cytoplasm in the same way as WT β-arrestin2. Previous literature has highlighted the retention or import of β-arrestin2 monomers in the nucleus, and that oligomerisation of arrestins (Milano *et al.*, 2006) maintains a pool of receptor accessible arrestins in the cytoplasm. Given the assumed position of the large Nluc tag when arrestin is inactive (above the N-domain) would sterically hinder oligomerization, we wanted to ensure β-arrestin2-FlAsH-Nluc sensors were available in the cytoplasm for receptor binding. As shown in the luminescence imaging in figure 4.3.1.1e, all β-arrestin2-FlAsH-Nluc sensors showed luminescence throughout the cytoplasm, indicating diffuse, cytoplasm localised β-arrestin2-FlAsH-Nluc sensors likely to be available for binding. Nuclear luminescence was much lower, and nuclei were clearly defined in each image, indicating the export of β-arrestin2-FlAsH-Nluc sensors from this compartment.

Further to this, the availability and functionality of the β-arrestin2-FlAsH-Nluc sensors was assessed by their ability to be recruited to the MOR. Bystander BRET assays were conducted in which a plasma membrane marker, K-Ras, was fused to a Venus fluorescent protein in order to detect an increase in BRET upon the recruitment of the β-arrestin2-FlAsH-Nluc sensors to the receptor, thereby bringing the Nluc close to the membrane and therefore the

membrane bound fluorophore (Donthamsetti *et al.*, 2015; Perry-Hauser *et al.*, 2021) . While less sensitive than a direct BRET assay in which both the recruited and recruiting molecules are tagged with a BRET donor or acceptor, this approach has two advantages, first, it allowed the use of the same β-arrestin2-FlAsH-Nluc sensors used for conformational change determination, and second, it allowed for the use of unmodified MOR, and makes altering the receptor used easier later in the chapter. All β-arrestin2-FlAsH-Nluc sensors exhibited some ability to be recruited to the membrane, except F6, which, while it produced luminescence in the correct cellular region, was unresponsive in any recruitment assay.

F1, 7, and 9 produced lower but detectable responses in this assay, whereas F0, 2, 3, 4, 5, and 10 exhibited more robust responses. This pattern is common amongst the recruitment assays conducted and may be due to the location of the FlAsH binding sequence. The FlAsH binding sequence in F1, 6, 7 and 9 is located on the C-edge, a region of arrestin known for its interaction and embedding in the plasma membrane (Lally *et al.*, 2017; Grimes *et al.*, 2023). As such, mutation of this region and the replacement of residues important for membrane interaction may remove the stability that membrane embedding supplies to the receptor-arrestin complex, and as such reduce recruitment and activation, resulting in lower membrane proximity and β-Adaptin2 recruitment. Receptor-arrestin interactions may occur, and as such induce the conformational changes we see later in the chapter; however, the complex formation may be more transient. F10, at the base of the C-edge, may be far enough away from the membrane binding region to avoid this effect and maintain the ability to be recruited and activate β-Adaptin2.

### 4.4.2 β-Adaptin2-YFP Assay Development and Validation

As discussed, agonist efficacies shown in the K-Ras recruitment assay are maintained in the β-Adaptin2 recruitment assay. This indicated that each of the β-arrestin2-FlAsH-Nluc sensors were able to execute the main downstream functions of β-arrestin2 recruitment to clathrin pits and scaffolding for MOR internalisation. For this, a BRET assay originally developed in the study of inhibitors for the binding between the β-arrestin2 and AP2, the adaptor protein for accessory binding to clathrin, was adapted for use with the β-arrestin2-FlAsH-Nluc sensors (Fessart *et al.*, 2007; Beautrait *et al.*, 2017). The accessory binding subunit of AP2, β-Adaptin2, known to bind arrestin directly (Fessart, Simaan and Laporte, 2005) was tagged with YFP, as described in Fessart *et al.*, 2007, and binding is detectable in a plate reader as described in Beautrait *et al.*, 2017, and can be interpreted as a proxy for receptor internalisation. This was validated against a well described β-arrestin2 recruitment assay, as used in Chapter 2, using a variety of opioid agonists. As shown in figure 4.3.2.1, while the BRET signal window is around 10 fold smaller than that seen in the β-arrestin2 recruitment assay,

the potency and response pattern for each ligand is identical and suggests that recruitment of arrestin leads to a proportional level of β-Adaptin2 recruitment, and subsequently implies a proportional level of internalisation. More work could go into improving the window through optimisation of the assay, which will likely reduce the variability in response.

In order to validate this assay with respect to internalisation, imaging studies of previously generated SNAP-hMOR HEK293T cells (see section 3.3.2) were conducted following treatment with the opioid ligands used in the previous assay. Images supported the profile shown in the β-Adaptin assay, with the observed gap in maximum efficacies between morphine and oliceridine appearing to be the threshold between observable internalisation.

### 4.4.3 Opioid Ligand Characterisation

The opioid ligand response exhibited in the assays described above (figure 4.3.2.1) and is characteristic of the opioid ligands used in an overexpressed GRK2 environment (Zhang *et al.*, 1998; Groer *et al.*, 2007; Gillis, Batista-Gondin, *et al.*, 2020a). DAMGO and fentanyl, high efficacy agonists, overlay at the maximum efficacy, with morphine, a partial agonist, exhibiting a log unit lower potency and around 75% efficacy compared to DAMGO. Oliceridine, a more partial agonist, exhibits 50% efficacy, although with similar potency to DAMGO and fentanyl. Naloxone, a well described MOR antagonist, shows a decrease in both assays, indicating some level of constitutive activity being inhibited. Not shown here is buprenorphine, which appeared to precipitate out in the assay buffer used in these experiments, resulting in highly variable responses.

The potency of each agonist assessed in the β-arrestin2 was not significantly different to previously reported potencies as determined by unpaired t-test (Gillis, Batista-Gondin, *et al.*, 2020a), and calculated maximal efficacy as a percentage of maximal DAMGO response was similarly not significantly different to previous reports (Gillis, Kliewer, *et al.*, 2020).

The efficacy data are supported further down the arrestin-dependent pathway by imaging studies, which show a similar pattern. Experiment on the whole confirm previous findings, that higher efficacy agonists can internalise the MOR at high concentration, and morphine is able to cause receptor internalisation when GRK2 is over-expressed. Oliceridine images are difficult to interpret, however previous work has highlighted the weaker ability of oliceridine activated MOR to internalise, even under GRK2 overexpression (Ehrlich *et al.*, 2019; Pedersen *et al.*, 2019).

### 4.4.4 Detection of Ligand-Directed Conformational Changes in β-arrestin2

We assessed the ability of the MOR to induce conformational change in both β-arrestin1 and β-arrestin2, however, despite sufficient expression, none of

the β-arrestin1 sensors exhibited a detectable conformational change when MOR was stimulated with DAMGO, in contrast to the observed responses for β-arrestin2 (data not shown), This is consistent with previous reports that the MOR preferentially couples to β-arrestin2 rather than β-arrestin1 (Zhang *et al.*, 1998; Bohn, Gainetdinov and Caron, 2004).

Under endogenous levels of GRK2 expression, there were no significant changes in net BRET ratio compared to vehicle (see fig 4.3.3.1) for any of the sensors in response to DAMGO stimulation. This is likely due to the insensitivity of the assay combined with the limited coupling of β-arrestin2 to the MOR under endogenous expression of GRK2, as shown in the cells lacking GRK2 treated with DAMGO and imaged in section 3.3.2.

This prompted the co-transfection of GRK2, which has been used in opioid studies to gain greater windows in assessing opioid ligands (Gillis, Batista-Gondin, *et al.*, 2020a). In the presence of over-expressed GRK2 and 1 μM of opioid ligand, significant conformational change was most easily detected by the F5 sensor with most other β-arrestin2-FlAsH-Nluc sensors producing significant change only with the higher efficacy agonists, the best of which was F3 (shown in figure 4.3.3.2, full results in appendix 4.3.3.2). As such, in the final assay a concentration of 10 μM of opioid ligand was used, based on the data from the β-arrestin2 recruitment assay shown in figure 4.3.2.1a, which indicated this was a saturating concentration for all ligands.

Under these condition, clear ligand-dependent changes in β-arrestin2 conformation were observed upon activation of MOR. While the relative extent of these changes was generally efficacy based, each β-arrestin2-FlAsH-Nluc sensor by itself provides interesting insight or arrestin rearrangement.

F5 has the FlAsH motif insertion in the upper N-domain loop (160-loop, (Scheerer and Sommer, 2017). This β-arrestin2-FlAsH-Nluc sensor generated the largest BRET changes upon ligand binding to MOR and showed a decrease in response as the ligand efficacy decreased.

This indicates F5 can act as a binding sensor, in that it can detect an active receptor even when activated by very weak agonists. This region of β-arrestin2 has been shown to interact directly with the receptor C-tail in other arrestins (Shukla *et al.*, 2013; Kang *et al.*, 2015). The position of this sensor close to the assumed Nluc inactive position (C-tail bound to N-domain groove), suggests the region would undergo large changes in conformation upon binding active receptor, which displaces the arrestin C-tail and thus the Nluc. With the Nluc moving away from the FlAsH binding site, BRET changes significantly decreases, making changes more obvious and weaker changes detectable (Haider, 2021).

It is worth noting, however, that in this assay changes in relative distance are being measured. As such, conformational changes in opposite directions

could result in similar distance changes, and as such show up as similar in this assay. This may be the case with naloxone; that an antagonising effect on β-arrestin2 recruitment blocks any constitutive activity, and therefore pushes the population into a more inactive pose, resulting in the movement of BRET donor and acceptor moving away from each other. Another explanation for the activity of naloxone in F5 is that naloxone may function as a very weak partial agonist. Naloxone has been shown to have some partial agonism at the MOR and Kappa-opioid receptor (Osterlitz and Watt, 1968; Fukuda *et al.*, 1998), and as such, could generate some active state able to influence arrestin conformation. This is supported by the response generated by buprenorphine, a well described weak partial agonist for the MOR, which generated a significant response. If this weak partial agonism is present, F5 can be thought of as a highly sensitive arrestin binding sensor, which may detect receptor-arrestin interactions that are too transient to be detected by population recruitment assays, but leaves a catalytic conformational change in arrestin, for example the displacement of the arrestin C-tail, that can be detected by this assay. Catalytic activation of arrestin has been shown previously (Eichel *et al.*, 2018b), and the addition of the Nluc tag to the C-tail may slow the rebinding of the arrestin C-tail to its inactive position. F5 is positioned to detect this change due to its close proximity to the assumed position of the Nluc tag when arrestin is in its inactive form, with the C-tail laying across the N-domain and binding in the N-domain groove (Scheerer and Sommer, 2017; Latorraca *et al.*, 2018). Displacement of the C-tail would then pull the Nluc tag down and away from F5, resulting in the large changes in BRET we see.

Different patterns occur for the F2, F3 and F4 sensors, despite their similar location to F5. In these sensors, high efficacy agonists and the higher efficacy partial agonist morphine generate robust responses, however upon efficacy decrease to oliceridine, buprenorphine, and naloxone, no significant responses are generated. This threshold effect is well characterised in other sensors and may be due to differences in C-tail displacement. Weaker agonists may have difficultly phosphorylating residues other than S375 on the receptor C tail, as has been shown previously. This has been shown both under endogenous conditions, where morphine is unable to stimulate phosphorylation other than S375, and overexpressed GRK2 conditions, as in this assay, where morphine becomes able to phosphorylate other residues, however lower efficacy agonists, such as buprenorphine, are not (Doll *et al.*, 2011; Just *et al.*, 2013; Miess *et al.*, 2018). This may lead to strong binding of some sections of the receptor C-tail to the arrestin N-domain, however other sections may not have similar affinity, and as such are unable to displace the tail fully, leading to the weaker, or absent, responses we see in some sensors compared to others. While the distance between F5 and the Nluc may

increase, the distance between F2, 3, and 4, and the Nluc, may remain the same, even if the position changes.

In F9, fentanyl generates the only significant response. F9 may show a greater change due to its previously described involvement in C-edge embedding in the membrane. Fentanyl, a highly lipophilic molecule (Kelly *et al.*, 2023), may disrupt the plasma membrane, or in some other way stabilise interactions with the membrane, such that F9 experiences conformational change once embedded inside it. Another explanation is that fentanyl generates a conformational change in the receptor in such a way that the receptor is able to confer conformational changes on arrestin that lead to the F9 loop changing conformation in a consistent way, similar to the activation stage for membrane embedding described by Lally *et al.*, 2017. This could lead to greater arrestin-receptor complex stability, and therefore the bias reported (Schmid *et al.*, 2017; Comer and Cahill, 2019; de Waal *et al.*, 2020; Kelly *et al.*, 2023).

The other sensors on the C-edge, F1, F6, F7, and F10, exhibit more variable responses, and F1 and 10 exhibit similar patterns to those described earlier. F6 and F7 display no changes that are significantly different from 0. This may be due to the insertion of the FlAsH binding motif at these locations having an effect on the function of the arrestin, supported by the functionality data shown in figure 4.3.1.1, however changes seen in figure 4.3.1.2 and 4.3.1.3 may dispute this.

The ligand-dependent changes observed above are likely to be transduced from the ligand to the arrestin by two possible mechanisms; either a distinct conformation of the receptor engenders a distinct arrestin conformation or, alternatively, that the C-tail of the MOR (as many other GPCR) encodes this information within its phosphorylation barcode. The first mechanism suggests differential receptor conformational changes upon ligand binding, is challenging to assess without structural studies such as crystallisation, cryo-EM or NMR, and would potentially require additional stabilisation of the MOR via nanobody or G protein, altering the final structure (Shukla *et al.*, 2014; Carpenter and Tate, 2016; Baidya, Kumari, Dwivedi-Agnihotri, *et al.*, 2020). However, advances are being made in these fields, using computational models to dock diverse opioid ligands (de Waal *et al.*, 2020; Qu *et al.*, 2023). In assessing the process by which a core interaction may cause arrestin conformational changes, other work has focused on the binding surfaces of receptor-arrestin complexes and may provide insights into the residues involved in this process, but assays of this kind have not yet been applied to the MOR (Böttke *et al.*, 2020).

The other alternative mechanism is much better studied through a variety of methods. The C-terminal tail of the MOR has multiple methods of encoding data, discussed in section 4.1.1. One is the formation of different secondary

structures causing different conformational change in arrestins, either induced by phosphorylation of certain sites, or induced following phosphorylation-dependent arrestin binding (Guillien *et al.*, 2023). The other is the formation of phosphorylation patterns on the C-tail of the receptor that are then 'read' by the arrestin, with changes in conformation of the arrestin induced by the location of phosphorylation, and the disruption these phosphate groups cause to residues on the arrestin (Liggett, 2011; Nobles *et al.*, 2011; Yang *et al.*, 2017; Latorraca *et al.*, 2020). Due to the available complexity in C-tail phosphorylation patterns both within receptor, and across receptors (Pándy-Szekeres *et al.*, 2023), it is therefore likely that this mechanism underlies the ligand-dependent changes observed using the above β-arrestin2-FlAsH-Nluc biosensors.

To assess whether differential recruitment of β-arrestin2-FlAsH-Nluc sensors by different ligands was a confounding factor in the patterns observed and the activity of naloxone, we conducted K-Ras recruitment assays for a subset (F0-F5) of the β-arrestin2-FlAsH-Nluc sensors with all ligands used, at identical concentrations. As shown in figure 4.3.4, recruitment remained efficacy based, and little difference was shown between β-arrestin2-FlAsH-Nluc sensors, indicating they function similarly upon recruitment. A drop in recruitment is seen between morphine and oliceridine, similar to the threshold effect seen in the conformational change assay. However, this drop also occurs in F5, which exhibits no threshold effect in the conformational change assay. Of note is the fact that little to no recruitment of β-arrestin2 is detected for oliceridine, buprenorphine, or naloxone but conformational changes are still observed, indicating the sensitivity of the conformational change assay over the K-Ras assay. This is supported by the arrestin recruitment assay shown in figure 4.3.2.1, which showed clear recruitment for oliceridine. As this assay is a direct-interaction BRET assay, it is therefore much more sensitive, rather than a bystander BRET assay as in the K-Ras assay.

### 4.4.5 Role of MOR C-tail Phosphorylation in Ligand-Induced Arrestin Conformational Changes

To ascertain the role of phosphorylation in transducing the ligand-dependent effects observed above, we used MORs in which serine and threonine residues on the C-terminal tail were mutated to alanine, thus removing their ability to be phosphorylated by kinases. This approach has been used previously (Just *et al.*, 2013; Miess *et al.*, 2018) and has highlighted the importance of such residues on MOR regulation. We used three phosphomutant MORs in this work. The first, S375/A, targets the main residue phosphorylated by opioid receptors, and is integral to the further phosphorylation of other sites. We also mutated the rest of the motif following S375, STANT/A, which has been shown to play a major role in

arrestin recruitment (Lau *et al.*, 2011; Williams *et al.*, 2013; Miess *et al.*, 2018). Finally, we mutated all phosphorylation sites in the MOR C-tail, named 11ST/A, shown to abolish DAMGO mediated internalisation (Just *et al.*, 2013). We assessed the effect of each phosphomutant in our K-Ras recruitment assay to measure arrestin recruitment to the membrane, as well as our β-Adaptin2 recruitment assay to measure internalisation.

In the bystander arrestin recruitment assay shown in figure 4.3.5a, we observed similar results to the direct recruitment assay shown in Miess *et al.*, 2018, in which S375/A exhibited slightly weaker responses at the 10 min timepoint, suggested to be due to weaker stability of interaction rather than reduced recruitment. However, arrestin recruitment to the MOR in the STANT/A mutant in Miess et al., was not completely abrogated as it is in our bystander assay, but was similar to the 11ST/A, with a significant reduction compared to WT MOR. This suggests that the assay used here is less sensitive than the direct recruitment assay shown by Miess, and subsequently does detect reduced, likely core mediated, interactions between the receptor and arrestin. However, the choice of this assay was preferred to allow the assessment of the recruitment of the different β-arrestin2-FlAsH-Nluc sensors to the membrane as well as the advantage to use non-C-terminally tagged receptors.

The β-Adaptin2 assay shows no detectable BRET between arrestin and adaptin with STANT/A and 11ST/A mutants, supporting the current literature (Just *et al.*, 2013). However, S375A appears to generate responses above that of WT MOR. One explanation for this is the catalytic activation of β-arrestin2 (Eichel *et al.*, 2018b), which occurs to greater extent upon S375/A mutation due to reduced stability of the receptor-arrestin complex, and thus causes unbound but activated arrestins to bind β-Adaptin2, as well as those that remain bound albeit transiently. This supports the theory that arrestin activation, and thus conformational change, does not require a receptor to be bound for the duration of the change.

No differences were shown between the recruitment of the β-arrestin2-FlAsH-Nluc sensors at different phosphomutants, although the β-arrestin2-FlAsH-Nluc sensors with FlAsH binding sequences on their C-edge performed consistently poorly compared to F10 or their N-domain counterparts. As with the previous K-Ras assay, STANT/A and 11STA exhibited no detectable change in recruitment across all β-arrestin2-FlAsH-Nluc sensors, and S375/A exhibited reduced recruitment compared to WT.

To investigate the role of receptor phosphorylation on the conformational changes of arrestin using β-arrestin2-FlAsH-Nluc sensors, we expressed the different phosphorylation site mutants together with the sensors and stimulated MOR using 10 uM DAMGO.

F5, the sensor earlier described as a binding sensor, again exhibited large responses. S375 mutation had little effect on conformational change, however knockout of the STANT motif generated significantly reduced changes, albeit still detectable. This supports the findings of the K-Ras and β-Adaptin2 recruitment assays, that knockout of the motif reduces binding stability and activation, however similarly to the Miess paper, some recruitment remains.

Surprisingly, the 11ST/A mutation exhibited responses not significantly different to wild type, indicating a return to similar conformational change. This has been supported by similar data from these β-arrestin2-FlAsH-Nluc sensors when studying the dopamine D2 receptor, with phosphorylation null Dopamine (D2) receptor, showing greater responses than WT D2 (Boldizsar *et al.*, 2022). Similar results were observed with β-arrestin2-FlAsH-Nluc sensors F1, 2, and 3.

There are a few potential explanations for these changes. First, is that the MOR C-tail is autoinhibitory, in that the C-tail binds the intracellular side of the MOR, occluding the β-arrestin2 binding site in some way. If binding of the C-tail to the receptor core could be inhibited by phosphorylation of the C-tail, arrestin would be free to make core interactions, or bind the now free C-tail. Theoretically the converse may be true, and the mutation of 11 residues on the C-tail, to alanine could inhibit binding in a different way, but similarly make available the C-tail and the core for β-arrestin2 binding and thus the detected conformational change.

The concept of the autoinhibitory C-tail was recently suggested in Asher *et al.*, 2022, in which truncation of the β2-adrenoceptor (β2AR) recruited β-arrestin2 to a greater extent than WT β2AR both in WT and GRK KO cells, in which the β2AR could not significantly recruit arrestin. This effect was specific to arrestin, and truncation had no effect on G protein recruitment. Similarly, the D2 receptor, with no C-tail, recruited β-arrestin2 in the absence of GRKs. Phosphorylation of the intracellular loops remains possible and was shown to increase arrestin recruitment with the truncated β2AR (Heng *et al.*, 2023). It is possible similar events occur within the MOR, provided the release of the C-tail, either by phosphorylation of the intracellular loops, which remain un-mutated in the 11ST/A MOR, or by virtue of the conversion of serine and/or threonine residues important for maintaining receptor C-tail-core binding. The abrogation of response in the STANT/A condition indicates this region is not involved in core binding, and one may assume phosphosites closer to the C-terminus, such as T385 or T396, may be involved.

Alternatively, inhibitory phosphosites may play a role in the effects observed in 11ST/A. Mutation of S363 and T370 has been shown to increase the rate and extent of internalisation (El Kouhen *et al.*, 2001), and so it becomes possible that other sites that would normally be phosphorylated and

subsequently inhibit arrestin binding or activation would be unphosphorylated in 11ST/A, blocking their inhibition and allowing activation.

Another explanation is that the C-tail secondary structure plays a role in the activation of arrestin. Assuming the C-tail is free, recent reports suggest arrestin recruitment and conformational change is highly dependent on the formation of secondary structure motifs, such as β-sheets and helices (Guillien *et al.*, 2023), in such C-tail. This is reported to occur upon phosphorylation, as mutation of a selection of receptor C-tails to a phospho-mimetic amino acid, glutamic acid, leads to increased formation of helices and β-sheets, predicted by secondary structure prediction servers and detected by NMR and biophysical analysis or purified protein (Guillien *et al.*, 2022). The formation of these secondary structures increases the affinity for arrestin to bind and has effects on arrestin conformation.

Secondary structure prediction servers use varied methods to predict secondary structure. Using one of these tools, RaptorX, a prediction server that doesn't rely on PDB homologs (Yang *et al.*, 2016), we assessed the effect of altering the 11 S/T residues to alanine, which highlighted the increased formation of helices. Notably, the probability of helix formation increases with mutation of phosphosites to alanine, shown in figure 4.4.5.1. In the absence of biophysical methods, this is a good indication that the mutations introduced will alter secondary structure of the mutant receptor C-tail, and as

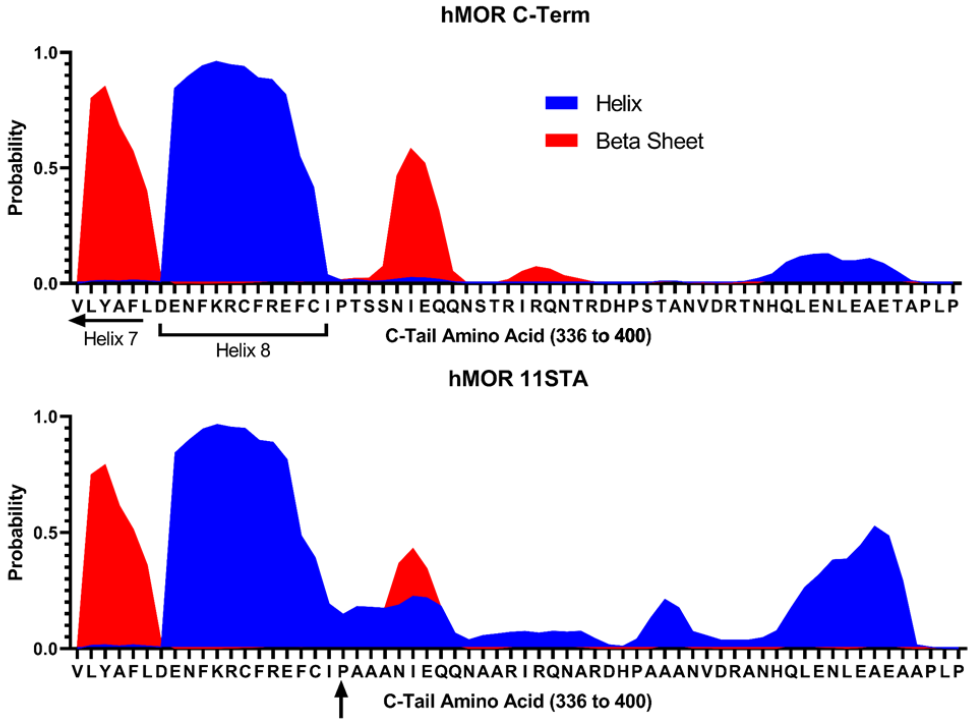


*Figure 4.4.5.1, Probability of secondary structure feature (Helix – Blue, Beta Sheet – Red) by amino acid in hMOR C-terminal tail sequences (Top – WT, Bottom – 11ST/A), as predicted by RaptorX secondary structure prediction server. End of hMOR helix 7, helix 8, and the start of the C-tail indicated by left arrow, bracket, and upwards arrow respectively.*

such, may have increased binding affinity for arrestin. However, this remains a hypothesis that will need to be tested experimentally.

Another common feature across multiple β-arrestin2-FlAsH-Nluc sensors, namely F1, 3, 4 and 6, is the slightly increased response generated by the S375/A phosphomutant. This may be due to a similar phenomenon as what we suggested as to the increase in β-Adaptin2 recruitment over baseline, in that catalytically activated, and therefore conformationally changed, β-arrestin2 generates a greater portion of the population that have these conformational change, and the lack of stability at the arrestin-receptor complex facilitates increased turnover of arrestins at the receptor, and some amplification of the conformational change signal. This is especially interesting for F6, which, despite showing poor limited changes with WT MOR, shows significantly different responses with phosphomutants S375/A. However, these differences may still be due to variability in the data and further experiments are necessary.

This effect is not present in the STANT/A mutant, which, as shown in F2, F3, and F5, exhibit significantly lower levels of conformational change than WT, as well as F1 and F4, which exhibit much reduced signal compared to S375/A. This is likely due to the lack of recruitment to the receptor, combined with an inability to induce conformational change in arrestin. When put into the context of the theoretical autoinhibitory C-tail, this indicates the tail may remain bound to the receptor, either requiring more phosphorylation to be released, or the lack of phosphorylation at STANT prevents hierarchical phosphorylation from occurring later in the C-tail (Miess *et al.*, 2018)

Interestingly, F7 and F9 do not fit the patterns described so far in other β-arrestin2-FlAsH-Nluc sensors. Phosphomutants STANT/A and 11ST/A cause decreases in net BRET ratio with F7, opposite to that exhibited with any of the ligands used in the previous conformational change assay. These changes are significantly different from WT, and, in combination with the response of F9, which exhibits a similar pattern though only with 11ST/A, highlight the possible role of core-only interaction having different effects on arrestin conformational change. Displacement of the Nluc-tagged C-tail may not occur, or the loops may shift in a differing way upon core only interaction.

The patterns described in this section are present when phosphomutants are treated with morphine, however responses are much weaker and therefore masked by the variability of the assay (see appendix 4.3.6.1). Of note is the lack of return to WT seen with 11ST/A, which may be a ligand specific event, or morphine lacks the efficacy to recruit arrestin in a core-only engagement.

In order to compare the stability of the conformational change to other assays described elsewhere (Miess *et al.*, 2018), we conducted time courses observing the conformational change. While results were variable, as shown in figure 4.3.6.2, the β-arrestin2-FlAsH-Nluc sensors with the greatest responses, F5 and F3, showed relatively stable responses, with conformational change peaking around 5 mins post ligand addition, and with only a slow reduction of around 5% in each by 30 mins post ligand. This is likely due to arrestins beginning to be internalised and stripped from receptors once inside endosomes, losing their conformational change under the different conditions. Each β-arrestin2-FlAsH-Nluc sensor exhibited similar levels of stability, although high levels of variability may mask changes (see appendix 4.3.6.2).

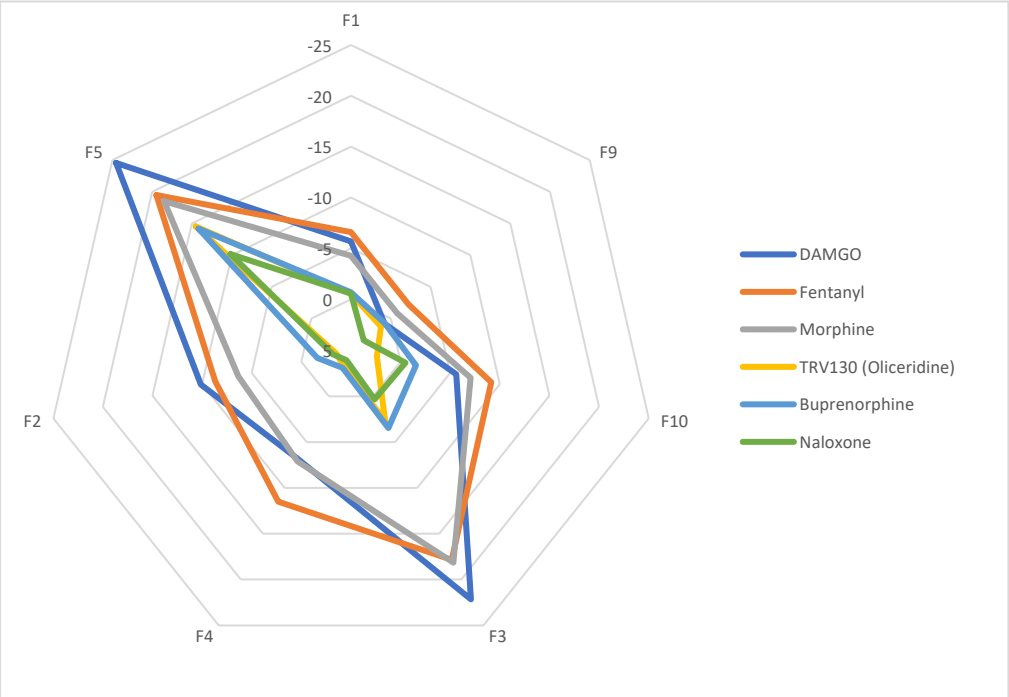


*Figure 4.4.5.2, Radar plot showing change as a percentage of baseline of net BRET ratio of β-arrestin2-FlAsH-Nluc intramolecular BRET conformational biosensors, with varying FlAsH binding sites producing the greatest levels of change following treatment with 10 μM opioid ligands, ordered by position on the β-arrestin2 of the FlAsH binding site(n=5, average).*

As shown in figure 4.4.5.2, when expressing the conformational changes observed in a radar plot, the shrinking of the shape created depicts the decrease in recruitment of arrestin, whereas subtle differences in the shape may highlight differential effects on conformation for each ligand. This is masked in the lower efficacy ligands, however.

While recruitment of arrestin correlates well with conformational change across ligands, the trend is less clear with the phosphomutants, and indicates there is a more complicated mechanism than first thought. To bypass the issue of recruitment affecting conformation, an arrestin tethered to the membrane, decreasing the 3D 'search' for active receptors to a 2D one, as discussed in section 1.1.5.1 (Grimes *et al.*, 2023), may make clearer the direct

effects of the C-tail or ligands have on arrestin conformation without adjusting for their intrinsic recruitment.

In conclusion, it has been shown that while conformational changes of β-arrestin2 following activation by the MOR by opioid ligands follow an efficacy based pattern, manipulation of phosphosites at the MOR C-tail has clear effects on the conformation of β-arrestin2. The conformational effects of opioid ligands can be altered following mutation of MOR C-tail phosphosites to alanine.

# Chapter 5: General Discussion

Phosphorylation of the MOR has been shown to facilitate β-arrestin binding, leading to desensitisation of the receptor and internalisation. The role of GRKs and PKC in agonist-dependent phosphorylation of the MOR is well established. (Bailey et al., 2009; Feng, Li and Wang, 2011). Current literature has gone further, with some phosphosites linked to the activity of individual kinases (El Kouhen et al., 2001; Glück et al., 2014). MOR phosphosites have been shown to become phosphorylated in a hierarchical manner, with phosphorylation of S375 being highlighted as the first and most phosphorylated site (Just et al., 2013). Knockout of this site has been shown to reduce phosphorylation of other sites in the MOR C-tail.

The role of C-tail phosphorylation in MOR signalling remains relatively understudied, especially given the reported role of the β-arrestin2 on MOR agonist side effects (Bohn et al., 1999; Bohn, Gainetdinov and Caron, 2004). While the interplay between G protein and β-arrestin2 pathways has confounded attempts to understand mechanisms by which many opioid side effects are caused, opioid tolerance has recently been shown to be caused by β-arrestin2 (Gillis and Christie, 2021; He et al., 2021; Muchhala et al., 2021).

Whilst the signalling pathways elicited by the MOR when activated by different ligands have been shown to be significantly correlated with the ligand efficacy (Kliewer et al., 2019, 2020; Gillis et al., 2020), the process by which β-arrestin2 directs MOR regulatory outcomes has only been partly elucidated, and the role of GRKs in this process has little mechanistic evidence (Just et al., 2013; Møller et al., 2020). In this thesis, we provide evidence linking opioid ligand pharmacology to both differential GRK recruitment as well as differential β-arrestin2 conformations.

In chapter 2, we found that GRK2 and GRK3 play the most significant roles in recruitment of β-arrestin2 by MOR phosphorylation, with GRK5 playing a more moderate role. GRK6 exhibited very limited activity at the MOR, however even in a null background, β-arrestin2 recruitment remains detectable. We also observed ligand specific effects of GRK knockout. In chapter 3, we did not observe changes in receptor organisation and diffusion upon knockout of GRKs, either under basal conditions or following DAMGO treatment. In chapter 4, we showed efficacy-based, phosphorylation-dependent changes in β-arrestin2 conformation induced by opioid ligands, indicating opioid ligands are able to dictate arrestin conformation.

Previously with the MOR, studies have focused on the role of GRK2 alone or GRK2 and 3 as a family, with regards to receptor regulation (Batista-Gondin et al., 2019; Stoeber et al., 2020). More recently, the introduction of the CRISPR-generated GRK knockout cells used here has allowed the study of single isoform knockdown (Møller et al., 2020; Drube et al., 2022). Assays

conducted in the presence of overexpressed GRK2 exhibited large increases in β-arrestin2 recruitment for all ligands, increasing overall and relative responses of each ligand, as expected. It was also observed that the WT HEK293T cells used in the Canals/Lane lab exhibited similar β-arrestin2 recruitment responses to the GRK2 knockout cell line, indicating low GRK expression in the WT cell line. While knockout of GRK 2/3/5/6 significantly decreased β-arrestin2 recruitment in response to high concentrations of DAMGO, β-arrestin2 recruitment was still detectable above basal levels. Compared to the effects of GRK knockout on β-arrestin2 recruitment, miniGsi recruitment remained relatively unaffected as expected, with limited differences likely associated with receptor number at the cell surface. These effects may be caused by altered GRK-mediated receptor turnover in cells with differing GRK expression.

Similar to this study, Møller et al., 2020 observed clear differences in the effects of GRK2 and 3 with differing ligands in β-arrestin2 recruitment assays, however these differences were dependent on the signalling outcome measured, as well as the time point observed.

We observed unexpected changes in ligand efficacy and potency in the β-arrestin2 recruitment assay upon knockout of GRK3, especially with morphine, whose potency and Emax increased, in contrast to the effects of GRK3 knockout on DAMGO and fentanyl. There are multiple reasons the observed potentiation of morphine response may occur, including the role of GRK3 as a G protein βγ scavenger (Matthees et al., 2021), or reduced affinity or catalytic activity compared to other GRKs that are removed upon CRISPR knockout. These data could also suggest that GRK3 may act as an inhibitor of other GRKs upon stimulation with morphine, potentially by competitively binding the receptor C-terminal tail and phosphorylating the receptor more slowly, or to a lesser extent than other GRK isoforms. However, these results may require further testing.

Future studies using the triple knockout cells, in which GRK2, 5 and 6, or when all four GRKs, are knocked out via CRISPR and a single kinase re-introduced, represent a better strategy to delineate the role of an individual GRK, rather than observing differences between its presence or absence in a background with all other GRKs present. Comparing the presence or absence of a particular GRK in an otherwise GRK-null background would allow us to assign specific roles to an individual GRK. Moreover, assessing the phosphorylation patterns generated in the GRK knockout cells used in this study would further the understanding of the mechanisms by which a phosphorylation barcode is generated by different activating ligands, and finally elucidate the contribution of GRK isoforms to MOR regulation.

Similarly, despite the previous literature suggesting that morphine induces GRK5-mediated phosphorylation of MOR (Glück et al., 2014), we did not

observe changes in β-arrestin2 recruitment upon single knockout of GRK5. This may be due to the redundancy provided by the other family member GRK6, or by GRK2/3. Assessment of the role of GRK5 in morphine-induced desensitisation in a triple GRK-null background, only harbouring GRK5 would provide further insight into the role of GRK5/6 isoforms.

Having observed the changes in miniGsi recruitment upon different GRK knockouts, and the lack of involvement of GRKs in this assay, we can assume the effects observed are due to differences in receptor cell surface expression or receptor state at the cell surface. With this in mind, future experiments may focus on the longer term implications of GRK knockout on the cellular location of receptors, differences in constitutive activity of the receptor, and differences in receptor trafficking. This could be answered in part by the differences between the cell lines assayed in chapter 3 using FCS, however extending these experiments to single and triple knockout cell lines would provide better insight into the effects of individual GRKs on trafficking of the receptor. Similarly, extending the confocal imaging studies into these cell lines would highlight differences in subcellular localisation of receptor under different GRK conditions, and the role each GRK plays not only in receptor endocytosis, but also in receptor biogenesis. While we have observed potential differences in acute responses to opioid ligands with regards to clustering and translocation, longer term effects of opioid treatment may expose potential mechanisms of cellular tolerance highlighted in certain GRK conditions, and point to individual GRKs in these processes.

In general, assessing the effects of GRK knockout on a panel of more varied opioid ligands may also yield further insight, as the selection used in chapter 2 was rather limited to two high efficacy ligands and morphine, however weaker partial agonists such as buprenorphine and oliceridine, antagonists such as naloxone, as well as non-classical opioids such as tianeptine may have interesting interactions with GRKs not previously observed. As shown in chapter 4, interesting β-arrestin2 conformational changes occur with low efficacy agonists and antagonists, and assuming these changes are mediated by phosphorylation, it is likely differences in GRK activity could underlie the effects of these ligands.

Similarly, while the work presented in chapter 4 investigated the conformations adopted by β-arrestin2 upon mutation of potential phosphosites in the MOR C-tail, assessing the effects of alteration of phosphorylation patterns on β-arrestin2 conformation could be further extended to assess the effects of individual GRKs using the triple and quadruple GRK knockouts similar to those characterised in chapter 2. The triple knockouts could be used to assess which GRKs induce conformational change, and whether conformational changes differ between GRKs upon inducing receptor activation with the same ligand. These conformations

generated in GRK knockout cells could be compared to conformations generated by phosphomutants and show functionally where each GRK phosphorylates without the need for phosphoantibodies.

Quadruple GRK knockout cells would also allow us to compare the differences between a lack of C-tail phosphorylation observed in the 11ST/A phosphomutant, and a lack of GRK induced phosphorylation. The implications for this is that this would block GRK-induced phosphorylation of any site across the intracellular side of the MOR, in addition to the eleven residues mutated in the 11ST/A. As the MOR has serine and threonine residues present in the intracellular loops, differences between conformations generated by the 11ST/A phosphomutant could be compared to conformations generated by a WT MOR in the Q-GRK knockout cell line, highlighting the role of GRK-induced phosphorylation of intracellular loops in generating conformational change of β-arrestin2. Moreover, this strategy would highlight phosphorylation driven by other intracellular kinases, for example PKC. In a quadruple GRK KO cell, PKC driven phosphorylation would remain; however, PKC inhibitors have been widely characterised and could be tested as to the role of PKC in generating phosphorylated MOR.

The effects of the receptor core on β-arrestin2 conformation could be further ascertained using a C-tail truncated MOR, leaving only the changes induced in β-arrestin2 conformation by core binding. The reverse could also be used to remove effects of core binding, by using MOR phosphorylated C-tail mimetic peptides to activate β-arrestin2 and induce conformational change, which could be generated in varying phosphomutant mimetic combinations.

Extending the phosphosites tested in the conformational change assay would allow assessment of finer phosphosite control of β-arrestin2 conformation by the MOR C-tail. The ability to assess individual phosphosites for their role, as well as different combinations of phosphosites, would allow improved testing of the determinants of the phosphorylation barcode. This has been tested in silico, where the effects of varied phosphorylation patterns of the vasopressin receptor C-tail on β-arrestin2 conformation have been screened (Latorraca et al., 2020). In silico testing may enable the identification of key phosphosites, however as shown previously, the fact that the MOR undergoes hierarchical phosphorylation may prevent some phosphorylation patterns from being formed physiologically (Just et al., 2013; Miess et al., 2018).

While GRKs have been shown to be the main mechanism by which phosphorylation sites become phosphorylated and thus β-arrestin2 conformation, the mechanism by which MOR ligands select GRKs is has not been fully elucidated. One of the mechanisms proposed is the direct interactions between the GPCR and GRKs. In this process, the GPCR forms a conformation upon ligand binding that increases affinity for one GRK or GRK

family over others, likely based on the GPCR intracellular cleft, similar to a GPCR's specificity for G proteins isoforms (Cato et al., 2021; Matthees et al., 2021).

One of the main limitations of this thesis is connecting the differences in conformation we observe in chapter 4 to specific cellular signalling outcomes. Downstream signalling assays for multiple effectors would allow us to link the input of an activating ligand, through the GRKs selected and the conformation of β-arrestin2 formed, to a specific signalling outcome, thus providing strong evidence for the purpose of the phosphorylation barcode in the MOR. Difficulty arises however with developing signalling assays for each of the effectors, and preventing the influence of G protein activation from masking β-arrestin2 mediated changes. One opportunity in this field would be to discover binding sites for these effectors on the β-arrestin2 binding surface, an area which has seen progression recently (Bhattacharya et al., 2002; Baillie et al., 2007; Berndt and Liebscher, 2021; Barsi-Rhyne, Manglik and von Zastrow, 2022). This would allow us to associate regions linked to effector binding to sensors described above, and using this, pair conformational changes observed to signalling outcomes.

One also has to take into consideration that the β-arrestin2 conformational biosensor data is somewhat abstract, in so much as the data itself compares only the relative positions of two points of the β-arrestin2, both of which have the capability of movement. Thus, a change in detected BRET could be due to the movement of either the donor or acceptor, or both, and equally, a lack of change may be caused by no movement of either the donor or acceptor, or a relative movement of both equally. To differentiate between these, an option would be to take the data generated in each condition and model conformational changes as if each sensor is on the same molecule. By combining both the known positions of the basal conformation, which could be validated by assessing basal BRET ratio, which is linked to distance, and the change in relative distance, one may be able to conduct in silico molecular modelling of the possible conformations that is in keeping with the data available.

In summary, through this work we have screened a selection of cells with differential GRK expression and highlighted the differing roles of each GRK in MOR β-arrestin2 recruitment, as well as the differing roles of each GRK depending on activating opioid ligand. We then used a selection of these cells and assessed the diffusion of the MOR under both basal and ligand treated conditions, observing little difference between treatments or GRK expression. Finally, we used a variety of opioid ligands and MOR phosphorylation mutants to understand their effects on arrestin conformation. In this, we observed changes in arrestin conformation correlated with ligand efficacy,

however upon mutation of phosphosites, large differences in conformation were observed.

Combined, these results highlight a mechanism by which MOR-regulated β-arrestin2 signalling is selected, with opioid ligands recruiting specific GRKs, and thus phosphorylating specific residues on the receptor C-tail. These patterns then induce different conformational changes in arrestin, which likely induce differing signalling and trafficking outcomes. We have observed that while the opioid ligands tested here induce similar conformational changes albeit to differing degrees, through differential phosphorylation different arrestin conformations are possible. β-arrestin2 signalling and opioid tolerance has been shown to be highly ligand dependant, and the processes described here may provide a mechanism by which this and other limiting opioid side effects are transduced.

# VII. References


Abrimian, A., Kraft, T. and Pan, Y.-X. (2021) 'Endogenous Opioid Peptides and Alternatively Spliced Mu Opioid Receptor Seven Transmembrane Carboxyl-Terminal Variants', *International Journal of Molecular Sciences*, 22(7), p. 3779. Available at: https://doi.org/10.3390/ijms22073779.

Al-Hasani, R. and Bruchas, M.R. (2011a) 'Molecular Mechanisms of Opioid Receptor-dependent Signaling and Behavior', *Anesthesiology*, 115(6), p. 1. Available at: https://doi.org/10.1097/ALN.0b013e318238bba6.

Al-Hasani, R. and Bruchas, M.R. (2011b) 'Molecular Mechanisms of Opioid Receptor-dependent Signaling and Behavior', *Anesthesiology*, 115(6), p. 1. Available at: https://doi.org/10.1097/ALN.0b013e318238bba6.

Alhosaini, K. *et al.* (2021) 'GPCRs: The most promiscuous druggable receptor of the mankind', *Saudi Pharmaceutical Journal*, 29(6), pp. 539–551. Available at: https://doi.org/10.1016/j.jsps.2021.04.015.

Angers, S. *et al.* (2000) 'Detection of β2-adrenergic receptor dimerization in living cells using bioluminescence resonance energy transfer (BRET)', *Proceedings of the National Academy of Sciences of the United States of America*, 97(7), pp. 3684–3689.

Arttamangkul, S. *et al.* (2018) 'Cellular tolerance at the μ-opioid receptor is phosphorylation dependent', *eLife*, 7. Available at: https://doi.org/10.7554/eLife.34989.

Arttamangkul, S. *et al.* (2019) 'Visualizing endogenous opioid receptors in living neurons using ligand-directed chemistry', *eLife*, 8. Available at: https://doi.org/10.7554/eLife.49319.

Asher, W.B. *et al.* (2022) 'GPCR-mediated β-arrestin activation deconvoluted with single-molecule precision.', *Cell* [Preprint]. Available at: https://doi.org/10.1016/J.CELL.2022.03.042.

Atwood, B.K. *et al.* (2011) 'Expression of G protein-coupled receptors and related proteins in HEK293, AtT20, BV2, and N18 cell lines as revealed by microarray analysis', *BMC Genomics*, 12(1), p. 14. Available at: https://doi.org/10.1186/1471-2164-12-14.

Ayoub, M.A. and Pfleger, K.D. (2010) 'Recent advances in bioluminescence resonance energy transfer technologies to study GPCR heteromerization', *Current Opinion in Pharmacology*, 10(1), pp. 44–52. Available at: https://doi.org/10.1016/j.coph.2009.09.012.

Azzam, A.A.H., McDonald, J. and Lambert, D.G. (2019) 'Hot topics in opioid pharmacology: mixed and biased opioids', *British Journal of Anaesthesia*, 122(6), pp. e136–e145. Available at: https://doi.org/10.1016/j.bja.2019.03.006.

Baidya, M., Kumari, P., Dwivedi-Agnihotri, H., *et al.* (2020) 'Genetically encoded intrabody sensors report the interaction and trafficking of β-arrestin 1 upon activation of G-protein–coupled receptors', *Journal of Biological Chemistry*, 295(30), pp. 10153–10167. Available at: https://doi.org/10.1074/jbc.RA120.013470.

Baidya, M., Kumari, P., Dwivedi-Agnihotri, H., *et al.* (2020) 'Key phosphorylation sites in GPCRs orchestrate the contribution of β-Arrestin 1 in ERK 1/2 activation', *EMBO reports*, 21(9). Available at: https://doi.org/10.15252/embr.201949886.

Bailey, C. *et al.* (2009) 'Involvement of PKCα and G-protein-coupled receptor kinase 2 in agonist-selective desensitization of μ-opioid receptors in mature brain neurons', *British Journal of Pharmacology*, 158(1), pp. 157–164. Available at: https://doi.org/10.1111/j.1476-5381.2009.00140.x.

Bailey, C.P. *et al.* (2009) 'Role of protein kinase C and μ-opioid receptor (MOPr) desensitization in tolerance to morphine in rat locus coeruleus neurons', *The European Journal of Neuroscience*, 29(2), pp. 307–318. Available at: https://doi.org/10.1111/j.1460-9568.2008.06573.x.

Baillie, G.S. *et al.* (2007) 'Mapping binding sites for the PDE4D5 cAMP-specific phosphodiesterase to the N- and C-domains of β-arrestin using spot-immobilized peptide arrays', *Biochemical Journal*, 404(1), pp. 71–80. Available at: https://doi.org/10.1042/BJ20070005.

Ballesteros, J.A. and Weinstein, H. (1995) '[19] Integrated methods for the construction of three-dimensional models and computational probing of structure-function relations in G protein-coupled receptors', in S.C. Sealfon (ed.) *Methods in Neurosciences*. Academic Press (Receptor Molecular Biology), pp. 366–428. Available at: https://doi.org/10.1016/S1043-9471(05)80049-7.

Barak, L.S. *et al.* (1994) 'A highly conserved tyrosine residue in G protein-coupled receptors is required for agonist-mediated beta 2-adrenergic receptor sequestration', *The Journal of Biological Chemistry*, 269(4), pp. 2790–2795.

Barak, L.S. *et al.* (1995) 'The conserved seven-transmembrane sequence NP(X)2,3Y of the G-protein-coupled receptor superfamily regulates multiple properties of the beta 2-adrenergic receptor', *Biochemistry*, 34(47), pp. 15407–15414. Available at: https://doi.org/10.1021/bi00047a003.

Barlic, J. *et al.* (2000) 'Regulation of tyrosine kinase activation and granule release through β-arrestin by CXCR1', *Nature Immunology*, 1(3), pp. 227–233. Available at: https://doi.org/10.1038/79767.

Barsi-Rhyne, B., Manglik, A. and von Zastrow, M. (2022) 'Discrete GPCR-triggered endocytic modes enable β-arrestins to flexibly regulate cell

signaling', *eLife*. Edited by S.R. Pfeffer and E. Kostenis, 11, p. e81563. Available at: https://doi.org/10.7554/eLife.81563.

Batista-Gondin, A. (2018) *Molecular mechanisms controlling μ-opioid receptor activation*. University of Nottingham.

Batista-Gondin, A. *et al.* (2019) 'GRK Mediates μ-Opioid Receptor Plasma Membrane Reorganization', *Frontiers in Molecular Neuroscience*, 12, p. 104. Available at: https://doi.org/10.3389/fnmol.2019.00104.

Beard, T.L. *et al.* (2021) 'Oliceridine is Associated with Reduced Risk of Vomiting and Need for Rescue Antiemetics Compared to Morphine: Exploratory Analysis from Two Phase 3 Randomized Placebo and Active Controlled Trials', *Pain and Therapy*, 10(1), pp. 401–413. Available at: https://doi.org/10.1007/s40122-020-00216-x.

Beaulieu, J.-M. *et al.* (2005) 'An Akt/β-Arrestin 2/PP2A Signaling Complex Mediates Dopaminergic Neurotransmission and Behavior', *Cell*, 122(2), pp. 261–273. Available at: https://doi.org/10.1016/j.cell.2005.05.012.

Beaulieu, J.-M. *et al.* (2008) 'A β-arrestin 2 Signaling Complex Mediates Lithium Action on Behavior', *Cell*, 132(1), pp. 125–136. Available at: https://doi.org/10.1016/j.cell.2007.11.041.

Beautrait, A. *et al.* (2017) 'A new inhibitor of the β-arrestin/AP2 endocytic complex reveals interplay between GPCR internalization and signalling', *Nature Communications*, 8(1), p. 15054. Available at: https://doi.org/10.1038/ncomms15054.

Benovic, J.L. *et al.* (1989) 'Inhibition of the beta-adrenergic receptor kinase by polyanions', *The Journal of Biological Chemistry*, 264(12), pp. 6707–6710.

Benredjem, B. *et al.* (2019) 'Exploring use of unsupervised clustering to associate signaling profiles of GPCR ligands to clinical response', *Nature Communications*, 10(1), p. 4075. Available at: https://doi.org/10.1038/s41467-019-11875-6.

Berman, D.M., Kozasa, T. and Gilman, A.G. (1996) 'The GTPase-activating Protein RGS4 Stabilizes the Transition State for Nucleotide Hydrolysis *', *Journal of Biological Chemistry*, 271(44), pp. 27209–27212. Available at: https://doi.org/10.1074/jbc.271.44.27209.

Bhandari, D. *et al.* (2007) 'Arrestin-2 Interacts with the Ubiquitin-Protein Isopeptide Ligase Atrophin-interacting Protein 4 and Mediates Endosomal Sorting of the Chemokine Receptor CXCR4', *Journal of Biological Chemistry*, 282(51), pp. 36971–36979. Available at: https://doi.org/10.1074/jbc.M705085200.

Bhattacharya, M. *et al.* (2002) ‘β-Arrestins regulate a Ral-GDS–Ral effector pathway that mediates cytoskeletal reorganization’, *Nature Cell Biology*, 4(8), pp. 547–555. Available at: https://doi.org/10.1038/ncb821.

Birdsong, W.T. *et al.* (2015) ‘Agonist Binding and Desensitization of the μ -Opioid Receptor Is Modulated by Phosphorylation of the C-Terminal Tail Domain’, *Molecular Pharmacology*, 88(4), pp. 816–824. Available at: https://doi.org/10.1124/mol.114.097527.

Bock, A. and Bermudez, M. (2021) ‘Allosteric coupling and biased agonism in G protein-coupled receptors’, *The FEBS Journal*, 288(8), pp. 2513–2528. Available at: https://doi.org/10.1111/febs.15783.

Boguth, C.A. *et al.* (2010) ‘Molecular basis for activation of G protein-coupled receptor kinases’, *EMBO Journal*, 29(19), pp. 3249–3259. Available at: https://doi.org/10.1038/EMBOJ.2010.206.

Bohn, L.M. *et al.* (1999) ‘Enhanced Morphine Analgesia in Mice Lacking β-Arrestin 2’, *Science*, 286(5449), pp. 2495–2498. Available at: https://doi.org/10.1126/science.286.5449.2495.

Bohn, L.M., Gainetdinov, R.R. and Caron, M.G. (2004) ‘G protein-coupled receptor kinase/β-arrestin systems and drugs of abuse’, *NeuroMolecular Medicine*, 5(1), pp. 41–50. Available at: https://doi.org/10.1385/NMM:5:1:041.

Boldizsar, N.M. *et al.* (2022) ‘G protein-coupled receptor kinases regulate &[beta]-arrestin interactions with the D2 dopamine receptor in an isoform-specific manner and in the absence of direct receptor phosphorylation’, *The FASEB Journal*, 36(S1). Available at: https://doi.org/10.1096/fasebj.2022.36.S1.R3465.

Böttke, T. *et al.* (2020) ‘Exploring GPCR-arrestin interfaces with genetically encoded crosslinkers’, *EMBO reports*, 21(11). Available at: https://doi.org/10.15252/embr.202050437.

Breitman, M. *et al.* (2012) ‘Silent Scaffolds’, *Journal of Biological Chemistry*, 287(23), pp. 19653–19664. Available at: https://doi.org/10.1074/jbc.M112.358192.

Briddon, S.J. *et al.* (2004) ‘Quantitative analysis of the formation and diffusion of A1-adenosine receptor-antagonist complexes in single living cells’, *Proceedings of the National Academy of Sciences*, 101(13), pp. 4673–4678. Available at: https://doi.org/10.1073/pnas.0400420101.

Briddon, S.J., Kilpatrick, L.E. and Hill, S.J. (2018) ‘Studying GPCR Pharmacology in Membrane Microdomains: Fluorescence Correlation Spectroscopy Comes of Age’, *Trends in Pharmacological Sciences*, 39(2), pp. 158–174. Available at: https://doi.org/10.1016/j.tips.2017.11.004.

Brown, S.M. *et al.* (2011) 'Buprenorphine metabolites, buprenorphine-3-glucuronide and norbuprenorphine-3-glucuronide, are biologically active', *Anesthesiology*, 115(6), pp. 1251–1260. Available at: https://doi.org/10.1097/ALN.0b013e318238fea0.

Brownstein, M.J. (1993) *Review A brief history of opiates, opioid peptides, and opioid receptors*, *Proc. Natl. Acad. Sci. USA*, pp. 5391–5393.

Bryant, B. and Knights, K. (2010) *Pharmacology for Health Professionals*. 3rd edn. Edited by K. Knights. Mosby Australia.

Butcher, A.J. *et al.* (2011) 'Differential G-protein-coupled Receptor Phosphorylation Provides Evidence for a Signaling Bar Code', *Journal of Biological Chemistry*, 286(13), pp. 11506–11518. Available at: https://doi.org/10.1074/jbc.M110.154526.

Butcher, A.J., Tobin, A.B. and Kong, K.C. (2011) 'Examining Site-Specific GPCR Phosphorylation', in *Methods in Molecular Biology*, pp. 237–249. Available at: https://doi.org/10.1007/978-1-61779-126-0_12.

Calebiro, D. *et al.* (2009) 'Persistent cAMP-Signals Triggered by Internalized G-Protein–Coupled Receptors', *PLoS Biology*. Edited by M. von Zastrow, 7(8), p. e1000172. Available at: https://doi.org/10.1371/journal.pbio.1000172.

Calebiro, D. *et al.* (2021) 'G protein-coupled receptor-G protein interactions: a single-molecule perspective', *Physiological Reviews*, 101(3), pp. 857–906. Available at: https://doi.org/10.1152/physrev.00021.2020.

Cario, G. and Franck, J. (1922) 'Über Zerlegung von Wasserstoffmolekülen durch angeregte Quecksilberatome', *Zeitschrift für Physik*, 11(1), pp. 161–166. Available at: https://doi.org/10.1007/BF01328410.

Carpenter, B. and Tate, C.G. (2016) 'Engineering a minimal G protein to facilitate crystallisation of G protein-coupled receptors in their active conformation', *Protein Engineering Design and Selection*, 29(12), pp. 583–593. Available at: https://doi.org/10.1093/protein/gzw049.

CDC Injury Center (2018) *Understanding the Epidemic*, *CDC*. Available at: https://www.cdc.gov/drugoverdose/epidemic/index.html (Accessed: 27 November 2019).

Charest, P.G., Terrillon, S. and Bouvier, M. (2005) 'Monitoring agonist-promoted conformational changes of β-arrestin in living cells by intramolecular BRET', *EMBO reports*, 6(4), pp. 334–340. Available at: https://doi.org/10.1038/sj.embor.7400373.

Chen, Q. *et al.* (2017) 'Structural basis of arrestin-3 activation and signaling', *Nature Communications*, 8(1), p. 1427. Available at: https://doi.org/10.1038/s41467-017-01218-8.

Chen, Q., Iverson, T.M. and Gurevich, V.V. (2018) 'Structural Basis of Arrestin-Dependent Signal Transduction', *Trends in Biochemical Sciences*, 43(6), pp. 412–423. Available at: https://doi.org/10.1016/j.tibs.2018.03.005.

Chen, Y.-J. *et al.* (2013) 'Identification of phosphorylation sites in the COOH-terminal tail of the μ-opioid receptor', *Journal of Neurochemistry*, 124(2), pp. 189–199. Available at: https://doi.org/10.1111/jnc.12071.

Christopoulos, A. (2002) 'Allosteric binding sites on cell-surface receptors: novel targets for drug discovery', *Nature Reviews Drug Discovery*, 1(3), pp. 198–210. Available at: https://doi.org/10.1038/nrd746.

Christopoulos, A. *et al.* (2014) 'International Union of Basic and Clinical Pharmacology. XC. Multisite Pharmacology: Recommendations for the Nomenclature of Receptor Allosterism and Allosteric Ligands', *Pharmacological Reviews*. Edited by E.H. Ohlstein, 66(4), pp. 918–947. Available at: https://doi.org/10.1124/pr.114.008862.

Christopoulos, A. and Kenakin, T. (2002) 'G Protein-Coupled Receptor Allosterism and Complexing', *Pharmacological Reviews*, 54(2), pp. 323–374. Available at: https://doi.org/10.1124/pr.54.2.323.

Claing, A. *et al.* (2001) 'β-Arrestin-mediated ADP-ribosylation Factor 6 Activation and β 2 -Adrenergic Receptor Endocytosis', *Journal of Biological Chemistry*, 276(45), pp. 42509–42513. Available at: https://doi.org/10.1074/jbc.M108399200.

Comer, S.D. and Cahill, C.M. (2019) 'Fentanyl: Receptor pharmacology, abuse potential, and implications for treatment', *Neurosci. Biobehav. Rev.*, 106, pp. 49–57. Available at: https://doi.org/10.1016/j.neubiorev.2018.12.005.

Conibear, A.E. and Kelly, E. (2019) 'A Biased View of μ -Opioid Receptors?', *Molecular Pharmacology*, 96(5), pp. 542–549. Available at: https://doi.org/10.1124/mol.119.115956.

Corder, G. *et al.* (2018) 'Endogenous and Exogenous Opioids in Pain', *Annual Review of Neuroscience*, 41(1), pp. 453–473. Available at: https://doi.org/10.1146/annurev-neuro-080317-061522.

Crews, K.R. *et al.* (2014) 'Clinical Pharmacogenetics Implementation Consortium Guidelines for Cytochrome P450 2D6 Genotype and Codeine Therapy: 2014 Update', *Clinical Pharmacology and Therapeutics*, 95(4), pp. 376–382. Available at: https://doi.org/10.1038/clpt.2013.254.

Crilly, S.E. *et al.* (2021) 'Conformational specificity of opioid receptors is determined by subcellular location irrespective of agonist', *eLife*, 10. Available at: https://doi.org/10.7554/eLife.67478.

Crivat, G. and Taraska, J.W. (2012) 'Imaging proteins inside cells with fluorescent tags', *Trends in biotechnology*, 30(1), pp. 8–16. Available at: https://doi.org/10.1016/j.tibtech.2011.08.002.

DeFea, K.A., Vaughn, Z.D., *et al.* (2000) 'The proliferative and antiapoptotic effects of substance P are facilitated by formation of a beta -arrestin-dependent scaffolding complex', *Proceedings of the National Academy of Sciences*, 97(20), pp. 11086–11091. Available at: https://doi.org/10.1073/pnas.190276697.

DeFea, K.A., Zalevsky, J., *et al.* (2000) 'β-Arrestin–Dependent Endocytosis of Proteinase-Activated Receptor 2 Is Required for Intracellular Targeting of Activated Erk1/2', *Journal of Cell Biology*, 148(6), pp. 1267–1282. Available at: https://doi.org/10.1083/jcb.148.6.1267.

Deng, H.B. *et al.* (2000) 'Role for the C-Terminus in Agonist-Induced μ Opioid Receptor Phosphorylation and Desensitization', *Biochemistry*, 39(18), pp. 5492–5499. Available at: https://doi.org/10.1021/bi991938b.

Dertinger, T. and Ewers, B. (2008) 'Unpublished Results'.

DeVree, B.T. *et al.* (2016) 'Allosteric coupling from G protein to the agonist binding pocket in GPCRs', *Nature*, 535(7610), pp. 182–186. Available at: https://doi.org/10.1038/nature18324.

DeWire, S.M. *et al.* (2008) 'β-Arrestin-mediated Signaling Regulates Protein Synthesis', *Journal of Biological Chemistry*, 283(16), pp. 10611–10620. Available at: https://doi.org/10.1074/jbc.M710515200.

DeWire, S.M. *et al.* (2013) 'A G Protein-Biased Ligand at the μ -Opioid Receptor Is Potently Analgesic with Reduced Gastrointestinal and Respiratory Dysfunction Compared with Morphine', *Journal of Pharmacology and Experimental Therapeutics*, 344(3), pp. 708–717. Available at: https://doi.org/10.1124/jpet.112.201616.

Doll, C. *et al.* (2011) 'Agonist-selective patterns of μ-opioid receptor phosphorylation revealed by phosphosite-specific antibodies', *British Journal of Pharmacology*, 164(2), pp. 298–307. Available at: https://doi.org/10.1111/j.1476-5381.2011.01382.x.

Doll, C. *et al.* (2012) 'Deciphering μ-opioid receptor phosphorylation and dephosphorylation in HEK293 cells', *British Journal of Pharmacology*, 167(6), pp. 1259–1270. Available at: https://doi.org/10.1111/j.1476-5381.2012.02080.x.

Donthamsetti, P. *et al.* (2015) 'Using Bioluminescence Resonance Energy Transfer (BRET) to Characterize Agonist-Induced Arrestin Recruitment to Modified and Unmodified G Protein-Coupled Receptors', *Current Protocols in*

*Pharmacology*, 70(1), p. 2.14.1-2.14.14. Available at: https://doi.org/10.1002/0471141755.ph0214s70.

Doudna, J.A. and Charpentier, E. (2014) 'The new frontier of genome engineering with CRISPR-Cas9', *Science*, 346(6213), p. 1258096. Available at: https://doi.org/10.1126/science.1258096.

Downes, G.B. and Gautam, N. (1999) 'The G Protein Subunit Gene Families', *Genomics*, 62(3), pp. 544–552. Available at: https://doi.org/10.1006/geno.1999.5992.

Drube, J. *et al.* (2022) 'GPCR kinase knockout cells reveal the impact of individual GRKs on arrestin binding and GPCR regulation', *Nature Communications*, 13(1), p. 540. Available at: https://doi.org/10.1038/s41467-022-28152-8.

Ehrlich, A.T. *et al.* (2019) 'Biased Signaling of the Mu Opioid Receptor Revealed in Native Neurons', *iScience*, 14, pp. 47–57. Available at: https://doi.org/10.1016/j.isci.2019.03.011.

Eichel, K. *et al.* (2018a) 'Catalytic activation of β-arrestin by GPCRs', *Nature*, 557(7705), pp. 381–386. Available at: https://doi.org/10.1038/s41586-018-0079-1.

Eichel, K. *et al.* (2018b) 'Catalytic activation of β-arrestin by GPCRs', *Nature*, 557(7705), pp. 381–386. Available at: https://doi.org/10.1038/s41586-018-0079-1.

Eichel, K. and von Zastrow, M. (2018) 'Subcellular Organization of GPCR Signaling', *Trends in Pharmacological Sciences*, 39(2), pp. 200–208. Available at: https://doi.org/10.1016/j.tips.2017.11.009.

El Kouhen, R. *et al.* (2001) 'Phosphorylation of Ser 363 , Thr 370 , and Ser 375 Residues within the Carboxyl Tail Differentially Regulates μ-Opioid Receptor Internalization', *Journal of Biological Chemistry*, 276(16), pp. 12774–12780. Available at: https://doi.org/10.1074/jbc.M009571200.

Erlandson, S.C., McMahon, C. and Kruse, A.C. (2018) 'Structural Basis for G Protein–Coupled Receptor Signaling', *Annual Review of Biophysics*, 47(1), pp. 1–18. Available at: https://doi.org/10.1146/annurev-biophys-070317-032931.

Feng, B., Li, Z. and Wang, J.B. (2011) 'Protein Kinase C-Mediated Phosphorylation of the μ-Opioid Receptor and Its Effects on Receptor Signaling', *Molecular Pharmacology*, 79(4), pp. 768–775. Available at: https://doi.org/10.1124/mol.110.069096.

Fernandes, D.D. *et al.* (2017) 'Characterization of Fluorescein Arsenical Hairpin (FlAsH) as a Probe for Single-Molecule Fluorescence Spectroscopy',

*Scientific Reports*, 7(1). Available at: https://doi.org/10.1038/s41598-017-13427-8.

Fessart, D. *et al.* (2007) 'Src-dependent phosphorylation of β2-adaptin dissociates the β-arrestin–AP-2 complex', *Journal of Cell Science*, 120(10), pp. 1723–1732. Available at: https://doi.org/10.1242/jcs.03444.

Fessart, D., Simaan, M. and Laporte, S.A. (2005) 'c-Src regulates clathrin adapter protein 2 interaction with beta-arrestin and the angiotensin II type 1 receptor during clathrin- mediated internalization', *Molecular Endocrinology (Baltimore, Md.)*, 19(2), pp. 491–503. Available at: https://doi.org/10.1210/me.2004-0246.

Flock, T. *et al.* (2017) 'Selectivity determinants of GPCR–G-protein binding', *Nature*, 545(7654), pp. 317–322. Available at: https://doi.org/10.1038/nature22070.

Főrster, T. (1959) '10th Spiers Memorial Lecture. Transfer mechanisms of electronic excitation', *Discussions of the Faraday Society*, 27(0), pp. 7–17. Available at: https://doi.org/10.1039/DF9592700007.

Fritzwanker, S., Schulz, S. and Kliewer, A. (2021) 'SR-17018 Stimulates Atypical μ-Opioid Receptor Phosphorylation and Dephosphorylation', *Molecules*, 26(15), p. 4509. Available at: https://doi.org/10.3390/molecules26154509.

Fukuda, K. *et al.* (1998) 'Partial Agonistic Activity of Naloxone on the Opioid Receptors Expressed from Complementary Deoxyribonucleic Acids in Chinese Hamster Ovary Cells', *Anesthesia & Analgesia*, 87(2), p. 450. Available at: https://doi.org/10.1213/00000539-199808000-00041.

Gaidarov, I. *et al.* (1999) 'Arrestin function in G protein-coupled receptor endocytosis requires phosphoinositide binding', *The EMBO Journal*, 18(4), pp. 871–881. Available at: https://doi.org/10.1093/emboj/18.4.871.

Galet, C. and Ascoli, M. (2008) 'Arrestin-3 is essential for the activation of Fyn by the luteinizing hormone receptor (LHR) in MA-10 cells☆', *Cellular Signalling*, 20(10), pp. 1822–1829. Available at: https://doi.org/10.1016/j.cellsig.2008.06.005.

Galligan, J.J. and Akbarali, H.I. (2014) 'Molecular Physiology of Enteric Opioid Receptors', *The American Journal of Gastroenterology Supplements*, 2(1), pp. 17–21. Available at: https://doi.org/10.1038/ajgsup.2014.5.

Gao, H. *et al.* (2004) 'Identification of β-Arrestin2 as a G Protein-Coupled Receptor-Stimulated Regulator of NF-κB Pathways', *Molecular Cell*, 14(3), pp. 303–317. Available at: https://doi.org/10.1016/S1097-2765(04)00216-3.

Ge, L. *et al.* (2003) 'A β-Arrestin-dependent Scaffold Is Associated with Prolonged MAPK Activation in Pseudopodia during Protease-activated Receptor-2-induced Chemotaxis', *Journal of Biological Chemistry*, 278(36), pp. 34418–34426. Available at: https://doi.org/10.1074/jbc.M300573200.

Gesty-Palmer, D. *et al.* (2005) 'β-Arrestin 2 Expression Determines the Transcriptional Response to Lysophosphatidic Acid Stimulation in Murine Embryo Fibroblasts', *Journal of Biological Chemistry*, 280(37), pp. 32157–32167. Available at: https://doi.org/10.1074/jbc.M507460200.

Ghosh, E. *et al.* (2019) 'Conformational Sensors and Domain Swapping Reveal Structural and Functional Differences between β-Arrestin Isoforms', *Cell reports*, 28(13), pp. 3287-3299.e6. Available at: https://doi.org/10.1016/j.celrep.2019.08.053.

Gillis, A., Kliewer, A., *et al.* (2020) 'Critical Assessment of G Protein-Biased Agonism at the μ-Opioid Receptor', *Trends in Pharmacological Sciences*, 41(12), pp. 947–959. Available at: https://doi.org/10.1016/j.tips.2020.09.009.

Gillis, A., Batista-Gondin, A., *et al.* (2020a) 'Low intrinsic efficacy for G protein activation can explain the improved side effect profiles of new opioid agonists', *Science Signaling*, 13(625), p. eaaz3140. Available at: https://doi.org/10.1126/scisignal.aaz3140.

Gillis, A., Batista-Gondin, A., *et al.* (2020b) 'Low intrinsic efficacy for G protein activation can explain the improved side effect profiles of new opioid agonists', *Science Signaling*, 13(625), p. eaaz3140. Available at: https://doi.org/10.1126/scisignal.aaz3140.

Glück, L. *et al.* (2014) 'Loss of Morphine Reward and Dependence in Mice Lacking G Protein-Coupled Receptor Kinase 5', *Biological psychiatry*, 76(10), pp. 767–774. Available at: https://doi.org/10.1016/j.biopsych.2014.01.021.

Goddard, A.D. and Watts, A. (2012) 'Regulation of G protein-coupled receptors by palmitoylation and cholesterol', *BMC Biology*, 10(1), p. 27. Available at: https://doi.org/10.1186/1741-7007-10-27.

Gomes, I. *et al.* (2020) 'Biased signaling by endogenous opioid peptides', *Proceedings of the National Academy of Sciences*, 117(21), pp. 11820–11828. Available at: https://doi.org/10.1073/pnas.2000712117.

Goodman, O.B. *et al.* (1996) 'β-Arrestin acts as a clathrin adaptor in endocytosis of the β2-adrenergic receptor', *Nature*, 383(6599), pp. 447–450. Available at: https://doi.org/10.1038/383447a0.

Grimes, J. *et al.* (2022) 'Single-molecule analysis of receptor-β-arrestin interactions in living cells'. bioRxiv, p. 2022.11.15.516577. Available at: https://doi.org/10.1101/2022.11.15.516577.

Grimes, J. *et al.* (2023) 'Plasma membrane preassociation drives β-arrestin coupling to receptors and activation', *Cell*, 0(0). Available at: https://doi.org/10.1016/j.cell.2023.04.018.

Groer, C.E. *et al.* (2007) 'An Opioid Agonist that Does Not Induce μ-Opioid Receptor—Arrestin Interactions or Receptor Internalization', *Molecular Pharmacology*, 71(2), pp. 549–557. Available at: https://doi.org/10.1124/mol.106.028258.

Guillien, M. *et al.* (2022) 'Structural Insights into the Intrinsically Disordered GPCR C-Terminal Region, Major Actor in Arrestin-GPCR Interaction', *Biomolecules*, 12(5), p. 617. Available at: https://doi.org/10.3390/biom12050617.

Guillien, M. *et al.* (2023) 'Phosphorylation motif dictates GPCR C-terminal domain conformation and arrestin interaction'. bioRxiv, p. 2023.02.23.529712. Available at: https://doi.org/10.1101/2023.02.23.529712.

Gurevich, E.V. *et al.* (2012) 'G protein-coupled receptor kinases: more than just kinases and not only for GPCRs', *Pharmacology & therapeutics*, 133(1), p. 40. Available at: https://doi.org/10.1016/j.pharmthera.2011.08.001.

Gurevich, E.V. and Gurevich, V.V. (2006) 'Arrestins: ubiquitous regulators of cellular signaling pathways', *Genome Biology*, 7(9), p. 236. Available at: https://doi.org/10.1186/gb-2006-7-9-236.

Gurevich, V.V. and Gurevich, E.V. (2004) 'The molecular acrobatics of arrestin activation', *Trends in Pharmacological Sciences*, 25(2), pp. 105–111. Available at: https://doi.org/10.1016/j.tips.2003.12.008.

Haider, R.S. (2021) *Differential Analysis of GPCR-Induced Dynamic Conformational Change in β-Arrestin1 and 2*. Friedrich-Schiller University Jena.

Haider, R.S. *et al.* (2022) 'β-arrestin1 and 2 exhibit distinct phosphorylation-dependent conformations when coupling to the same GPCR in living cells', *Nature Communications*, 13(1), p. 5638. Available at: https://doi.org/10.1038/s41467-022-33307-8.

Halls, M.L. *et al.* (2016) 'Plasma membrane localization of the μ-opioid receptor controls spatiotemporal signaling', *Science Signaling*, 9(414), pp. 1–13. Available at: https://doi.org/10.1126/scisignal.aac9177.

Hanlon, C.D. and Andrew, D.J. (2015) 'Outside-in signaling - a brief review of GPCR signaling with a focus on the Drosophila GPCR family', *Journal of Cell Science*, 128(19), pp. 3533–3542. Available at: https://doi.org/10.1242/jcs.175158.

Hanson, S.M. *et al.* (2006) 'Visual Arrestin Binding to Microtubules Involves a Distinct Conformational Change', *Journal of Biological Chemistry*, 281(14), pp. 9765–9772. Available at: https://doi.org/10.1074/jbc.M510738200.

Hanson, S.M. *et al.* (2007) 'Arrestin Mobilizes Signaling Proteins to the Cytoskeleton and Redirects their Activity', *Journal of Molecular Biology*, 368(2), pp. 375–387. Available at: https://doi.org/10.1016/j.jmb.2007.02.053.

Hanson, S.M. *et al.* (2008) 'Opposing Effects of Inositol Hexakisphosphate on Rod Arrestin and Arrestin2 Self-Association †', *Biochemistry*, 47(3), pp. 1070–1075. Available at: https://doi.org/10.1021/bi7021359.

Heng, J. *et al.* (2023) 'Function and dynamics of the intrinsically disordered carboxyl terminus of β2 adrenergic receptor', *Nature Communications*, 14(1), p. 2005. Available at: https://doi.org/10.1038/s41467-023-37233-1.

Hill, R. *et al.* (2018) 'The novel μ-opioid receptor agonist PZM21 depresses respiration and induces tolerance to antinociception', *British Journal of Pharmacology*, 175(13), pp. 2653–2661. Available at: https://doi.org/10.1111/bph.14224.

Homan, K.T., Wu, E., Cannavo, A., *et al.* (2014) 'Identification and Characterization of Amlexanox as a G Protein-Coupled Receptor Kinase 5 Inhibitor', *Molecules*, 19(10), pp. 16937–16949. Available at: https://doi.org/10.3390/molecules191016937.

Homan, K.T., Wu, E., Wilson, M.W., *et al.* (2014) 'Structural and functional analysis of g protein-coupled receptor kinase inhibition by paroxetine and a rationally designed analog', *Molecular Pharmacology*, 85(2), pp. 237–248. Available at: https://doi.org/10.1124/mol.113.089631.

Houndolo, T., Boulay, P.-L. and Claing, A. (2005) 'G Protein-coupled Receptor Endocytosis in ADP-ribosylation Factor 6-depleted Cells', *Journal of Biological Chemistry*, 280(7), pp. 5598–5604. Available at: https://doi.org/10.1074/jbc.M411456200.

Hwang, E., Song, J. and Zhang, J. (2019) 'Integration of Nanomaterials and Bioluminescence Resonance Energy Transfer Techniques for Sensing Biomolecules', *Biosensors*, 9(1), p. 42. Available at: https://doi.org/10.3390/bios9010042.

Ikeda, S., Kaneko, M. and Fujiwara, S. (2007) 'Cardiotonic agent comprising grk inhibitor'. Available at: https://patents.google.com/patent/WO2007034846A1/en (Accessed: 5 April 2023).

Illing, S., Mann, A. and Schulz, S. (2014) 'Heterologous regulation of agonist-independent μ-opioid receptor phosphorylation by protein kinase C', *British*

*Journal of Pharmacology*, 171(5), pp. 1330–1340. Available at: https://doi.org/10.1111/bph.12546.

Imamura, T. *et al.* (2001) 'β-Arrestin-mediated Recruitment of the Src Family Kinase Yes Mediates Endothelin-1-stimulated Glucose Transport', *Journal of Biological Chemistry*, 276(47), pp. 43663–43667. Available at: https://doi.org/10.1074/jbc.M105364200.

Inouye, K. and The Svedberg (1911) 'Zur Kenntnis der Struktur ultramikroskopischer Teilchen', *Zeitschrift für Chemie und Industrie der Kolloide*, 9(2), pp. 49–53. Available at: https://doi.org/10.1007/BF01466005.

Irannejad, R. *et al.* (2017) 'Functional selectivity of GPCR-directed drug action through location bias', *Nature Chemical Biology*, 13(7), pp. 799–806. Available at: https://doi.org/10.1038/nchembio.2389.

Irannejad, R. and von Zastrow, M. (2014) 'GPCR signaling along the endocytic pathway', *Current Opinion in Cell Biology*, 27(1), pp. 109–116. Available at: https://doi.org/10.1016/j.ceb.2013.10.003.

Isaikina, P. *et al.* (2022) 'A key GPCR phosphorylation motif discovered in arrestin2•CCR5 phosphopeptide complexes'. bioRxiv, p. 2022.10.10.511578. Available at: https://doi.org/10.1101/2022.10.10.511578.

James, A. and Williams, J.T. (2020) 'Basic Opioid Pharmacology — An Update', *British Journal of Pain*, 14(2), pp. 115–121. Available at: https://doi.org/10.1177/2049463720911986.

Janetzko, J. *et al.* (2022) 'Membrane phosphoinositides regulate GPCR-β-arrestin complex assembly and dynamics', *Cell*, 185(24), pp. 4560-4573.e19. Available at: https://doi.org/10.1016/j.cell.2022.10.018.

Jones, G.A. and Bradshaw, D.S. (2019) 'Resonance Energy Transfer: From Fundamental Theory to Recent Applications', *Frontiers in Physics*, 7(JULY), p. 100. Available at: https://doi.org/10.3389/fphy.2019.00100.

Juillerat, A. *et al.* (2003) 'Directed Evolution of O6-Alkylguanine-DNA Alkyltransferase for Efficient Labelling of Fusion Proteins with Small Molecules In Vivo', *Chemistry & Biology*, 10(4), pp. 313–317. Available at: https://doi.org/10.1016/S1074-5521(03)00068-1.

Just, S. *et al.* (2013) 'Differentiation of Opioid Drug Effects by Hierarchical Multi-Site Phosphorylation', *Molecular Pharmacology*, 83(3), pp. 633–639. Available at: https://doi.org/10.1124/mol.112.082875.

Kallmann, H. and London, F. (1929) 'Über quantenmechanische Energieübertragung zwischen atomaren Systemen', *Zeitschrift für Physikalische Chemie*, 2B(1), pp. 207–243. Available at: https://doi.org/10.1515/zpch-1929-0214.

Kang, Y. *et al.* (2015) 'Crystal structure of rhodopsin bound to arrestin by femtosecond X-ray laser', *Nature*, 523(7562), pp. 561–567. Available at: https://doi.org/10.1038/nature14656.

Karlsson, M. *et al.* (2021) 'A single–cell type transcriptomics map of human tissues', *Science Advances*, 7(31), p. eabh2169. Available at: https://doi.org/10.1126/sciadv.abh2169.

Kelly, B. *et al.* (2021) 'Delineating the Ligand-Receptor Interactions That Lead to Biased Signaling at the μ-Opioid Receptor', 61(7), pp. 3696–3707. Available at: https://doi.org/10.1021/ACS.JCIM.1C00585.

Kelly, E. *et al.* (2023) 'The anomalous pharmacology of fentanyl', *British Journal of Pharmacology*, 180(7), pp. 797–812. Available at: https://doi.org/10.1111/bph.15573.

Kendall, R.T. *et al.* (2011) 'The β-Arrestin Pathway-selective Type 1A Angiotensin Receptor (AT 1A ) Agonist [Sar 1 ,Ile 4 ,Ile 8 ]Angiotensin II Regulates a Robust G Protein-independent Signaling Network', *Journal of Biological Chemistry*, 286(22), pp. 19880–19891. Available at: https://doi.org/10.1074/jbc.M111.233080.

Kennedy, N.M. *et al.* (2018) 'Optimization of a Series of Mu Opioid Receptor (MOR) Agonists with High G Protein Signaling Bias', *Journal of Medicinal Chemistry*, 61(19), pp. 8895–8907. Available at: https://doi.org/10.1021/acs.jmedchem.8b01136.

Kenski, D.M. *et al.* (2005) 'Chemical Genetic Engineering of G Protein-coupled Receptor Kinase 2 *', *Journal of Biological Chemistry*, 280(41), pp. 35051–35061. Available at: https://doi.org/10.1074/jbc.M507594200.

Khan, S.M. *et al.* (2013) 'The Expanding Roles of G βγ Subunits in G Protein–Coupled Receptor Signaling and Drug Action', *Pharmacological Reviews*. Edited by E.L. Barker, 65(2), pp. 545–577. Available at: https://doi.org/10.1124/pr.111.005603.

Khoury, E. *et al.* (2014) 'Differential Regulation of Endosomal GPCR/β-Arrestin Complexes and Trafficking by MAPK', *Journal of Biological Chemistry*, 289(34), pp. 23302–23317. Available at: https://doi.org/10.1074/jbc.M114.568147.

Kim, J. *et al.* (2005) 'Functional antagonism of different G protein-coupled receptor kinases for β-arrestin-mediated angiotensin II receptor signaling', *Proceedings of the National Academy of Sciences of the United States of America*, 102(5), pp. 1442–1447. Available at: https://doi.org/10.1073/pnas.0409532102.

Kim, Y.J. *et al.* (2013) 'Crystal structure of pre-activated arrestin p44', *Nature*, 497(7447), pp. 142–146. Available at: https://doi.org/10.1038/nature12133.

Kliewer, A. *et al.* (2019) 'Phosphorylation-deficient G-protein-biased μ-opioid receptors improve analgesia and diminish tolerance but worsen opioid side effects.', *Nature communications*, 10(1), p. 367. Available at: https://doi.org/10.1038/s41467-018-08162-1.

Kliewer, A. *et al.* (2020) 'Morphine-induced respiratory depression is independent of ß-arrestin2 signalling', *British Journal of Pharmacology* [Preprint]. Available at: https://doi.org/10.1111/bph.15004.

Kosterlitz, H.W. and Waterfield, A.A. (1975) 'In Vitro Models in the Study of Structure-Activity Relationships of Narcotic Analgesics', *Annual Review of Pharmacology*, 15(1), pp. 29–47. Available at: https://doi.org/10.1146/annurev.pa.15.040175.000333.

Kovacs, J.J. *et al.* (2008) '-Arrestin-Mediated Localization of Smoothened to the Primary Cilium', *Science*, 320(5884), pp. 1777–1781. Available at: https://doi.org/10.1126/science.1157983.

Krupnick, J.G. *et al.* (1997) 'Arrestin/Clathrin Interaction', *Journal of Biological Chemistry*, 272(23), pp. 15011–15016. Available at: https://doi.org/10.1074/jbc.272.23.15011.

Kuhr, F.K. *et al.* (2010) 'ß-Arrestin 2 is required for B1 receptor-dependent post-translational activation of inducible nitric oxide synthase', *The FASEB Journal*, 24(7), pp. 2475–2483. Available at: https://doi.org/10.1096/fj.09-148783.

Lally, C.C.M. *et al.* (2017) 'C-edge loops of arrestin function as a membrane anchor', *Nature Communications*, 8(1), p. 14258. Available at: https://doi.org/10.1038/ncomms14258.

Laporte, S.A. *et al.* (1999) 'The 2-adrenergic receptor/ arrestin complex recruits the clathrin adaptor AP-2 during endocytosis', *Proceedings of the National Academy of Sciences*, 96(7), pp. 3712–3717. Available at: https://doi.org/10.1073/pnas.96.7.3712.

Laporte, S.A. *et al.* (2000) 'The Interaction of β-Arrestin with the AP-2 Adaptor Is Required for the Clustering of β 2 -Adrenergic Receptor into Clathrin-coated Pits', *Journal of Biological Chemistry*, 275(30), pp. 23120–23126. Available at: https://doi.org/10.1074/jbc.M002581200.

Latorraca, N.R. *et al.* (2018) 'Molecular mechanism of GPCR-mediated arrestin activation', *Nature*, 557(7705), pp. 452–456. Available at: https://doi.org/10.1038/s41586-018-0077-3.

Latorraca, N.R. *et al.* (2020) 'How GPCR Phosphorylation Patterns Orchestrate Arrestin-Mediated Signaling', *Cell*, 183(7), pp. 1813-1825.e18. Available at: https://doi.org/10.1016/j.cell.2020.11.014.

Lau, E.K. *et al.* (2011) 'Quantitative Encoding of the Effect of a Partial Agonist on Individual Opioid Receptors by Multisite Phosphorylation and Threshold Detection', *Science Signaling*, 4(185), pp. ra52–ra52. Available at: https://doi.org/10.1126/scisignal.2001748.

Lay, J. *et al.* (2016) 'Distribution and trafficking of the μ-opioid receptor in enteric neurons of the guinea pig', *American Journal of Physiology-Gastrointestinal and Liver Physiology*, 311(2), pp. G252–G266. Available at: https://doi.org/10.1152/ajpgi.00184.2016.

Lee, M.-H. *et al.* (2016) 'The conformational signature of β-arrestin2 predicts its trafficking and signalling functions', *Nature*, 531(7596), pp. 665–668. Available at: https://doi.org/10.1038/nature17154.

Lefkowitz, R.J. (2013) 'A Brief History of G-Protein Coupled Receptors (Nobel Lecture)', *Angewandte Chemie International Edition*, 52(25), pp. 6366–6378. Available at: https://doi.org/10.1002/anie.201301924.

Li, J. *et al.* (2003) 'Agonist-induced Formation of Opioid Receptor-G Protein-coupled Receptor Kinase (GRK)-Gβγ Complex on Membrane Is Required for GRK2 Function in Vivo', *Journal of Biological Chemistry*, 278(32), pp. 30219–30226. Available at: https://doi.org/10.1074/jbc.M302385200.

Liggett, S.B. (2011) 'Phosphorylation Barcoding as a Mechanism of Directing GPCR Signaling', *Science Signaling*, 4(185), pp. pe36–pe36. Available at: https://doi.org/10.1126/scisignal.2002331.

Lima-Fernandes, E. *et al.* (2011) 'Distinct functional outputs of PTEN signalling are controlled by dynamic association with β-arrestins', *The EMBO Journal*, 30(13), pp. 2557–2568. Available at: https://doi.org/10.1038/emboj.2011.178.

Lin, F.-T. *et al.* (1999) 'Feedback Regulation of β-Arrestin1 Function by Extracellular Signal-regulated Kinases', *Journal of Biological Chemistry*, 274(23), pp. 15971–15974. Available at: https://doi.org/10.1074/jbc.274.23.15971.

Liu, W. *et al.* (1998) 'Mechanism of Allosteric Regulation of the Rod cGMP Phosphodiesterase Activity by the Helical Domain of Transducin α Subunit *', *Journal of Biological Chemistry*, 273(51), pp. 34284–34292. Available at: https://doi.org/10.1074/jbc.273.51.34284.

Lohse, M.J. and Hoffmann, C. (2014) 'Arrestin Interactions with G Protein-Coupled Receptors', in *Handbook of Experimental Pharmacology*. Springer New York LLC, pp. 15–56. Available at: https://doi.org/10.1007/978-3-642-41199-1_2.

Lowe, J.D. *et al.* (2015) 'Role of G Protein–Coupled Receptor Kinases 2 and 3 in μ-Opioid Receptor Desensitization and Internalization', *Molecular*

*Pharmacology*, 88(2), pp. 347–356. Available at: https://doi.org/10.1124/mol.115.098293.

Luttrell, L.M. *et al.* (1999) 'β-Arrestin-Dependent Formation of β 2 Adrenergic Receptor-Src Protein Kinase Complexes', *Science*, 283(5402), pp. 655–661. Available at: https://doi.org/10.1126/science.283.5402.655.

Luttrell, L.M. *et al.* (2001) 'Activation and targeting of extracellular signal-regulated kinases by -arrestin scaffolds', *Proceedings of the National Academy of Sciences*, 98(5), pp. 2449–2454. Available at: https://doi.org/10.1073/pnas.041604898.

Lymperopoulos, A., Rengo, G. and Koch, W.J. (2012) 'GRK2 Inhibition in Heart Failure: Something Old, Something New', *Current Pharmaceutical Design*, 18(2), pp. 186–191.

Magde, D., Elson, E. and Webb, W.W. (1972) 'Thermodynamic Fluctuations in a Reacting System—Measurement by Fluorescence Correlation Spectroscopy', *Physical Review Letters*, 29(11), pp. 705–708. Available at: https://doi.org/10.1103/PhysRevLett.29.705.

Magde, D., Elson, E.L. and Webb, W.W. (1974) 'Fluorescence correlation spectroscopy. II. An experimental realization', *Biopolymers*, 13(1), pp. 29–61. Available at: https://doi.org/10.1002/bip.1974.360130103.

Manglik, A. *et al.* (2016) 'Structure-based discovery of opioid analgesics with reduced side effects', *Nature*, 537(7619), pp. 185–190. Available at: https://doi.org/10.1038/nature19112.

Mann, A. *et al.* (2015) 'Different mechanisms of homologous and heterologous μ-opioid receptor phosphorylation', *British Journal of Pharmacology*, 172(2), pp. 311–316. Available at: https://doi.org/10.1111/bph.12627.

Mann, A. *et al.* (2019) 'Agonist-selective NOP receptor phosphorylation correlates in vitro and in vivo and reveals differential post-activation signaling by chemically diverse agonists', *Science signaling*, 12(574), p. eaau8072. Available at: https://doi.org/10.1126/scisignal.aau8072.

Mann, A. *et al.* (2020) 'Agonist-induced phosphorylation bar code and differential post-activation signaling of the delta opioid receptor revealed by phosphosite-specific antibodies', *Scientific Reports*, 10(1), p. 8585. Available at: https://doi.org/10.1038/s41598-020-65589-7.

Marion, S. *et al.* (2006) 'A β-arrestin binding determinant common to the second intracellular loops of rhodopsin family G protein-coupled receptors', *Journal of Biological Chemistry*, 281(5), pp. 2932–2938. Available at: https://doi.org/10.1074/jbc.M508074200.

Markova, V. *et al.* (2021) 'β-Arrestin 1 and 2 similarly influence μ-opioid receptor mobility and distinctly modulate adenylyl cyclase activity', *Cellular Signalling*, 87, p. 110124. Available at: https://doi.org/10.1016/j.cellsig.2021.110124.

May, L.T., Leach, K., *et al.* (2007) 'Allosteric modulation of G protein-coupled receptors', *Annual Review of Pharmacology and Toxicology*, 47, pp. 1–51. Available at: https://doi.org/10.1146/annurev.pharmtox.47.120505.105159.

May, L.T., Avlani, V.A., *et al.* (2007) 'Structure-Function Studies of Allosteric Agonism at M2 Muscarinic Acetylcholine Receptors', *Molecular Pharmacology*, 72(2), pp. 463–476. Available at: https://doi.org/10.1124/mol.107.037630.

McDonald, P.H. (2000) 'beta -Arrestin 2: A Receptor-Regulated MAPK Scaffold for the Activation of JNK3', *Science*, 290(5496), pp. 1574–1577. Available at: https://doi.org/10.1126/science.290.5496.1574.

McPherson, J. *et al.* (2010) 'μ-Opioid Receptors: Correlation of Agonist Efficacy for Signalling with Ability to Activate Internalization', *Molecular Pharmacology*, 78(4), pp. 756–766. Available at: https://doi.org/10.1124/mol.110.066613.

Melkes, B., Hejnova, L. and Novotny, J. (2016) 'Biased μ-opioid receptor agonists diversely regulate lateral mobility and functional coupling of the receptor to its cognate G proteins', *Naunyn-Schmiedeberg's Archives of Pharmacology*, 389(12), pp. 1289–1300. Available at: https://doi.org/10.1007/s00210-016-1293-8.

Miess, E. *et al.* (2018) 'Multisite phosphorylation is required for sustained interaction with GRKs and arrestins during rapid μ-opioid receptor desensitization', *Science Signaling*, 11(539), p. eaas9609. Available at: https://doi.org/10.1126/scisignal.aas9609.

Milano, S.K. *et al.* (2006) 'Nonvisual Arrestin Oligomerization and Cellular Localization Are Regulated by Inositol Hexakisphosphate Binding', *Journal of Biological Chemistry*, 281(14), pp. 9812–9823. Available at: https://doi.org/10.1074/jbc.M512703200.

Miller, W.E. *et al.* (2000) 'β-Arrestin1 Interacts with the Catalytic Domain of the Tyrosine Kinase c-SRC', *Journal of Biological Chemistry*, 275(15), pp. 11312–11319. Available at: https://doi.org/10.1074/jbc.275.15.11312.

Møller, T.C. *et al.* (2020) 'Dissecting the roles of GRK2 and GRK3 in μ-opioid receptor internalization and β-arrestin2 recruitment using CRISPR/Cas9-edited HEK293 cells', *Scientific Reports*, 10(1), p. 17395. Available at: https://doi.org/10.1038/s41598-020-73674-0.

Morita, K. and North, R.A. (1982) 'Opiate activation of potassium conductance in myenteric neurons: inhibition by calcium ion', *Brain Research*, 242(1), pp. 145–150. Available at: https://doi.org/10.1016/0006-8993(82)90504-2.

Moritz, A. *et al.* (2021) 'Phosphorylation of the D1 Dopamine Receptor by G Protein-Coupled Receptor Kinases: phosphorylation site identification and linkage to functional effects', *The FASEB Journal*, 35(S1). Available at: https://doi.org/10.1096/fasebj.2021.35.S1.02732.

Moulédous, L. *et al.* (2012) 'GRK2 Protein-mediated Transphosphorylation Contributes to Loss of Function of μ-Opioid Receptors Induced by Neuropeptide FF (NPFF2) Receptors', *Journal of Biological Chemistry*, 287(16), pp. 12736–12749. Available at: https://doi.org/10.1074/jbc.M111.314617.

Nehmé, R. *et al.* (2017) 'Mini-G proteins: Novel tools for studying GPCRs in their active conformation', *PLoS ONE*, 12(4), p. e0175642. Available at: https://doi.org/10.1371/journal.pone.0175642.

Nelson, C.D. *et al.* (2007) 'Targeting of Diacylglycerol Degradation to M1 Muscarinic Receptors by -Arrestins', *Science*, 315(5812), pp. 663–666. Available at: https://doi.org/10.1126/science.1134562.

Nelson, C.D. *et al.* (2008) 'β-Arrestin Scaffolding of Phosphatidylinositol 4-Phosphate 5-Kinase Iα Promotes Agonist-stimulated Sequestration of the β2-Adrenergic Receptor', *Journal of Biological Chemistry*, 283(30), pp. 21093–21101. Available at: https://doi.org/10.1074/jbc.M800431200.

Nobles, K.N. *et al.* (2011) 'Distinct Phosphorylation Sites on the β2-Adrenergic Receptor Establish a Barcode That Encodes Differential Functions of β-Arrestin', *Science Signaling*, 4(185), pp. ra51–ra51. Available at: https://doi.org/10.1126/scisignal.2001707.

Noma, T. *et al.* (2007) 'β-Arrestin–mediated β1-adrenergic receptor transactivation of the EGFR confers cardioprotection', *Journal of Clinical Investigation*, 117(9), pp. 2445–2458. Available at: https://doi.org/10.1172/JCI31901.

Nuber, S. *et al.* (2016) 'β-Arrestin biosensors reveal a rapid, receptor-dependent activation/deactivation cycle', *Nature*, 531(7596), pp. 661–664. Available at: https://doi.org/10.1038/nature17198.

Oakley, R.H. *et al.* (2001) 'Molecular determinants underlying the formation of stable intracellular G protein-coupled receptor-beta-arrestin complexes after receptor endocytosis*', *The Journal of biological chemistry*, 276(22), pp. 19452–19460. Available at: https://doi.org/10.1074/JBC.M101450200.

Oishi, A., Dam, J. and Jockers, R. (2020) 'β-Arrestin-2 BRET Biosensors Detect Different β-Arrestin-2 Conformations in Interaction with GPCRs', *ACS Sensors*, 5(1), pp. 57–64. Available at: https://doi.org/10.1021/acssensors.9b01414.

Osterlitz, H.W. and Watt, A.J. (1968) 'Kinetic parameters of narcotic agonists and antagonists, with particular reference to N-allylnoroxymorphone (naloxone).', *British Journal of Pharmacology and Chemotherapy*, 33(2), pp. 266–276.

Ozawa, K. *et al.* (2008) 'S-Nitrosylation of β-Arrestin Regulates β-Adrenergic Receptor Trafficking', *Molecular Cell*, 31(3), pp. 395–405. Available at: https://doi.org/10.1016/j.molcel.2008.05.024.

Palczewski, K. *et al.* (1991) 'Binding of inositol phosphates to arrestin', *FEBS Letters*, 295(1–3), pp. 195–199. Available at: https://doi.org/10.1016/0014-5793(91)81416-6.

Pándy-Szekeres, G. *et al.* (2018) 'GPCRdb in 2018: adding GPCR structure models and ligands', *Nucleic Acids Research*, 46(D1), pp. D440–D446. Available at: https://doi.org/10.1093/nar/gkx1109.

Pándy-Szekeres, G. *et al.* (2023) 'GPCRdb in 2023: state-specific structure models using AlphaFold2 and new ligand resources', *Nucleic Acids Research*, 51(D1), pp. D395–D402. Available at: https://doi.org/10.1093/nar/gkac1013.

Pasternak, G.W. and Pan, Y.-X. (2013) 'Mu Opioids and Their Receptors: Evolution of a Concept', *Pharmacological Reviews*, 65(4), pp. 1257–1317. Available at: https://doi.org/10.1124/pr.112.007138.

Pathan, H. and Williams, J.T. (2012) 'Basic opioid pharmacology: an update', *British Journal of Pain*, 6(1), pp. 11–16. Available at: https://doi.org/10.1177/2049463712438493.

Pedersen, M.F. *et al.* (2019) 'Biased agonism of clinically approved μ-opioid receptor agonists and TRV130 is not controlled by binding and signaling kinetics', *Neuropharmacology*, 166, p. 107718. Available at: https://doi.org/10.1016/j.neuropharm.2019.107718.

Pedersen, M.F. *et al.* (2020) 'Dissecting the roles of GRK2 and GRK3 in μ-opioid receptor internalization and β-arrestin2 recruitment using CRISPR/Cas9-edited HEK293 cells', *bioRxiv*, p. 2020.01.08.898338. Available at: https://doi.org/10.1101/2020.01.08.898338.

Penela, P. *et al.* (2001) 'β-arrestin- and c-Src-dependent degradation of G-protein-coupled receptor kinase 2', *The EMBO Journal*, 20(18), pp. 5129–5138. Available at: https://doi.org/10.1093/emboj/20.18.5129.

Penela, P. *et al.* (2010) 'The complex G protein-coupled receptor kinase 2 (GRK2) interactome unveils new physiopathological targets', *British Journal of*

*Pharmacology*, 160(4), pp. 821–832. Available at: https://doi.org/10.1111/j.1476-5381.2010.00727.x.

Perrin, J. (1927) 'Fluorescence et induction moléculaire par résonance', 184, pp. 1097--1100.

Perry, S.J. (2002) 'Targeting of Cyclic AMP Degradation to beta 2-Adrenergic Receptors by beta -Arrestins', *Science*, 298(5594), pp. 834–836. Available at: https://doi.org/10.1126/science.1074683.

Perry-Hauser, N.A. *et al.* (2021) 'Assays for detecting arrestin interaction with GPCRs', in *Methods in cell biology*. Methods Cell Biol, pp. 43–65. Available at: https://doi.org/10.1016/bs.mcb.2021.06.007.

Peterson, Y.K. and Luttrell, L.M. (2017) 'The Diverse Roles of Arrestin Scaffolds in G Protein–Coupled Receptor Signaling', *Pharmacological Reviews*. Edited by M.C. Michel, 69(3), pp. 256–297. Available at: https://doi.org/10.1124/pr.116.013367.

Pfleger, K.D.G. and Eidne, K.A. (2006) 'Illuminating insights into protein-protein interactions using bioluminescence resonance energy transfer (BRET)', *Nature Methods*, 3(3), pp. 165–174. Available at: https://doi.org/10.1038/nmeth841.

Pfleger, K.D.G., Seeber, R.M. and Eidne, K.A. (2006) 'Bioluminescence resonance energy transfer (BRET) for the real-time detection of protein-protein interactions', *Nature Protocols*, 1(1), pp. 337–345. Available at: https://doi.org/10.1038/nprot.2006.52.

Pitcher, J.A., Freedman, N.J. and Lefkowitz, R.J. (1998) 'G protein-coupled receptor kinases.', *Annual review of biochemistry*, 67, pp. 653–92. Available at: https://doi.org/10.1146/annurev.biochem.67.1.653.

Podlewska, S. *et al.* (2020) 'Molecular Modelling of μ Opioid Receptor Ligands with Various Functional Properties: PZM21, SR-17018, Morphine, and Fentanyl—Simulated Interaction Patterns Confronted with Experimental Data', *Molecules*, 25(20), p. 4636. Available at: https://doi.org/10.3390/molecules25204636.

Potter, R.M. *et al.* (2002) 'Arrestin Variants Display Differential Binding Characteristics for the Phosphorylated N-Formyl Peptide Receptor Carboxyl Terminus', *Journal of Biological Chemistry*, 277(11), pp. 8970–8978. Available at: https://doi.org/10.1074/jbc.M111086200.

Premont, R.T. *et al.* (1996) 'Characterization of the G Protein-coupled Receptor Kinase GRK4: IDENTIFICATION OF FOUR SPLICE VARIANTS (∗)', *Journal of Biological Chemistry*, 271(11), pp. 6403–6410. Available at: https://doi.org/10.1074/jbc.271.11.6403.

Qiu, Y. *et al.* (2011) 'Cholesterol Regulates μ-Opioid Receptor-Induced β-Arrestin 2 Translocation to Membrane Lipid Rafts', *Molecular Pharmacology*, 80(1), pp. 210–218. Available at: https://doi.org/10.1124/mol.110.070870.

Qu, Q. *et al.* (2023) 'Insights into distinct signaling profiles of the μOR activated by diverse agonists', *Nature Chemical Biology*, 19(4), pp. 423–430. Available at: https://doi.org/10.1038/s41589-022-01208-y.

Quillinan, N. *et al.* (2011) 'Recovery from μ-Opioid Receptor Desensitization after Chronic Treatment with Morphine and Methadone', *The Journal of Neuroscience*, 31(12), pp. 4434–4443. Available at: https://doi.org/10.1523/JNEUROSCI.4874-10.2011.

Raehal, K.M. *et al.* (2009) 'Morphine-Induced Physiological and Behavioural Responses in Mice Lacking G Protein-Coupled Receptor Kinase 6', *Drug and alcohol dependence*, 104(3), pp. 187–196. Available at: https://doi.org/10.1016/j.drugalcdep.2009.04.011.

Raehal, K.M., Walker, J.K.L. and Bohn, L.M. (2005) 'Morphine Side Effects in β-Arrestin 2 Knockout Mice', *Journal of Pharmacology and Experimental Therapeutics*, 314(3), pp. 1195–1201. Available at: https://doi.org/10.1124/jpet.105.087254.

Raveh, A. *et al.* (2010) 'Nonenzymatic Rapid Control of GIRK Channel Function by a G Protein-Coupled Receptor Kinase', *Cell*, 143(5), pp. 750–760. Available at: https://doi.org/10.1016/j.cell.2010.10.018.

Reichel, M. *et al.* (2022) 'Suitability of GRK Antibodies for Individual Detection and Quantification of GRK Isoforms in Western Blots', *International Journal of Molecular Sciences*, 23(3), p. 1195. Available at: https://doi.org/10.3390/ijms23031195.

Reilly, S.M. *et al.* (2013) 'An inhibitor of the protein kinases TBK1/IKKε improves obesity-related metabolic dysfunctions', *Nature medicine*, 19(3), pp. 313–321. Available at: https://doi.org/10.1038/nm.3082.

Ren, X.-R. *et al.* (2005) 'Different G protein-coupled receptor kinases govern G protein and β-arrestin-mediated signaling of V2 vasopressin receptor', *Proceedings of the National Academy of Sciences of the United States of America*, 102(5), pp. 1448–1453. Available at: https://doi.org/10.1073/pnas.0409534102.

Reyes-Alcaraz, A. *et al.* (2018) 'Conformational signatures in β-arrestin2 reveal natural biased agonism at a G-protein-coupled receptor', *Communications Biology*, 1, p. 128. Available at: https://doi.org/10.1038/s42003-018-0134-3.

Ribas, C. *et al.* (2007) 'The G protein-coupled receptor kinase (GRK) interactome: Role of GRKs in GPCR regulation and signaling', *Biochimica et*

*Biophysica Acta (BBA) - Biomembranes*, 1768(4), pp. 913–922. Available at: https://doi.org/10.1016/j.bbamem.2006.09.019.

Rogacki, M.K. *et al.* (2018) 'Dynamic lateral organization of opioid receptors (kappa, mu wt and mu N40D ) in the plasma membrane at the nanoscale level', *Traffic*, 19(9), pp. 690–709. Available at: https://doi.org/10.1111/tra.12582.

Ross, E.M. (2008) 'Coordinating Speed and Amplitude in G-Protein Signaling', *Current Biology*, 18(17), pp. R777–R783. Available at: https://doi.org/10.1016/j.cub.2008.07.035.

Salahpour, A. *et al.* (2012) 'BRET biosensors to study GPCR biology, pharmacology, and signal transduction', *Frontiers in Endocrinology*, 3(AUG), p. 105. Available at: https://doi.org/10.3389/FENDO.2012.00105/BIBTEX.

Sanjana, N.E., Shalem, O. and Zhang, F. (2014) 'Improved vectors and genome-wide libraries for CRISPR screening', *Nature methods*, 11(8), pp. 783–784. Available at: https://doi.org/10.1038/nmeth.3047.

Saulière-Nzeh, A.N. *et al.* (2010) 'Agonist-selective Dynamic Compartmentalization of Human Mu Opioid Receptor as Revealed by Resolutive FRAP Analysis', *Journal of Biological Chemistry*, 285(19), pp. 14514–14520. Available at: https://doi.org/10.1074/jbc.M109.076695.

Scheerer, P. and Sommer, M.E. (2017) 'Structural mechanism of arrestin activation', *Current Opinion in Structural Biology*, 45, pp. 160–169. Available at: https://doi.org/10.1016/j.sbi.2017.05.001.

Schleicher, A., Kühn, H. and Hofmann, K.P. (1989) *Kinetics, Binding Constant, and Activation Energy of the 48-kDa Protein–Rhodopsin Complex by Extra-Metarhodopsin*, *Biochemistry*, pp. 1770–1775. Available at: https://doi.org/10.1021/bi00430a052.

Schmid, C.L. *et al.* (2017) 'Bias Factor and Therapeutic Window Correlate to Predict Safer Opioid Analgesics', *Cell*, 171(5), pp. 1165-1175.e13. Available at: https://doi.org/10.1016/j.cell.2017.10.035.

Schneider, S., Provasi, D. and Filizola, M. (2016) 'How Oliceridine (TRV-130) Binds and Stabilizes a μ-Opioid Receptor Conformational State That Selectively Triggers G Protein Signaling Pathways', *Biochemistry*, 55(46), pp. 6456–6466. Available at: https://doi.org/10.1021/acs.biochem.6b00948.

Schulz, S. *et al.* (2004) 'Morphine induces terminal μ-opioid receptor desensitization by sustained phosphorylation of serine-375', *The EMBO Journal*, 23(16), pp. 3282–3289. Available at: https://doi.org/10.1038/sj.emboj.7600334.

Schwille, P. *et al.* (1999) 'Molecular dynamics in living cells observed by fluorescence correlation spectroscopy with one- and two-photon excitation.', *Biophysical Journal*, 77(4), pp. 2251–2265.

Scott, M.G.H. *et al.* (2006) 'Cooperative Regulation of Extracellular Signal-Regulated Kinase Activation and Cell Shape Change by Filamin A and β-Arrestins', *Molecular and Cellular Biology*, 26(9), pp. 3432–3445. Available at: https://doi.org/10.1128/MCB.26.9.3432-3445.2006.

Seta, K. *et al.* (2002) 'AT1 Receptor Mutant Lacking Heterotrimeric G Protein Coupling Activates the Src-Ras-ERK Pathway without Nuclear Translocation of ERKs', *Journal of Biological Chemistry*, 277(11), pp. 9268–9277. Available at: https://doi.org/10.1074/jbc.M109221200.

Shenoy, S.K. (2001) 'Regulation of Receptor Fate by Ubiquitination of Activated beta 2-Adrenergic Receptor and beta -Arrestin', *Science*, 294(5545), pp. 1307–1313. Available at: https://doi.org/10.1126/science.1063866.

Shenoy, S.K. *et al.* (2007) 'Ubiquitination of β-Arrestin Links Seven-transmembrane Receptor Endocytosis and ERK Activation', *Journal of Biological Chemistry*, 282(40), pp. 29549–29562. Available at: https://doi.org/10.1074/jbc.M700852200.

Shenoy, S.K. *et al.* (2008) 'Nedd4 Mediates Agonist-dependent Ubiquitination, Lysosomal Targeting, and Degradation of the β 2 -Adrenergic Receptor', *Journal of Biological Chemistry*, 283(32), pp. 22166–22176. Available at: https://doi.org/10.1074/jbc.M709668200.

Shenoy, S.K. *et al.* (2009) '-Arrestin-dependent signaling and trafficking of 7-transmembrane receptors is reciprocally regulated by the deubiquitinase USP33 and the E3 ligase Mdm2', *Proceedings of the National Academy of Sciences*, 106(16), pp. 6650–6655. Available at: https://doi.org/10.1073/pnas.0901083106.

Shenoy, S.K. and Lefkowitz, R.J. (2003) 'Trafficking Patterns of β-Arrestin and G Protein-coupled Receptors Determined by the Kinetics of β-Arrestin Deubiquitination', *Journal of Biological Chemistry*, 278(16), pp. 14498–14506. Available at: https://doi.org/10.1074/jbc.M209626200.

Shukla, A.K. *et al.* (2008) 'Distinct conformational changes in β-arrestin report biased agonism at seven-transmembrane receptors', *Proceedings of the National Academy of Sciences of the United States of America*, 105(29), pp. 9988–9993. Available at: https://doi.org/10.1073/pnas.0804246105.

Shukla, A.K. *et al.* (2013) 'Structure of active β-arrestin-1 bound to a G-protein-coupled receptor phosphopeptide', *Nature*, 497(7447), pp. 137–141. Available at: https://doi.org/10.1038/nature12120.

Shukla, A.K. *et al.* (2014) 'Visualization of arrestin recruitment by a G-protein-coupled receptor', *Nature*, 512(7513), pp. 218–222. Available at: https://doi.org/10.1038/nature13430.

Smith, J.S. and Rajagopal, S. (2016) 'The β-Arrestins: Multifunctional Regulators of G Protein-coupled Receptors', *Journal of Biological Chemistry*, 291(17), pp. 8969–8977. Available at: https://doi.org/10.1074/jbc.R115.713313.

Smrcka, A.V. (2008) 'G protein βγ subunits: Central mediators of G protein-coupled receptor signaling', *Cellular and Molecular Life Sciences*, 65(14), pp. 2191–2214. Available at: https://doi.org/10.1007/s00018-008-8006-5.

Song, X. *et al.* (2006) 'Visual and Both Non-visual Arrestins in Their "Inactive" Conformation Bind JNK3 and Mdm2 and Relocalize Them from the Nucleus to the Cytoplasm', *Journal of Biological Chemistry*, 281(30), pp. 21491–21499. Available at: https://doi.org/10.1074/jbc.M603659200.

Sorkin, A. and von Zastrow, M. (2002) 'Signal transduction and endocytosis: close encounters of many kinds', *Nature Reviews Molecular Cell Biology*, 3(8), pp. 600–614. Available at: https://doi.org/10.1038/nrm883.

Sorkin, A. and von Zastrow, M. (2009) 'Endocytosis and signalling: intertwining molecular networks', *Nature Reviews Molecular Cell Biology*, 10(9), pp. 609–622. Available at: https://doi.org/10.1038/nrm2748.

Sternini, C. *et al.* (1996) 'Agonist-selective endocytosis of mu opioid receptor by neurons in vivo.', *Proceedings of the National Academy of Sciences of the United States of America*, 93(17), pp. 9241–9246. Available at: https://doi.org/10.1073/pnas.93.17.9241.

Stoddart, L.A. *et al.* (2015) 'Application of BRET to monitor ligand binding to GPCRs', *Nature Methods*, 12(7), pp. 661–663. Available at: https://doi.org/10.1038/nmeth.3398.

Stoeber, M. *et al.* (2018) 'A Genetically Encoded Biosensor Reveals Location Bias of Opioid Drug Action', *Neuron*, 98(5), pp. 963-976.e5. Available at: https://doi.org/10.1016/j.neuron.2018.04.021.

Stoeber, M. *et al.* (2020) 'Agonist-selective recruitment of engineered protein probes and of GRK2 by opioid receptors in living cells', *eLife*, 9, p. 866780. Available at: https://doi.org/10.7554/eLife.54208.

Sun, Y. *et al.* (2002) 'β-Arrestin2 Is Critically Involved in CXCR4-mediated Chemotaxis, and This Is Mediated by Its Enhancement of p38 MAPK Activation', *Journal of Biological Chemistry*, 277(51), pp. 49212–49219. Available at: https://doi.org/10.1074/jbc.M207294200.

Sungkaworn, T. *et al.* (2017) 'Single-molecule imaging reveals receptor–G protein interactions at cell surface hot spots', *Nature*, 550(7677), pp. 543–547. Available at: https://doi.org/10.1038/nature24264.

Surprenant, A. *et al.* (1990) 'Inhibition of calcium currents by noradrenaline, somatostatin and opioids in guinea-pig submucosal neurones.', *The Journal of Physiology*, 431(1), pp. 585–608. Available at: https://doi.org/10.1113/jphysiol.1990.sp018349.

Sutkeviciute, I. and Vilardaga, J.-P.P. (2020) 'Structural insights into emergent signaling modes of G protein–coupled receptors', *Journal of Biological Chemistry*, 295(33), pp. 11626–11642. Available at: https://doi.org/10.1074/jbc.REV120.009348.

Thal, D.M. *et al.* (2011) 'Molecular Mechanism of Selectivity among G Protein-Coupled Receptor Kinase 2 Inhibitors', *Molecular Pharmacology*, 80(2), pp. 294–303. Available at: https://doi.org/10.1124/mol.111.071522.

*The Human Protein Atlas* (no date). Available at: https://www.proteinatlas.org/ (Accessed: 7 April 2023).

Thomsen, A.R.B. *et al.* (2016) 'GPCR-G Protein-β-Arrestin Super-Complex Mediates Sustained G Protein Signaling', *Cell*, 166(4), pp. 907–919. Available at: https://doi.org/10.1016/j.cell.2016.07.004.

Toll, L. *et al.* (2016) 'Nociceptin/Orphanin FQ Receptor Structure, Signaling, Ligands, Functions, and Interactions with Opioid Systems', *Pharmacological Reviews*. Edited by M.J. Christie, 68(2), pp. 419–457. Available at: https://doi.org/10.1124/pr.114.009209.

Trapaidze, N. *et al.* (2000) 'Opioid receptor endocytosis and activation of MAP kinase pathway', *Molecular Brain Research*, 76(2), pp. 220–228. Available at: https://doi.org/10.1016/S0169-328X(00)00002-4.

Tsvetanova, N.G. and von Zastrow, M. (2014) 'Spatial encoding of cyclic AMP signaling specificity by GPCR endocytosis', *Nature Chemical Biology*, 10(12), pp. 1061–1065. Available at: https://doi.org/10.1038/nchembio.1665.

Usoskin, D. *et al.* (2015) 'Unbiased classification of sensory neuron types by large-scale single-cell RNA sequencing', *Nature Neuroscience*, 18(1), pp. 145–153. Available at: https://doi.org/10.1038/nn.3881.

Verweij, E.W.E. *et al.* (2020) 'Differential Role of Serines and Threonines in Intracellular Loop 3 and C-Terminal Tail of the Histamine H 4 Receptor in β-Arrestin and G Protein-Coupled Receptor Kinase Interaction, Internalization, and Signaling', *ACS Pharmacology & Translational Science*, 3(2), pp. 321–333. Available at: https://doi.org/10.1021/acsptsci.0c00008.

Vo, Q.N. *et al.* (2021) 'How μ-opioid receptor recognizes fentanyl', *Nature Communications*, 12(1), p. 984. Available at: https://doi.org/10.1038/s41467-021-21262-9.

Vukojević, V. *et al.* (2008) 'Ethanol/Naltrexone Interactions at the mu-Opioid Receptor. CLSM/FCS Study in Live Cells', *PLoS ONE*. Edited by A. Jenkins, 3(12), p. e4008. Available at: https://doi.org/10.1371/journal.pone.0004008.

de Waal, P.W. *et al.* (2020) 'Molecular mechanisms of fentanyl mediated β-arrestin biased signaling', *PLOS Computational Biology*. Edited by B.L. de Groot, 16(4), p. e1007394. Available at: https://doi.org/10.1371/journal.pcbi.1007394.

Wan, Q. *et al.* (2018) 'Mini G protein probes for active G protein–coupled receptors (GPCRs) in live cells', *The Journal of Biological Chemistry*, 293(19), pp. 7466–7473. Available at: https://doi.org/10.1074/jbc.RA118.001975.

Wang, H.-L. *et al.* (2002) 'Identification of two C-terminal amino acids, Ser355 and Thr357, required for short-term homologous desensitization of μ-opioid receptors', *Biochemical Pharmacology*, 64(2), pp. 257–266. Available at: https://doi.org/10.1016/S0006-2952(02)01114-0.

Wang, P. *et al.* (2003) 'β-Arrestin 2 Functions as a G-Protein-coupled Receptor-activated Regulator of Oncoprotein Mdm2', *Journal of Biological Chemistry*, 278(8), pp. 6363–6370. Available at: https://doi.org/10.1074/jbc.M210350200.

Wang, P. and DeFea, K.A. (2006) 'Protease-Activated Receptor-2 Simultaneously Directs β-Arrestin-1-Dependent Inhibition and Gαq-Dependent Activation of Phosphatidylinositol 3-Kinase †', *Biochemistry*, 45(31), pp. 9374–9385. Available at: https://doi.org/10.1021/bi0602617.

Wang, Y. *et al.* (2006) 'Association of β-arrestin and TRAF6 negatively regulates Toll-like receptor–interleukin 1 receptor signaling', *Nature Immunology*, 7(2), pp. 139–147. Available at: https://doi.org/10.1038/ni1294.

Wang, Y. *et al.* (2023) 'Structures of the entire human opioid receptor family', *Cell*, 186(2), pp. 413-427.e17. Available at: https://doi.org/10.1016/j.cell.2022.12.026.

Weis, W.I. and Kobilka, B.K. (2018) 'The Molecular Basis of G Protein–Coupled Receptor Activation', *Annual Review of Biochemistry*, 87(1), pp. 897–919. Available at: https://doi.org/10.1146/annurev-biochem-060614-033910.

Wettschureck, N. and Offermanns, S. (2005) 'Mammalian G Proteins and Their Cell Type Specific Functions', *Physiological Reviews*, 85(4), pp. 1159–1204. Available at: https://doi.org/10.1152/physrev.00003.2005.

Whistler, J.L. and von Zastrow, M. (1998) 'Morphine-activated opioid receptors elude desensitization by -arrestin', *Proceedings of the National Academy of Sciences of the United States of America*, 95(17), pp. 9914–9919. Available at: https://doi.org/10.1073/pnas.95.17.9914.

White, C.W. *et al.* (2017) 'Using nanoBRET and CRISPR/Cas9 to monitor proximity to a genome-edited protein in real-time', *Scientific Reports*, 7(1), p. 3187. Available at: https://doi.org/10.1038/s41598-017-03486-2.

Williams, J.T. *et al.* (2013) 'Regulation of μ -Opioid Receptors: Desensitization, Phosphorylation, Internalization, and Tolerance', *Pharmacological Reviews*. Edited by A.C. Dolphin, 65(1), pp. 223–254. Available at: https://doi.org/10.1124/pr.112.005942.

Witherow, D.S. *et al.* (2004) '-Arrestin inhibits NF- B activity by means of its interaction with the NF- B inhibitor I B', *Proceedings of the National Academy of Sciences*, 101(23), pp. 8603–8607. Available at: https://doi.org/10.1073/pnas.0402851101.

Wolf, R. *et al.* (1999) 'Replacement of Threonine 394 by Alanine Facilitates Internalization and Resensitization of the Rat μ Opioid Receptor', *Molecular Pharmacology*, 55(2), pp. 263–268. Available at: https://doi.org/10.1124/mol.55.2.263.

Wu, N. *et al.* (2006) 'Arrestin Binding to Calmodulin: A Direct Interaction Between Two Ubiquitous Signaling Proteins', *Journal of Molecular Biology*, 364(5), pp. 955–963. Available at: https://doi.org/10.1016/j.jmb.2006.09.075.

Xiao, K.-H. *et al.* (2007) 'Functional specialization of beta-arrestin interactions revealed by proteomic analysis', *Proceedings of the National Academy of Sciences*, 104(29), pp. 12011–12016. Available at: https://doi.org/10.1073/pnas.0704849104.

Yang, F. *et al.* (2015) 'Phospho-selective mechanisms of arrestin conformations and functions revealed by unnatural amino acid incorporation and 19F-NMR', *Nature Communications*, 6(1), p. 8202. Available at: https://doi.org/10.1038/ncomms9202.

Yang, X. *et al.* (2012) 'β-Arrestin prevents cell apoptosis through pro-apoptotic ERK1/2 and p38 MAPKs and anti-apoptotic Akt pathways', *Apoptosis*, 17(9), pp. 1019–1026. Available at: https://doi.org/10.1007/s10495-012-0741-2.

Yang, Y. *et al.* (2016) 'Sixty-five years of the long march in protein secondary structure prediction: the final stretch?', *Briefings in Bioinformatics*, 19(3), pp. 482–494. Available at: https://doi.org/10.1093/bib/bbw129.

Yang, Z. *et al.* (2017) 'Phosphorylation of G Protein-Coupled Receptors: From the Barcode Hypothesis to the Flute Model', *Molecular Pharmacology*, 92(3), pp. 201–210. Available at: https://doi.org/10.1124/mol.116.107839.

Yeh, H.-W. *et al.* (2017) 'Red-shifted luciferase–luciferin pairs for enhanced bioluminescence imaging', *Nature Methods*, 14(10), pp. 971–974. Available at: https://doi.org/10.1038/nmeth.4400.

Yousuf, A. *et al.* (2015) 'Role of Phosphorylation Sites in Desensitization of μ -Opioid Receptor', *Molecular Pharmacology*, 88(4), pp. 825–835. Available at: https://doi.org/10.1124/mol.115.098244.

Yu, M.-C. *et al.* (2008) 'An essential function for β-arrestin 2 in the inhibitory signaling of natural killer cells', *Nature Immunology*, 9(8), pp. 898–907. Available at: https://doi.org/10.1038/ni.1635.

Zhang, J. *et al.* (1998) 'Role for G protein-coupled receptor kinase in agonist-specific regulation of -opioid receptor responsiveness', *Proceedings of the National Academy of Sciences of the United States of America*, 95(12), pp. 7157–7162. Available at: https://doi.org/10.1073/pnas.95.12.7157.

Zhao, M. *et al.* (2004) 'Arrestin Regulates MAPK Activation and Prevents NADPH Oxidase-dependent Death of Cells Expressing CXCR2', *Journal of Biological Chemistry*, 279(47), pp. 49259–49267. Available at: https://doi.org/10.1074/jbc.M405118200.

Zhou, X.E. *et al.* (2017) 'Identification of Phosphorylation Codes for Arrestin Recruitment by G Protein-Coupled Receptors', *Cell*, 170(3), pp. 457-469.e13. Available at: https://doi.org/10.1016/j.cell.2017.07.002.

Zimmerman, B. *et al.* (2009) 'c-Src-mediated phosphorylation of AP-2 reveals a general mechanism for receptors internalizing through the clathrin pathway', *Cellular Signalling*, 21(1), pp. 103–110. Available at: https://doi.org/10.1016/j.cellsig.2008.09.013.

Zoudilova, M. *et al.* (2007) 'β-Arrestin-dependent Regulation of the Cofilin Pathway Downstream of Protease-activated Receptor-2', *Journal of Biological Chemistry*, 282(28), pp. 20634–20646. Available at: https://doi.org/10.1074/jbc.M701391200.

Zoudilova, M. *et al.* (2010) 'β-Arrestins Scaffold Cofilin with Chronophin to Direct Localized Actin Filament Severing and Membrane Protrusions Downstream of Protease-activated Receptor-2', *Journal of Biological Chemistry*, 285(19), pp. 14318–14329. Available at: https://doi.org/10.1074/jbc.M109.055806.

# VIII. Appendices

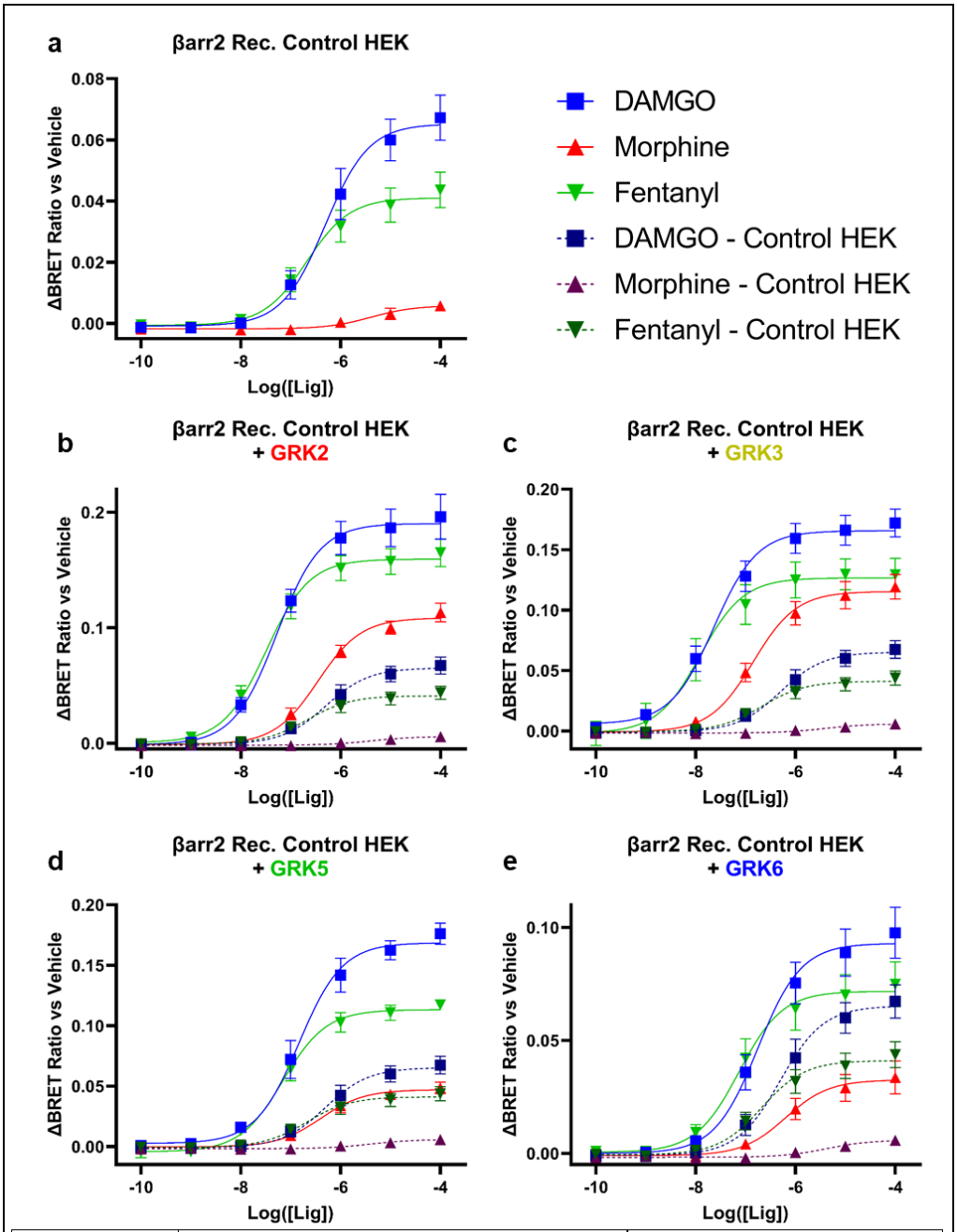


**f**

| Cell Line | Potency (Log(EC50)) | | | | | | | | | | | | % Max DAMGO Response | | | | | | | |
|---|---|---|---|---|---|---|---|---|---|---|---|---|---|---|---|---|---|---|---|---|
| | DAMGO | | | | Morphine | | | | Fentanyl | | | | Morphine | | | | Fentanyl | | | |
| | Mean | SEM | N | Sig. | Mean | SEM | N | Sig. | Mean | SEM | N | Sig. | Mean | SEM | N | Sig. | Mean | SEM | N | Sig. |
| Control HEK | -6.26 | 0.16 | 5 | | -5.37 | 0.32 | 5 | | -6.63 | 0.15 | 5 | | 13.8 | 1.88 | 5 | | 63.8 | 3.26 | 5 | |
| Control HEK + GRK2 | -7.31 | 0.11 | 5 | ** | -6.46 | 0.11 | 5 | * | -7.49 | 0.10 | 5 | ** | 58.3 | 3.00 | 5 | **** | 84.6 | 2.60 | 5 | ** |
| Control HEK + GRK3 | -7.66 | 0.15 | 5 | *** | -6.83 | 0.10 | 5 | ** | -7.89 | 0.11 | 5 | *** | 69.7 | 2.78 | 5 | **** | 78.5 | 5.54 | 5 | |
| Control HEK + GRK5 | -6.78 | 0.17 | 6 | | -6.32 | 0.14 | 6 | * | -7.11 | 0.14 | 6 | * | 28.4 | 2.58 | 6 | ** | 68.1 | 3.42 | 6 | |
| Control HEK + GRK6 | -6.75 | 0.14 | 5 | | -6.18 | 0.11 | 5 | * | -7.10 | 0.11 | 5 | * | 36.0 | 6.25 | 5 | * | 77.3 | 6.03 | 5 | |

*Appendix 2.3.1.1, β-arrestin2-YFP recruitment to MOR-Nluc mean ± SEM concentration response curves with varied opioid ligands (log(M)) (DAMGO (Blue), Morphine (Red), Fentanyl (Green) in a) Control HEK293 cells. b, c, d, e) Control HEK293 cell concentration response curves (dashed lines) overlaid (DAMGO – Dark Blue, Morphine – Purple, Fentanyl – Dark Green) on concentration response curves conducted in control GRK knockout HEK293 cells co-transfected with b) ΔGRK2 cells. c) ΔGRK3 cells. d) ΔGRK5. e) GRK6. f) Table showing EC50 and maximum response as a % of maximum DAMGO response for each ligand in each cell condition, with standard error of the mean (SEM), N-number (N), and significance as a difference from Control HEK in an unpaired T-Test, corrected for multiple comparisons using a Holm-Šídák test (*: p ≤ 0.05; **: p ≤ 0.005; ***: p ≤ 0.0005; ****: p ≤ 0.00005).*

| Cell Line | Potency (Log(EC50)) | | | %DAMGO Resp. | |
|---|---|---|---|---|---|
| | DAMGO | Morphine | Fentanyl | Morphine | Fentanyl |
| | P Value | P Value | P Value | P Value | P Value |
| WT HEK | - | - | - | - | - |
| WT HEK + GRK2 | 0.000237 | 0.005094 | 0.008525 | 0.000002 | 0.000015 |
| WT HEK + Cmpd101 | 0.206585 | 0.011633 | 0.222407 | 0.000156 | 0.005578 |

| Cell Line | Potency (Log(EC50)) | | | %DAMGO Resp. | |
|---|---|---|---|---|---|
| | DAMGO | Morphine | Fentanyl | Morphine | Fentanyl |
| | P Value | P Value | P Value | P Value | P Value |
| WT HEK | - | - | - | - | - |
| Control HEK | 0.967830 | 0.742029 | 0.589973 | 0.985019 | 0.006162 |
| ΔGRK2 | 0.171821 | 0.357748 | 0.629679 | 0.954644 | 0.678931 |

| Cell Line | Potency (Log(EC50)) | | | %DAMGO Resp. | |
|---|---|---|---|---|---|
| | DAMGO | Morphine | Fentanyl | Morphine | Fentanyl |
| | P Value | P Value | P Value | P Value | P Value |
| Control HEK | - | - | - | - | - |
| ΔGRK2 | 0.140864 | 0.476789 | 0.914333 | 0.920387 | 0.008301 |
| ΔGRK3 | 0.185359 | 0.007929 | 0.159267 | 0.013033 | 0.430119 |
| ΔGRK2/3 | 0.122192 | 0.023176 | 0.177373 | 0.001284 | 0.094882 |

| Cell Line | Potency (Log(EC50)) | | | %DAMGO Resp. | |
|---|---|---|---|---|---|
| | DAMGO | Morphine | Fentanyl | Morphine | Fentanyl |
| | P Value | P Value | P Value | P Value | P Value |
| Control HEK | - | - | - | - | - |
| ΔGRK5 | 0.628861 | 0.127054 | 0.334598 | 0.078766 | 0.387304 |
| ΔGRK6 | 0.792674 | 0.069254 | 0.621852 | 0.078766 | 0.387304 |
| ΔGRK5/6 | 0.449413 | 0.251438 | 0.655554 | 0.913692 | 0.333335 |

| Cell Line | Potency (Log(EC50)) | | | %DAMGO Resp. | |
|---|---|---|---|---|---|
| | DAMGO | Morphine | Fentanyl | Morphine | Fentanyl |
| | P Value | P Value | P Value | P Value | P Value |
| Control HEK | - | - | - | - | - |
| ΔQ-GRK | 0.500320 | 0.172336 | 0.161098 | 0.005437 | 0.251420 |

| Cell Line | Potency (Log(EC50)) | | | %DAMGO Resp. | |
|---|---|---|---|---|---|
| | DAMGO | Morphine | Fentanyl | Morphine | Fentanyl |
| | P Value | P Value | P Value | P Value | P Value |
| Control HEK | - | - | - | - | - |
| ΔQ-GRK | 0.500320 | 0.172336 | 0.161098 | 0.005437 | 0.251420 |
| ΔQ-GRK + GRK2 | 0.000002 | 0.000444 | 0.000009 | 0.000001 | 0.000164 |
| ΔQ-GRK + GRK3 | 0.000042 | 0.000976 | 0.000147 | 0.000001 | 0.000479 |
| ΔQ-GRK + GRK5 | 0.007276 | 0.006399 | 0.032929 | 0.001629 | 0.597589 |
| ΔQ-GRK + GRK6 | 0.073415 | 0.026454 | 0.056078 | 0.000261 | 0.225106 |

| Cell Line | Potency (Log(EC50)) | | | %DAMGO Resp. | |
|---|---|---|---|---|---|
| | DAMGO | Morphine | Fentanyl | Morphine | Fentanyl |
| | P Value | P Value | P Value | P Value | P Value |
| Control HEK | - | - | - | - | - |
| Control HEK + GRK2 | 0.000635 | 0.010874 | 0.001252 | 0.000001 | 0.001055 |
| Control HEK + GRK3 | 0.000237 | 0.002261 | 0.000111 | 0.000001 | 0.051776 |
| Control HEK + GRK5 | 0.056463 | 0.016427 | 0.046394 | 0.001756 | 0.394718 |
| Control HEK + GRK6 | 0.053750 | 0.040691 | 0.032630 | 0.009458 | 0.084244 |

*Appendix 2.3.1.2, table showing P values from unpaired Tests, assessing significant difference from equivalent ligand potency and response in WT or control HEKs for β-arrestin2 recruitment, corrected for multiple comparisons using a Holm-Šídák test.*

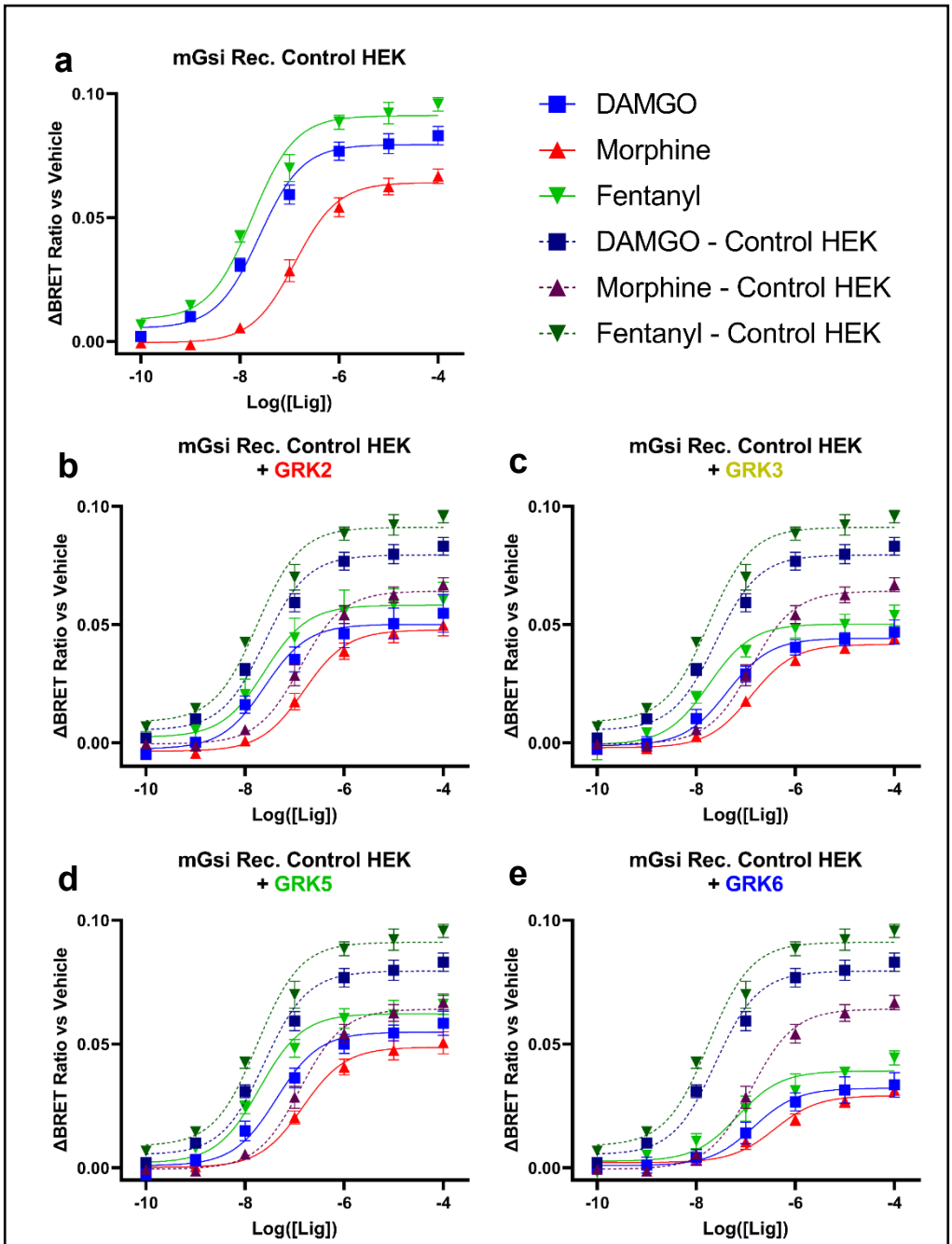


| Cell Line | Potency (Log(EC50)) | | | | | | | | | | | | % Max DAMGO Response | | | | | | | |
|---|---|---|---|---|---|---|---|---|---|---|---|---|---|---|---|---|---|---|---|---|
| | DAMGO | | | | Morphine | | | | Fentanyl | | | | Morphine | | | | Fentanyl | | | |
| | Mean | SEM | N | Sig. | Mean | SEM | N | Sig. | Mean | SEM | N | Sig. | Mean | SEM | N | Sig. | Mean | SEM | N | Sig. |
| Control HEK | -7.61 | 0.05 | 5 | | -6.88 | 0.09 | 5 | | -7.74 | 0.04 | 5 | | 89.7 | 8.68 | 5 | | 108.3 | 6.50 | 5 | |
| Control HEK + GRK2 | -7.60 | 0.15 | 5 | | -6.81 | 0.08 | 5 | | -7.55 | 0.16 | 5 | | 97.5 | 7.03 | 5 | | 116.1 | 10.59 | 5 | |
| Control HEK + GRK3 | -7.42 | 0.13 | 5 | | -6.88 | 0.09 | 5 | | -7.74 | 0.10 | 5 | | 97.2 | 8.71 | 5 | | 113.7 | 11.73 | 5 | |
| Control HEK + GRK5 | -7.42 | 0.15 | 5 | | -6.84 | 0.12 | 5 | | -7.70 | 0.08 | 5 | | 90.0 | 4.31 | 5 | | 113.2 | 2.29 | 5 | |
| Control HEK + GRK6 | -6.92 | 0.28 | 5 | * | -6.65 | 0.45 | 5 | | -7.09 | 0.50 | 5 | | 99.0 | 11.53 | 5 | | 142.4 | 23.06 | 5 | |

*Appendix 2.3.2.1, miniGsi-Venus recruitment to MOR-Nluc mean ± SEM concentration response curves with varied opioid ligands (log(M)) (DAMGO (Blue), Morphine (Red), Fentanyl (Green) in a) Control HEK293 cells. b, c, d, e) Control HEK293 cell concentration response curves (dashed lines) overlaid (DAMGO – Dark Blue, Morphine – Purple, Fentanyl – Dark Green) on concentration response curves conducted in control GRK knockout HEK293 cells co-transfected with b) ΔGRK2 cells. c) ΔGRK3 cells. d) ΔGRK5. e) GRK6. f) Table showing EC50 and maximum response as a % of maximum DAMGO response for each ligand in each cell condition, with standard error of the mean (SEM), N-number (N), and significance as a difference from Control HEK in an unpaired T-Test, corrected for multiple comparisons using a Holm-Šídák test (*: $p \leq 0.05$).*

*Appendix 2.3.2.2, table showing P values from unpaired Tests, assessing significant difference from equivalent ligand potency and response in WT or control HEKs for miniGsi recruitment, corrected for multiple comparisons using a Holm-Šídák test.*

| | Potency (Log(EC50)) | | | %DAMGO Resp. | |
|---|---|---|---|---|---|
| | DAMGO | Morphine | Fentanyl | Morphine | Fentanyl |
| Cell Line | P Value | P Value | P Value | P Value | P Value |
| WT HEK | - | - | - | - | - |
| WT HEK + GRK2 | 0.119001 | 0.087051 | 0.022227 | 0.149284 | 0.332735 |
| WT HEK + Cmpd101 | 0.259210 | 0.352042 | 0.524782 | 0.016564 | 0.071074 |

| | Potency (Log(EC50)) | | | %DAMGO Resp. | |
|---|---|---|---|---|---|
| | DAMGO | Morphine | Fentanyl | Morphine | Fentanyl |
| Cell Line | P Value | P Value | P Value | P Value | P Value |
| WT HEK | - | - | - | - | - |
| Control HEK | 0.087174 | 0.173078 | 0.033871 | 0.019802 | 0.094162 |
| ΔGRK2 | 0.509613 | 0.536195 | 0.612759 | 0.082836 | 0.192452 |

| | Potency (Log(EC50)) | | | %DAMGO Resp. | |
|---|---|---|---|---|---|
| | DAMGO | Morphine | Fentanyl | Morphine | Fentanyl |
| Cell Line | P Value | P Value | P Value | P Value | P Value |
| Control HEK | - | - | - | - | - |
| ΔGRK2 | 0.019179 | 0.045623 | 0.000561 | 0.133313 | 0.382719 |
| ΔGRK3 | 0.088451 | 0.237016 | 0.030795 | 0.855033 | 0.168549 |
| ΔGRK2/3 | 0.520655 | 0.579417 | 0.512721 | 0.286798 | 0.525374 |

| | Potency (Log(EC50)) | | | %DAMGO Resp. | |
|---|---|---|---|---|---|
| | DAMGO | Morphine | Fentanyl | Morphine | Fentanyl |
| Cell Line | P Value | P Value | P Value | P Value | P Value |
| Control HEK | - | - | - | - | - |
| ΔGRK5 | 0.702111 | 0.498508 | 0.315797 | 0.857890 | 0.038174 |
| ΔGRK6 | 0.489726 | 0.559279 | 0.768623 | 0.523513 | 0.747917 |
| ΔGRK5/6 | 0.843391 | 0.642898 | 0.061904 | 0.375132 | 0.174142 |

| | Potency (Log(EC50)) | | | %DAMGO Resp. | |
|---|---|---|---|---|---|
| | DAMGO | Morphine | Fentanyl | Morphine | Fentanyl |
| Cell Line | P Value | P Value | P Value | P Value | P Value |
| Control HEK | - | - | - | - | - |
| ΔQ-GRK | 0.014161 | 0.606434 | 0.000328 | 0.242026 | 0.330522 |

| | Potency (Log(EC50)) | | | %DAMGO Resp. | |
|---|---|---|---|---|---|
| | DAMGO | Morphine | Fentanyl | Morphine | Fentanyl |
| Cell Line | P Value | P Value | P Value | P Value | P Value |
| Control HEK | - | - | - | - | - |
| ΔQ-GRK | 0.014161 | 0.606434 | 0.000328 | 0.242026 | 0.330522 |
| ΔQ-GRK + GRK2 | 0.792773 | 0.665794 | 0.936823 | 0.341676 | 0.898304 |
| ΔQ-GRK + GRK3 | 0.049256 | 0.672933 | 0.006814 | 0.235300 | 0.409069 |
| ΔQ-GRK + GRK5 | 0.213199 | 0.419695 | 0.118924 | 0.187467 | 0.236056 |
| ΔQ-GRK + GRK6 | 0.022848 | 0.091293 | 0.016582 | 0.391431 | 0.421833 |

| | Potency (Log(EC50)) | | | %DAMGO Resp. | |
|---|---|---|---|---|---|
| | DAMGO | Morphine | Fentanyl | Morphine | Fentanyl |
| Cell Line | P Value | P Value | P Value | P Value | P Value |
| Control HEK | - | - | - | - | - |
| Control HEK + GRK2 | 0.955880 | 0.595789 | 0.288832 | 0.505612 | 0.547371 |
| Control HEK + GRK3 | 0.221555 | 0.978244 | 0.988121 | 0.560929 | 0.694856 |
| Control HEK + GRK5 | 0.269687 | 0.819618 | 0.720559 | 0.979738 | 0.493132 |
| Control HEK + GRK6 | 0.041515 | 0.629323 | 0.234488 | 0.538434 | 0.192403 |

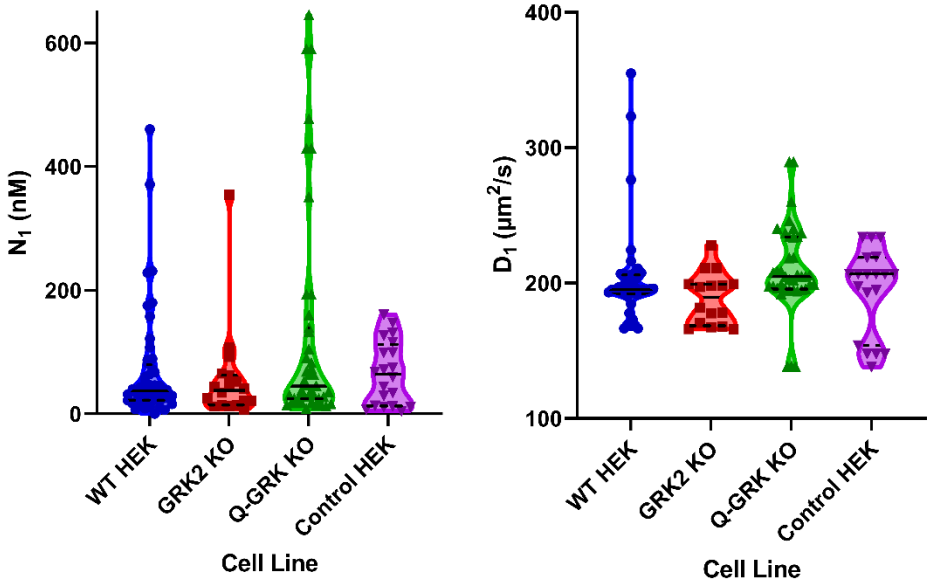


| | WT HEK | | GRK2 KO | | Q-GRK KO | | Control HEK | |
|---|---|---|---|---|---|---|---|---|
| | Mean | ± SEM | Mean | ± SEM | Mean | ± SEM | Mean | ± SEM |
| $N_1$ (nM) | 70.91 | 13.24 | 57.07 | 18.69 | 127.8 | 27.11 | 66.23 | 11.48 |
| $D_1$; µm$^2$/s | 202.7 | 5.435 | 188.6 | 4.789 | 210.1 | 5.177 | 194.8 | 7.297 |
| No. Cells | 48 | | 18 | | 43 | | 20 | |

*Appendix 3.4.2, a) Number of particles (nM) and b) diffusion coefficient (µm$^2$/s) of particles described by the first component, black lines indicate median, dashed lines indicate upper and lower quartiles. c) table summarising autocorrelation analysis parameters for each cell line (mean ±SEM). Data collected from at least 20 individual cells per cell line over 3 independent experimental days.*

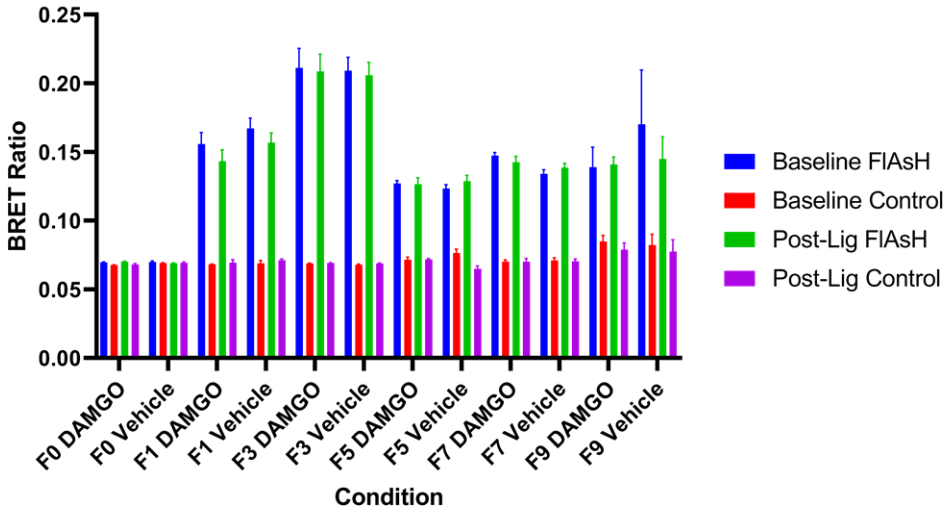


*Appendix 4.3.3.1, BRET ratio of β-arrestin2-FlAsH-NLuc intramolecular BRET conformational biosensors, with varying FlAsH binding sites, before and after treatment with 1 μM DAMGO or vehicle in the absence of GRK2 overexpression, following labelling with either control or FlAsH buffer (n=1, error bars show ± SD)*

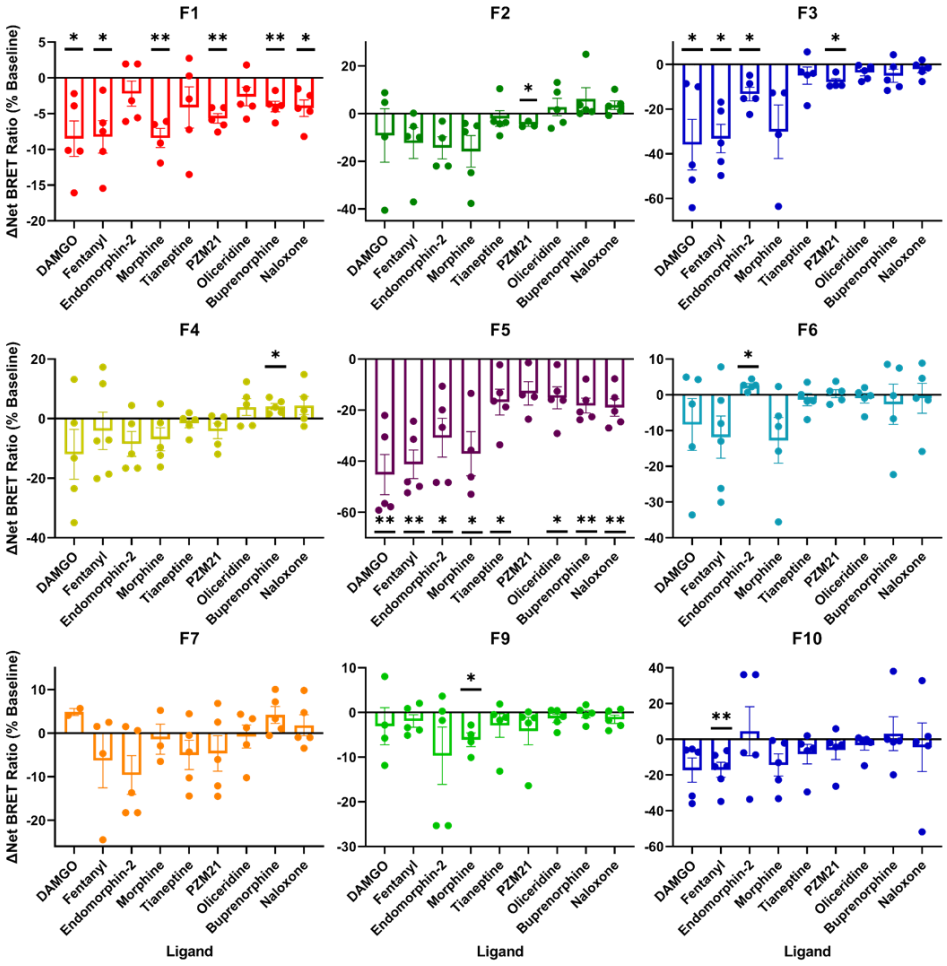


*Appendix 4.3.3.2, Change as a percentage of baseline of net BRET ratio of β-arrestin2-FlAsH-NLuc intramolecular BRET conformational biosensors, with varying FlAsH binding sites (F1, Red, residue 331; F2, Dark Green, residue 154; F3, Dark Blue, residue 49; F4, Yellow, residue 150; F5, Purple, residue 157; F6, Teal, residue 326; F7, Orange, residue 335; F9, Light Green, residue 225; F10, Blue, residue 263), following treatment with 1 μM opioid ligands (n=5, average ± SEM, T-Test for significant difference from 0: *: p ≤ 0.05; **: p ≤ 0.005).*

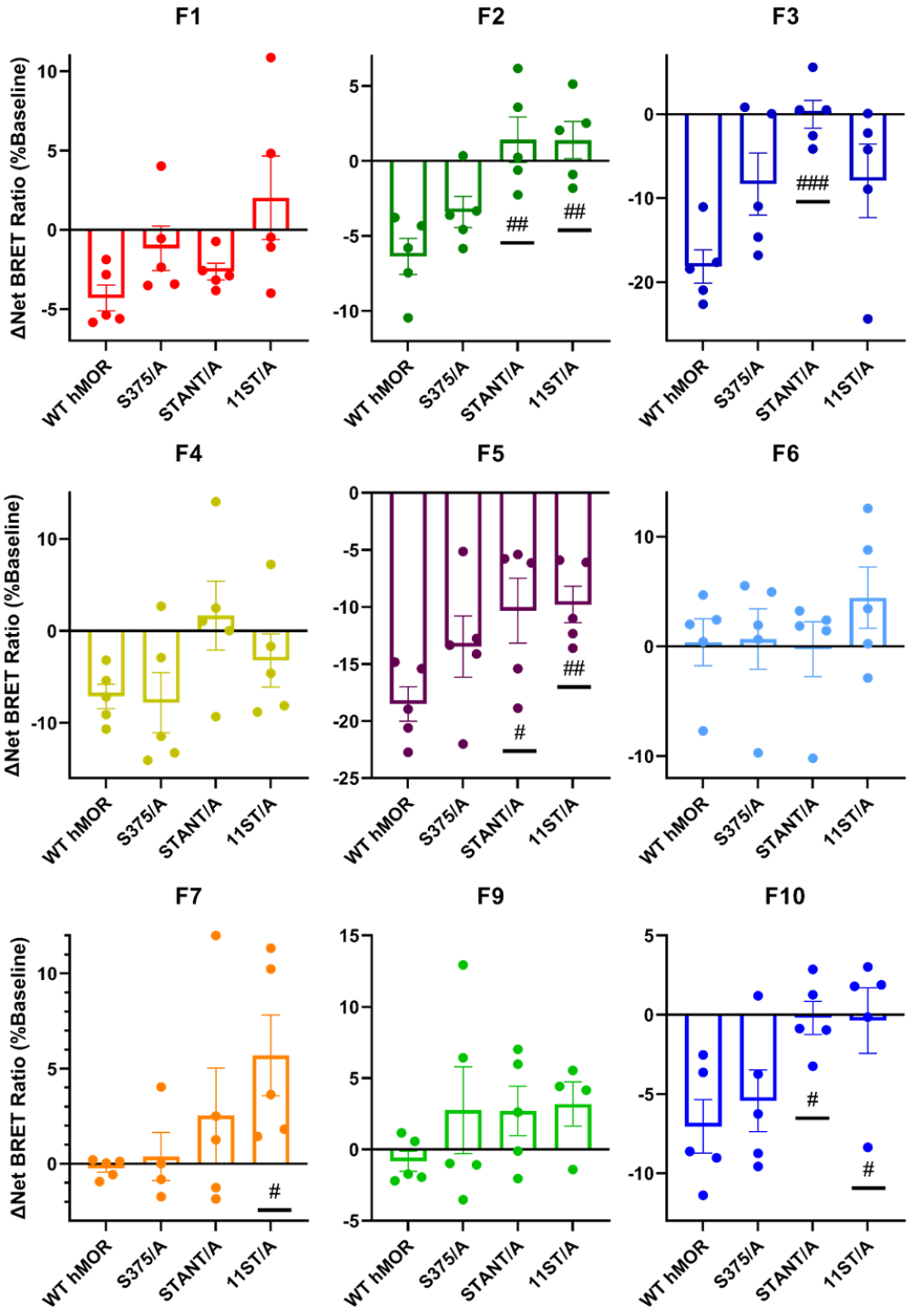


*Appendix 4.3.6.1, Change as a percentage of baseline of net BRET ratio of β-arrestin2-FlAsH-NLuc intramolecular BRET conformational biosensors, with varying FlAsH binding sites (F1, Red, residue 331; F2, Dark Green, residue 154; F3, Dark Blue, residue 49; F4, Yellow, residue 150; F5, Purple, residue 157; F6, Teal, residue 326; F7, Orange, residue 335; F9, Light Green, residue 225; F10, Blue, residue 263), following treatment of MORs with phosphosites mutated to alanine with 10 µM morphine (n=5, average ± SEM).*

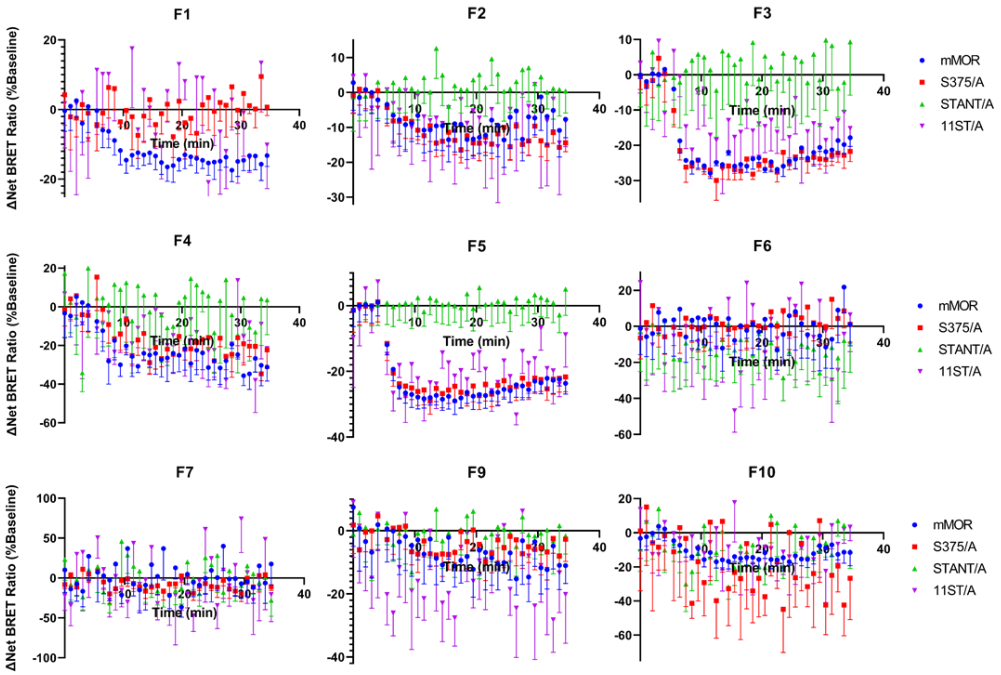


*Appendix 4.3.6.2, Change as a percentage of baseline over time of net BRET ratio of β-arrestin2-FlAsH-NLuc intramolecular BRET conformational biosensors, with varying FlAsH binding sites (F1, Red, residue 331; F2, Dark Green, residue 154; F3, Dark Blue, residue 49; F4, Yellow, residue 150; F5, Purple, residue 157; F6, Teal, residue 326; F7, Orange, residue 335; F9, Light Green, residue 225; F10, Blue, residue 263), following treatment of MORs with phosphosites mutated to alanine with 10 µM morphine (n=1, average of quadruplicate wells, error bars show SD).*